Production of Pentanol in Metabolically Engineered *Escherichia coli*

By

Hsien-Chung Tseng

B.S. Chemical Engineering
National Taiwan University, 2004

SUBMITTED TO THE DEPARTMENT OF CHEMICAL ENGINEERING IN PARTIAL FULFILLMENT OF THE REQUIREMENTS FOR THE DEGREE OF

DOCTOR OF PHILOSOPHY IN CHEMICAL ENGINEERING
AT THE
MASSACHUSETTS INSTITUTE OF TECHNOLOGY
JUNE 2011

Signature of Author: _____
Department of Chemical Engineering
May 5, 2011

Certified by: _____
Kristala L. Jones Prather
Associate Professor of Chemical Engineering
Thesis Supervisor

Accepted by: _____
William M. Deen
Professor of Chemical Engineering
Chairman, Committee for Graduate Students

Production of Pentanol in Metabolically Engineered *Escherichia coli*

By

Hsien-Chung Tseng

Submitted to the Department of Chemical Engineering on May 5, 2011 in Partial Fulfillment of the Requirements for the Degree of Doctor of Philosophy in Chemical Engineering

ABSTRACT

Public concerns about global warming and energy security contribute to an ever-increasing focus on biologically-derived fuels, leading to significant interest in several candidate molecules capable of complementing petroleum-derived fuel resources. Ethanol, one of the most developed biofuels, is used extensively as a gasoline additive. However, the high water miscibility of ethanol creates corrosion problems when transporting the fuel by pipelines. Furthermore, the low energy density of ethanol limits its fuel efficiency. Thus, it is important to explore alternative biofuels with properties that are more similar to conventional gasoline. With a higher energy density, enhanced physical properties that would allow better integration with current infrastructure, pentanol represents an excellent alternative, and has the potential to be a replacement for gasoline. The primary objective of my thesis work is to construct pentanol biosynthetic pathways in *Escherichia coli*, offering the possibility of producing pentanol from renewable carbon sources through microbial fermentations.

We used butanol synthesis as a platform from which microbial synthesis of pentanol can be obtained. To explore the possibility of employing the butanol pathway enzymes for pentanol biosynthesis, we implemented a bypass/feeding strategy to thoroughly evaluate the ability of those enzymes to act on five-carbon substrates. Additionally, by boosting the intracellular NADH availability, we achieved up to 85 mg/L pentanol from glucose and propionate, providing an initial proof-of-concept of a functional and feasible pentanol biosynthetic pathway in *E. coli*. Furthermore, a platform pathway was established for synthesis of value-added chiral 3-hydroxyalkanoic acids with applications ranging from chiral building blocks to high-value pharmaceuticals. Of significance, such pathway was constructed as one portion of the pentanol pathway, illustrating versatility of our pentanol pathway as it can be modularized for synthesis of various valuable chemicals.

Altogether, our results suggest that direct microbial synthesis of pentanol solely from glucose or glycerol can be realized once an efficient redox balancing within the recombinant strains is ensured. As construction of desired biosynthetic pathways is just the first step toward economically viable pentanol production, increasing the titer, yield, and productivity will ultimately determine the feasibility of such pathways.

Thesis Supervisor: Kristala L. Jones Prather

Title: Associate Professor of Chemical Engineering

This thesis is dedicated to my lovely family overseas in Taiwan - my Mom, Dad, and Brother.

ACKNOWLEDGEMENTS

My thesis work would not have been possible without the help and support of my advisor, committee members, colleagues, collaborators, fellow students, and friends throughout the past five years. I am especially fortunate to have a great thesis advisor, Kris Prather, for her guidance, enthusiasm, and optimism, keeping me firmly on track to achieve my goals. My thesis committee members – Greg Stephanopoulos, Charles Cooney, and Tony Sinskey – also deserve my gratitude for the guidance they have given to me. I would like express my special thanks to Dave Nielsen for spending countless hours mentoring me when I first joined the lab. He not only taught me a lot about scientific research, but helped me learn to live a meaningful life. I really enjoyed hanging out and drinking beer with him! I am also very grateful for the tremendous help from Effendi Leonard, Collin Martin, and Sang-Hwal Yoon. Without their help in the work of butanol and 3-hydroxybutyrate biosynthesis, I would have never been able to finish my thesis work in such a short period of time. Thanks also to Himanshu Dhamankar, Micah Sheppard, and Catey Harwell for their assistance in construction of chiral 3-hydroxyalkanoic acid pathway. During my time at MIT, I have had the pleasure of collaborating with Curt Fischer with acyl-CoA pool size measurement to troubleshoot the *Clostridial* butanol biosynthesis pathway, and colleagues in the Shell biofuel team with construction of metabolic pathways for production of novel biofuels. In addition, I have had a wonderful time in Prather lab with amazing people working on interesting research projects. Many thanks to Gwen Wilcox for her tremendous help in all facets of my life at MIT. I also appreciate the funding of the SynBERC, MITEI, and Shell. Last but certainly not least, I would like to express my gratitude to all my friends. Without their help in countless ways, it was not possible for me to complete my thesis.

TABLE OF CONTENTS

ABSTRACT **2**
ACKNOWLEDGEMENTS **4**
TABLE OF CONTENTS **5**
LIST OF FIGURES **9**
LIST OF TABLES **11**
LIST OF ABBREVIATIONS **12**

CHAPTER 1: Introduction 13
1.1 Background on Historical Perspective of Biofuels 14
1.1.1 Renewable biomass 14
1.1.2 Conversion of biomass to liquid fuels 15
1.1.3 Ethanol as a transportation fuel 16
1.1.4 Conventional ethanol 16
1.1.5 Cellulosic ethanol 17
1.1.6 Advanced biofuels 17
1.1.7 Butanol as a liquid transportation fuel 18
1.1.8 Metabolic engineering of novel biocatalysts 19
1.2 Motivation and Objectives 21
1.3 Metabolic Pathway Design 23
1.4 Thesis Organization 26

CHAPTER 2: Reconstruction of *Clostridial* Butanol Pathway **29**
2.1 Introduction 30
2.2 Materials and Methods 34
2.2.1 Microbial strains 34
2.2.2 Plasmid construction 34
2.2.3 Strain development and culture conditions 37
2.2.4 Butanol challenge 40
2.2.5 Metabolite analysis 40
2.3 Results 41
2.3.1 Construction of butanol-producing *E. coli* 41
2.3.2 Expression of NADH-regenerating and glycolytic flux-enhancing enzymes 43
2.3.3 Engineering *P. putida* and *B. subtilis* for butanol biosynthesis 46
2.3.4 Assessing the butanol tolerance of *E. coli*, *P. putida*, and *B. subtilis* ... 48
2.4 Discussion 50
2.5 Conclusions 55

CHAPTER 3: Chiral 3-Hydroxybutyrate Biosynthesis as In Vivo Assessment of the Top Butanol Pathway **57**
3.1 Introduction 58
3.2 Materials and Methods 61

3.2.1 Microorganisms 61
3.2.2 Plasmid construction 61
3.2.3 Culture conditions 63
3.2.4 Metabolite analysis and dry cell weight determination 64
3.2.5 Methyl esterification of 3HB 64
3.2.6 Chiral HPLC analysis of methyl-3HB 65
3.2.7 Enzyme assays 65
3.2.8 Quantification of intracellular cofactor levels 65
3.3 Results 66
3.3.1 Production of chiral 3HB in BL21Star(DE3) 66
3.3.2 Production of chiral 3HB in MG1655(DE3) 67
3.3.3 Confirmation of 3HB stereochemistry 68
3.3.4 Measurement of specific activities of 3HB synthesis enzymes expressed in *E. coli* 70
3.3.5 Measurement of cofactor levels in engineered MG1655(DE3) strains 71
3.3.6 Enhanced 3HB production 72
3.4 Discussion 73
3.4.1 *E. coli* B versus *E. coli* K-12 in chiral 3HB production 73
3.4.2 Effect of alternative acetoacetyl-CoA thiolases on chiral 3HB production 74
3.4.3 TesB versus Ptb-Buk as a CoA removal system 75
3.4.4 Discrepancies between enzyme activities of Hbd and PhaB and production titers of (*S*)-3HB and (*R*)-3HB 76
3.5 Conclusions 77

CHAPTER 4: Chiral 3-Hydroxyvalerate Biosynthesis from Single Carbon Sources as In Vivo Assesment of the Top Pentanol Pathway 79
4.1 Introduction 80
4.2 Materials and Methods 84
4.2.1 Microorganisms 84
4.2.2 Plasmid construction 85
4.2.3 Culture conditions 87
4.2.4 Metabolite analysis 88
4.2.5 Chiral analysis of 3HV 88
4.3 Results 89
4.3.1 3HV synthesis from glucose and propionate 89
4.3.2 3HV synthesis from glucose and 2-ketobutyrate 90
4.3.3 3HV synthesis from glucose and threonine 92
4.3.4 3HV synthesis from glucose 92
4.3.5 3HV synthesis from glycerol 94
4.3.6 Confirmation of 3HV stereochemistry 95
4.4 Discussion 96
4.5 Conclusions 100

CHAPTER 5: Microbial Synthesis of Pentanol **101**
5.1 Introduction 102
5.2 Materials and Methods 104
5.2.1 Plasmids and primers 104
5.2.2 Strains 105
5.2.3 Culture conditions 107
5.2.4 Metabolite analysis 109
5.3 Results 109
5.3.1 Construction of pentanol biosynthetic pathway 109
5.3.2 Trans-2-pentenoate synthesis from glucose and propionate 110
5.3.3 Pentanol synthesis from valerate 112
5.3.4 Pentanol synthesis from trans-2-pentenoate 114
5.3.5 Validation of the pentanol pathway by butanol synthesis 117
5.3.6 Pentanol synthesis from glucose and propionate 118
5.3.7 Pentanol synthesis solely from glucose or glycerol 119
5.4 Discussion 120
5.5 Conclusions 123

CHAPTER 6: Biosynthesis of Structurally Diverse 3-Hydroxyalkanoic Acids **125**
6.1 Introduction 126
6.2 Materials and Methods 128
6.2.1 Strains 128
6.2.2 Plasmids and primers 129
6.2.3 Culturing conditions 131
6.2.4 Metabolite analysis 131
6.3 Results 134
6.3.1 Production of 3HV from glucose and propionate 134
6.3.2 Production of 4M3HV from glucose and isobutyrate and 3HH from glucose and butyrate 137
6.3.3 Production of DHBA and 3HBL from glucose and glycolate 138
6.3.4 DHBA to 3HBL conversion by acid treatment 139
6.4 Discussion 140
6.5 Conclusions 143

CHAPTER 7: Conclusions and Recommendations **145**
7.1 Conclusions 146
7.2 Recommendations for Future Works 147

REFERENCES **149**

APPENDIX A: Assessment of *Clostridium acetobutylicum* Butanol and Butyrate Pathway Activity by CoA Pool Size Measurements **161**
A.1 Introduction 162

A.2 Materials and Methods..... 163
A.2.1 Strains..... 163
A.2.2 Plasmids..... 164
A.2.3 Culturing conditions..... 165
A.2.4 Stoichiometric modeling of the pal strain..... 165
A.2.5 Determination of intracellular acyl CoAs..... 166
A.2.6 Calculation of $\Delta_{IPTG}\Delta G'$..... 168
A.3 Results..... 169
A.3.1 Design of the pal strain and a stoichiometric driving force for butyrate production..... 169
A.3.2 Assessment of butyrate pathway activity by CoA pool size measurements in three strain sets..... 171
A.3.3 A thermodynamic framework for relating pool size measurements to pathway activity..... 174
A.3.4 Unexpected behavior of Ptb and Buk..... 176
A.4 Discussion..... 178
A.5 Conclusions..... 179

APPENDIX B: Theoretical Yield Analysis for the Pentanol Biosynthetic Pathway. 180
APPENDIX C: Sequences of Synthesized Genes..... 183

LIST OF FIGURES

Figure 1-1 | Schematic of biorefinery for biofuel production. **15**

Figure 1-2 | Scheme for metabolic engineering of novel biocatalysts. **20**

Figure 1-3 | Schematic of proposed pentanol biosynthetic pathway. **22**

Figure 1-4 | Schematic diagram of research plans for pentanol biosynthesis. **23**

Figure 1-5 | Schematic of metabolic pathways for synthesis of pentanol from glucose or glycerol in engineered *E. coli* and schematic structure of my thesis. **26**

Figure 2-1 | The Acetone-Butanol-Ethanol fermentation pathway of *C. acetobutylicum.* **31**

Figure 2-2 | A comparison of the maximum butanol titers for all strains constructed in this study, including those which utilize polycistronic gene expression (A) or individual gene expression (B). **41**

Figure 2-3 | Engineering the central metabolic pathway of *E. coli* to increase glycolytic flux and promote NADH regeneration in support of butanol synthesis. **43**

Figure 2-4 | Effects of co-expression of *gapA* and/or *fdh1* on butanol production by strains EB4.0 (control, solid squares), EB4.G (*gapA*$^+$, open circles), EB4.F (*fdh1*$^+$, solid circles), and EB4.GF (*gapA*$^+$ *fdh1*$^+$, half-filled circles) as a function of time. **44**

Figure 2-5 | Metabolite byproduct formation by strains EB4.0 (black), EB4.G (dark gray), EB4.F (light gray), and EB4.GF (white). **45**

Figure 2-6 | Effect of butanol addition on growing cultures of *E. coli* BL21 (DE3), *P. putida* S12, and *B. subtilis* KS438 as determined by viable cell concentration and optical density. **49**

Figure 3-1 | Schematic representation of (*S*)-3HB or (*R*)-3HB synthesis from glucose in engineered *E. coli*. **59**

Figure 3-2 | Extracellular production of chiral 3HB by *E. coli* BL21Star(DE3) and MG1655(DE3) grown in shake flasks. **68**

Figure 3-3 | HPLC spectra of (A) methyl-(*R*)-3HB and methyl-(*S*)-3HB standards, (B) culture medium from *E. coli* BL21Star(DE3) expressing *bktB, phaB* and *tesB* after boiling in methanol, (C) culture medium from *E. coli* BL21Star(DE3) expressing *bktB, hbd* and *tesB* after boiling in methanol, and (D) culture medium from *E. coli* BL21Star(DE3) after boiling in methanol as a control. **69**

Figure 3-4 | Effects of media composition on the production of chiral 3HB. **72**

Figure 4-1 | Schematic representation of chiral 3HV production via the threonine biosynthesis pathway in metabolically engineered *E. coli.* **81**

Figure 4-2 | 3HV biosynthesis from glucose and propionate. **90**

Figure 4-3 | 3HV biosynthesis from glucose and 2-ketobutyrate. **91**

Figure 4-4 | 3HV biosynthesis from glucose and threonine. **92**

Figure 4-5 | 3HV biosynthesis solely from glucose. **93**

Figure 4-6 | 3HV biosynthesis solely from glycerol. **95**

Figure 4-7 | Determination of the stereochemistry of 3HV. **96**

Figure 5-1 | Schematic of *Clostridial* butanol biosynthetic pathway (left panel), poly(3HB-co-3HV) biosynthetic pathway (in blue), and proposed pentanol biosynthetic pathway (right panel). **103**

Figure 5-2 | Schematic of metabolic pathway and plasmids constructed for direct micriobial production of pentanol from glucose or glycerol. **110**

Figure 5-3 | Schematic of trans-2-pentenoate biosynthetic pathway (Top) and titers of products synthesized by recombinant *E. coli* grown under various conditions (Bottom). **111**

Figure 5-4 | Schematic diagram of pentanol synthesis from valerate and titers of substrates consumed and products synthesized by recombinant *E. coli*. **113**

Figure 5-5 | Schematic diagram of pentanol synthesis from trans-2-pentenoate and titers of products resulting from the feeding of trans-2-pentenoate. **115**

Figure 5-6 | Comparson of the *Clostridial* butanol pathway and the newly constructed pentanol pathway. **117**

Figure 5-7 | Butanol synthesis from glucose via newly constructed pentanol pathways. **118**

Figure 5-8 | Pentanol synthesis from glucose and propionate. **119**

Figure 5-9 | Pentanol synthesis solely from glucose or glycerol. **120**

Figure 5-10 | Schematic representation of correlations between dissolved oxygen and various variables (cofactor ratios, ATP, and observed product ratios). **121**

Figure 6-1 | Schematic representation of the 3-hydroxyalkanoic acid pathway. **127**

Figure 6-2 | Variation of equilibrium constant K with pH post acid treatment of DHBA standards in LB. **133**

Figure 6-3 | Biosynthesis of 3-hydroxyalkanoic acids through pathways with different pathway genes with feeding of various precursor substrates. **135**

Figure 6-4 | Time course data in residual propionate and produced 3HV. **136**

Figure 6-5 | Metabolite profile of the various recombinant *E. coli* cultures supplemented with various precursor substrates. **136**

Figure 6-6 | 4M3HV biosynthesis from glucose and isobutyrate. **138**

Figure 6-7 | DHBA and 3HBL titers before and after acid treatment. **140**

Figure 6-8 | Endogenous supply of pathway substrates from *E. coli* internal metabolism instead of exogenous supplementation of precursor acids. **143**

Figure A-1 | Pathways of butyrate and butanol biosynthesis from acetyl-CoA (AcCoA) in *Clostridium acetobutylicum*. **162**

Figure A-2 | Stoichiometrically feasible region for the anaerobic biosynthesis of (a) succinate and *E. coli* cell biomass from glucose and carbon dioxide; (b) butyric acid and *E. coli* cell biomass from glucose as the sole carbon source. **169**

Figure A-3 | The change from adding IPTG inducer in measured $\Delta G'$ values for component reactions of the clostridial butyrate or butanol biosynthesis pathway. **175**

Figure A-4 | Unexpected activity of the clostridial *ptb-buk* operons in recombinant *E. coli*. **177**

Figure B-1 | Pentanol biosynthetic pathway with cofactor and energy requirement shown in green. **181**

LIST OF TABLES

Table 1-1 | Comparison of physical-chemical properties of various biofuels and gasoline. **18**

Table 2-1 | Plasmids used or constructed in this study. **37**

Table 2-2 | Strains of *E. coli*, *P. putida*, and *B. subtilis* engineered for this study. **38**

Table 2-3 | Comparing butanol production (mg/L) by engineered strains of *P. putida* S12 (PS) and *B. subtilis* KS438 (BK) in different media, and under different growth conditions. **46**

Table 3-1 | *E. coli* strains, plasmids and oligonucleotides used. **62**

Table 3-2 | Extracellular production of chiral 3HB by *E. coli* BL21Star(DE3) grown in shake flasks. **66**

Table 3-3 | Enzyme specific activities (U mg^{-1}) of crude extracts of *E. coli* BL21Star(DE3) and MG1655(DE3). **70**

Table 3-4 | Levels and ratios of NAD^+, NADH, $NADP^+$, and NADPH cofactors in engineered MG1655(DE3) strains. **71**

Table 4-1 | *E. coli* strains, plasmids and oligonucleotides used. **86**

Table 5-1 | *E. coli* strains and plasmids used in this work. **106**

Table 6-1 | List of DNA oligonucleotide primers used in the cloning of genes for the 3-hydroxyalkanoic acid pathway. **129**

Table 6-2 | *E. coli* strains and plasmids used in the 3-hydroxyalkanoic acid pathway. **130**

Table A-1 | Strains and plasmids used in this study. **171**

Table A-2 | AcCoA pool sizes in induced cultures of strain set I, expressing clostridial butyrate biosynthesis genes from low and medium copy plasmids using P_{LTetO1}-derived promoters. **172**

Table A-3 | Intracellular pool sizes in pmol/(A600·mL) of free coenzyme A, acyl CoAs, and adenosine phosphates in *E. coli* strains expressing clostridial butanol biosynthesis genes. **174**

LIST OF ABBREVIATIONS

Abbreviation	Full Name
3HB	3-Hydroxybutyrate
3HV	3-Hydroxyvalerate
3HBL	3-Hydroxybutyrolactone
3HH	3-Hydroxyhexanoate
4M3HV	4-Methyl-3-hydroxyvalerate
ADP	Adenosine Diphosphate
ATP	Adenosine Triphosphate
B. subtilis	*Bacillus subtilis*
CoA	Coenzyme A
C. boidinii	*Candida boidinii*
C. acetobutylicum	*Clostridium acetobutylicum*
DHBA	3,4-Dihydroxybutyrate
E. coli	*Escherichia coli*
HPLC	High Pressure Liquid Chromatography
LB	Luria-Bertani (Medium)
LC/MS	Liquid Chromatography / Mass Spectrometry
MCS	Multi-Cloning Site
M. elsdenii	*Megasphaera elsdenii*
NAD^+	Nicotinamide Adenine Dinucleotide
$NADP^+$	Nicotinamide Adenine Dinucleotide Phosphate
PHA	Polyhydroxyalkanoate
PHB	Poly-3-hydroxybutyric acid
P. putida	*Pseudomonas putida*
P. aeruginosa	*Pseudomonas aeruginosa*
RBS	Ribosome Binding Site
R. eutropha	*Ralstonia eutropha*
S. cerevisiae	*Saccharomyces cerevisiae*
TB	Terrific broth (Medium)

CHAPTER 1

Introduction

Abstract

This chapter first describes background information on the field of biofuel research and the motivation for my thesis project on construction of biosynthetic pathways in *E. coli* for production of petanol. The metabolic pathway design and construction for pentanol biosynthesis will next be provided. Finally, this chapter concludes with the thesis organization.

1.1 Background on Historical Perspective of Biofuels

One of the main problems the world is facing today is the energy crisis. With the development of industry, the world has consumed a huge amount of energy. The supplies of energy are running short now while energy is of great importance to us. It is obvious that oil is becoming more expensive and less available. To solve the energy crisis, much work has been studied on alternative energies to replace traditional oil and gas, including fuel cell technology, hydrogen fuel, solar energy, geothermal energy, tidal energy, wind energy, fusion power and biofuels. Of those energy alternatives, biomass-derived liquid fuels have received ever-increasing attention over the past two decades, leading to significant interest in several candidate molecules, such as ethanol, capable of complementing petroleum-derived fuel resources. This thesis is about construction of novel biocatalysts that can transform fermentable sugars into pentanol, one of the advanced liquid transportation fuels with properties more similar to conventional gasoline than ethanol.

1.1.1 Renewable biomass

Biomass comprises all the living matter present on earth, deriving from growing plants including algae, trees and crops. The biomass resources are the organic matters in which the solar energy is stored in chemical bonds. Specifically, the process of photosynthesis uses energy from the sun to convert carbon dioxide into carbohydrates. Cellulosic biomass, sometimes referred to as lignocellulosic biomass, is an abundant renewable resource (*Rubin, 2008, Zhang, 2008*). The three main components of lignocellulose are cellulose, hemicellulose and lignin with typical composition of 75-90 wt% of sugar polymers and 10-25 wt% of lignin. Cellulose, the main structural component of plant cell walls, is a long chain of glucose units. Hemicellulose, the second most abundant constituent of lignocellulosic biomass, is not a chemically well defined compound but rather a family of polysaccharides, composed of 5- and 6-carbon monosaccharide units. Lastly lignin, a three-dimensional polymer, can be regarded as the cellular glue that provides the cell wall with stiffness and the plant tissue with

compressive strength.

The use of biomass has advantages in its renewability, versatility, and domestic availability while it also has its limitations. For example, the energy density of biomass is low compared to that of coal, liquid petroleum, or petroleum-derived fuels (*Saxena et al., 2009*). In addition, most biomass has a high amount of water content. Thus, without substantial drying, the energy content of a certain biomass per unit mass would be even less. As a result, in order to conquer those inherent characteristics and limitations of biomass for the application on the liquid fuels, it is crucial and necessary to develop efficient methods to transform and upgrade biomass to useful forms of liquid fuels.

1.1.2 Conversion of biomass to liquid fuels

Conversion of biomass may release the energy directly, in the form of heat or electricity, or may convert it to another form, such as liquid fuels. In general, there are two strategies for production of liquid fuels from biomass, including the thermochemical platform and biochemical platform (**Fig. 1-1**) (*Foust et al., 2009*).

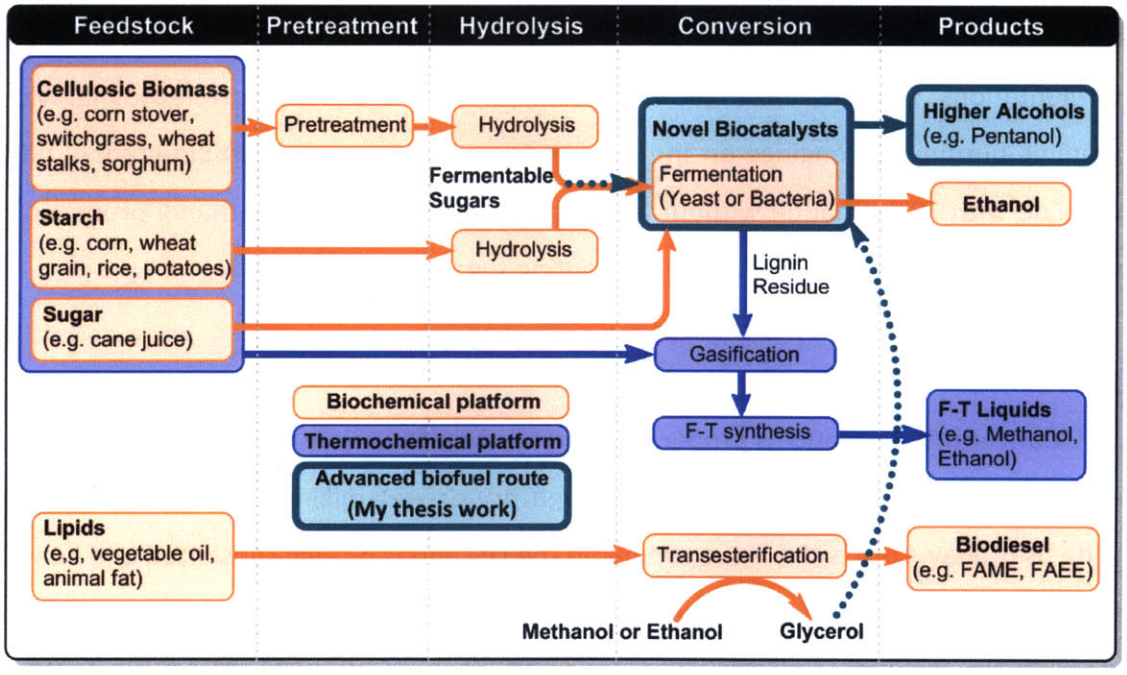

Figure 1-1| Schematic of biorefinery for biofuel production.

The thermochemical platform (also called syngas platform) aims at converting biomass to intermediates such as pyrolysis oil and syngas. These intermediates can be used directly as raw fuels or further be upgraded to produce liquid fuels by a classical Fischer-Tropsch process (**Fig. 1-1**).The biochemical platform (also called sugar platform) is based on the breakdown of biomass into raw component sugars using chemical and biological pretreatment, followed by enzymatic depolymerization by cellulases. The resulting fermentable sugars can then be used to make useful liquid fuels by microorganisms. Therefore, construction of novel biocatalysts enabling liquid fuel synthesis from simple sugars is the main scope of my thesis work.

1.1.3 Ethanol as a transportation fuel

Liquid fuels are molecules that can be harnessed to create mechanical energy, usually producing kinetic energy, via energy-generating or combustion process. Most liquid fuels are derived from fossil fuel through crude oil refineries. In general, gasoline is the most widely used liquid fuel while diesel is a mixture of long chain aliphatic hydrocarbons. When petroleum is not readily available, biotechnology can offer possibility of producing useful liquid fuels from biomass through microbial fermentations. One clear example is ethanol, which is often added to gasoline. Most gasoline-burning car engines on the road today will operate on E10 bio-ethanol (90% gasoline with 10% ethanol) without modification, and most of the ethanol produced in the world today is "bio-ethanol," by fermenting sugar with yeast.

1.1.4 Conventional ethanol

Conventional ethanol is produced using food crops such as corn, wheat, sugarcane and soybeans, and processed either through dry or wet milling. Of the feedstocks in wide use today, corn is the most popular in the US, and is heavily subsidized and heavily fertilized and sprayed with pesticides; the latter two are very energy-intensive where many of the fertilizers are petroleum-based (*Bischoff et al., 2009, Secchi et al., 2009, Wakeley et al., 2009*). Further, because corn-derived ethanol requires a lot of the crop,

the growth of it as a fuel source has wide-ranging agricultural implications, from the price of corn to the substantial land use to grow the crop (*Regalbuto, 2009, Rubin, 2008*). The corn-derived ethanol is usually referred to as a first generation biofuel.

1.1.5 Cellulosic ethanol

Ethanol made from cellulose, as opposed to ethanol made from corn, is a second generation biofuel. The difference from the first generation biofuels is that second generation biofuels are made from biomass sources like dedicated energy crops and wood products, which lead to much lower environmental impact. Cellulosic ethanol has the potential to make ethanol a much more energy-efficient fuel. Because every plant contains cellulose, a huge variety of feedstocks could be used (*Kwok, 2009, Lau & Dale, 2009, Waltz, 2009*). The ideal cellulosic ethanol technology enables conversion of most sugars found in cellulosic biomass, including both five-carbon and six-carbon sugars, into ethanol. This efficiency advantage, combined with the low input cost of cellulosic biomass, results in superior economics in the production of ethanol. However, there are several technical and economic challenges associated with the large-scale production of ethanol from cellulosic biomass, including collection and transport of the biomass raw material, pretreatment, dilute acid hydrolysis, and enzymatic conversion of pretreated cellulosic material to sugars (*Kwok, 2009, Lau & Dale, 2009, Waltz, 2009*), making cellulosic ethanol somewhat less economical to produce than conventional ethanol. As a result, solving the above challenges has grown into an active research field over the past few years.

1.1.6 Advanced biofuels

Although ethanol represents an initial success as a biofuel due to its high production yield and efficiency, it does not compare favorably to gasoline. As shown in **Table 1-1**, it has a lower energy density (approximately 34% less energy per unit volume than gasoline, resulting in a 34% reduction in miles per gallon), a low vapor pressure, and a high hygroscopicity, possibly leading to corrosion in pipelines and engines.

Furthermore, ethanol raises the vapor pressure of the mixture when blended to gasoline, although this is partially offset by an increase in octane number.

Table 1-1 | Comparison of physical-chemical properties of various biofuels and gasoline

Fuels	Air-Fuel Ratio	Vapor Pressure (psi)	Energy density (MJ/kg)	Fits current infrastructure?
Gasoline	14.6	0.1-30	42.7	Yes
Ethanol	9.0	1.1	29.7	No
Butanol	11.2	0.077	36.1	Yes
Isobutanol	11.2	0.17	36.1	Yes
Pentanol	12.5	0.039	37.7	Yes

Perry's handbook and *http://www2.dupont.com/Biofuels/en_US/*

On the contrary, advanced biofuels, including butanol, isobutanol and pentanol, have better physical-chemical properties, such as higher energy densities, low hygroscopicities as well as lower vapor pressure for gasoline blends. While the octane number of n-butanol is slightly less than gasoline, branched-chain isomers such as isobutanol have higher octane numbers, allowing for more flexibility in fuel design. Furthermore, as carbon length increases, the amount of air needed to combust unit amount of fuel also increases (**Table 1-1**). Because standard gasoline engines can only adjust the air-fuel ratio to accommodate variations in the fuel within certain limits, the closer to 14.6 the air-fuel ratio of the fuels, the better the engine's efficiency. Therefore, long-chain alcohols are preferable fuel alternatives. Of those biofuels, butanol represents an interesting alternative and has gained a renewed interest in a classical process of acetone-butanol-ethanol (ABE) production as described below (*Jones & Woods, 1986*).

1.1.7 Butanol as a liquid transportation fuel

Currently, butanol's primary use is as an industrial solvent. With a lower oxygen content than ethanol, higher volumetric concentrations of butanol could be blended into gasoline while still adhering to oxygen limits. On top of that, butanol has a nearly 50% higher energy density than ethanol (**Table 1-1**), representing about 90% of the energy density of gasoline, and has physical, chemical, and thermodynamic properties that are more similar to conventional gasoline, thus making it more compatible with

current automotive designs, better integration into the infrastructure, and a more attractive prospect as a substitute for gasoline. In fact, it has been claimed that today's vehicles can be fueled with high concentrations of biobutanol (up to 100%) with minor or no vehicle modifications (*Keasling & Chou, 2008*).

Butanol, a 4-carbon alcohol, can be produced from biomass feedstocks and is traditionally produced by fermentation of biomass by the ABE process by *Clostridium acetobutylicum*, also known as the Weizmann organism. The historical ABE fermentation technology produces a variety of fermentation products with a 6:3:1 ratio of butanol, acetone and ethanol (*Gheshlaghi et al., 2009, Jarboe et al., Ni & Sun, 2009, Zheng et al., 2009*). *C. acetobutylicum* was the first isolated and identified between 1912 and 1914, and then used to develop an industrial starch-based ABE fermentation process, aiming to produce acetone for gunpowder production, by Chaim Weizmann during World War I. During the 1920s and 1930s, increased demand for butanol led to the establishment of large fermentation factories. However, due to the establishment of more cost-effective petrochemical processes during the 1950s, the ABE process was almost abandoned. The rise in oil prices during the 1970s stimulated renewed interest in the ABE process as well as in the genetic manipulation of *C. acetobutylicum* and related species to improve the yield and purity of solvents from a broader range of fermentation substrates.

1.1.8 Metabolic engineering of novel biocatalysts

Another big innovation in biofuel field has been the growing utilization of genetically engineered microorganisms to convert renewable biomass or its derived simple sugars into hydrocarbon-based fuels. Naturally, microorganisms are evolved for survival in competitive natural environments, but not for production of chemicals desired by humans. To achieve so, we can utilize several metabolic engineering tools, for example, to amplify or short-circuit their internal machinery as well as insert some genes form other organisms into the target producers (*Alper & Stephanopoulos, 2009, Aristidou & Penttil, 2000, Atsumi et al., 2008, Connor & Liao, 2008, Steen et al., 2008*), making them able to convert precursor molecules directly into desired liquid fuels. The

metabolic engineering of microorganisms can be achieved using a variety of metabolic redesign tools (**Fig. 1-2**), including protein-level recruitment from all kinds of organisms, reengineering of enzymes, and pathway-level efforts to design and assemble these enzymes (*Martin et al., 2009*).

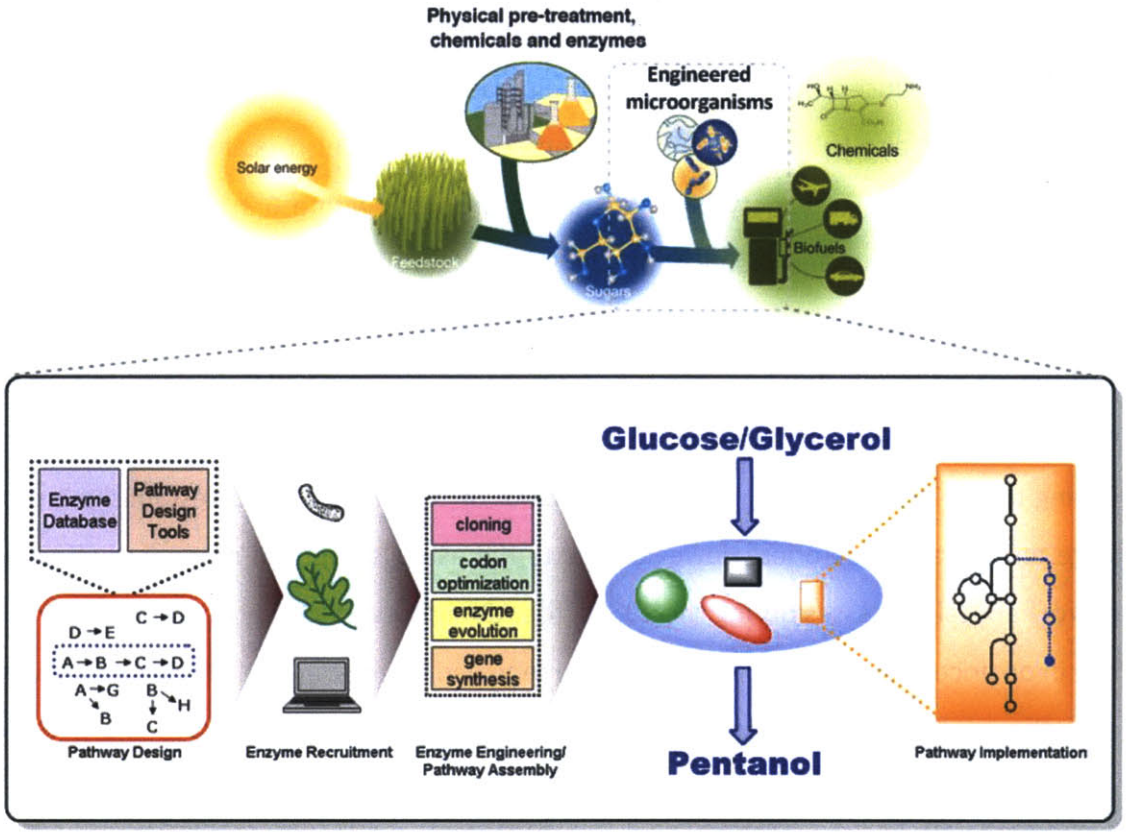

Figure 1-2 | Scheme for metabolic engineering of novel biocatalysts (modified from (*Martin et al., 2009*)).

In recent years, metabolic engineering of microorganisms, such as *Escherichia coli* and yeast *Saccharomyces cerevisiae*, has shown significant progress for production of advanced biomass-derived liquid fuels, turning them into biofuel factories. For example, microbial production of fatty acid derived fuels, as known as biodiesel, from hemicelluloses or glucose has recently been achieved by metabolically engineered *E. coli (Steen et al., 2010).* The beauty of it was that the *E. coli* took in the sugar, transformed it directly into diesel, and the diesel was secreted outside the cell. In fact, several companies, including Codexis, Amyris Biotechnologies, LS9 and Craig Venter's Synthetic Genomics, are making progress and have had some good initial results in engineering

novel biocatalysts capable of converting biomass or its derived fermentable sugars into liquid biofuels (*Clomburg & Gonzalez, 2010, Li et al., 2010*).

1.2 Motivation and Objectives

As described earlier, ethanol has several undesirable properties as a fuel, including its water miscibility, which creates problems in transporting the fuel by pipelines, and low energy density (*Keasling & Chou, 2008*). Thus, there is much interest in developing biofuels that are more hydrophobic and spontaneously partition out of the aqueous phase as well as having energy content closer to gasoline. Pentanol, with a higher energy density, enhanced physical properties that would allow better integration with current infrastructure, represents an excellent candidate, and has the potential to be a replacement for gasoline (**Table 1-1**). Existing methods for production of pentanol include hydroformylation of butenes, hydrolysis of chloropentanes, and hydration of pentenes, relying on the use of fossil fuels, such as natural gas and oil, as precursor molecules. However, negative environmental consequences of fossil fuels and concerns about petroleum supplies have spurred research on synthesis of biofuels from renewable resources via bio-processing.

Currently, however, there are no known microorganisms that are capable of producing pentanol from renewable feedstocks. Butanol, on the other hand, can be produced biologically by the ABE fermentation of *C. acetobutylicum*. We have identified a potential synthetic pathway for the biosynthesis of pentanol which combines elements of the natural butanol biosynthesis pathway with pathways of the poly(3HB-co-3HV) biosynthesis of *Ralstonia eutropha* and threonine biosynthesis of *E. coli* (**Fig. 1-3**) (*Slater et al., 1998*). Meanwhile, due to a relatively unknown genetic system and complex physiology of *C. acetobutylicum*, the pentanol biosynthesis will be investigated in a user-friendly host, *E. coli.* Overall, my thesis focuses on the construction of synthetic metabolic pathways in *E. coli* for pentanol biosynthesis, giving promise to alleviating the energy shortage through the synthesis of biofuels with enhanced properties.

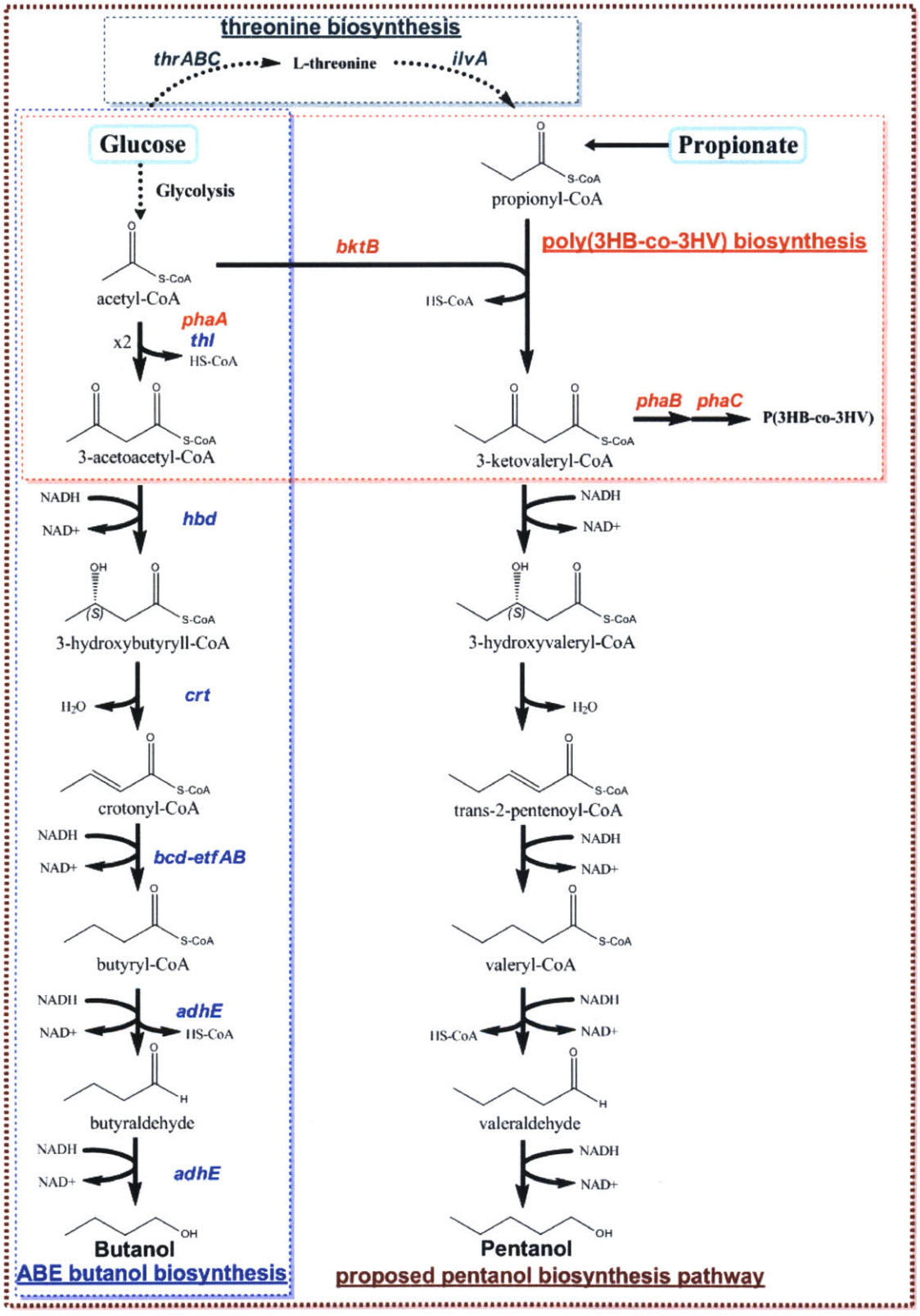

Figure 1-3 | Schematic of proposed pentanol biosynthetic pathway.

1.3 Metabolic Pathway Design

The aim of my thesis is to explore microbial biosynthetic routes for production of pentanol from renewable feedstocks (**Fig. 1-4**), providing an attractive way to alleviate the energy shortage while reducing the use of fossil fuels.

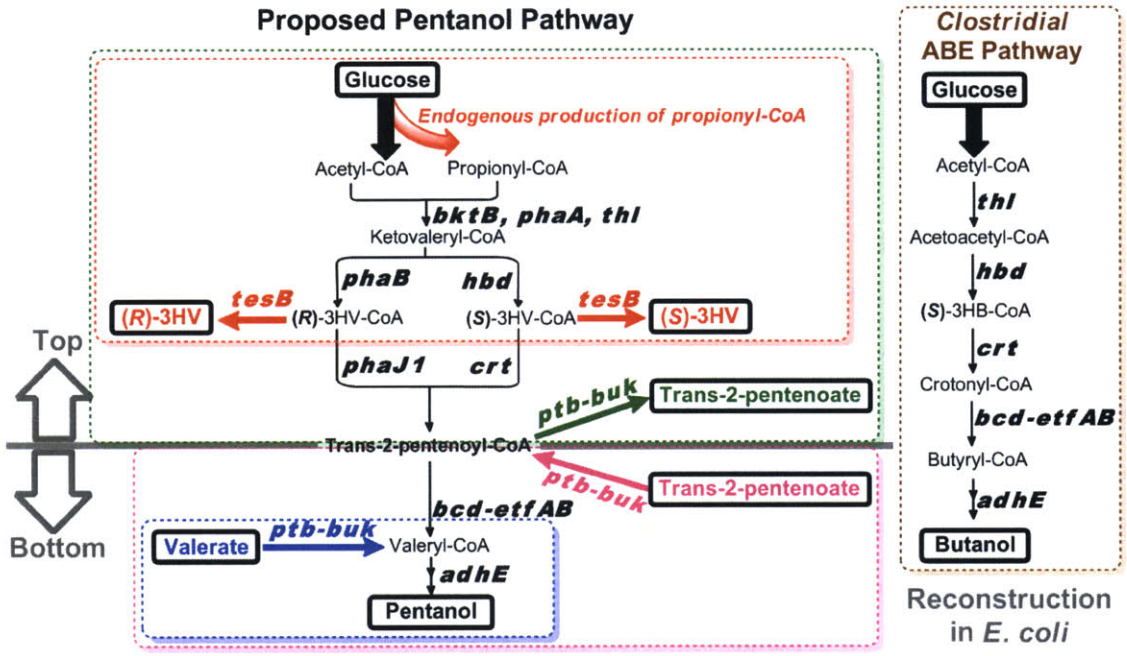

Figure 1-4 | Schematic diagram of research plans for pentanol biosynthesis.

The pentanol biosynthesis begins with condensation of one acetyl-CoA and one propionyl-CoA to form 3-ketovaleryl-CoA. This reaction is catalyzed by an acetoacetyl-CoA thiolase from *R. eutropha* H16, which is encoded by *bktB, phaA,* or *thl*. The genes encoding for enzyme activities for the step-wise conversion of 3-ketovaleryl-CoA to valeryl-CoA are clustered together in a polycistronic operon, consisting of genes *crt*, *bcd*, *etfAB*, and *hbd* from *C. acetobutylicum*, encoding for crotonase, butyryl-CoA dehydrogenase, electron transfer proteins, and 3-hydroxybutyryl-CoA dehydrogenase, respectively. A bi-functional aldehyde/alcohol dehydrogenase, encoded by *adhE* from *C. acetobutylicum*, catalyzes the final steps of pentanol synthesis from valeryl-CoA. Alternatively, both *hbd* and *crt* genes can be replaced with *phaB* from *R. eutropha* H16 and *phaJ1* from *Pseudomonas aeruginosa*, respectively, to convert ketovaleryl-CoA to trans-2-pentenoyl-CoA.

Acetyl-CoA is an obligate central intermediate occurring in any organism and under any physiological condition; however, this is not the case for propionyl-CoA. Given that synthesis of 3-ketovaleryl-CoA requires propionyl-CoA biosynthesis, a pathway allowing for endogenous propionyl-CoA synthesis from glucose or glycerol is also introduced. Specifically, up-regulation of *L*-threonine biosynthesis by over-expressing the *E. coli thrABC* operon along with over-expression of *ilvA* (encoding threonine deaminase) can enhance synthesis of 2-ketobutyrate, a common keto-acid intermediate for isoleucine biosynthesis, which can further be converted to propionyl-CoA by the endogenous pyruvate dehydrogenase complex (PDHc) or pyruvate-formate lyase (PflB).

To examine the synthetic pentanol pathway, a bypass strategy has been implemented to evaluate capability of the pathway enzymes (**Fig. 1-4**). Particularly, certain coenzyme A (CoA) derivatives synthesized via reduction reactions along the pentanol pathway are targeted to be converted to their respective free acid forms, allowing for their extracellular detection; alternatively, certain carboxylic acids are fed to serve as precursors of targeted CoA intermediates, both which can be achieved through the use of CoA-addition/removal tools, including broad-substrate-range enzymes of Ptb-Buk (from *C. acetobutylicum*) and TesB (from *E. coli*). The outline below describes the overall strategy for construction of the pentanol biosynthetic pathways.

1. **Reconstruction of the *Clostridial* Butanol Pathway in *E. coli*:**
   - ✓ Due to poor characterization and a lack of compatible genetic tools in the natural biocatalyst *C. acetobutylicum*, we have explored the prospects of engineering butanol biosynthesis in *E. coli*, a well-characterized and tractable microorganism that has repeatedly been employed as a robust industrial workhorse for the synthesis of fuels and chemicals. A successful reconstruction of the *Clostridial* butanol pathway in *E. coli* would provide an avenue towards pentanol biosynthesis.
2. **Top Pentanol Pathway:**
   - ✓ Modification of the *Clostridial* butanol biosynthetic pathway requires the ability of the upstream thiolase enzyme to condense propionyl-CoA with acetyl-CoA.

The thiolase reaction is the first step of the pathway and establishes the core carbon skeleton with respect to the number of carbons. A library of thiolase enzymes were examined by the production of 3-hydroxybutyrate (3HB) and 3-hydroxyvalerate (3HV) where 3HB-CoA and 3HV-CoA synthesized via reduction reactions along the pentanol pathway were converted to 3HB and 3HV, respectively, catalyzed by TesB.

- ✓ Furthermore, a pathway allowing for endogenous propionyl-CoA synthesis from glucose or glycerol, through the threonine metabolic pathway intermediate 2-ketobutyrate, was introduced to circumvent the need of feeding propionate.
- ✓ In addition, to test one additional enzyme that converts 3HV-CoA to trans-2-pentenoyl-CoA, the pentanol pathway was shortcut towards production of trans-2-pentenoate with over-expression of the *ptb-buk* operon. Here, two distinct metabolic routes towards pentanol synthesis, including one through (*S*)-3HV-CoA with an *hbd-crt* gene pair and the other through (*R*)-3HV-CoA with a *phaB-phaJ1* gene pair, were examined.

3. Bottom Pentanol Pathway:

- ✓ To evaluate the capacity of butyryl-CoA dehydrogenase (encoded by *bcd-etfAB*) and alcohol/aldehyde dehydrogenase (encoded by *adhE*) of *C. acetobutylicum* on catalyzing reactions of non-natural five-carbon analogues, valerate was initially supplemented to the culture in addition to glucose to test the capability of AdhE enzyme on catalyzing valeryl-CoA to pentanol.
- ✓ One additional enzymatic step upstream to the AdhE reaction was then examined through feeding of trans-2-pentenoate. It was first converted to trans-2-pentenoyl-CoA catalyzed by Ptb-Buk, followed by sequential conversion to pentanol, catalyzed by Bcd and AdhE.

1.4 Thesis Organization

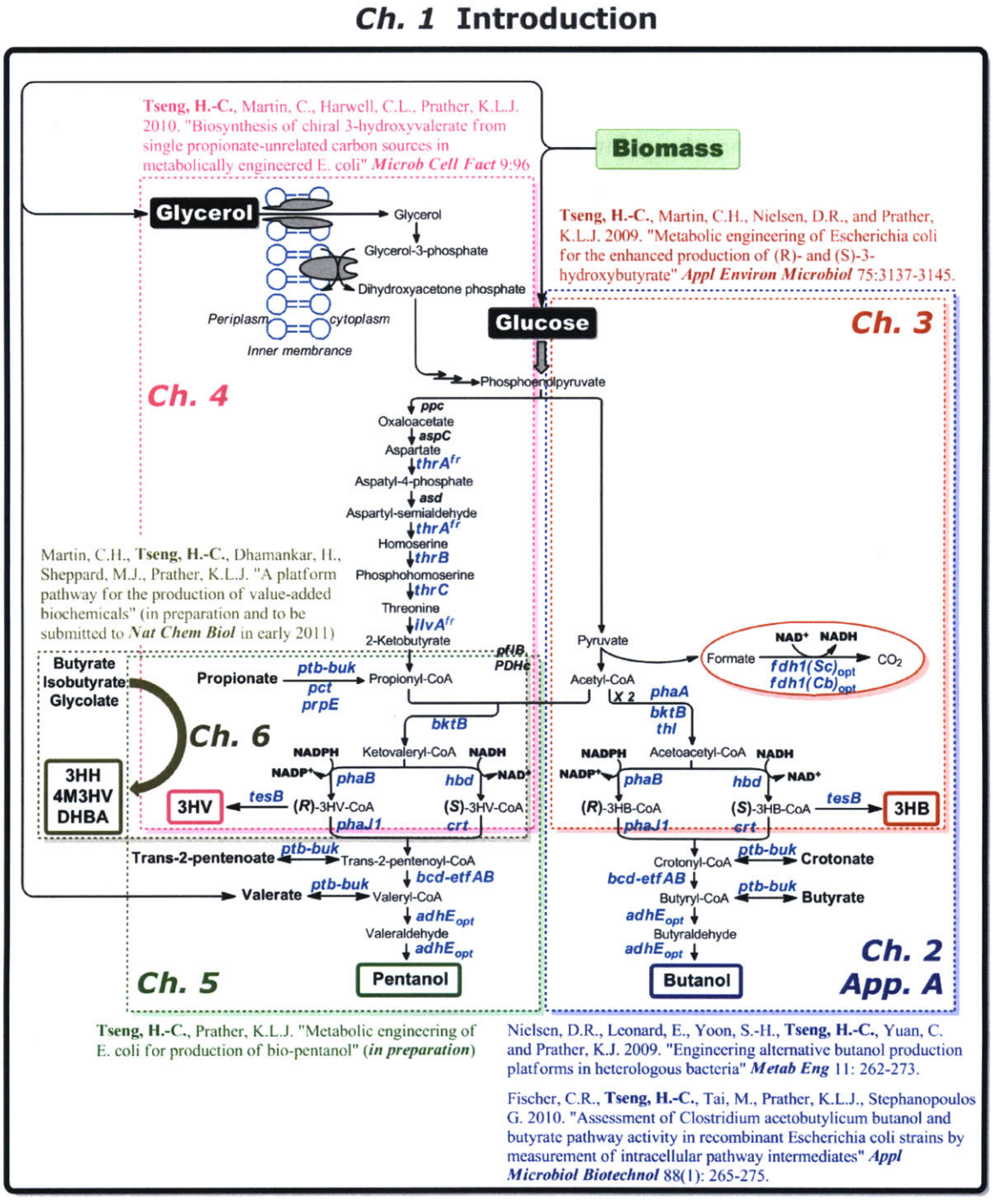

Figure 1-5 | Schematic of metabolic pathways for synthesis of pentanol from glucose or glycerol in engineered *E. coli* and schematic structure of my thesis. Genes in light blue and italic are over-expressed. Chapters in the thesis are shown in the categorization scheme with corresponding manuscripts submitted, or to be submitted, for publication.

This thesis is organized into seven chapters and each chapter is systemically organized to contain the many spectrums involved in this project (**Fig. 1-5**). Chapter 1 provides background into historical perspective of biofuels as well as the design of metabolic pathways and assembly of such pathway in cell factories, enabling production of pentanol through microbial fermentations. Chapter 2 describes prospects of manipulating *E. coli* cells that do not naturally produce butanol to produce this fuel through reconstruction of the *Clostridial* ABE butanol pathway by metabolic engineering. A successful reconstruction of butanol pathway in *E. coli* will provide a feasible platform for achieving our goal on pentanol biosynthesis. Also, to better understand the *Clostridial* butanol pathway, Chapter 3 describes a strategy in which the ABE butanol biosynthetic pathway was bypassed towards 3HB synthesis as a way to access the top butanol pathway. Besides, we recruited enzymes from polyhydroxyalkanoates (PHA) biosynthesis in place of the first two enzymes in the butanol pathway to support 3HB production, which will also be discussed in Chapter 3. In addition, a complementary technique to the bypass strategy was developed to measure acyl-CoA and related pool sizes in a number of *E. coli* strains expressing *Clostridial* genes for butyrate and butanol biosynthesis, which will be described in Appendix A. As mentioned earlier, pentanol synthesis requires the ability of the upstream thiolase enzyme to condense propionyl-CoA with acetyl-CoA to establish the five-carbon skeleton. Therefore, in Chapter 4, selection of such thiolase enzyme will be discussed in the context of 3HV biosynthesis. Furthermore, construction of a pathway allowing for endogenous propionyl-CoA supply from glucose or glycerol will also be described in Chapter 4. Chapter 5 illustrates a substrate feeding study used for investigation on the bottom pentanol biosynthetic pathway as a means to evaluate the capacity of downstream pathway enzymes to catalyze reactions of non-natural five-carbon analogues. Direct microbial synthesis of pentanol from glucose supplemented with propionate or solely from glucose or glycerol will also be discussed in Chapter 5. Chapter 6 focuses on the construction of a novel pathway, as an extension of the 3HV biosynthetic pathway described in Chapter 4, for production of value-added chiral 3-hydroxyalkanoic acids,

such as 3,4-dihydroxybutyrate and its related lactone, 3-hydroxy-γ-butyrolactone. Finally, Chapter 7 summarizes all of the pathways, products, and titers presented in Chapters 2-6, and concludes by providing discussion and recommendations for future work.

CHAPTER 2

Reconstruction of *Clostridial* Butanol Pathway

Abstract

This chapter describes engineering of alternative biocatalysts for butanol biosynthesis. The butanol synthetic pathway of *Clostridium acetobutylicum* was first re-constructed in *Escherichia coli* to establish a baseline for comparison to other hosts. Whereas polycistronic expression of the pathway genes resulted in the production of 34 mg/L butanol, individual expression of pathway genes elevated titers to 200 mg/L. Improved titers were achieved by co-expression of *Saccharomyces cerevisiae* formate dehydrogenase while overexpression of *E. coli* glyceraldehyde 3-phosphate dehydrogenase to elevate glycolytic flux improved titers to 580 mg/L. *Pseudomonas putida* and *Bacillus subtilis* were also explored as alternative production hosts. Polycistronic expression of butanol biosynthetic genes yielded butanol titers of 120 mg/L and 24 mg/L from *P. putida* and *B. subtilis*, respectively. Production in the obligate aerobe *P. putida* was dependent upon expression of *bcd-etfAB*. These results demonstrate the potential of engineering butanol biosynthesis in a variety of heterologous microorganisms, including those cultivated aerobically. Most importantly, the successful reconstruction of the *Clostridial* butanol pathway in *E. coli* provides a feasible platform for pentanol biosynthesis.

This chapter was published as:

Nielsen, D.R., Leonard, E., Yoon, S.-H., Tseng, H.-C., Yuan, C. and Prather, K.J. 2009. "Engineering alternative butanol production platforms in heterologous bacteria" ***Metab Eng*** 11: 262–273.

2.1 Introduction

With applications as a feedstock in plastic manufacturing and as an industrial solvent, the current butanol market in the United States alone is about 2.9 billion lbs per annum. However, chemical synthesis of butanol relies upon propylene feedstock, a petroleum-based substrate (*Ezeji et al., 2007*). Alternatively, butanol (biobutanol) can be naturally synthesized by solventogenic bacteria of the genus *Clostridium* through fermentation of renewable substrates, such as glucose. The once prosperous Acetone-Butanol-Ethanol (ABE) fermentation has garnered resurgent interest as a result of unprecedented economic and political concerns associated with increasing demand of nonrenewable energy resources. In this regard, biobutanol has also emerged as a promising renewable liquid transportation fuel. With thermodynamic and physical properties that are highly akin to those of gasoline, biobutanol can be used either as a blending agent or direct fuel replacement in conventional vehicles (*Antoni et al., 2007*). More specifically, butanol possesses a nearly 50% higher energy density than ethanol, representing about 95% of the energy density of gasoline (*Cascone, 2008*). Since it is nearly 12-times more hydrophobic than ethanol, butanol can also be distributed and utilized within existing transportation fuel infrastructures without corrosive consequences.

The suitability of Clostridial biocatalysts for use in industrial fermentations suffers from several phenotypic disadvantages, including spore formation that can result in the loss of butanol forming abilities. Additionally, stresses caused by butanol toxicity have been attributed to the loss of pSOL1, a mega-plasmid encoding several essential solvent-forming genes (*Borden & Papoutsakis, 2007*). Furthermore, the metabolic shift from acidogenesis to solventogenesis in *Clostridium* presents additional complications for continuous culture (*Antoni et al., 2007*). Overall, despite efforts to improve the biobutanol production efficiency of *Clostridium* (*Harris et al., 2000, Mermelstein et al., 1994, Sillers et al., 2008, Tomas et al., 2003*), relatively poor characterization and a lack of compatible genetic tools remain as central obstacles impeding natural biocatalyst progression.

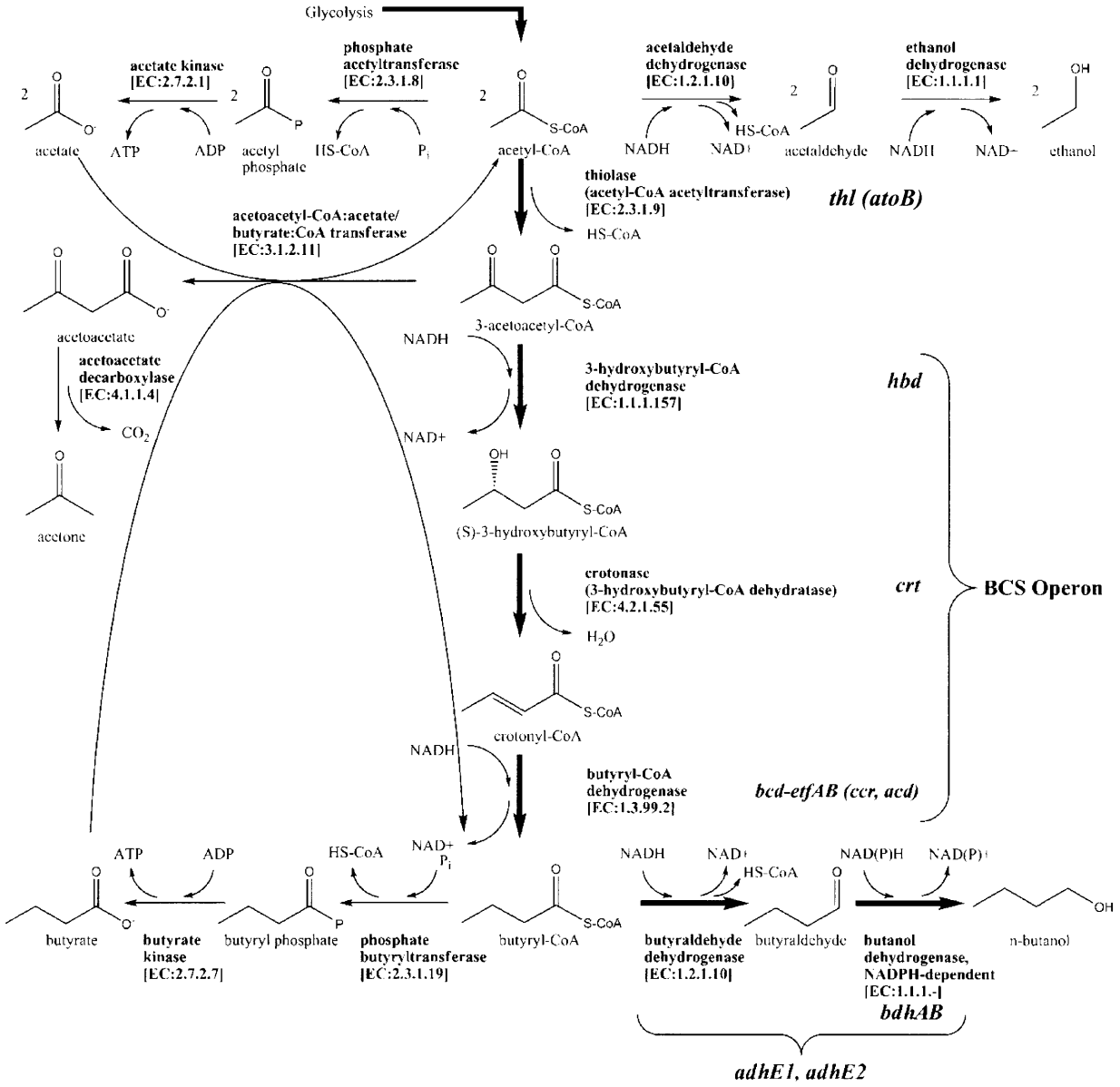

Figure 2-1 | The Acetone-Butanol-Ethanol (ABE) fermentation pathway of *C. acetobutylicum*. Enzymatic steps used to reconstruct the biobutanol pathway are shown in bold. Relevant *C. acetobutylicum* genes are also indicated, while those genes encoding enzymes of homologous function from alternative genetic sources are shown in parentheses.

In addition to phenotypic instabilities associated with Clostridial biocatalysts, the productivity of butanol fermentations is routinely limited by the effects of product cytotoxicity. Butanol has been found to accumulate primarily within the cytoplasmic membrane of *Clostridium* (*Bowles & Ellefson, 1985*) where it leads to disruption of the ordered structure of the phospholipid bilayer. This phenomenon produces an increase in

membrane fluidity (*Osborne et al., 1990*) which results in the loss of intracellular molecules (including proteins, RNA, and ATP), as well as an inability to maintain transmembrane ion gradients (*Isken & de Bont, 1998*). The resultant feed-back inhibition precludes butanol accumulation in culture media to titers above ~13 g/L for wild-type strains (*Jones & Woods, 1986*).

In *C. acetobutylicum*, butanol biosynthesis begins with the condensation of two molecules of acetyl-CoA to yield acetoacetyl-CoA. This reaction is catalyzed by a thiolase which is encoded by *thl* (**Fig. 2-1**). The genes encoding for enzyme activities for the step-wise conversion of acetoacetyl-CoA to butyryl-CoA are clustered together in the polycistronic BCS operon. This operon is comprised of the genes *crt*, *bcd*, *etfAB*, and *hbd*, encoding for crotonase, butyryl-CoA dehydrogenase, electron transfer proteins, and 3-hydroxybutyryl-CoA dehydrogenase, respectively. A bi-functional aldehyde/alcohol dehydrogenase, encoded by either *adhE1* or *adhE2*, catalyzes the final steps of butanol synthesis from butyryl-CoA (**Fig. 2-1**). Although *C. acetobutylicum adhE1* can catalyze the conversion of butyryl-CoA to butyraldehyde and then butanol with a single enzyme, it can also mediate the synthesis of ethanol from acetyl-CoA (through acetaldehyde). *C. acetobutylicum* also possesses two distinct butanol dehydrogenase isozymes, encoded by *bdhA* and *bdhB* which have been found to have a high specificity for the conversion of butyraldehyde to butanol (*Welch et al., 1989*). In that same study, it was also reported that *bdhB* provided a significantly higher catalytic turn over rate of butyraldehyde than *bdhA*. Recently, different groups have successfully re-constructed the butanol biosynthetic pathway of *C. acetobutylicum* using heterologous microorganisms, including *E. coli* (*Atsumi et al., 2008, Inui et al., 2008*) and *S. cerevisiae* (*Steen et al., 2008*). Although *S. cerevisiae* has been found to possess favorable industrial attributes, including moderate butanol tolerance (*Fischer et al., 2008, Knoshaug & Zhang, 2008*), preliminary attempts to engineer butanol biosynthesis in yeast have resulted in the production of merely 2.5 mg/L (*Steen et al., 2008*). Meanwhile, butanol titers in *E. coli* engineered to express the *Clostridium* butanol pathway have been reported as high as 552 mg/L (*Atsumi et al., 2008*). The

biosynthesis of butanol, as well as other higher alcohols of interest, from keto-acid precursors (typically used in amino acid biosynthesis) has also been explored as an alternative route towards biofuel production (*Atsumi et al., 2008*). In subsequent studies it was shown that through this non-natural pathway, butanol could be produced in excess of 800 mg/L as a co-product with n-propanol (*Shen & Liao, 2008*). Although the effects of product inhibition were likely to have remained unnoticed given the relatively low titers achieved in each of these previous studies, the butanol toxicity threshold of *E. coli* is known to be below that of *Clostridium* (*Fischer et al., 2008, Knoshaug & Zhang, 2008*). Thus, it is anticipated that modest inhibitory thresholds of these strains will ultimately limit their achievable outputs as their productivity is further engineered to that which is required of production-level strains.

Solvent tolerant phenotypes consist of evolved mechanisms by which many opportunistic microorganisms have developed the means to survive in extreme environments. Notable naturally solvent tolerant bacteria include species of *Rhodococcus*, *Bacillus*, and *Pseudomonas* (*de Bont, 1998*). For example, *P. putida* S12 derives its solvent tolerance from an increased proportion of *trans*-unsaturated fatty acids in its cytoplasmic membrane (*Heipieper & Debont, 1994*), as well as through the use of active efflux pump systems. Such mechanisms permit maintenance of cytoplasmic membrane integrity in the presence of high concentrations of organic solvents, and have allowed *P. putida* S12 to demonstrate moderate tolerance to butanol in previous studies (*de Carvalho et al., 2004*). For these same reasons, *P. putida* S12 has also previously been employed as an engineered host strain for the biosynthesis of phenol (*Wierckx et al., 2005*) and cinnamic acid (*Nijkamp et al., 2005*). Meanwhile, solvent tolerant species of *Bacillus* have also been isolated that can tolerate butanol concentrations as high as 2.5-3.7% (wt./vol.) (*Sardessai & Bhosle, 2002*), by incorporating tolerance mechanisms that can include adaptations to the cell wall composition and through the use of stress response proteins (*Kang et al., 2007*). In an effort to explore an alternative paradigm towards the engineering of robust biocatalysts, we have re-constructed the butanol biosynthesis pathway in heterologous hosts with

known natural solvent tolerance and high industrial utility (*Schmid et al., 2001*). More specifically, we have engineered functional pathway expression strategies to allow biobutanol synthesis by both *Pseudomonas putida* and *Bacillus subtilis*. To provide a baseline for comparison, our study begins by also engineering butanol biosynthesis in *E. coli*. In contrast to previous works, we apply alternative strategies for functional pathway construction and continue on to explore the effects of the overexpression of enzymes involved in increasing glycolytic flux or regenerating NADH on butanol production.

2.2 Materials and Methods

2.2.1 Microbial strains

C. acetobutylicum ATCC 824 and *P. putida* S12 were purchased from the American Type Culture Collection (ATCC, Manassas, VA). *B. subtilis* KS438, a sporulation deficient strain, was kindly provided by Dr. Alan Grossman of the Department of Biology at the Massachusetts Institute of Technology, USA. *E. coli* DH10B and XL1-Blue (Stratagene, La Jolla, CA) were used for cloning and plasmid maintenance. *E. coli* BL21Star(DE3) (Invitrogen, Carlsbad, CA) was used as the host strain to allow the expression of genes under the T7*lac* promoter.

2.2.2 Plasmid construction

Genes derived from *C. acetobutylicum* ATCC 824 (*thl*, *hbd*, *crt*, *bcd*, *etfAB*, *adhE1*, *adhE2*), *E. coli* K-12 (*atoB* and *gapA*), and *P. putida* KT2440 (*acd*) were obtained via polymerase chain reaction (PCR) using genomic DNA (gDNA) templates. All gDNA samples were prepared using the Wizard Genomic DNA Purification Kit (Promega, Madison, WI). *S. cerevisiae fdh1* chromosomal DNA (cDNA) fragment was obtained from mRNA using SuperScript One-Step RT-PCR (Invitrogen, Carlsbad, CA). RNA was isolated from *S. cerevisiae* grown overnight in YPD medium (Difco, Franklin Lakes, NJ). Custom oligonucleotides (primers) were purchased for all PCR amplifications (Sigma-Genosys, St. Louis, MO).

The natural butanol biosynthesis pathway of *C. acetobutylicum* (**Fig. 2-1**) was first re-constructed using two broad host range compatible expression vectors, pMMB206G and pRK415 ((*Keen et al., 1988*); kindly donated by Dr. Keith Poole, Department of Microbiology and Immunology, Queen's University, Canada), which possess the RSF1010 and RK2 replicons, respectively. pMMB206G contains a *taclac* (*tac-lac*UV5 in tandem) promoter and a gentamycin resistance selective marker while pRK415 contains a *lac* promoter and a tetracyclin resistance marker. pMMB206G was constructed by ligating the Klenow-filled, *Mlu*I-*Mlu*I gentamycin resistance cassette from pBSL141 (ATCC; (*Alexeyev et al., 1995*)) into the *Xmn*I site of pMMB206 (ATCC; (*Morales et al., 1991*)), thereby disrupting the original chloramphenicol resistance marker. To construct pmT, *thl* was first ligated into the *Bam*HI site of pMMB206G. pmTA1 was then generated by ligation of *adhE1* between the *Sal*I – *Pst*I sites of pmT. *bdhB* was then ligated into the *Sal*I site of pmTA1 to yield pmTBA1. prBCS was constructed by inserting the 4.7-kb BCS operon (containing *crt*, *bcd*, *etfAB*, and *hbd*) into the *BamH*I site of pRK415. To investigate the effects of background butyryl-CoA dehydrogenase activity in *P. putida* strains, prCCS was constructed by first digesting prBCS with *Apa*LI and *Dra*III. The linearized, 14.4 kb fragment was gel purified then Klenow-filled to generate a blunt-end product. This truncated fragment was then re-ligated with itself to create prCCS (a bcd^- and $etfB^-$ derivative of prBCS).

Compatible vectors pETDuet-1, pCDFDuet-1, pACYCDuet-1, and pCOLADuet-1 (Novagen, Darmstadt, Germany) were used to provide individual expression of each gene under a T7*lac* promoter and a ribosome binding site (RBS). *thl* was inserted between the *Nde*I and *Xho*I sites of pETDuet-1 to create peT plasmid. *atoB* was inserted between the *Bgl*II and *Xho*I sites of pETDuet-1 to form peA plasmid. Plasmid pcHC was prepared by inserting *hbd* and *crt* between the *EcoR*I and *Pst*I, and *Nde*I and *Xho*I sites, respectively, in pCDFDuet-1 vector. *bcd* and *etfAB* fragments were inserted between the *BamH*I and *Sal*I and *Xho*I and *Pac*I sites, respectively, in pCOLADuet-1 to create pkBE. As an alternative to *bcd*, *acd*, encoding an acyl-CoA dehydrogenase from *P. putida* was inserted between the *SalI* and *HindIII* sites in vector pCOLADuet-1 to create plasmid pkA.

Additionally, the gene encoding for *Streptomyces collinus* crotonyl-CoA reductase (*ccr*) was synthetically constructed (DNA2.0, Menlo Park, CA) with codon usage optimized for expression in *E. coli.* The synthetic *ccr* fragment was inserted between the *EcoR*I and *Hind*III sites in vector pCOLADuet-1 to create plasmid pkC. The *adhE1* fragment was inserted into pACYCDuet-1 vector between the *EcoR*I and *Pst*I sites to create plasmid paA1. The *adhE2* fragment was inserted into pACYCDuet-1 vector between the *BamH*I and *Sal*I sites to create plasmid paA2. Three plasmids containing genes encoding enzymes to promote greater glycolytic flux or NADH regeneration were constructed. Plasmid peAG was created by inserting *gapA* into the *BamH*I and *Sac*I sites of peA. Cloning *fdh1* between the *Nco*I and *Pst*I sites of peA resulted in plasmid peAF. Together with the T7*lac* promoter fragment, *fdh1* was inserted into peAG between the *Sac*I and *Pst*I sites to create plasmid peAGF.

To re-construct the butanol biosynthetic pathway in *B. subtilis*, the BCS operon was first ligated between the *Nhe*I and *Sph*I sites of pDR111 ((*Britton et al., 2002*); donated by Dr. Alan Grossman, MIT) to create pdBCS. pJBN1 and pDRPyr-Kan were each constructed by ligating the 1.8-kb *Eco*RI – *Bam*HI fragment containing the hyper-spank promoter, multi-cloning site, and *lacI* from pDR111 with *Eco*RI – *Bam*HI linearized pDG1664 ((*Guerout-Fleury et al., 1996*); obtained from the *Bacillus* Genetic Stock Center at The Ohio State University) and pPyr-Kan ((*Middleton & Hofmeister, 2004*); obtained from the *Bacillus* Genetic Stock Center), respectively. *thl* was cloned into the *Nhe*I site of pJBN1 resulting in pjT while *adhE2* was ligated between the *Sal*I and *Sph*I sites of pDRPyr-Kan, yielding ppA2. Plasmid construction and cloning was performed using *E. coli* DH10B.

In all cases, the Expand High Fidelity PCR System (Roche, Basel, Switzerland) or Phusion High Fidelity DNA Polymerase (Finnzymes, Espoo, Finland) was used for DNA amplification. Restriction enzymes and T4 DNA ligase were purchased from New England Biolabs (Ipswich, MA). All positive constructs were identified via restriction digest and nucleotide sequencing. Plasmids constructed in the present work are listed in **Table 2-1**.

Table 2-1 | Plasmids used or constructed in this study.

Plasmid	Description	Source
pRK415	Tet^r, *lac*	(*Keen et al., 1988*)
pMMB206	Cm^r, *lacI, taclac*	(*Morales et al., 1991*)
pMMB206G	Gm^r, *lacI, taclac*	This study
pETDuet-1	Ap^r, *lacI,* T7*lac*	Novagen
pCDFDuet-1	Sm^r, *lacI,* T7*lac*	Novagen
pCOLADuet-1	Km^r, *lacI,* T7*lac*	Novagen
pACYCDuet-1	Cm^r, *lacI,* T7*lac*	Novagen
pDG1664	Ap^r (*E. coli*), Em^r (*B. subtilis*), *thrC* locus	(*Guerout-Fleury et al., 1996*)
pPyr-Kan	Ap^r Km^r (*E. coli*), Km^r (*B. subtilis*), *pyrD* locus	(*Middleton & Hofmeister, 2004*)
pDR111	Ap^r (*E. coli*), Sp^r (*B. subtilis*), *lac I, hyper-spank, amyE* locus	(*Britton et al., 2002*)
pJBN1	Ap^r (*E. coli*), Em^r (*B. subtilis*), *lac I, hyper-spank, thrC* locus	This study
pDRPyr-Kan	Ap^r Km^r (*E. coli*), Km^r (*B. subtilis*), *lac I, hyper-spank, pyrD* locus	This study
prBCS	Tet^r, *lac:* BCS (*crt, bcd, etfAB, hbd*)	This study
prCCS	Tet^r, *lac:* BCS (*crt, etfA, hbd*)	This study
pmTA1	Gm^r, *lacI, taclac: thl, adhE1*	This study
pmTBA1	Gm^r, *lacI, taclac: thl, bdhB, adhE1*	This study
peT	Ap^r, *lacI,* T7*lac: thl*	This study
peA	Ap^r, *lacI,* T7*lac: atoB*	This study
pcHC	Sm^r, *lacI,* T7*lac: hbd,* T7*lac: crt*	This study
pkBE	Km^r, *lacI,* T7*lac: bcd,* T7*lac: etfAB*	This study
pkA	Km^r, *lacI,* T7*lac: acd*	This study
pkC	Km^r, *lacI,* T7*lac: Synccr*	This study
paA1	Cm^r, *lacI,* T7*lac: adhE1*	This study
paA2	Cm^r, *lacI,* T7*lac: adhE2*	This study
peAF	Ap^r, *lacI,* T7*lac: atoB,* T7*lac: fdh1*	This study
peAG	Ap^r, *lacI,* T7*lac: atoB,* T7*lac: gapA*	This study
peAGF	Ap^r, *lacI,* T7*lac: atoB,* T7*lac: gapA,* T7*lac: fdh1*	This study
pdBCS	Ap^r (*E. coli*), Sp^r (*B. subtilis*), *lac I, hyper-spank:* BCS	This study
pjT	Ap^r (*E. coli*), Em^r (*B. subtilis*), *lac I, hyper-spank: thl*	This study
ppA2	Ap^r Km^r (*E. coli*), Km^r (*B. subtilis*), *lac I, hyper-spank: adhE2*	This study

2.2.3 Strain development and culture conditions

E. coli ED1.0 was obtained by transforming *E. coli* DH10B with prBCS and pmTA1 whereas ED2.0 resulted from the transformation of *E. coli* DH10B with prBCS and pmTBA1. Positive transformants were isolated on LB plates containing gentamycin (20 mg/L) and tetracycline (10 mg/L). To create *E. coli* strain EB1.0, BL21Star(DE3) was transformed with plasmids peT, pcHC, pkBE, and paA1. To test the utility of *acd* and *ccr*, EB2.A and EB2.C were created by replacing pkBE in strain EB1.0 with either pkA or pkC, respectively. Replacement of peT with peA in strain EB1.0 yielded strain EB3.0. Strain

EB4.0 was created by replacing paA1 with paA2 in EB1.0 to compare the effect of *adhE2* expression with *adhE1*. In order to explore the possibility of improving butanol synthesis by increasing intracellular NADH or glycolytic flux towards precursors, strains EB4.F and EB4.G were created by replacing peA in EB4.0 with peAF and peAG, respectively. To investigate the effects of both glyceraldehyde 3-phosphate dehydrogenase and formate dehydrogenase expression on butanol biosynthesis, strain EB4.GF was created by replacing peA in EB4.0 with peAGF. Cells containing all compatible plasmids were isolated on LB plates containing ampicillin (30 mg/L), streptomycin (25 mg/L), kanamycin (25 mg/L), and chloramphenicol (8 mg/L). Deletions of *adhE* and *ldhA* in *E. coli* BL21Star(DE3) strains were performed according to a previously reported method (*Datsenko & Wanner, 2000*). All recombinant strains developed in this study are listed in **Table 2-2**.

Table 2-2 | Strains of *E. coli*, *P. putida*, and *B. subtilis* engineered for this study.

Strain	Genotype or plasmid inserted	Source
E. coli strains		
DH10B	F⁻ *mcr*A Δ(*mrr-hsd*RMS-*mcr*BC) ϕ80*lacZ*ΔM15 Δ*lacX74 recA1 endA1 araD139*Δ(*ara, leu*)7697 *galU galK* λ⁻ *rpsL nupG*	Invitrogen
ED1.0	prBCS, pmTA1	This study
ED2.0	prBCS, pmTBA1	This study
BL21Star(DE3)	F⁻ *ompT hsdS*$_B$(r_B^- m_B^-) *gal dcm* (DE3)	Invitrogen
EB1.0	peT, pcHC, pkBE, paA1	This study
EB2.A	peT, pcHC, pkA, paA1	This study
EB2.C	peT, pcHC, pkC, paA1	This study
EB3.0	peA, pcHC, pkBE, paA1	This study
EB4.0	peA, pcHC, pkBE, paA2	This study
EB4.F	peAF, pcHC, pkBE, paA2	This study
EB4.G	peAG, pcHC, pkBE, paA2	This study
EB4.GF	peAGF, pcHC, pkBE, paA2	This study
P. putida strains		
S12	Wild type	ATCC
PS1.0	prBCS, pmTA1	This study
PS1.A	prCCS, pmTA1	This study
PS2.0	prBCS, pmTBA1	This study
PS2.A	prCCS, pmTBA1	This study
B. subtilis strains		
KS438	*spoIIAI SPβ^o*	(*Errington & Mandelstam, 1983*)
BK1.0	Δ *amyE::*pdBCS, Δ *thrC* ::pjT, Δ *pyrD::*ppA2	This study

Fermentation experiments using ED and EB strains were initiated by culturing the recombinant strains in 6 mL TB using 15-mL tubes overnight at 37°C, in a shaker rotating at 225 rpm. The preinoculum was used to seed 150 mL TB medium supplemented with 5 g/L glucose or glycerol in 250-mL screw-capped flasks, at an initial optical density at 600 nm (OD_{600}) of 0.05. Both aerobic and anaerobic culture conditions were studied. Anaerobic cultures were first grown under aerobic conditions in sealed shake flasks to promote biomass production. With a limited headspace volume, these closed cultures became naturally depleted of oxygen after 3-5 h (as indicated by the addition of 5 mg/L resazurin to the culture medium). Cultures were incubated at 37°C in a rotary shaker until OD_{600} reached 0.8. At this point, 0.1 mM IPTG was added to the cultures to induce recombinant protein expression. Following induction, cells were cultivated at 30°C. In all cases, TB medium was supplemented with 20 mg/L gentamycin and 10 mg/L tetracycline (ED strains), or 30 mg/L ampicillin, 25 mg/L streptomycin, 25 mg/L kanamycin, and 8 mg/L chloramphenicol (EB strains). The addition of formic acid to cultures at an initial concentration of 1 g/L was also investigated to promote greater cofactor regeneration in cultures of EB4.F and EB4.0 (control). Culture media were sampled at 24 h intervals for up to 72 h. Samples were centrifuged to pellet cells while the aqueous supernatant was collected for HPLC analysis.

P. putida S12 was co-transformed with prBCS and pmTA1 to construct PS1.0, or with prBCS and pmTBA1 to yield PS2.0. Meanwhile, construction of strains PS1.A and PS2.A was accomplished by co-transformation of *P. putida* S12 with prCCS or pmTA1 or pmTBA1, respectively. Selection of these strains was performed using LB plates containing 20 mg/L gentamycin and 10 mg/L tetracycline. Butanol production in both PS strains was performed at 30°C in 250 mL shake flasks containing 50 mL TB medium with 0.5% (wt./vol.) glucose or glycerol. Induction protocols were performed as described for *E. coli*, though using 1 mM IPTG. All media were supplemented with gentamycin (20 mg/L) and tetracycline (10 mg/L). Aerobic conditions were promoted throughout the study due to the obligately aerobic nature of *P. putida*.

Competent *B. subtilis* KS438 cells were sequentially transformed with pdBCS, pjT, and ppA2 where they were integrated into the chromosome at the *amyE*, *thrC*, and *pyrD* loci, respectively, via double-crossover homologous recombination. The resultant strain, BK1.0, was *amyE*$^-$ *thrC*$^-$ *pyrD*$^-$. LB plates containing 100 mg/L spectinomycin, 12.5 mg/L lincomycin, 0.5 mg/L erythromycin, and 5 mg/L kanamycin were used for selection of transformants, as appropriate. Butanol fermentation experiments with BK1.0 were performed as described above for *E. coli* strains, except that induction was performed using 1 mM IPTG. Antibiotics were not required for the maintenance of BK1.0, and thus were not added to the fermentation medium.

2.2.4 Butanol challenge

50 mL of TB medium was inoculated with preinoculum of *E. coli* BL21Star(DE3), *P. putida* S12, or *B. subtilis* KS438 to give an initial OD_{600} of 0.05. Cultures were incubated at 30°C while shaking at 250 rpm. After reaching mid-exponential growth stage (OD_{600} ≈ 1.5), challenges were applied by butanol addition to a final concentration between 0 and 2% (wt./vol.). Growth and viability were then monitored for 24 hours post butanol addition through optical density measurements and plate counts, respectively. Culture samples were diluted in phosphate buffer (pH 7.0) prior to absorbance readings to yield an average OD_{600} measurement of 0.5. Culture samples were serially diluted by up to 10^{-7} in phosphate buffer prior to plating 100 µL of each dilution on LB agar and incubated at 30°C overnight. Counts were made on all plates yielding a countable number of distinct colony forming units (CFUs), and expressed as CFU/mL of original culture. Error was estimated at one standard deviation of all plates counted for each sample at each time point (typically 2-3).

2.2.5 Metabolite analysis

Solvents and fermentation products were analyzed via HPLC using an Agilent 1100 series instrument equipped with a refractive index detector (RID). Analyte separation was achieved using an Aminex® HPX-87H anion exchange column (Bio-Rad Laboratories, Hercules, CA) according to the method of Buday et al. (*Buday et al., 1990*)

using 5mM H_2SO_4 as the mobile phase. External standards provided calibration for titer determination.

2.3 Results

2.3.1 Construction of butanol-producing *E. coli*

Butanol synthesis in *E. coli* was first investigated via polycistronic expression of the Clostridial genes. DH10B was transformed with prBCS and pmTA1 (strain ED1.0) or with prBCS and pmTBA1 (strain ED2.0). Both strains were cultured in TB medium supplemented with either 0.5% (wt./vol.) glucose or glycerol to assess their ability to synthesize butanol. Following induction with IPTG, butanol was detected in the culture broth of both ED1.0 and ED2.0 after about 48 h, but only when the TB medium was supplemented with glycerol (a more reduced substrate than glucose). Specifically, butanol synthesis by ED1.0 and ED2.0 reached up to 34 ± 5 mg/L and 33 ± 2 mg/L, respectively (**Fig. 2-2**). These results are comparable with earlier efforts to reconstruct the butanol pathway in *E. coli* (*Atsumi et al., 2008*). Co-expression of *bdhB* with *adhE1* in strain ED2.0 had no impact on butanol titer.

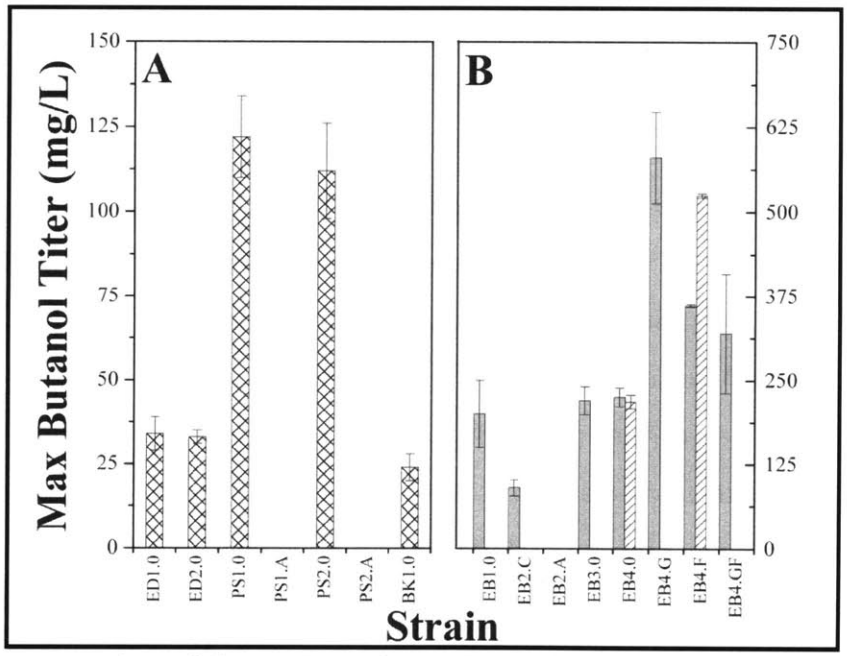

Figure 2-2 | A comparison of the maximum butanol titers for all strains constructed in this study, including those which utilize polycistronic gene expression (A) or individual gene expression (B). All strains cultured in TB media with 0.5% (wt./vol.) glycerol with (diagonal) or without (hashed and gray) supplementation with 1 g/L formate.

The establishment of *E. coli* strains expressing polycistronic constructs provides a baseline for comparison of productivity with the other heterologous hosts. However, we hypothesized that butanol biosynthesis in *E. coli* could also potentially be improved by promoting greater expression of the heterologous Clostridial enzymes. The effects of different strategies of expressing a heterologous multi-gene biosynthetic pathway on metabolite production in *E. coli* have been explored (*Hwang et al., 2003*). Specifically, the polycistronic expression in *E. coli* of a heterologous pathway was compared with the simultaneous individual expression of each gene under a promoter and a ribosome binding site. By using the latter strategy, it was demonstrated that the production of each recombinant protein in the biosynthetic pathway was improved, translating into increased production of non-native metabolites.

We tested the effect of individual expression of *thl*, *hbd*, *crt*, *bcd*, *etfAB*, and *adhE1* under a T7*lac* promoter and a ribosome binding site in *E. coli* EB1.0. Since butanol production was not improved by expression of *bdhB* in strain ED2.0 (relative to ED1.0), *bdhB* was excluded in the construction of all EB strains. Butanol production after 48 h from EB1.0 was 200 mg/L, which is approximately a five-fold improvement over the production from strain ED1.0 (**Fig. 2-2**). It has repeatedly been demonstrated that butyryl-CoA dehydrogenase, isolated from either *C. acetobutylicum* or from recombinant *E. coli*, failed to exhibit enzymatic activity *in vitro* (*Atsumi et al., 2008, Boynton et al., 1996, Hartmanis & Gatenbeck, 1984*). Furthermore, *in vivo* butyryl-CoA dehydrogenase activity is also dependent upon the coordinated functional expression of electron transfer flavoproteins *etfA* and *etfB*. Since the functionality of the butyryl-CoA dehydrogenase complex could possibly be a rate-limiting step in the butanol synthesis pathway, we explored the utility of crotonyl-CoA reductase (*ccr*) derived from *Streptomyces collinus* to mediate the conversion of crotonyl-CoA to butyryl-CoA (strain EB2.C). *ccr* has been previously characterized and functionally expressed in *E. coli* (*Wallace et al., 1995*). As was also noted in previous studies (*Atsumi et al., 2008*), we found this particular substitution to provide inferior results, as butanol production decreased by 55% compared with strain EB1.0. The utility of other non-Clostridial

source enzyme homologs also provided unsubstantial improvements to the maximum butanol titer. In contrast to previously published work (*Atsumi et al., 2008*), the replacement of *thl* with *atoB* from *E. coli* in strain EB3.0, led to only a modest improvement in titer, to 220 mg/L butanol. The replacement of *C. acetobutylicum adhE1* in strain EB3.0 with *adhE2* led to only 230 mg/L butanol (strain EB4.0; **Fig. 2-2**). Although it was reported that *adhE2* was the most highly active of these homologs in alcohologenic cultures of *C. acetobutylicum* (*Fontaine et al., 2002*), little difference between these two homologs was observed in our system.

2.3.2 Expression of NADH-regenerating and glycolytic flux-enhancing enzymes

In the butanol biosynthetic pathway, four moles of NADH are consumed (by oxidation to NAD+) per each mole of butanol produced from acetyl-CoA (**Fig. 2-1**). In an effort to improve butanol synthesis by strain EB4.0, we explored the effects of introducing formate dehydrogenase (*fdh1*) from *Saccharomyces cerevisiae*. Yeast formate dehydrogenase catalyzes the conversion of formate to CO_2 while producing one molecule of NADH (**Fig. 2-3**).

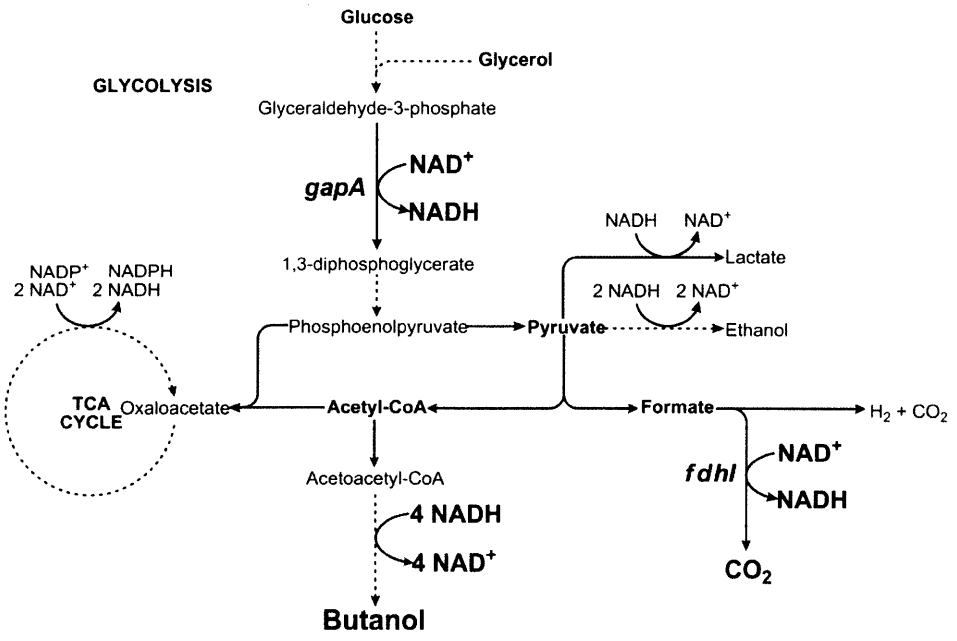

Figure 2-3 | Engineering the central metabolic pathway of *E. coli* to increase glycolytic flux and promote NADH regeneration in support of butanol synthesis.

While formate dehydrogenase also exists in *E. coli*, the bacterial enzyme catabolizes formate to CO_2 and H_2 without generation of NAD(P)H. For this reason, yeast formate dehydrogenase has been exploited in a variety biocatalytic applications requiring ample NADH molecules for product formation (*Berrios-Rivera et al., 2002, Harris et al., 2000, Kaup et al., 2004, Sanchez et al., 2005, Tishkov & Popov, 2004*). Expression of *fdh1* in strain EB4.0 resulted in the generation of strain EB4.F. As shown in **Figure 2-4**, the optimum biobutanol synthesis from strain EB4.F was achieved after 48 h, similar to that of strain EB4.0. Expression of the yeast *fdh1* also resulted in ~74% butanol production improvement over EB4.0, reaching as high as 400 mg/L. Supplementation of the media with 1 g/L formate, increased maximum butanol titers up to 520 mg/L with EB4.F, whereas no difference was observed with EB4.0 (**Fig. 2-2**).

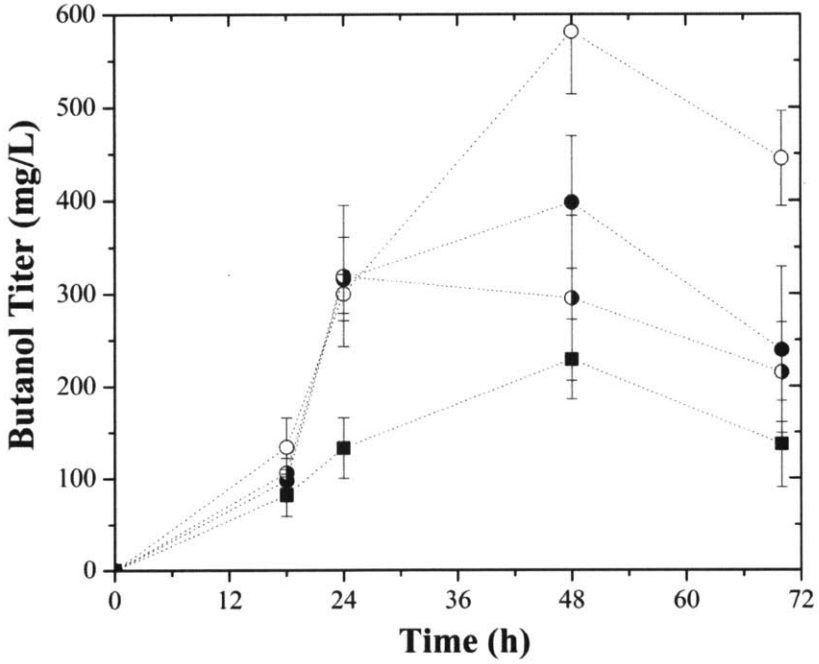

Figure 2-4 | Effects of co-expression of *gapA* and/or *fdh1* on butanol production by strains EB4.0 (control, solid squares), EB4.G (*gapA*$^+$, open circles), EB4.F (*fdh1*$^+$, solid circles), and EB4.GF (*gapA*$^+$ *fdh1*$^+$, half-filled circles) as a function of time. Error bars shown at one standard deviation.

In *E. coli*, glyceraldehyde 3-phosphate dehydrogenase mediates the conversion of glyceraldehyde 3-phosphate to 1,3-diphosphateglycerate in the glycolytic pathway (**Fig. 2-3**). Thus, overexpression of glyceraldehyde 3-phosphate dehydrogenase (*gapA*)

should promote higher rates of substrate flux through the glycolytic pathway. Expression of *gapA* in strain EB4.0 resulted in the generation of strain EB4.G. Again, the maximum biobutanol titer from strain EB4.G was achieved after 48 h, and reached a butanol titer of 580 mg/L, demonstrating that *gapA* overexpression resulted in ~150% greater butanol production (relative to EB4.0). The effects of simultaneously expressing both *gapA* and *fdh1* was tested in strain EB4.GF. Interestingly, however, butanol synthesis from strain EB4.GF was only up to 320 mg/L, which was lower than either EB4.G or EB4.F (**Fig. 2-2** and **Fig. 2-4**). It is possible that simultaneous overexpression of *gapA* and *fdh1* along with the Clostridial enzymes negatively impacted host fitness.

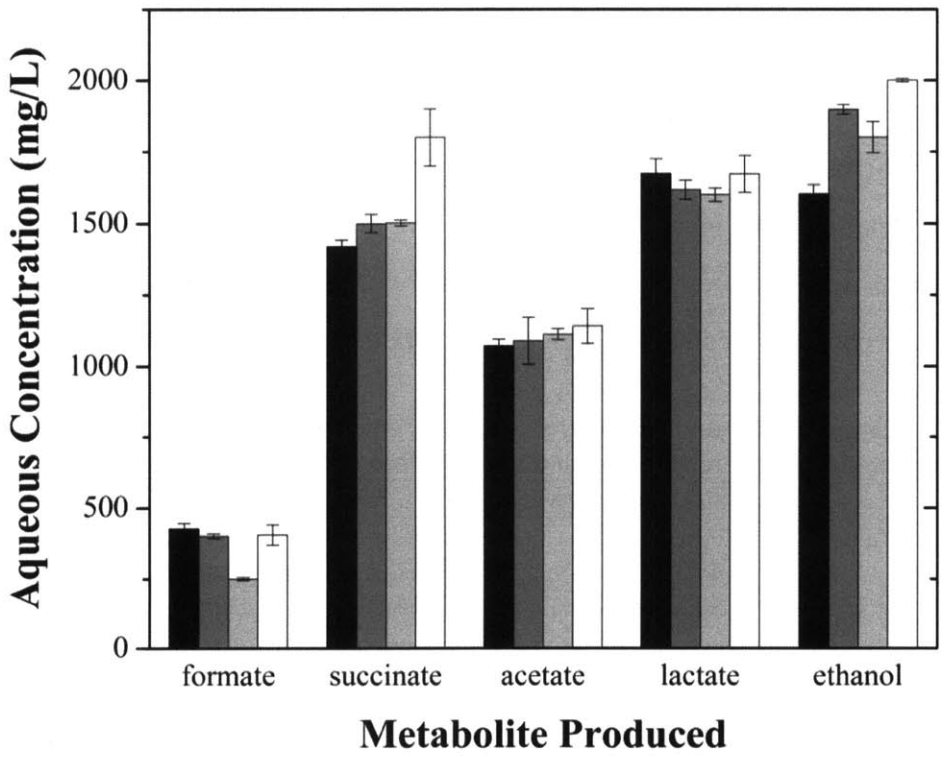

Figure 2-5 | Metabolite byproduct formation by strains EB4.0 (black), EB4.G (dark gray), EB4.F (light gray), and EB4.GF (white). Error bars shown at one standard deviation.

Characterization of EB4.0 fermentation byproducts revealed that after 48 h, succinate, lactate, and ethanol constituted the majority of the end-products, at concentrations of 1400 mg/L, 1700 mg/L, and 1600 mg/L, respectively (**Fig. 2-5**). Overexpression of *gapA* in EB4.G not only resulted in butanol production increase, but

also increased ethanol production by ~18%, likely as a result of increased availability of the precursor acetyl-CoA. The expression of *fdh1* in strain EB4.F resulted in a ~42% decrease of formate accumulation compared to EB4.0, down to 250 mg/L. In addition to an increase in butanol production, *fdh1* co-expression in strain EB4.F also caused ethanol production to increase by ~12% (**Fig. 2-5**). In fact, with the exception of lactate, flux through each of the natural NADH-consuming fermentative pathways of *E. coli* (i.e., ethanol and succinate) was enhanced when *fdh1* was co-expressed. Deletions of *adhE* and/or *ldhA* did not improve carbon flux and/or NADH availability, instead resulting in a decrease in growth rate and butanol production in all strains tested (data not shown).

2.3.3 Engineering *P. putida* and *B. subtilis* for butanol biosynthesis

The previously observed sensitivity of *E. coli* to elevated butanol concentrations motivated the engineering of alternative butanol production platforms in more tolerant, yet still well-characterized, strains. *P. putida* strains PS1.0 and PS2.0 were obtained by co-transformation with either prBCS and pmTA1 or prBCS and pmTBA1, respectively. These strains were cultured in TB supplemented with 0.5% glucose or glycerol, however only aerobic conditions could be studied as *P. putida* is an obligately aerobic organism.

Table 2-3 | Comparing butanol production (mg/L) by engineered strains of *P. putida* S12 (PS) and *B. subtilis* KS438 (BK) in different media, and under different growth conditions.

	Aerobic, TB media with 0.5% (wt./vol.)		Anaerobic, TB media with 0.5% (wt./vol.)	
P. putida strains	Glucose	Glycerol	Glucose	Glycerol
PS1.0	44 ± 6	122 ± 12	n.a. [1]	n.a. [1]
PS2.0	50 ± 6	112 ± 14	n.a. [1]	n.a. [1]
B. subtilis strains				
BK1.0	n.d.	n.d.	23 ± 4	24 ± 4

n.a., not applicable
n.d., not detected
[1] note that *P. putida* is obligately aerobic

As seen in **Table 2-3**, PS1.0 and PS2.0 achieved initial butanol titers of 44 ± 6 and 50 ± 6 mg/L with glucose, respectively, and 122 ± 12 and 112 ± 14 mg/L with glycerol, respectively. As with *E. coli*, butanol production was highest when using the more reduced substrate, glycerol. In this case butanol production by PS1.0 and PS2.0 was

~260% (3.6-fold) and ~240% (3.4-fold) greater than their respective *E. coli* counterparts (ED1.0 and ED2.0, respectively; **Fig. 2-2**). Again, the co-expression of *bdhB* was found to yield an insignificant effect on butanol production. The capacity to produce such butanol titers under aerobic conditions in engineered strains of *P. putida* is of particular phenomenological interest because it questions the longstanding and generally accepted position that the *bcd-etfAB* complex of *C. acetobutylicum* is inactive in the presence of oxygen. For instance, a recent report has shown that the activity of *C. kluyveri* butyryl-CoA dehydrogenase could in fact be demonstrated *in vitro*, but only when the enzymes were prepared under a strict oxygen-free environment, and in the presence of FAD (*Li et al., 2008*). The presence of an acyl-CoA dehydrogenase (*acd*) in *P. putida* KT2440 with catalytic activity on crotonyl-CoA/butyryl-CoA under aerobic conditions has recently been reported (*McMahon et al., 2005*). To determine if the heterologous *bcd-etfAB* complex was responsible for providing butyryl-CoA dehydrogenase activity in butanol-producing strains of *P. putida*, or whether this activity was perhaps alternatively derived from an endogenous *acd* or other homologous protein, we constructed a *bcd*- and *etfB*-deficient derivative of the BCS operon which was expressed from pRK415 as prCCS (strains PS1.A, PS2.A). After 72 h of culture, no butanol production was detected in the culture medium with either strain PS1.A or PS2.A (**Fig. 2-2**). In a complementary experiment, expression of *acd* from *P. putida* instead of *bcd-etfAB* in *E. coli* (strain EB2.A) abolished butanol biosynthesis. These two experiments provide strong evidence that the *bcd-etfAB* complex is in fact functional under aerobic conditions.

Reconstruction of the butanol biosynthetic pathway in *B. subtilis* was achieved by serial transformation with each of plasmids pdBCS, pjT, and ppA2, producing strain BK1.0. In this case, the expression of the polycistronic BCS operon was performed using a single, strong (*hyper-spank*) promoter. Although it had demonstrated no distinct benefits in strain EB4.0, *adhE2* was chosen among aldehyde/alcohol dehydrogenase homologs based on its previously demonstrated activity in *C. acetobutylicum* (*Fontaine et al., 2002*). *bdhB*, on the other hand, was excluded from this design because it

demonstrated no beneficial effects in either *E. coli* or *P. putida*. BK1.0 was cultured in TB medium supplemented with 0.5% glucose or glycerol, under both aerobic and anaerobic conditions. As seen in **Table 2-3**, no butanol production was detected under aerobic conditions. However, after 72 h under anaerobic conditions, BK1.0 produced a maximum of 23 ± 4 and 24 ± 4 mg/L butanol with glucose and glycerol supplementation, respectively. Therefore, despite sharing greater phylogentic similarity with *Clostridium* than both *E. coli* and *P. putida*, expression of Clostridial genes in *B. subtilis* did not improve the apparent activity of this heterologous pathway.

2.3.4 Assessing the butanol tolerance of *E. coli*, *P. putida*, and *B. subtilis*

To assess the production potential of the various butanol-producing strains constructed, we studied the inhibitory effects of butanol on the dynamic and steady-state growth phenotypes of *E. coli*, *P. putida*, and *B. subtilis*. As seen in **Figure 2-6**, the addition of at least 0.5% (wt./vol.) butanol to cultures of *E. coli* and *P. putida*, or at least 1.0% (wt./vol.) butanol to *B. subtilis* cultures, resulted in rapid and markedly negative effects on both the growth rate and biomass yield. Addition of 2.0% (wt./vol.) butanol was completely lethal to all cultures tested within about 30 min. The addition of butanol at 0.5% (wt./vol.) or higher to *E. coli* cultures caused a rapid decrease (within 30 minutes) in growth rate and OD_{600} relative to the control culture. Viability, however, was only observed to decrease significantly in the presence of at least 1.0% (wt./vol.) butanol over the same time period. Adaptation to the solvent stresses was observed for *E. coli* cultures with between 0.5 and 0.75% (wt./vol.) butanol, as shown by increases in viable cell concentration after approximately 100 minutes. *P. putida* and *B. subtilis* also demonstrated similar behaviors, though with respect to different characteristic butanol concentrations. A pseudo-steady state at which there was nearly no net change in OD_{600} or culture viability relative to that at the time of butanol addition occurred after addition of 0.75, 1.0, and 1.25% (wt./vol.) butanol to cultures of *P. putida*, *E. coli*, and *B. subtilis*, respectively. Above these respective concentrations, however, decreases in both measurements were observed.

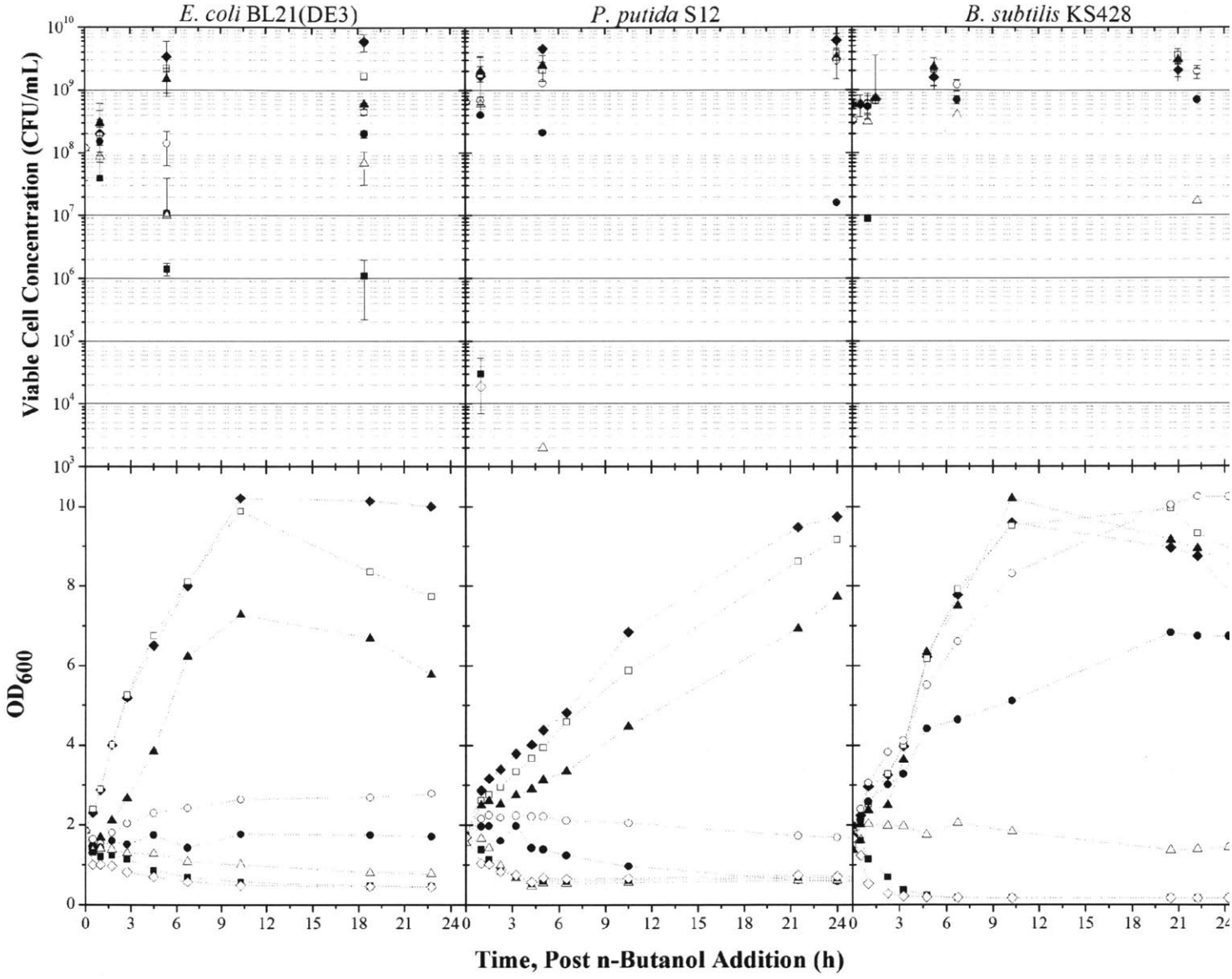

Figure 2-6 | Effect of butanol addition on growing cultures of *E. coli* BL21 (DE3), *P. putida* S12, and *B. subtilis* KS438 as determined b viable cell concentration and optical density. Butanol was added to mid-exponential stage cultures at final aqueous concentration (% wt./vol.) of: 0 (solid diamonds), 0.25 (open squares), 0.5 (solid triangles), 0.75 (open circles), 1.0 (solid circles), 1.25 (open triangles), 1. (solid squares), and 2.0 (open diamonds). Note that series data were excluded when zero viable cells were obtained, as was observe after 1.5 and/or 2% (wt./vol.) butanol addition. Error bars shown at one standard deviation.

2.4 Discussion

Although the bacterium *E. coli* is a well-characterized microorganism from both a genetic and metabolic perspective and boasts a vast availability of genetic tools for its engineering, the susceptibility of *E. coli* to high butanol concentrations complicates its development as a butanol production strain. Nevertheless, we selected *E. coli* as our first prototype strain for the development of an alternative butanol producer in order to provide a baseline for comparison with our other non-native hosts, as well as with other works recently reported in the literature. Enhanced expression of the butanol pathway genes was achieved via replacement of the polycistronic BCS operon to provide expression using individual promoter-RBS sequences and resulted in nearly a six-fold improvement in product titer. It has recently been shown that the expression levels of several butanol biosynthetic genes were significantly higher in a butanol hyper-producing mutant of *C. beijerinckii* than that of the wild-type strain (*Chen & Blaschek, 1999*). Recruitment of enzymes with homologous function from alternative genetic sources had limited results, which is consistent with previous reports (*Atsumi et al., 2008*).

Co-expression of *fdh1* from yeast to provide cofactor regeneration in *E. coli* resulted in further improvement of butanol titers up to 400 mg/L in shake flask cultures. However, it was expected that this strategy could provide only limited improvements as endogenous formate levels were quite low (**Fig. 2-5**). By provision of exogenous formate, flux through the butanol pathway was increased, presumably as a result of elevated rates of NADH regeneration. Although supplementation of the culture media with formate does not represent a sustainable practice for butanol fermentations, it does suggest that an insufficient supply of intracellular NADH may limit the activity of the heterologous butanol pathway in engineered *E. coli*. Meanwhile, overexpression of *gapA* from *E. coli* to promote greater glycolytic flux and increase the acetyl-CoA pool resulted in final butanol titers of 580 mg/L. This titer is comparable to the maximum reported by Atsumi et al. (2008) and did not require the deletion of endogenous genes. As shown in **Figure 2-5**, the co-expression of both *gapA* and *fdh1* resulted in a notable

increase in succinate production, a phenomenon that can be explained two-fold. Firstly, the overexpression of *gapA* increases the flux through phosphoenolpyruvate carboxylase towards the synthesis of oxaloacetate, a precursor of succinate (*Causey et al., 2004*). Since the overexpression of *gapA* was also likely to result in increased accumulation of acetyl-CoA (as indicated by observed increases in ethanol accumulation; **Fig. 2-5**), a substrate of malate synthase, this would ultimately lead to increased production of malate and succinate. Secondly, the NADH regenerated via *fdh1* co-expression can also serve as an electron donor for both malate dehydrogenase and fumarate reductase (*Causey et al., 2004*), two enzymes involved in succinate biosynthesis. Overall, the elevation of fermentative byproducts reflects an increase in the intracellular $NADH/NAD^+$ ratio (*de Graef et al., 1999*).

One means of reducing carbon flux towards fermentative byproducts and affecting the co-factor balance could involve deletions of *adhE* and *ldhA*, the primary enzymes responsible for the production of ethanol and lactate, respectively. In this study, deletion of either or both of these genes led to decreases in butanol productivity. These two deletions were previously found to improve butanol titers from glucose in engineered *E. coli* when combined with additional gene deletions (*Atsumi et al., 2008*). Similarly, glucose flux to pyruvate was significantly enhanced when *adhE* and *ldhA* deletions were included among several genetic modifications (*Causey et al., 2004*). Thus, it may be that additional mutations (e.g., *frd* deletion) are required to observe the positive effect associated with *adhE* and/or *ldhA* deletions. 1,2-Propanediol productivity was previously improved in an *ldh* mutant of *E. coli*, but only with glucose as a substrate (*Berrios-Rivera et al., 2003*). Considering this observation, our use of the more reduced glycerol as a substrate may also have impacted these results. Finally, it should be noted that our experiments were performed with BL21(DE3), a B strain, while each of the previous studies utilized K-12 strains. The reported differences in metabolic activity between these strains (*Phue et al., 2005, Phue & Shiloach, 2004*) may have also contributed to the observed lack of effect of *adhE* and *ldhA* in this study.

Ultimately, the availability of excess reducing equivalents and/or enhanced metabolite flux could only provide limited improvements towards butanol production due likely to the slow enzyme kinetics of the engineered butanol pathway. Our results support those of previous studies (*Li et al., 2008*) in suggesting that the slow turn-over rate of the *Clostridium* butyryl-CoA dehydrogenase complex likely limited the capacity of the engineered butanol pathway. In *C. kluyveri*, activity of the enzyme encoded by the *bcd-etf* complex has recently been found to be rate-limiting in butyraldehyde synthesis. It was postulated that the slow kinetics demonstrated by this enzyme complex may result from complexities associated with the endergonic reduction of ferredoxin with NADH and the exergonic reduction of crotonyl-CoA with NADH (*Li et al., 2008*). *In vitro* activity of *bcd-etfAB* could not be detected from any of the strains constructed in this study. Previous works have also highlighted the difficulty associated with confirming the *in vitro* activity of *bcd-etfAB* as expressed in recombinant *E. coli* (*Boynton et al., 1996*) or from *C. acetobutylicum* itself (*Hartmanis & Gatenbeck, 1984*), often citing the possible sensitivity of this enzyme complex to oxygen. Although product titers were quite low, functional expression of the butanol pathway has previously been achieved in *E. coli* under aerobic conditions, despite the inability to assay *bcd-etfAB* activity *in vitro* (*Atsumi et al., 2008*). Compared to that work, butanol titers obtained under aerobic conditions in this study were improved by nearly 15-fold using *P. putida* as the host organism (122 mg/L vs. ~8 mg/L). If *C. acetobutylicum bcd-etfAB* did in fact suffer from decreased activity in the presence of oxygen, then the functional pathway construction in *P. putida* under aerobic conditions could have been aided by the activity of native isozymes catalyzing the same reaction of crotonyl-CoA to butyryl-CoA. However, as we have demonstrated, butanol production was dependent upon the presence of *bcd-etfAB* and expression of *acd* did not complement butanol biosynthesis in our engineered strains of *E. coli*, indicating that background enzymatic activity alone was insufficient for catalyzing this reaction under the culture conditions studied. These results support the notion that it may be the method of analysis, and not the sensitivity of this enzyme to

dissolved oxygen, that is in fact responsible for the inability to assay this step of the butanol biosynthetic pathway.

The susceptibility of *E. coli* to the toxic effects of butanol prompted our interest in engineering of butanol-producing strains of both *P. putida* and *B. subtilis*. In this case, we found that *B. subtilis* displayed elevated butanol tolerance, when compared with *P. putida* and *E. coli*. The polycistronic expression of *C. acetobutylicum* genes in *B. subtilis* resulted in butanol synthesis at similar titers to engineered *E. coli* ED strains. This result represents a step toward the generation of an alternative butanol production platform with improved solvent tolerant characteristics. As with *E. coli*, we anticipate the butanol titers from *P. putida* and *B. subtilis* could now be substantially improved through host-specific strategies. Significant improvements of butanol biosynthesis were achieved in *E. coli* as a result of an improved gene expression strategy that involved individual promoter and RBS sequences associated with each pathway enzyme, as well as through the overexpression of enzymes to increase glycolytic flux or facilitate cofactor regeneration. Furthermore, as has been previously demonstrated in *E. coli*, *in vivo* evolution of heterologous pathway elements can also lead to improved productivities in a non-native host (*Meynial Salles et al., 2007*). In *P. putida* strains, improved expression could also be achieved through the use of a *Pseudomonas*-derived promoter as opposed to the *E. coli*-derived *lac* promoter employed in this study. Furthermore, the lack of extensive natural product biosynthesis in *Pseudomonas* sp. also reduces the potential for molecular cross-talk, contamination, and competition with native pathways in heterologous production efforts (*Zhang et al., 2008*). The functional expression of the butanol biosynthesis pathway in *P. putida* and *B. subtilis* further illustrates the potential of these under-utilized, yet industrially relevant, strains as production hosts.

In addition to n-butanol, *E. coli* has also recently been engineered for the production of other potential biofuels consisting of higher alcohols such as iso-butanol (*Atsumi et al., 2008*), 2-methyl-1-butanol (*Cann & Liao, 2008*), 3-methyl-1-butanol (*Connor & Liao, 2008*), as well as n-pentanol, 3-methyl-1-pentanol, and n-hexanol

(*Zhang et al., 2008*). Despite their favorable thermodynamic properties, it has been thoroughly demonstrated that the cytotoxicity of an alcohol is elevated with an increasing carbon chain length (*Heipieper & Debont, 1994, Osborne et al., 1990, Vermue et al., 1993*). Thus, the problems associated with the cytotoxicity of both conventional and second-generation biofuels will remain apparent, and represent an increasing requirement for robust biocatalyst platforms.

The pseudo-steady state behavior observed with respect to butanol inhibition represents a critical condition above which growth and viability became most severely inhibited, and below which cultures remained prosperous. This state was found to be a distinguishing feature of each organism, however the characteristic range of critical butanol concentrations was found to be seemingly narrow (0.75 to 1.25%). This finding is consistent with a previous study which found that a selection of Gram-positive and Gram-negative bacteria, including *Arthrobacter*, *Norcadia*, *Acinetobacter*, and *Pseudomonas* sp., each displayed very similar tolerance to a series of n-alkanol solvents, including butanol (*Vermue et al., 1993*). More recently, the inhibitory effects of butanol on the growth of 24 different microorganisms, including several species of bacteria and yeast, was investigated (*Knoshaug & Zhang, 2008*). Although *Pseudomonas* and *Bacillus* were excluded from that study, those findings also confirmed the existence of a narrow range of toxic thresholds (between 1 and 2% (wt./vol.)) for most strains. Two strains of *Lactobacillus*, however, were found to capable of maintaining growth in butanol concentrations as high as 3%. Meanwhile, additional strains of *Lactobacillus* and the phylogenetically related species *Enterococcus* have also been reported as capable of tolerating up to 2.5% (wt./vol.) butanol on solid media (*Bramucci et al., 2007, Bramucci et al., 2008*). Interspecies similarity of butanol toxic threshold concentrations is likely a result of high homology between the cytoplasmic membrane structures of the studied organisms particularly when it is considered that the inhibitory mechanism involves membrane accumulation leading to structural distortion. Although the specific strains of *P. putida* investigated here showed a relatively low sensitivity threshold to butanol, evolved strains of *P. putida* that can grow

in the presence of up to 6% (wt./vol.) butanol have recently been isolated (*Ruhl et al., 2009*). Since the *P. putida* pathway reconstruction strategy outlined here would be compatible with these novel organisms, these hosts would make excellent candidates as alternative butanol production strains.

Solvent tolerance can be further engineered, for example, as it was in *Clostridium* through the overexpression of stress (heat shock) proteins (*Tomas et al., 2003*). Other widely employed approaches towards enhancing the desired phenotypes of industrial biocatalysts most frequently rely upon mutagenic techniques. However, the identification of enhanced phenotypes obtained via stochastic mutation procedures typically requires laborious screening and selection processes. Such techniques can also elicit an unforeseen impact on host fitness and decrease its overall industrial utility (*Bonomo et al., 2006*). Furthermore, since complex phenotypes such as solvent tolerance are not monogenic (*Alper et al., 2006*), several distinct mutation events would be required to be performed in highly specific combinations. In contrast, broader mechanisms utilizing global transcription machinery engineering (gTME) have been successfully demonstrated for the elevation of ethanol tolerance in yeast (*Alper et al., 2006*) and *E. coli* (*Alper & Stephanopoulos, 2007*). The use of naturally solvent tolerant microorganisms as host productions strains does not negate the relevance or applicability of previously developed molecular techniques. Rather, the selection of an appropriate host as a starting point is a critical challenge for the for the engineering of solvent tolerant phenotypes via such combinatorial procedures (*Fischer et al., 2008*). The outlined approach thus remains compatible with such emerging techniques while providing an elevated baseline of natural solvent tolerance from which next generation butanol producing microorganisms can be engineered.

2.5 Conclusions

Although *Clostridia* are the traditional organisms employed in biobutanol production, a significant and growing amount of research is centered on the engineering of more robust strains capable of elevated production. Because systematic approaches

to improve butanol production traits of *Clostridium* are currently impeded by a lack of characterization and genetic tools, this work has focused on the generation of a variety of tractable strains which allow for versatile manipulations with the objective of improving butanol fermentation. Functional butanol pathways were successfully constructed in *E. coli*, *P. putida*, and *B. subtilis*. Experimental titers were highest in *E. coli* and benefited from optimized expression strategies. Although *B. subtilis* displayed the most solvent tolerant phenotype among the studied strains, thus providing it with the greatest production potential, it was found to be the poorest producing strain. Preliminary titers obtained in engineered strains of *P. putida* were superior to those obtained by *E. coli* under aerobic conditions in previous studies, and titers from both *P. putida* and *B. subtilis* were notably better than those recently achieved in yeast (*Steen et al., 2008*). Although the specific strain studied displayed sensitivity to butanol, with concurrent work on the evolution of more solvent tolerant strains of *P. putida*, pseudomonads may constitute an effective butanol production host in the future. Overall, this work has demonstrated the engineering of butanol biosynthesis in heterologous, solvent-tolerant microorganisms.

Furthermore, the successful production of butanol in *E. coli* with titers up to 580 mg/L demonstrated the feasibility of a synthetic butanol pathway in *E. coli*, giving a feasible platform for pentanol biosynthesis. The proposed synthesis of pentanol involves six reaction steps proceeding from acetyl-CoA and propionyl-CoA as the starting substrates. To better understand the pentanol pathway, we utilized two sets of CoA-removing enzymes, the phosphotransbutyrylase (Ptb) and butyrate kinase (Buk) system encoded by the *ptb-buk* operon from *C. acetobutylicum* ATCC 824, and acyl-CoA thioesterase II (TesB) from *E. coli* MG1655, as diagnostic tools to test enzyme plasticity on catalyzing formation of the five-carbon precursor to pentanol. Removal of the CoA moieties also leads to the production of high value-added chiral hydroxybutyrates and hydroxyvalerates, which will be discussed in Chapter 3 and Chapter 4, respectively.

CHAPTER 3

Chiral 3-Hydroxybutyrate Biosynthesis as In Vivo Assessment of the Top Butanol Pathway

Abstract

This chapter describes construction of synthetic metabolic pathways for production of enantiopure (*R*)- and (*S*)-3-hydroxybutyrate (3HB) from glucose in recombinant *E. coli* as a way to assess the top butanol pathway. To promote maximal activity, we profiled three thiolase homologs (BktB, Thl, and PhaA) and two CoA-removal mechanisms (Ptb-Buk and TesB). In addition, two enantioselective 3-hydroxybutyryl-CoA dehydrogenases (PhaB, producing the (*R*)-enantiomer and Hbd, producing the (*S*)-enantiomer) were utilized to control the 3HB chirality across two *E. coli* backgrounds, BL21Star(DE3) and MG1655(DE3), representing *E. coli* B and *E. coli* K-12 derived strains, respectively. MG1655(DE3) was found to be superior for the production of each 3HB stereoisomer although the recombinant enzymes exhibited lower *in vitro* specific activities compared to BL21Star(DE3). Hbd *in vitro* activity was significantly higher than PhaB in both strains. The engineered strains achieved high titer production of enantiopure (*R*)-3HB and (*S*)-3HB in shake flask cultures within two days. The NADPH/$NADP^+$ ratio was found to be two- to three-fold higher than the NADH/NAD^+ ratio under the culture conditions examined, presumably affecting *in vivo* activities of PhaB and Hbd and resulting in greater production of (*R*)-3HB than (*S*)-3HB. To the best of our knowledge, this study reports the highest (*S*)-3HB titer achieved in shake flask *E. coli* cultures to date.

The majority of this chapter was published as:

Tseng, H.-C., Martin, C.H., Nielsen, D.R., and Prather, K.L.J. 2009. "Metabolic engineering of *Escherichia coli* for the enhanced production of (R)- and (S)-3-hydroxybutyrate" ***Appl Environ Microbiol*** 75:3137–3145.

4-1 Introduction

The synthesis of chiral molecules is of significant interest in the pharmaceutical industry because frequently one stereoisomer of a drug has efficacy while the other has either substantially reduced or no activity, or may even have adverse effects (*Patel, 2006, Pollard & Woodley, 2007*). Additionally, chiral molecules serve as building blocks for many pharmaceuticals and high value compounds. Thus, the ability to prepare chiral molecules with high optical purity is important. Stereoselective chemical processes generally employ expensive chiral catalysts, require harsh physical conditions and solvents, and suffer from extensive byproduct formation. In contrast, enzyme-catalyzed reactions are highly stereoselective and can be performed in aqueous solutions under mild conditions (*Patel, 2000*). As a result, the use of biological processes for chiral molecule production has been extensively investigated (*Chen & Wu, 2005, Shiraki et al., 2006, Tokiwa & Calabia, 2008, Zhao et al., 2003*). One example of such a process is the biosynthesis of 3-hydroxybutyric acid (3HB), a versatile chiral molecule containing one hydroxyl group and one carboxyl group, used as a building block for the synthesis of optically-active fine chemicals, such as vitamins, antibiotics, pheromones, and flavor compounds (*Chiba & Nakai, 1987, Chiba & Nakai, 1985, Mori, 1981, Seebach et al., 1986*).

The biosynthesis of 3HB has typically been achieved using two different mechanisms: depolymerization (*in vitro* or *in vivo*) of microbially synthesized poly-(*R*)-3-hydroxybutyric acid (PHB) (*de Roo et al., 2002, Lee & Lee, 2003*), or direct synthesis of 3HB without a PHB intermediate (*Gao et al., 2002, Lee et al., 2008, Liu et al., 2007*). However, due to the stereospecific constraints of PHB synthesis, in which polymers are composed exclusively of (*R*)-3HB monomer units, the synthesis of (*S*)-3HB from PHB is effectively impossible. In contrast, direct synthesis of both enantiopure (*R*)-3HB and (*S*)-3HB is possible. Pathways facilitating (*R*)-3HB synthesis have been constructed in *Escherichia coli* by simultaneous expression of *phaA* (encoding acetoacetyl-CoA thiolase) and *phaB* (encoding (*R*)-3-hydroxybutyryl-CoA dyhydrogenase) from *Ralstonia eutropha* H16, and *ptb* (encoding phosphotransbutyrylase) and *buk*

(encoding butyrate kinase) from *Clostridium acetobutylicum* ATCC 824 (*Gao et al., 2002*). In addition to the use of *ptb* and *buk* to catalyze the conversion of (*R*)-3HB-CoA to (*R*)-3HB, *tesB* (encoding thioesterase II from *E. coli*) has also been used for the direct hydrolysis of (*R*)-3HB-CoA to yield (*R*)-3HB (*Liu et al., 2007*). The production of (*S*)-3HB in *E. coli* has recently been reported using a biosynthetic pathway consisting of *phaA* from *R. eutropha* H16, *hbd* (encoding (*S*)-3-hydroxybutyryl-CoA dehydrogenase) from *C. acetobutylicum* ATCC 824, and *bch* (encoding 3-hydroxyisobutyryl-CoA hydrolase) from *Bacillus cereus* ATCC 14579 (*Lee et al., 2008*).

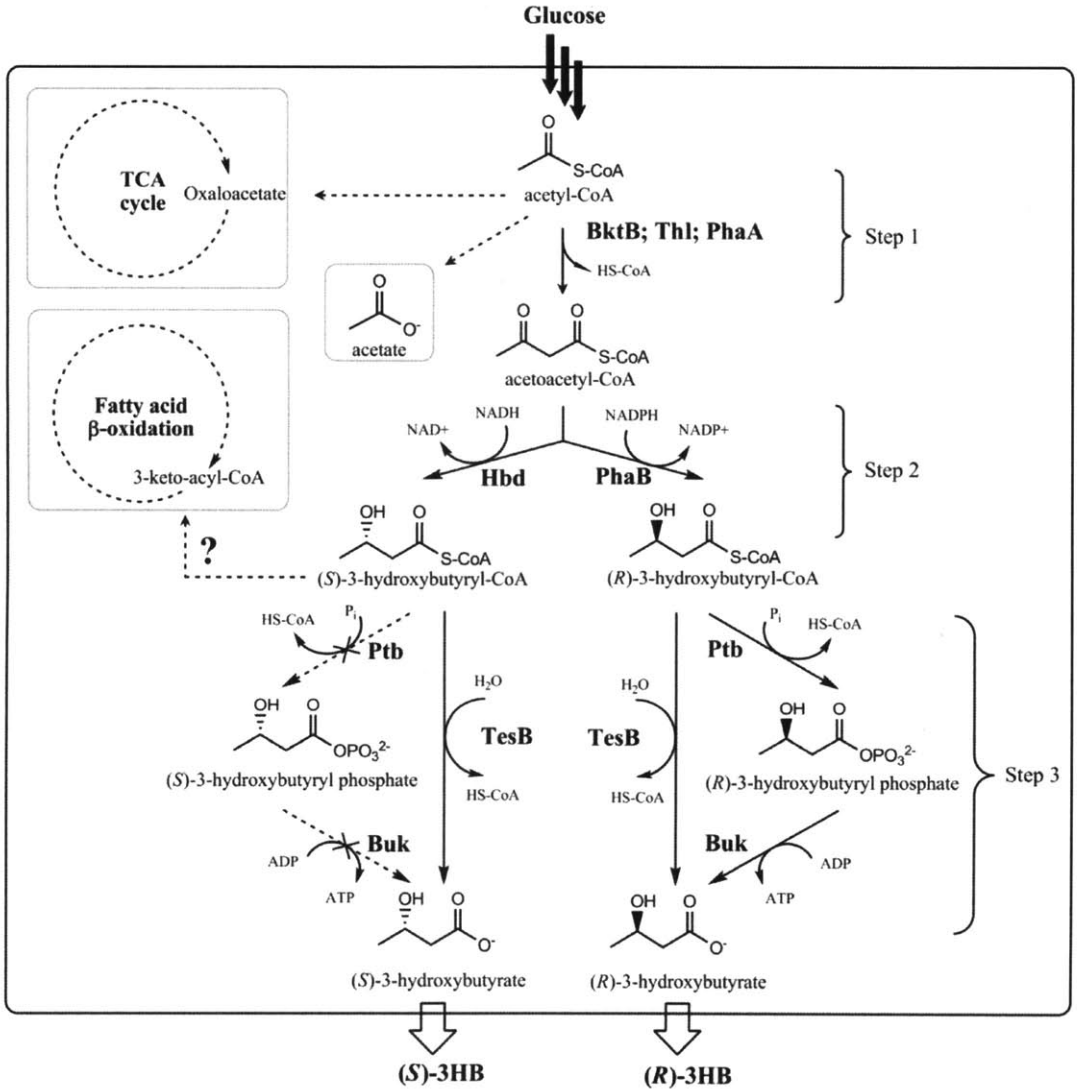

Figure 3-1 | Schematic representation of (*S*)-3HB or (*R*)-3HB synthesis from glucose in engineered *E. coli*.

In *E. coli*, the synthesis of both enantiomers of 3HB begins with the condensation of two molecules of acetyl-CoA, catalyzed by a thiolase, to give acetoacetyl-CoA (**Fig. 3-1**). The acetoacetyl-CoA is then reduced either to (*R*)-3-hydroxybutyryl-CoA ((*R*)-3HB-CoA) via ketone reduction mediated by an NADPH-dependent (*R*)-3-hydroxybutyryl-CoA dehydrogenase (PhaB), or to (*S*)-3-hydroxybutyryl-CoA ((*S*)-3HB-CoA) via an NADH-dependent (*S*)-3-hydroxybutyryl-CoA dehydrogenase (Hbd). (*R*)-3HB-CoA and (*S*)-3HB-CoA can each be further modified via a suitable CoA-removal reaction to form (*R*)-3HB and (*S*)-3HB, respectively. In an effort to increase chiral 3HB production, it is essential to identify a thiolase capable of efficiently catalyzing the first reaction in the 3HB biosynthetic pathways, to draw acetyl-CoA from competing endogenous pathways. Thus, we examined three different thiolases, BktB and PhaA from *R. eutropha* H16, and Thl from *C. acetobutylicum* ATCC 824, to determine which is most proficient for 3HB synthesis. (*R*)-3HB-CoA and (*S*)-3HB-CoA synthesized via the reduction reaction catalyzed by PhaB and Hbd, respectively, must be converted to their respective free acid forms before transport or diffusion out of the cell. We have compared two sets of CoA-removing enzyme mechanisms, including the phosphotransbutyrylase (Ptb) and butyrate kinase (Buk) system encoded by the *ptb-buk* operon from *C. acetobutylicum* ATCC 824, and acyl-CoA thioesterase II (TesB) from *E. coli* MG1655. Moreover, it has long been argued whether B strains or K-12 strains of *E. coli* would serve as better hosts for the biosynthesis of small molecules. Microarrays and Northern blot analyses have suggested that several metabolic pathways, including the TCA cycle, glyoxylate shunt, glycolysis, and fatty acid degradation are different between these two strains (*Phue et al., 2005, Schneider et al., 2002, Walle & Shiloach, 1998, Xia et al., 2008*), implying that they may differ significantly in their ability to supply significant levels of acetyl-CoA as the precursor for 3HB synthesis. Thus, we have also compared 3HB synthesis across two representative *E. coli* strains: *E. coli* BL21Star(DE3) (B strain) and *E coli* MG1655(DE3) (K-12 strain). 3HB chirality was examined and verified by high performance liquid chromatography (HPLC) analysis using a chiral stationary phase to provide separation.

Altogether, we have explored the production of each stereoisomer of 3HB across different strains of *E. coli*, different thiolases, and different CoA-removal systems to engineer *E. coli* for enhanced chiral 3HB production.

3.2 Materials and Methods

3.2.1 Microorganisms

The bacterial strains used are listed in **Table 3-1**. *C. acetobutylicum* ATCC 824 was purchased from the American Type Culture Collection (ATCC, Manassas, VA). *R. eutropha* H16 was provided by Professor Anthony Sinskey of the Department of Biology at the Massachusetts Institute of Technology, USA. *E. coli* DH10B (Invitrogen, Carlsbad, CA) and ElectroTen-Blue (Stratagene, La Jolla, CA) were used for transformation of cloning reactions and propagation of all plasmids. BL21Star(DE3) (Invitrogen, Carlsbad, CA) and MG1655(DE3) were used as host strains for the biosynthesis of chiral 3HB, where MG1655(DE3) was constructed using a λDE3 Lysogenization Kit (Novagen, Darmstadt, Germany) for site-specific integration of λDE3 prophage into *E. coli* MG1655 (kindly donated by Professor Gregory Stephanopoulos of the Department of Chemical Engineering at the Massachusetts Institute of Technology, USA).

3.2.2 Plasmid construction

Genes derived from *C. acetobutylicum* ATCC 824 (*thl*, *hbd*, and *ptb-buk* operon), *R. eutropha* H16 (*phaA*, *bktB*, and *phaB*), and *E. coli* K-12 (*tesB*) were obtained by polymerase chain reaction (PCR) using genomic DNA (gDNA) templates. All gDNAs were prepared using the Wizard Genomic DNA Purification Kit (Promega, Madison, WI). Custom oligonucleotides (primers) were purchased for all PCR amplifications (Sigma-Genosys, St. Louis, MO) as shown in **Table 3-1**. In all cases, HotStar HiFidelity Polymerase (QIAGEN, Valencia, CA) was used for DNA amplification. Restriction enzymes and T4 DNA ligase were purchased from New England Biolabs (Ipswich, MA). Recombination DNA techniques were performed according to standard procedures (*Sambrook & Russell, 2001*).

Table 3-1 | *E. coli* strains, plasmids and oligonucleotides used.

Name	Relevant Genotype	Reference
Strains		
DH10B	F⁻ *mcr*A Δ(*mrr-hsd*RMS-*mcr*BC) ϕ80*lacZ*ΔM15 Δ*lacX74 recA1 endA1 araD139*Δ(*ara, leu*)7697 *galU galK* λ⁻ *rpsL nupG*	Invitrogen
ElectroTen-Blue	Δ(*mcrA*)*183* Δ*(mcrCB-hsdSMR-mrr)173 endA1 supE44 thi-1 recA1 gyrA96 relA1 lac* Kan^r [F′ *proAB lacI*^{q}ZΔM15 Tn*10* (Tet^r)]	Stratagene
MG1655	F⁻ λ⁻ *ilvG- rfb-50 rph-1*	ATCC 700926
BL21Star(DE3)	F⁻ *ompT hsdS*$_B$ (r_B^- m_B^-) *gal dcm rne131* (DE3)	Invitrogen
MG1655(DE3)	F⁻ λ⁻ *ilvG- rfb-50 rph-1* (DE3)	This study
Plasmids		
pGEM-T easy	PCR cloning vector; F1 *ori,* Amp^r	Promega
pETDuet-1	ColE1(pBR322) *ori*, *lacI,* T7*lac*, Amp^r	Novagen
pCDFDuet-1	CloDF13 *ori*, *lacI,* T7*lac*, Str^r	Novagen
pET-H	pETDuet-1 harboring *hbd* from *C. acetobutylicum* ATCC 824	This study
pET-H-B[a]	pETDuet-1 harboring *bktB* from *R. eutropha* H16, and *hbd* from *C. acetobutylicum* ATCC 824	This study
pET-H-T[a]	pETDuet-1 harboring *thl* and *hbd* from *C. acetobutylicum* ATCC824	This study
pET-H-P[a]	pETDuet-1 harboring *phaA* from *R. eutropha* H16, and *hbd* from *C. acetobutylicum* ATCC 824	This study
pET-P	pETDuet-1 harboring *phaB* from *R. eutropha* H16	This study
pET-P-B[a]	pETDuet-1 harboring *bktB* and *phaB* from *R. eutropha* H16	This study
pET-P-T[a]	pETDuet-1 harboring *thl* from *C. acetobutylicum* ATCC 824, and *phaB* from *R. eutropha* H16	This study
pET-P-P[a]	pETDuet-1 harboring *phaA* and *phaB* from *R. eutropha* H16	This study
pCDF-T	pCDFDuet-1 harboring *tesB* from *E. coli* MG1655	This study
pCDF-PB	pCDFDuet-1 harboring *ptb-buk* operon from *C. acetobutylicum* ATCC 824	This study
Primers	**Sequence 5'→3'[b]**	
bktB_US_EcoRI	*GAATTC*ATGACGCGTGAAGTGGTAGTG	Sigma-Genosys
bktB_DS_XhoI	*CTCGAG*CGCAAGGCTAACCTCAGAT	Sigma-Genosys
thl_US_EcoRI	ATA*GAATTC*CATGAGAGATGTAGTAATAGTAAGTG	Sigma-Genosys
thl_DS_XhoI	TATTGAACCTC*CTCGAG*AACTTAGTTATAT	Sigma-Genosys
phaA_US_EcoRI	*GAATTC*GACTACACAATGACTGACGTTGTC	Sigma-Genosys
phaA_DS_XhoI	*CTCGAG*AAAACCCCTTCCTTATTTGC	Sigma-Genosys
hbd_US_EcoRI	*GAATTC*GGGAGGTCTGTTTAATGAAAA	Sigma-Genosys
hbd_DS_NotI	*GCGGCCGC*TGTAAACTTATTTTG	Sigma-Genosys
phaB_US_EcoRI	*GAATTC*AACGAAGCCAATCAAGGAG	Sigma-Genosys
phaB_DS_NotI	*GCGGCCGC*GCAGGTCAGCCCATATG	Sigma-Genosys
tesB_US_EcoRI	*GAATTC*TACTGGAGAGTTATATGAGTCAGG	Sigma-Genosys
tesB_DS_SalI	*GTCGAC*TTAATTGTGATTACGCATC	Sigma-Genosys

[a] Each gene is under the control of the T7*lac* promoter with a ribosome binding site.
[b] Restriction enzyme sites used in the cloning are shown in underlined italics.

Two co-replicable vectors, pETDuet-1 and pCDFDuet-1 (Novagen, Darmstadt, Germany), were used for construction of chiral 3HB biosynthetic pathways (*Tolia & Joshua-Tor, 2006*). Both Duet vectors contain two multiple cloning sites (MCS), each of which is preceded by a T7*lac* promoter and a ribosome binding site (RBS), affording high-level expression of each individual gene.

For cloning genes, PCR products incorporated with desired restriction sites within the 5' and 3' primers were first cloned into pGEM-T Easy vector (Promega, Madison, WI) using TA cloning. The resulting plasmids were then digested and the genes were subcloned into pETDuet-1 or pCDFDuet-1. The *hbd* gene was inserted in between the *EcoR*I and *Not*I sites (MCS I) of pETDuet-1 to create pET-H. The *phaB* gene was inserted between the *Nco*I and *Not*I sites (MCS I) of pETDuet-1 to create pET-P. Plasmids of pET-H-B, pET-H-T, and pET-H-P were constructed by inserting *bktB*, *thl*, and *phaA*, respectively, between the *Mfe*I and *Xho*I sites (MCS II) of pET-H. In a similar manner, plasmids pET-P-B, pET-P-T, and pET-P-P were constructed by inserting *bktB*, *thl*, and *phaA*, respectively, between the *Mfe*I and *Xho*I sites (MCS II) of pET-P. Plasmid pCDF-PB was created by inserting the *ptb-buk* operon between the *EcoR*I and *Sal*I sites of pCDFDuet-1. Cloning the *tesB* gene between the *EcoR*I and *Sal*I sites of pCDFDuet-1 resulted in plasmid pCDF-T. All constructs were confirmed to be correct by restriction enzyme digestion and nucleotide sequencing. Plasmids constructed in the present work are listed in **Table 3-1**.

3.2.3 Culture conditions

Seed cultures of the recombinant strains were grown in LB medium at 30°C overnight on a rotary shaker at 250 rpm. For the biosynthesis of chiral 3HB, the seed cultures were used to inoculate 50 mL LB medium in 250 mL flasks supplemented with 20 g L^{-1} glucose at an inoculation volume of 5%. Cultures were incubated at 30°C on a rotary shaker until OD_{600} reached 0.4~0.8. At this point, 1 mM IPTG was added to the cultures to induce recombinant protein expression. In all cases, LB medium was supplemented with 50 mg L^{-1} ampicillin and 25 mg L^{-1} streptomycin, and cultures were

incubated aerobically. Culture broth was sampled at 4 h post-induction for enzyme assays, and at 48 h post-induction for HPLC analysis.

3.2.4 Metabolite analysis and dry cell weight determination

Samples were centrifuged to pellet cells while the aqueous supernatant was collected for HPLC analysis. Concentrations of 3HB, glucose, and acetate were analyzed via HPLC using an Agilent 1100 series instrument equipped with a refractive index detector (RID). Analyte separation was achieved using an Aminex® HPX-87H anion exchange column (Bio-Rad Laboratories, Hercules, CA) according to the method of Buday et al. (*Buday et al., 1990*) using 5 mM H_2SO_4 as the mobile phase.

The dry cell weight (DCW) was determined in triplicates by filtering culture broth (25 mL) through a pre-weighed filter paper (0.45-μm cellulose acetate filters, Whatman, Maidstone, UK), followed by washing with deionized water (25 mL). The filter paper was then dried for two days in a 70°C oven and weighed for DCW determination. One OD_{600} unit was equivalent to 0.42 g-DCW L^{-1} for BL21Star(DE3) and 0.39 g-DCW L^{-1} for MG1655(DE3).

3.2.5 Methyl esterification of 3HB

50 mL of 3HB-containing LB microbial culture was centrifuged at 6000 x *g* for 10 min and the supernatant was transferred to an evaporation dish for evaporating overnight in a 50°C oven, resulting in a brown residue. To this residue, 2 mL of acidic methanol (4:1 methanol:concentrated HCl) was added and the dish was shaken for two minutes to remove 3HB from the residue. The methanol solution was transferred into a test tube, sealed, and heated at 100°C for 3 hours. After heating, the solution was allowed to cool to room temperature. After cooling, 200 μL of the methanol solution was mixed with 1 mL of pure isopropanol in a 1.7 mL tube, vortexed, and allowed to stand for 5 minutes. Precipitate in this sample was removed by centrifugation at 13,200 x *g* for 10 minutes. The supernatant was taken for chiral HPLC analysis.

3.2.6 Chiral HPLC analysis of methyl-3HB

Chiral HPLC analysis was performed on an Agilent 1100 Series instrument equipped with a Chiralcel OD-H column (0.46 cm ϕ x 25 cm) purchased from Daicel Chemical Industries (West Chester, PA). The column temperature was maintained at 40°C. Methyl-3HB was detected on a diode array detector at 210 nm. The mobile phase was 9:1 *n*-hexane:isopropanol and the flow rate through the column was 0.7 mL min^{-1}. Methyl-(*R*)-3HB and methyl-(*S*)-3HB purchased from Sigma-Aldrich (St. Louis, MO) were used as standards and had retention times of 7.78 and 9.37 min, respectively.

3.2.7 Enzyme assays

Samples of 5 mL culture broth were centrifuged at 5,000 × *g* and 4°C for 10 min. The pellets were resuspended in 200 µL of lysing buffer (1 Roche protease inhibitor cocktail tablet in 10.5 mL of 10 mM Tris-HCl supplemented with 1 mg mL^{-1} lysozyme; pH = 8.0). Crude cell lysates were prepared by freeze-thaw lysis, carried out by subjecting cells to five cycles of freezing in liquid nitrogen followed by thawing at 37°C. After centrifugation at 14,000 × *g* and 4°C for 20 min, the supernatant was taken for enzyme assays. The total protein concentration of this supernatant was determined by the method of Bradford (*Bradford, 1976*) using bovine serum albumin as a standard.

Activities of thiolases, including BktB, Thl, and PhaA, were assayed using acetoacetyl-CoA and CoA as substrates, and the decrease in acetoacetyl-CoA concentration was followed at 303 nm (*Inui et al., 2008*). Activities of PhaB and Hbd were assayed using acetoacetyl-CoA as substrate and NADPH or NADH as cofactor, respectively. The decrease of NADPH or NADH concentration resulting from 3-hydroxybutyryl-CoA formation from acetoacetyl-CoA was measured at 340 nm (*Inui et al., 2008, Schubert et al., 1988*).

3.2.8 Quantification of intracellular cofactor levels

The NAD^+, NADH, $NADP^+$, and NADPH were each determined using Enzychrom™ NAD^+/NADH and $NADP^+$/NADPH assay kits (Bioassay Systems, Hayward, CA).

Manufacturer's protocols were followed except that for sample preparation cells were resuspended in 100 µl extraction buffer and sonicated for 10 seconds on ice before heat extraction. The assays utilized alcohol dehydrogenase and glucose dehydrogenase for NAD(H) and NADP(H) quantifications, respectively, and colorimetric changes in the samples were measured at 565 nm.

3.3 Results

3.3.1 Production of chiral 3HB in BL21Star(DE3)

We first constructed the chiral 3HB pathways in BL21Star(DE3), an *E. coli* B strain, by co-transforming one pETDuet-1 derivative (pET-H-B, pET-H-T, pET-H-P, pET-P-B, pET-P-T, or pET-P-P) and one pCDFDuet-1 derivative (pCDF-T or pCDF-PB) (**Table 3-1**). All strains were cultured at 30°C for 48 h in LB medium supplemented with 20 g L^{-1} glucose, and accumulation of chiral 3HB in the culture medium was measured. We then compared capabilities of two sets of CoA-removing enzymes, Ptb-Buk and TesB, on (*R*)-3HB or (*S*)-3HB production.

Table 3-2 | Extracellular production of chiral 3HB by *E. coli* BL21Star(DE3) grown in shake flasks[a, b]

	3HB Synthesis Pathways			Acetate ($g\ L^{-1}$)	3HB ($g\ L^{-1}$)	3HB specific content ($g\ g\text{-}DCW^{-1}$)	3HB yield ($g\ g\text{-}Glucose^{-1}$)
	Step 1	Step 2	Step 3				
(S)-3HB	BktB	Hbd	Ptb-Buk	1.53 ± 0.13	<0.1	NA[c]	NA
	Thl			1.79 ± 0.03	<0.1	NA	NA
	PhaA			1.55 ± 0.14	<0.1	NA	NA
(R)-3HB	BktB	PhaB		1.33 ± 0.02	1.23 ± 0.06	1.19 ± 0.05	0.18 ± 0.01
	Thl			1.66 ± 0.08	1.03 ± 0.02	0.69 ± 0.01	0.15 ± 0.01
	PhaA			1.41 ± 0.11	1.26 ± 0.06	1.19 ± 0.15	0.20 ± 0.03
(S)-3HB	BktB	Hbd	TesB	0.89 ± 0.07	1.55 ± 0.05	1.50 ± 0.09	0.27 ± 0.01
	Thl			1.09 ± 0.12	1.58 ± 0.07	1.22 ± 0.06	0.24 ± 0.01
	PhaA			1.01 ± 0.03	1.44 ± 0.04	1.43 ± 0.04	0.26 ± 0.02
(R)-3HB	BktB	PhaB		0.88 ± 0.03	2.41 ± 0.04	2.24 ± 0.04	0.30 ± 0.00
	Thl			1.20 ± 0.03	1.90 ± 0.06	1.52 ± 0.03	0.26 ± 0.01
	PhaA			1.05 ± 0.09	2.36 ± 0.08	2.06 ± 0.17	0.30 ± 0.02

[a] Cells were grown aerobically in LB media with the addition of 2% glucose at 30°C for 48 h. 1 mM IPTG was added when OD_{600} reached 0.4~0.8.
[b] Data are presented as the average value and standard deviation of measurements from three independent cultures.
[c] NA: not applicable

TesB successfully removed the CoA moiety from both (*R*)-3HB-CoA and (*S*)-3HB-CoA to release the free acids (**Table 3-2**). In comparison, Ptb-Buk could also convert (*R*)-3HB-CoA but was essentially inactive on (*S*)-3HB-CoA. Titers as high as 1.58 g L^{-1} and 2.41 g L^{-1} of (*S*)-3HB and (*R*)-3HB, respectively, could be achieved when TesB was used to remove CoA. In the case of Ptb-Buk, only trace amount of (*S*)-3HB (less than 0.10 g L^{-1}) was produced, and 1.26 g L^{-1} of (*R*)-3HB was observed. It was also noted that less acetate, 1.02 g L^{-1} on average, was produced with the TesB system compared to that with the Ptb-Buk system, which was 1.55 g L^{-1} on average.

The efficacies of three different thiolases on chiral 3HB production were then compared. Both BktB and PhaA were found to yield similar titers of (*R*)-3HB when co-expressed with PhaB and Ptb-Buk (~1.25 g L^{-1}) or PhaB and TesB (~2.39 g L^{-1}). However, Thl gave approximately 20% lower titers of (*R*)-3HB and increased acetate production compared to BktB and PhaA. This phenomena was not observed in (*S*)-3HB production, where each of the thiolases resulted in similar titers of (*S*)-3HB, with an average of 1.52 g L^{-1}. In general, TesB could outperform Ptb-Buk for CoA removal, resulting in significantly higher titers of both (*R*)-3HB and (*S*)-3HB (**Table 3-2**).

3.3.2 Production of chiral 3HB in MG1655(DE3)

Since TesB was identified as the most effective enzyme among those tested for CoA removal in BL21Star(DE3), further investigation of MG1655(DE3), an *E. coli* K-12 strain, exclusively employed 3HB pathways using TesB. In all cases, (*R*)-3HB or (*S*)-3HB production was substantially higher with MG1655(DE3) than with BL21Star(DE3) under the same culture conditions (**Fig. 3-2**). MG1655(DE3) produced up to 2.08 g L^{-1} of (*S*)-3HB and 2.92 g L^{-1} of (*R*)-3HB, ~30% and ~20% higher titers, respectively, than those produced by BL21Star(DE3). It is also interesting to note that generally less acetate was produced in MG1655(DE3) than in BL21Star(DE3), suggesting that more acetyl-CoA carbon flux was directed towards 3HB biosynthesis in MG1655(DE3) than towards acetate production. These two production systems were also compared in terms of 3HB specific content (g g-DCW^{-1}) and 3HB yield (g g-$Glucose^{-1}$). 3HB specific contents

in MG1655(DE3) strains were ~50-120% greater than their respective BL21Star(DE3) counterparts as a result of increased 3HB production and reduced biomass accumulation (**Fig. 3-2**). The comparison of 3HB yield on glucose shows that the efficiency of 3HB production from glucose in MG1655(DE3) was higher than in BL21Star(DE3). Generally, MG1655(DE3) was able to produce more chiral 3HB and less acetate, while also accumulating less biomass than BL21Star(DE3).

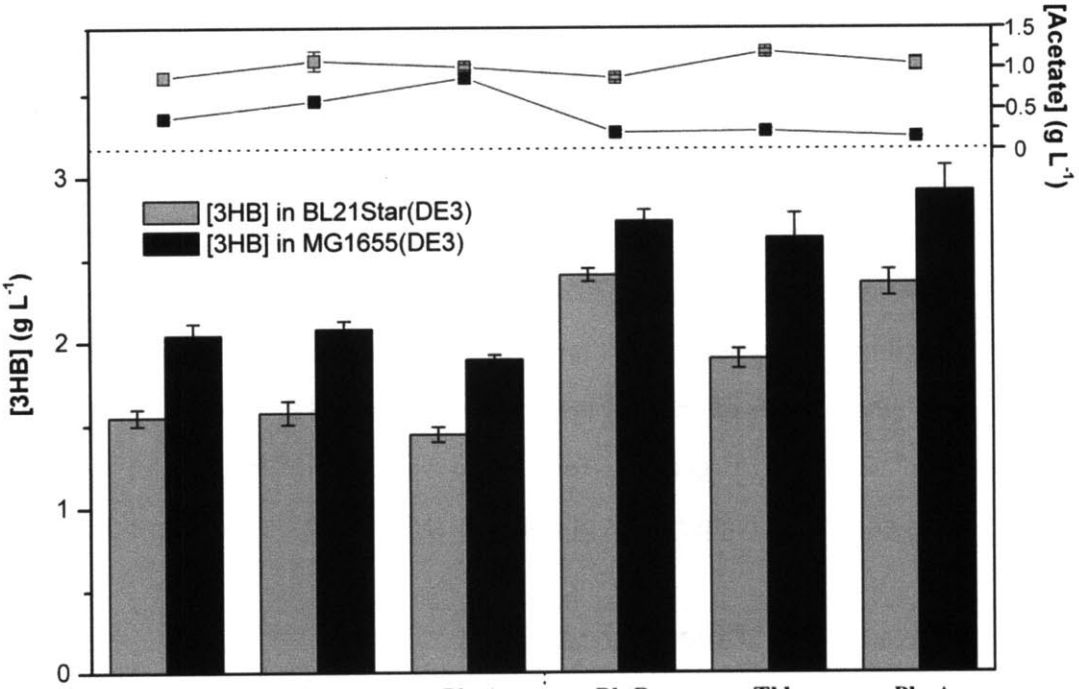

Thiolases	BktB		Thl		PhaA		BktB		Thl		PhaA	
3HB specific content (g g-DCW^{-1})	1.50	**2.31**	1.22	**2.62**	1.43	**2.42**	2.24	**3.41**	1.52	**3.41**	2.06	**3.63**
3HB Yield (g g-Glucose^{-1})	0.27	**0.34**	0.24	**0.31**	0.26	**0.27**	0.30	**0.43**	0.26	**0.38**	0.30	**0.41**
	(*S*)-3HB Biosynthesis Pathways (Hbd/TesB)						**(*R*)-3HB Biosynthesis Pathways (PhaB/TesB)**					

Figure 3-2 | Extracellular production of chiral 3HB by *E. coli* BL21Star(DE3) and MG1655(DE3) grown in shake flasks. *(S)*-3HB was produced when Hbd was employed (left), while *(R)*-3HB was produced when PhaB was employed (right). In all cases, TesB was used to mediate CoA removal.

3.3.3 Confirmation of 3HB stereochemistry

E. coli BL21Star(DE3) harboring *bktB*, *tesB*, and either *phaB* or *hbd* was grown at 30°C in 50 mL LB supplemented with 20 g L^{-1} glucose for 48 hours. The stereochemistry of the resulting 3HB in the media from these cultures was determined by methyl esterification of the 3HB present followed by chiral HPLC analysis as described in the Materials and Methods. The results confirm previous reports that cells

harboring a thiolase and CoA-removal enzyme produce (*R*)-3HB if the cells are concomitantly expressing *phaB* and synthesize (*S*)-3HB if they are expressing *hbd* (**Fig. 3-3**) (*Lee et al., 2008, Liu et al., 2007*).

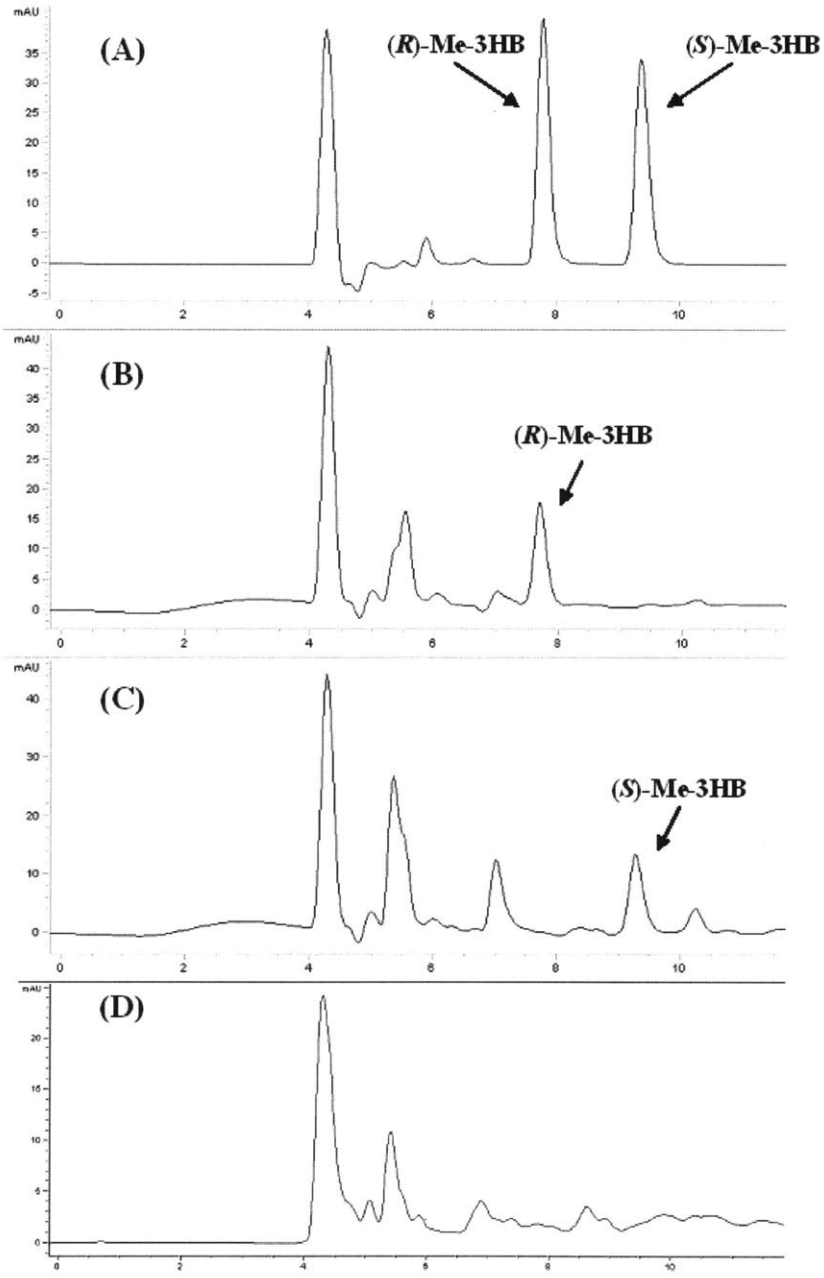

Figure 3-3 | HPLC spectra of (A) methyl-(*R*)-3HB and methyl-(*S*)-3HB standards, (B) culture medium from *E. coli* BL21Star(DE3) expressing *bktB, phaB* and *tesB* after boiling in methanol, (C) culture medium from *E. coli* BL21Star(DE3) expressing *bktB, hbd* and *tesB* after boiling in methanol, and (D) culture medium from *E. coli* BL21Star(DE3) after boiling in methanol as a control.

3.3.4 Measurement of specific activities of 3HB synthesis enzymes expressed in *E. coli*

To better understand the differences in 3HB titers between the different 3HB pathways in *E. coli* BL21Star(DE3) and MG1655(DE3), we sought to find a correlation between *in vivo* chiral 3HB production and *in vitro* enzyme activities. The activities of BktB, Thl, PhaA, Hbd and PhaB were measured in recombinant *E. coli* BL21Star(DE3) and MG1655(DE3).

Table 3-3 | Enzyme specific activities (U mg^{-1})[a] of crude extracts of *E. coli* BL21Star(DE3) and MG1655(DE3).

Enzymes		*E. coli* Strains[b]	
		BL21Star(DE3)	MG1655(DE3)
Acetoacetyl-CoA Thiolase	Control	0.04 ± 0.01	0.03 ± 0.00
	BktB	5.05 ± 0.69	1.10 ± 0.24
	Thl	29.66 ± 3.87	6.85 ± 0.97
	PhaA	5.90 ± 0.87	2.56 ± 0.36
3-Hydroxybutyryl-CoA Dehydrogenase	Control	ND[c]	ND
	Hbd	58.78 ± 7.76	40.76 ± 8.08
	PhaB	0.41 ± 0.18	0.33 ± 0.05

[a] One unit was defined as the conversion of 1 μmol of substrate to product per min at 25°C.
[b] Data are presented as the average value and standard deviation of measurements from three independent cultures.
[c] ND: not detected

The background acetoacetyl-CoA thiolase activities in *E. coli* BL21Star(DE3) and MG1655(DE3) were very weak (<0.04 U mg $protein^{-1}$), and there were undetectable 3-hydroxybuytyryl-CoA dehydrogenase activities (**Table 3-3**). Plasmid-based expression of BktB, Thl, PhaA, Hbd and PhaB was able to give functional enzymes in both *E. coli* strains (**Table 3-3**). It is interesting to note that all enzymes analyzed had greater specific activities in BL21Star(DE3) than in MG1655(DE3), showing approximately 130% to 360% higher thiolase activity and 24% to 44% higher 3-hydroxybuytyryl-CoA dehydrogenase activity, although 3HB production was lower. For comparison of alternative acetoacetyl-CoA thiolases, Thl had approximately 6-fold higher specific activity than BktB and PhaA in BL21Star(DE3), and 6-fold and 3-fold higher specific activity than BktB and PhaA, respectively, in MG1655(DE3). For 3-hydroxybuytyryl-CoA dehydrogenase activities of PhaB and Hbd, results show that the activities of Hbd

(NADH-dependent) were approximately 140-fold and 120-fold higher than those of PhaB (NADPH-dependent) in BL21Star(DE3) and MG1655(DE3), respectively.

3.3.5 Measurement of cofactor levels in engineered MG1655(DE3) strains

Although Hbd consistently showed higher *in vitro* activity than PhaB, the accumulated titers of (*S*)-3HB were lower than for (*R*)-3HB. Since these two enzymes have different pyridine nucleotide cofactor (NADPH/NADH) specificities, we measured intracellular levels of the reduced and oxidized cofactors to gain additional insights (**Table 3-4**). At the late exponential phase (4 h post-induction), the specific contents of NADH and NADPH in all tested recombinant strains were found to be significantly lower than those of their respective oxidized forms (NAD^+ and $NADP^+$), with the ratios of NADH/NAD^+ and NADPH/$NADP^+$ ranging from 0.08-0.16 and 0.26-0.31, respectively. At the stationary phase (24 h post-induction), reduced cofactor increased concomitantly with the decrease of oxidized cofactor, resulting in higher ratios of NADH/NAD^+ and NADPH/$NADP^+$ ranging from 0.20-0.44 and 0.79-0.99, respectively. Consistent with previously published reports (*Brumaghim et al., 2003, Lee et al., 1996*), in general NADH was found to be the predominant reducing equivalent in our *E. coli* strains while the NADPH/$NADP^+$ ratio was considerably higher than the NADH/NAD^+ ratio under the culture conditions examined.

Table 3-4 | Levels and ratios of NAD^+, NADH, $NADP^+$, and NADPH cofactors in engineered MG1655(DE3) strains.

Constructs		pET-H-P pCDF-T		pET-P-P pCDF-T		pETDuet pCDFDuet	
Post-induction time (hr)		4	24	4	24	4	24
Cofactor levels[a] (nmol/mg-DCW)	NAD^+	6.15 ± 0.75	3.95 ± 0.29	7.11 ± 0.08	4.94 ± 0.13	8.05 ± 1.09	4.79 ± 0.44
	NADH	0.97 ± 0.11	1.75 ± 0.02	0.59 ± 0.07	1.49 ± 0.21	0.85 ± 0.08	0.96 ± 0.06
	$NADP^+$	1.58 ± 0.16	0.96 ± 0.08	1.89 ± 0.18	1.22 ± 0.05	2.12 ± 0.04	1.12 ± 0.12
	NADPH	0.50 ± 0.08	0.94 ± 0.09	0.49 ± 0.03	0.97 ± 0.23	0.59 ± 0.02	0.97 ± 0.09
Cofactor ratios	NADH/NAD^+	0.16 ± 0.00	0.44 ± 0.03	0.08 ± 0.01	0.30 ± 0.03	0.11 ± 0.00	0.20 ± 0.01
	NADPH/$NADP^+$	0.31 ± 0.02	0.99 ± 0.18	0.26 ± 0.01	0.79 ± 0.16	0.28 ± 0.02	0.87 ± 0.01

[a]Data are presented as the average and standard deviation of measurements from two independent cultures.

3.3.6 Enhanced 3HB production

To further investigate the effect of intracellular cofactor levels on the chiral 3HB production, an independent project was assigned to a group of students in the course 10.28 (Chemical-Biological Engineering Laboratory) under my supervision. In that project, students investigated the effects of culture media on cell redox state and the production of 3HB in recombinant *E. coli*. Their research focused on optimizing the composition of culture media to affect cell redox state and increase the production of enantiopure (*R*)-3HB and (*S*)-3HB. Specifically, they focused on modifying various components of the culture medium, including base medium and carbon source, as well as adding metabolites and reducing agents to the medium. Overall, they obtained higher titers of both enantiomers of 3HB than our previously reported values by delaying induction during the late exponential phase at OD_{600} around 0.8 and supplementing dithiothreitol (DTT), a reducing agent that may result in higher levels of the cofactors NADH and NADPH. In addition, they further boosted production of both (*S*)-3HB and (*R*)-3HB with titers up to 3.47 g L^{-1} and 4.03 g L^{-1}, respectively, with supplementation of pyruvate, which can be metabolized to acetyl-CoA with generation of NADH (**Fig. 3-4**).

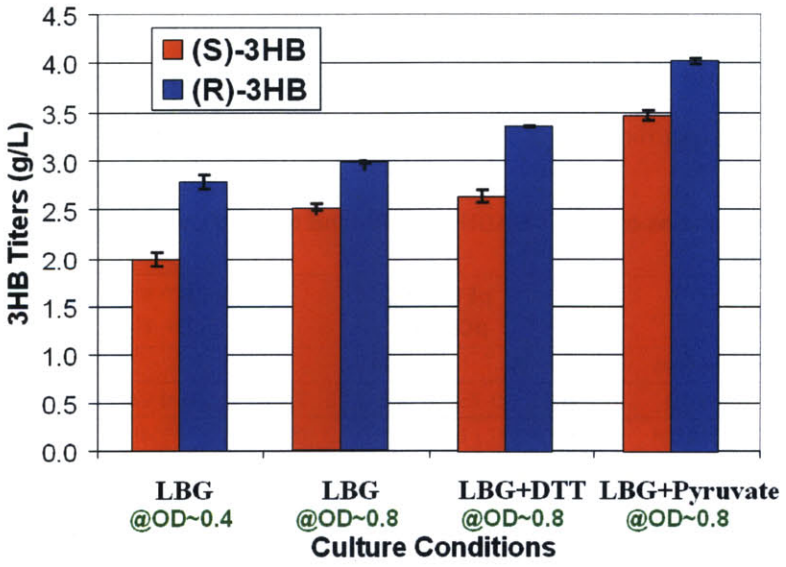

Figure 3-4 | Effects of media composition on the production of chiral 3HB. LBG denotes LB medium supplemented with 2% glucose. DTT or pyruvate was added at the time of induction by IPTG. Data are presented as the average and standard deviation of duplicates.

3.4 Discussion

The underlying objective of this study was to explore the high level production of both (*R*)- and (*S*)-3HB in recombinant *E. coli* by investigating different host strains, thiolase homologs, and CoA-removal mechanisms. We have achieved shake flask-scale production of enantiomerically pure (*R*)-3HB and (*S*)-3HB to concentrations of up to 2.92 g L^{-1} and 2.08 g L^{-1}, respectively. During the preparation of this manuscript, biosyntheis of enantiopure (*S*)-3HB was reported at titers of 0.61 g L^{-1} (*Lee et al., 2008*), which we believe is the highest reported concentration prior to this study.

3.4.1 *E. coli* B versus *E. coli* K-12 in chiral 3HB production

As previously described (*Phue et al., 2005*), there exist several intrinsic differences in metabolic pathways between *E. coli* B and K-12 strains, suggesting that the availability of metabolic intermediates as precursors for engineered biosynthetic pathways may also differ between these two strains. In addition, it has been generally concluded that the *E. coli* B strains are capable of producing greater amounts of proteins than the *E. coli* K-12 strains, making *E. coli* B strains better for protein production (*Terpe, 2006*). However, in terms of their role as microbial chemical factories, higher expression levels of recombinant proteins may not necessarily result in higher product titers, especially when substrate availability rather than enzymatic activity is rate limiting in the pathway. The results presented here support the hypothesis that host strain selection can critically influence the activity of recombinant enzymes as well as the productivity of a non-natural pathway. Although strains constructed in BL21Star(DE3) showed much higher acetoacetyl-CoA thiolase and 3-hydroxybuytyryl-CoA dehydrogenase activities than those constructed in MG1655(DE3), the chiral 3HB titers from recombinant BL21Star(DE3) were roughly 20% to 30% lower than those from MG1655(DE3). Such discrepancy between product titers and enzyme activities in those strains suggests that distribution of precursors, i.e., acetyl-CoA, and not enzyme expression levels was the limiting factor for chiral 3HB production. It further implies that metabolic networks play an important role in chiral

3HB synthesis (*Stelling et al., 2002*). This hypothesis is supported by the observation that significantly more cell mass (data not shown) and acetate were accumulated in BL21Star(DE3) probably due to a large fraction of carbon flux drawn into the TCA cycle and acetate production pathway at the acetyl-CoA node (**Fig. 3-1** and **3-2**). This flux distribution resulted in less acetyl-CoA directed into engineered chiral 3HB pathways in BL21Star(DE3). In contrast, MG1655(DE3), likely with a different distribution within its metabolic network, achieved high-level production of chiral 3HB while accumulating less cell mass and acetate despite its relatively lower enzyme activities. Since excess accumulation of cell mass and byproduct formation represent an inefficient use of carbon resources that will reduce the yield of desired products, MG1655(DE3) served as the superior production strain by better balancing its growth while maintaining efficient production of chiral 3HB.

3.4.2 Effect of alternative acetoacetyl-CoA thiolases on chiral 3HB production

It was originally anticipated that the three different acetoacetyl-CoA thiolases (Step 1 of **Fig. 3-1**) examined in this work would differ in terms of chiral 3HB production by directing different amounts of carbon flux (in the form of acetyl-CoA) into the engineered 3HB pathways. With the exception of Thl for (*R*)-3HB synthesis in BL21Star(DE3), the choice of thiolase had little effect on chiral 3HB titers even though the enzymes were found to display different specific activities *in vitro* in both recombinant strains (**Table 3-3**). Thl showed the highest *in vitro* specific activity in both strains, but recombinant BL21Star(DE3) with either Thl/PhaB/TesB or Thl/PhaB/Ptb-Buk yielded reduced (*R*)-3HB titers compared to other BL21Star(DE3) counterparts. To explain this contradiction, it should be noted that *in vitro* thiolase activity was assayed in the thiolytic direction, where two acetyl-CoA molecules were synthesized from one acetoacetyl-CoA and one CoA molecule. Thus, as a result of the combined effect of a hundred-fold lower PhaB activity compared to Hbd and a higher Thl activity compared to BktB and PhaA in BL21Star(DE3), the acetoacetyl-CoA synthesized by Thl could accumulate in the cell. Since the thiolytic reaction is highly

exergonic, thiolysis of acetoacetyl-CoA by thiolase is thermodynamically favored (*Masamune et al., 1989*). The accumulated acetoacetyl-CoA would then be cleaved into two acetyl-CoA molecules in the thiolytic direction, thereby supplying more acetyl-CoA to cell mass and acetate accumulation. In contrast, this did not occur in MG1655(DE3) probably due to the less active competing pathways towards cell mass and acetate accumulation and a negligible thiolytic reaction as a result of lower enzyme activities compared to BL21Star(DE3).

3.4.3 TesB versus Ptb-Buk as a CoA removal system

It has been suggested that the efficient removal of CoA from (*R*)-3HB-CoA can lead to enhanced (*R*)-3HB production (*Gao et al., 2002*), which could also be true for (*S*)-3HB production. To test this concept, two CoA-removal systems were assessed. The first is Ptb-Buk, encoded by an operon from *C. acetobutylicum*, which has been used for direct synthesis of polyhydroxyalkanoate (PHA) together with a PHA synthase utilizing the reverse reaction (i.e., the formation of the CoA thioester) (*Liu & Steinbuchel, 2000*). The second is TesB from *E. coli*, which is reported to possess a broad substrate specificity but unknown physiological function in *E. coli* (*Zheng et al., 2004*). While Ptb-Buk uses a two-step CoA-removal scheme through a phosphorylated intermediate, TesB catalyzes one-step CoA-removal by direct hydrolysis (**Fig. 3-1**). More chiral 3HB was likely produced in the TesB system than in the Ptb-Buk system due to the essentially irreversible hydrolysis by TesB. In addition, it was noted that pathways incorporating the Ptb-Buk system do not yield (*S*)-3HB (**Table 3-2**), which is consistent with a previous report by Lee et al. (*Lee et al., 2008*). The low level production (<0.10 g L^{-1}) of (*S*)-3HB produced by strains containing the Ptb-Buk system may have been due to the endogenous TesB activity in *E. coli*. In fact, in recombinant strains of *E. coli* BL21Star(DE3) in which *phaA* and *hbd* were solely expressed (i.e., no over-expression of *tesB* or *ptb-buk*), similarly low levels of (*S*)-3HB were also produced (data not shown).

3.4.4 Discrepancies between enzyme activities of Hbd and PhaB and production titers of (*S*)-3HB and (*R*)-3HB

Although Hbd demonstrated much higher *in vitro* specific activities than PhaB, significantly lower titers of (*S*)-3HB than (*R*)-3HB were achieved in all strains expressing Hbd (**Table 3-2** and **3-3**). This contradictory behavior may have been influenced by the following three factors *in vivo*: (1) the cofactor balance between NADH and NADPH and their respective oxidized counterparts; (2) the substrate preference of TesB for (*R*)-3HB-CoA over (*S*)-3HB-CoA; and (3) the competing pathway of fatty acid β-oxidation where (*S*)-3HB-CoA is an intermediate.

Given that Hbd and PhaB are NADH- and NADPH-dependent dehydrogenases, respectively, the physiological levels of NADH and NADPH and their redox ratios in *E. coli* most likely influences the *in vivo* catalytic activities of Hbd and PhaB, affecting chiral 3HB titers accordingly. Since NADH is the predominant reducing equivalent found in *E. coli* under normal conditions (*Brumaghim et al., 2003*) as well as conditions examined here (**Table 3-4**), these results indicate that Hbd should theoretically show higher *in vivo* activity than PhaB resulting in greater (*S*)-3HB than (*R*)-3HB production. The opposite, however, was observed in this study, suggesting that the physiological NADH/NADPH ratio alone can not resolve the contradiction. It may instead be explained by differences in the physiological ratios of $NADH/NAD^+$ and $NADPH/NADP^+$. We have shown that the ratio of $NADPH/NADP^+$ is substantially higher than that of $NADH/NAD^+$ in *E. coli* MG1655(DE3) under our culture conditions. These results, together with previous findings that the PHB synthesis is likely affected by the intracellular $NADPH/NADP^+$ ratio (*Lee et al., 1996*), suggest that in the case of chiral 3HB synthesis, a higher $NADPH/NADP^+$ ratio may result in more favorable reduction by PhaB while reduction by Hbd may be limited by the lower $NADH/NAD^+$ ratio. Overall, these observations are consistent with correspondingly higher yields of (*R*)-3HB than (*S*)-3HB in the present study.

In a similar manner to the substrate preference of Ptb-Buk for (*R*)-3HB-CoA, TesB might cleave (*R*)-3HB-CoA more efficiently than (*S*)-3HB-CoA. To verify this possibility,

it will be informative to perform *in vitro* enzyme assays using (*S*)-3HB-CoA and (*R*)-3HB-CoA as substrates. Unfortunately, the unavailability of these chemicals prevented us from pursuing this experiment.

The third hypothesis was tested using an *E. coli* mutant with an impaired fatty acid β-oxidation pathway. The *E. coli* MG1655(DE3) mutant was created using the method of Datsenko and Wanner (*Datsenko & Wanner, 2000*) by insertional inactivation of *fadB*, encoding 3-hydroxyacyl-CoA dehydrogenase. This *fadB* mutation should presumably attenuate or block the fatty acid β-oxidation cycle, thereby reducing the degradation of (*S*)-3HB-CoA. However, this mutant failed to achieve higher titers of (*S*)-3HB compared to its native counterpart (data not shown). It is possible that other FadB homologs were involved in the degradation of (*S*)-3HB-CoA. For example, *fadJ* (previously called *yfcX*), encodes a subunit of enoyl-CoA hydratase that has been shown to possess the same catalytic function as FadB (*Si Jae Park, 2004, Snell et al., 2002*).

3.5 Conclusions

The findings of this study suggest that the distribution of acetyl-CoA is likely the key factor affecting the production of chiral 3HB between *E. coli* BL21Star(DE3) and MG1655(DE3). Thus, in order to alter the distribution, further research should focus on blocking competing pathways for acetyl-CoA, for example, by deletion of acetate synthesis pathways comprised of acetate kinase and phosphotransacetylase (encoded by *ackA-pta*) or pyruvate oxidase (encoded by *poxB*) (*Lin et al., 2005*). Also, we can not entirely rule out the possibility that the overall higher titers of chiral 3HB in recombinant MG1655(DE3) might have been due to their higher TesB specific activities compared to BL21Star(DE3) counterparts in the case where CoA-removal is rate-limiting. Therefore, *in vitro* enzyme assays of both TesB and Ptb-Buk should be able to further elucidate the cause of superior titers of chiral 3HB in MG1655(DE3) than in BL21Star(DE3). Overall, production of ~3 g L^{-1} (*R*)-3HB and ~2 g L^{-1} (*S*)-3HB were achieved in shake flask cultures within two days. Further strain engineering should lead to more economical production of chiral 3HB.

Altogether, in Chapter 3, we showed the functional expression of various thiolase enzymes and 3-hydroxybutyryl-CoA dehydrogenase enzymes, resulting in chiral 3HB production. Those results suggest that a significant amount of carbon flux can be directed into synthesis of 3-hydroxybutyryl-CoA (3HB-CoA) that can further be reduced to a four-carbon alcohol, butanol, by the downstrean butanol pathway enzymes. To explore the possibility of employing the butanol pathway enzymes for pentanol biosynthesis, a similar approach to the 3HB production was conducted to assess the capability of the pathway enzymes to act on five carbon substrate analogues. Specifically, synthesis of 3-hydroxyvalerate (3HV), a five-carbon analogue to 3HB, was examined, and the results are described in Chapter 4.

CHAPTER 4

Chiral 3-Hydroxyvalerate Biosynthesis from Single Carbon Sources as In Vivo Assesment of the Top Pentanol Pathway

Abstract

Pentanol synthesis requires the ability of the upstream thiolase enzyme to condense propionyl-CoA with acetyl-CoA to establish a five-carbon skeleton. Therefore, Chapter 4 describes selection of such thiolase enzyme to support 3HV biosynthesis. Furthermore, construction of a pathway allowing for endogenous propionyl-CoA supply from glucose or glycerol is also described in this chapter. Here, we report the selective biosynthesis of each 3HV stereoisomer from a single, renewable carbon source using synthetic metabolic pathways in recombinant strains of *Escherichia coli*. The product chirality was controlled by utilizing two reductases of opposing stereoselectivity. Improvement of the biosynthetic pathway activity and host background was carried out to elevate both the 3HV titers and 3HV/3HB ratios. Overall, shake-flask titers as high as 0.31 g/L and 0.50 g/L of (*S*)-3HV and (*R*)-3HV, respectively, were achieved in glucose-fed cultures, whereas glycerol-fed cultures yielded up to 0.19 g/L and 0.96 g/L of (*S*)-3HV and (*R*)-3HV, respectively. Our work represents the first report of direct microbial production of enantiomerically pure 3HV from a single carbon source. Continued engineering of host strains and pathway enzymes will ultimately lead to more economical production of chiral 3HV.

This chapter was published as:

Tseng, H.-C., Harwell, C.L., Martin, C., Prather, K.L.J. 2010. "Biosynthesis of chiral 3-hydroxyvalerate from single propionate-unrelated carbon sources in metabolically engineered *E. coli*" ***Microb Cell Fact*** 9:96

4.1 Introduction

The efficient production of enantio-pure chemicals from renewable resources has gained considerable attention especially in the fine chemical/pharmaceutical industry. Stereo-selective chemical processes generally employ expensive chiral catalysts, require harsh physical conditions and solvents, and suffer from extensive byproduct formation. In contrast, enzyme-catalyzed reactions are highly stereo-selective and can be performed in aqueous solutions under mild conditions (*Patel, 2000*). As a result, replacing chemical processes by biological ones for the synthesis of chiral compounds has been extensively investigated not only due to superior stereo-selectivity of enzymatic reactions but also due to sustainability as an implementation of green chemistry (*Chen & Wu, 2005, Shiraki et al., 2006, Tokiwa & Calabia, 2008, Zhao et al., 2003*). One example is the production of hydroxyacids, a family of versatile chiral molecules containing one hydroxyl group and one carboxyl group (*Ren et al.*). These molecules have the potential to serve as useful chiral building blocks for a diverse range of products, including polyhydroxyalkanoates (PHAs) (biodegradable polymers) and optically-active fine chemicals, such as pharmaceuticals, vitamins, antibiotics, and flavor compounds (*Chiba & Nakai, 1987, Chiba & Nakai, 1985, Mori, 1981, Seebach et al., 1986*). Naturally, hydroxyacids are primarily found to be polymerized as PHAs where they serve as intracellular storage materials for numerous microbes. Those PHAs consist mostly of monomers with 3-hydroxy, 4-hydroxy, and 5-hydroxy groups with different lengths of main and side chains (*Steinbuchel & Valentin, 1995*).

Among the hydroxyacid monomers, 3-hydroxybutyrate (3HB) is the most prolific, with several reports on engineering *E. coli* for its production from renewable feedstocks. Biosynthesis of 3HB begins with the condensation of two acetyl-CoA molecules, a commonly found cellular metabolite regardless of carbon source (**Fig. 4-1**). However, economically-feasible production of longer-chain hydroxyacids is complicated by issues such as low yields and high prices of feedstocks due to the need to supplement a second carbon source. One example of such hydroxyacids is 3-hydroxyvalerate (3HV). The production of 3HV has been realized by the hydroxylation of valeric acid through

fermentation of *Candida rugosa* (*Hasegawa J, 1981*). It has also been reported that 3-hydroxyvaleronitrile can be converted into 3HV using the nitrilase activity of *Comamonas testosteroni* (*Bramucci, 2006*).

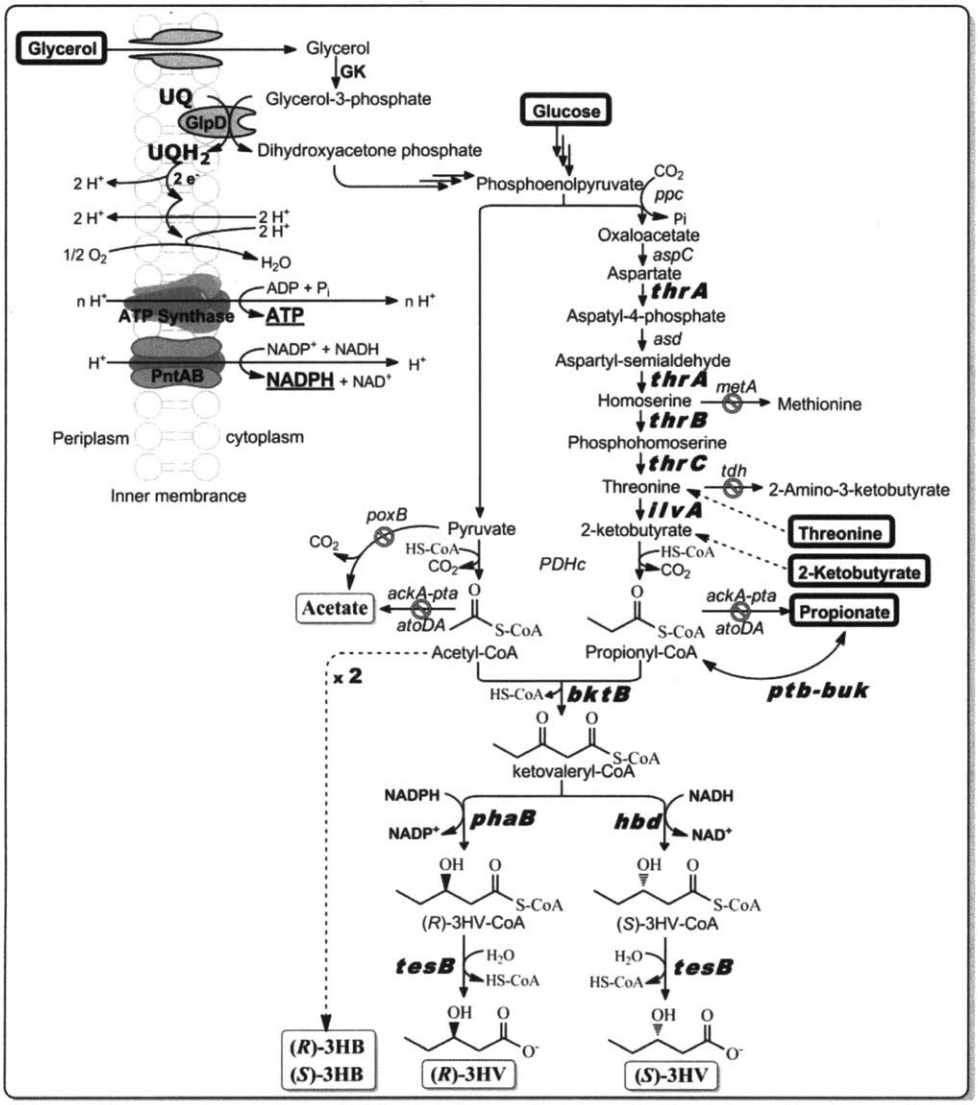

Figure 4-1 | Schematic representation of chiral 3HV production via the threonine biosynthesis pathway in metabolically engineered *E. coli*. Genes in bold are overexpressed while disrupted pathway steps are indicted by the "no" symbols. The carbon sources and main metabolic products in the system are enclosed by rectangular boxes with thick and thin lines, respectively. For glycerol utilization (*Abramson et al., 2000, Yeh et al., 2008*), a glycerol kinase (GK) phosphorylates glycerol to glycerol-3-phosphate, followed by oxidation to dihydroxyacetone phosphate that enters glycolysis. The oxidation reaction is catalyzed by a membrane enzyme called glycerol-3-phosphate dehydrogenase (GlpD) with concomitant production of ubiquinol (UQH_2) from ubiquinone (UQ). Electrons stored in the ubiquinol are then transferred through the aerobic respiratory chain coupled with proton translocation from cytoplasm to periplasm. Both ATP and NADPH can be synthesized by an H^+-driven proton movement from periplasm to cytoplasm, catalyzed by an ATP synthase and a membrane-bound transhydrogenase (PntAB), respectively.

More recently, direct biological production of 3HV was demonstrated using recombinant *P. putida* KT2440 and levulinic acid as substrate, although the levulinic acid metabolism pathway in *P. putida* KT2440 has not yet been fully elucidated (*Martin & Prather, 2009*). In the aforementioned cases, valeric acid, 3-hydroxyvaleronitrile, and levulinic acid were supplied as secondary carbon sources (in addition to glucose). Additionally, the chirality and/or enantiopurity of the 3HV produced in the above-mentioned studies is unclear as they did not report whether the synthesized 3HV was in the *R*, *S*, or racemic form. Alternatively, 3HV can be obtained through either the *in vivo* or *in vitro* enzymatic depolymerization of synthesized poly(3-hydroxybutyrate-co-3-hydroxyvalerate) (PHBV), a well known biodegradable polymer marketed as Biopol™ which is produced by the natural PHA accumulating bacterium *Ralstonia eutropha* when grown on glucose and propionate (*Slater et al., 1998*). The production of PHBV has also been reported in recombinant *E. coli* upon introduction of the PHA biosynthesis genes of *R. eutropha* and when grown in glucose medium supplemented with valine or threonine (*Eschenlauer et al., 1996*). Regardless of whether the end product is 3HV or PHBV, it can be generally concluded that supplementation of a second carbon source, such as valeric acid, 3-hydroxyvaleronitrile, levulinic acid, propionate, valine, or threonine in addition to glucose, is necessary to provide the 5-carbon unit precursor of 3HV. Unfortunately, the high price and/or toxicity of the added second carbon sources could limit industrial production of 3HV (*Poirier et al., 1995*). Therefore, synthesis of 3HV from a single carbon source has been proposed as an efficient and sustainable avenue in contrast to the above-mentioned systems.

A novel pathway for the production of PHBV solely from glycerol has been established in recombinant *Salmonella enterica* Serovar Typhimurium, containing a heterologous pathway that converts succinyl-CoA to propionyl-CoA, the essential precursor molecule of 3HV-CoA in PHBV synthesis (*Aldor et al., 2002*). However, expensive cyanocobalamin (CN-B_{12}) was supplemented to the medium to provide the precursor of coenzyme B_{12} required for the activity of one of the enzymes in the

B_{12}-dependent biosynthetic pathway. It should also be noted that the pathway only functioned in *S. enterica*, a pathogen, but not *E. coli*, thus limiting its applicability to other industrially-relevant host organisms. In this study, we proposed an alternative biosynthetic pathway that does not require coenzyme B_{12} for its functionality to synthesize 3HV from glucose or glycerol. Specifically, we metabolically engineered *E. coli* to exploit its native metabolism for endogenous supply of propionyl-CoA via the threonine biosynthesis pathway, and introduced a heterologous pathway for chiral 3HV biosynthesis using acetyl-CoA and propionyl-CoA as precursor molecules. As stated above, several previous methods for producing 3HV did not focus on enantiopure synthesis. Similarly, due to the stereospecific constraints of PHBV synthesis, in which polymers are composed exclusively of (*R*)-3HB and (*R*)-3HV monomer units, the synthesis of (*S*)-3HV from PHBV remains effectively impossible. On the contrary, our proposed pathway makes possible the direct synthesis of both enantiomerically pure (*R*)-3HV and (*S*)-3HV.

We have identified a pathway which combines elements of our previously developed chiral 3HB biosynthesis pathway together with the natural threonine biosynthesis pathway of *E. coli* for direct biosynthesis of chiral 3HV (**Fig. 4-1**). In the proposed pathway, chiral 3HV is produced from direct hydrolysis of 3HV-CoA catalyzed by a thioesterase II (encoded by *tesB*) where 3HV-CoA is obtained from condensation of one acetyl-CoA and one propionyl-CoA to form 3-ketovaleryl-CoA catalyzed by a thiolase (encoded by *bktB*), followed by a reduction of the 3-ketovaleryl-CoA to 3HV-CoA catalyzed by a 3-hydroxybutyryl-CoA dehydrogenase. Here, two enantio-selective 3-hydroxybutyryl-CoA dehydrogenases were utilized to control the chirality of 3HV-CoA produced. The NADPH-dependent dehydrogenase encoded by *phaB* produces (*R*)-3HV-CoA while the NADH-dependent dehydrogenase encoded by *hbd* produces (*S*)-3HV-CoA. It should be noted that in order to yield the highest 3HV titers and 3HV/3HB ratios, BktB was used as the thiolase in this study as opposed to other thiolases such as PhaA from *R. eutropha* H16 or Thl from *C. acetobutylicum* ATCC 824 because BktB has been shown to have highest *in vitro* enzyme activity towards the C_5

substrate while PhaA and Thl were specific towards the C_4 substrate (*Slater et al., 1998*). Next, a pathway allowing for endogenous propionyl-CoA synthesis from glucose or glycerol, through the threonine metabolic pathway intermediate 2-ketobutyrate, was introduced to circumvent the need for feeding propionate. To examine the upstream pathway for endogenous supply of propionyl-CoA, we used a bottom-up approach where 2-ketobutyrate and threonine were, at first, fed to provide propionyl-CoA, in addition to glucose, to support 3HV production. In the final stage, a single carbon source of glucose or glycerol was used to provide both acetyl-CoA and propionyl-CoA to support 3HV biosynthesis in our metabolically engineered *E. coli*.

Overall, in this study we successfully demonstrated the direct biological production of enantiomerically pure (*R*)-3HV and (*S*)-3HV from a single carbon source. Improvements of the biosynthetic pathway and *E. coli* host strains have also been carried out to elevate 3HV titers and 3HV/3HB ratios.

4.2 Materials and Methods

4.2.1 Microorganisms

The bacterial strains used are listed in Table 1. *C. acetobutylicum* ATCC 824, *C. glutamicum* ATCC 13032, and a threonine hyper-producer *E. coli* ATCC 21277 were purchased from the American Type Culture Collection (ATCC, Manassas, VA). *R. eutropha* H16 was provided by Professor Anthony Sinskey of the Department of Biology at the Massachusetts Institute of Technology (Cambridge, MA, USA). *E. coli* DH10B (Invitrogen, Carlsbad, CA) and ElectroTen-Blue (Stratagene, La Jolla, CA) were used for transformation of cloning reactions and propagation of all plasmids. MG1655 (kindly donated by Professor Gregory Stephanopoulos of the Department of Chemical Engineering at the Massachusetts Institute of Technology, USA) was used as the parental strain for genetic modification. Host gene deletions of *endA*, *recA*, *atoDA*, *ackA-pta*, *poxB*, *tdh*, *metA*, and *atoB* were achieved with P1 transduction using the Keio collection strains as donor cells (*Baba et al., 2006*). The kanamycin cassette was removed using plasmid pCP20 as described by Datsenko and Wanner (*Datsenko &*

Wanner, 2000) and the successfully constructed mutant strains were verified by colony PCR using appropriate primers. Strains carrying a λDE3 lysogen were constructed using a λDE3 Lysogenization Kit (Novagen, Darmstadt, Germany) for site-specific integration of λDE3 prophage into each host.

4.2.2 Plasmid construction

Genes derived from *C. acetobutylicum* ATCC 824 (*hbd* and *ptb-buk* operon), *R. eutropha* H16 (*bktB* and *phaB*), *C. glutamicum* ATCC 13032 (*ilvA*), *E. coli* MG1655 (*tesB, ilvA, and thrABC* opeon), and *E. coli* ATCC 21277 ($thrA^{G1297A}BC$ opeon) were obtained by polymerase chain reaction (PCR) using genomic DNA (gDNA) templates. All gDNAs were prepared using the Wizard Genomic DNA Purification Kit (Promega, Madison, WI). Custom oligonucleotides (primers) were purchased for all PCR amplifications (Sigma-Genosys, St. Louis, MO) as listed in **Table 4-1**. In all cases, Phusion High Fidelity DNA polymerase (Finnzymes, Espoo, Finland) was used for DNA amplification. Restriction enzymes and T4 DNA ligase were purchased from New England Biolabs (Ipswich, MA). Recombinant DNA techniques were performed according to standard procedures (*Sambrook & Russell, 2001*). Three co-replicable vectors, pETDuet-1, pCDFDuet-1, and pCOLADuet-1 (Novagen, Darmstadt, Germany), were used for construction of chiral 3HV biosynthetic pathways (*Tolia & Joshua-Tor, 2006*). All vectors contain two multiple cloning sites (MCS), each of which is preceded by a T7*lac* promoter and a ribosome binding site (RBS), affording high-level expression of each individual gene.

Plasmids constructed in the present work are listed in **Table 4-1**. For cloning genes, PCR products incorporated with desired restriction sites within the 5' and 3' primers were digested, and the resulting DNA fragments were then cloned into pETDuet-1, pCDFDuet-1, or pCOLADuet-1. The *bktB* gene was inserted in between the *Mfe*I and *Xho*I sites (MCS II) of pETDuet-1 to create pET-B. The *ptb-buk* gene, digested from pCDF-PB with EcoRI and NotI (*Tseng et al., 2009*), was inserted between the *Eco*RI and *Not*I sites (MCS I) of pET-B to create pET-PB-B. Plasmid pCDF-H was created by

inserting the *hbd* gene between the *Nde*I and *Avr*II sites (MCS II) of pCDFDuet-1. Cloning the *tesB* gene between the *Nco*I and *Not*I sites (MCS I) of pCDFDuet-1 resulted in plasmid pCDF-T. Plasmid pCDF-T-H was then created by inserting the *hbd* gene between the *Nde*I and *Avr*II sites (MCS II) of pCDF-T. In a similar manner, plasmid pCDF-P was created by inserting the *phaB* gene between the *Mfe*I and *Avr*II sites (MCS II) of pCDFDuet-1. Plasmid pCDF-T-P was created by inserting the *phaB* gene between the *Mfe*I and *Avr*II sites (MCS II) of pCDF-T. Plasmids of pCOLA-Iec and pCOLA-Icg were constructed by inserting the *E. coli ilvA* and *C. glutamicum ilvA*, respectively, between the *Nde*I and *Avr*II sites (MCS II) of pCOLADuet-1. The *thrABC* operon from MG1655 was inserted in between the *Nco*I and *Sal*I sites (MCS I) of pCOLADuet-1 to create pCOLA-Tec. Plasmid pCOLA-Tec-Icg was then created by inserting the *C. glutamicum ilvA* gene between the *Nde*I and *Avr*II sites (MCS II) of pCOLA-Tec. To construct plasmid pCOLA-Tecm-Icg, the *thrA*^{G1997A}*BC* operon from *E. coli* ATCC 21277 was inserted in between the *BamH*I and *Sal*I sites (MCS I) of pCOLA-Icg. All constructs were confirmed to be correct by restriction enzyme digestion and nucleotide sequencing.

Table 4-1 | *E. coli* strains, plasmids and oligonucleotides used.

Name	Relevant Genotype	Reference
Strains		
DH10B	F$^-$ *mcr*A Δ(*mrr-hsd*RMS-*mcr*BC) ϕ80*lacZ*ΔM15 Δ*lacX74 recA1 endA1 araD139*Δ(*ara, leu*)7697 *galU galK* λ$^-$ *rpsL nupG*	Invitrogen
ElectroTen-Blue	Δ(*mcrA*)*183* Δ*(mcrCB-hsdSMR-mrr)173 endA1 supE44 thi-1 recA1 gyrA96 relA1 lac* Kan^r [F′ *proAB lacI*^{q}ZΔM15 Tn*10* (Tet^r)]	Stratagene
MG1655	F$^-$ λ$^-$ *ilvG- rfb-50 rph-1*	ATCC 700926
HCT 10	MG1655 Δ*endA* Δ*recA* (DE3)	This study
HCT 11	MG1655 Δ*endA* Δ*recA* Δ*atoB* (DE3)	This study
HCT 20	MG1655 Δ*endA* Δ*ackA-pta* Δ*atoDA* Δ*poxB* (DE3)	This study
HCT 21	MG1655 Δ*endA* Δ*ackA-pta* Δ*atoDA* Δ*poxB* Δ*metA* Δ*tdh* (DE3)	This study
Plasmids		
pETDuet-1	ColE1(pBR322) *ori*, *lacI*, T7*lac*, Amp^R	Novagen
pCDFDuet-1	CloDF13 *ori*, *lacI*, T7*lac*, Strep^R	Novagen
pCOLADuet-1	COLA *ori*, *lacI*, T7*lac*, Kan^R	Novagen
pET-B	pETDuet-1 harboring *bktB* from *R. eutropha* H16	This study
pET-PB-B	pETDuet-1 harboring *ptb-buk* operon from *C. acetobutylicum* ATCC 824, and *bktB* from *R. eutropha* H16	This study
pCDF-H	pCDFDuet-1 harboring *hbd* from *C. acetobutylicum* ATCC 824	This study
pCDF-T-H	pCDFDuet-1 harboring *tesB* from *E. coli* MG1655, and *hbd* from *C. acetobutylicum* ATCC 824	This study

pCDF-P	pCDFDuet-1 harboring *phaB* from *R. eutropha* H16	This study
pCDF-T-P	pCDFDuet-1 harboring *tesB* from *E. coli* MG1655, and *phaB* from *R. eutropha* H16	This study
pCOLA-Iec	pCOLADuet-1 harboring *ilvA* from *E. coli* MG1655	This study
pCOLA-Icg	pCOLADuet-1 harboring *ilvA* from *C. Glutamicum*	This study
pCOLA-Tec-Icg	pCOLADuet-1 harboring *thrABC* operon from *E. coli* MG1655, and *ilvA* from *C. glutamicum* ATCC 13032	This study
pCOLA-Tecm-Icg	pCOLADuet-1 harboring *thrA*^{G1297A}*BC* operon from *E. coli* ATCC 21277, and *ilvA* from *C. glutamicum* ATCC 13032	This study

Primers	**Sequence 5'→3'**[a]	
bktB_US_EcoRI	*GAATTC*ATGACGCGTGAAGTGGTAGTG	Sigma-Genosys
bktB_DS_XhoI	*CTCGAG*CGCAAGGCTAACCTCAGAT	Sigma-Genosys
hbd_US_NdeI	ATT*CATATG*AAAAAGGTATGTGTTATAGG	Sigma-Genosys
hbd_DS_AvrII	ATT*CCTAGG*CAGGTCGACTCTAGAACTTA	Sigma-Genosys
phaB_US_MfeI	ATT*CAATTG*ACGAAGCCAATCAAGGAG	Sigma-Genosys
phaB_DS_AvrII	ATT*CCTAGG*GGTCAGCCCATATGCAG	Sigma-Genosys
tesB_US_NcoI	ATT*CCATGG*GCATGAGTCAGGCGCTAA	Sigma-Genosys
tesB_DS_NotI	ATT*GCGGCCGCG*ACTCTAGAGACTTAATTGTG	Sigma-Genosys
ilvAec_US_NdeI	ATTA*CATATG*GCTGACTCGCAAC	Sigma-Genosys
ilvAec_DS_AvrII	ATTA*CCTAGG*CATTTTTCCCTAACC	Sigma-Genosys
ilvAcg_US_NdeI	ATTA*CATATG*AGTGAAACATACGTGTC	Sigma-Genosys
ilvAcg_DS_AvrII	ATTA*CCTAGG*CCTTCAGCTATGTTTA	Sigma-Genosys
thrABC_US_BamHI	ATTA*GGATCC*AAGGAGATATATCATGCGAGTGTTGAAG	Sigma-Genosys
thrABC_US_NcoI	ATTA*CCATGG*GCATGCGAGTGTTGAAG	Sigma-Genosys
thrABC_DS_SalI	ATTA*GTCGAC*GATAATGAATAGATTTTACTGATG	Sigma-Genosys

[a] Restriction enzyme sites used in the cloning are shown in underlined italics.

4.2.3 Culture conditions

Seed cultures of the recombinant strains were grown in LB medium at 30°C overnight on a rotary shaker at 250 rpm. For the biosynthesis of chiral 3HV, the seed cultures were used to inoculate 50 mL LB medium supplemented with 20 g/L glucose or 20 g/L glycerol at an inoculation volume of 2% in 250 mL flasks. Cultures were then incubated at 30°C on a rotary shaker until OD_{600} reached 0.8~1.0. At this point, 1 mM IPTG was added to the cultures to induce recombinant protein expression. Following induction, cells were cultivated at 30°C and sampled at 24 h intervals for up to 72 h post-induction for HPLC analysis. We found that both 3HB and 3HV titers did not reach a plateau until 48 h and that there was essentially no difference in the titers between 48 h and 72 h. Accordingly, only the peak titers observed at 48 h were reported in this study. In some experiments as indicated, 20 mM (~1.92 g/L) sodium propionate, 3 g/L sodium

2-ketobutyrate, or 3 g/L threonine was added into the cultures at the same time of induction. In all cases, LB medium was supplemented with 50 mg/L ampicillin, 50 mg/L streptomycin, and 30 mg/L kanamycin, as appropriate. In general, experiments were performed in triplicates, and data are presented as the averages and standard deviations of the results.

4.2.4 Metabolite analysis

Samples were centrifuged to pellet cells while the aqueous supernatant was collected for HPLC analysis. Products of interest, including 3HB, 3HV, glucose, glycerol, 2-ketobutyrate, acetate, and propionate, were analyzed via HPLC using an Agilent 1100 series instrument equipped with a refractive index detector (RID) and a diode array detector (DAD). Given that the 3HB peak is overlapped with the glycerol peak in the RID chromatogram, detection of 3HB in the glycerol-fed cultures was achieved using the DAD at 210 nm. Analyte separation was achieved using an Aminex® HPX-87H anion exchange column (Bio-Rad Laboratories, Hercules, CA) with 5 mM H_2SO_4 as the mobile phase. The mobile phase was pumped at a constant rate of 0.6 mL/min, and the column and detector temperatures were each set at 35°C throughout. Concentrations were determined by linear extrapolation from calibration of external standards.

4.2.5 Chiral analysis of 3HV

The stereochemistry of 3HV produced was determined by methyl esterification of the 3HV present in the medium followed by chiral HPLC analysis as described in a previously reported method (*Tseng et al., 2009*). The chiral analysis was performed on an Agilent 1100 Series instrument equipped with a Chiralcel OD-H column (0.46 cm ϕ x 25 cm) purchased from Daicel Chemical Industries (West Chester, PA). Methyl-3HV was detected on a DAD at 210 nm. The mobile phase was 9:1 *n*-hexane:isopropanol and the flow rate through the column was 0.7 mL/min. Due to unavailability of standards of Methyl-(*R*)-3HV and Methyl-(*S*)-3HV, these spectra were compared to a racemic 3HV standard (Epsilon Chimie, Brest, France) derivatized by methyl esterification.

4.3 Results

4.3.1 3HV synthesis from glucose and propionate

Acetyl-CoA is an obligate central intermediate occurring in any organism and under any physiological condition; however, this is not the case for propionyl-CoA, which is only synthesized under special physiological conditions and from only few substrates (*Madison & Huisman, 1999*). Therefore, synthesis of 3HV-CoA requires propionyl-CoA biosynthesis. To validate our 3HV biosynthesis pathway, propionate was initially fed to provide propionyl-CoA as a precursor molecule to ensure the downstream pathway was capable of making chiral 3HV. It has been reported that the *R. eutropha* PHA biosynthesis genes can be functionally expressed in *E. coli,* resulting in homopolymer PHB production from glucose (*Slater et al., 1992*). However, low levels of 3HV monomer within the synthesized co-polymer PHBV was observed in recombinant *E. coli* when propionate was co-fed with glucose in a way analogous to the procedure used for *R. eutropha* (*Slater et al., 1992*). One explanation for the low content of 3HV monomer is that *E. coli* does not possess an efficient system for importing and/or converting propionate to propionyl-CoA. Therefore, to address the propionate utilization problem, a CoA-activation mechanism (encoded by the *ptb-buk* operon (*Liu & Steinbuchel, 2000*)) was incorporated into our previously developed 3HB pathway to investigate the substrate elasticity of the pathway for 3HV production.

Our results show that, in the absence of the CoA-activation mechanism, i.e. Ptb-Buk, only trace amount of 3HV was produced (**Fig. 4-2**). On the contrary, introducing Ptb-Buk into the pathway yielded up to 2 g/L of both enantiomers of 3HV. It was noted that for strains expressing Ptb-Buk but leaving out TesB, only (*R*)-hydroxyacids (when PhaB was employed) were produced, consistent with a previous report that Ptb-Buk forms a reversible, stereo-seletive enzyme system (*Lee et al., 2008*). Overall, these results indicate that CoA-activation was crucial for propionate utilization and, most importantly, all enzymes originally utilized for 3HB biosynthesis were able to catalyze synthesis of C_5 molecules.

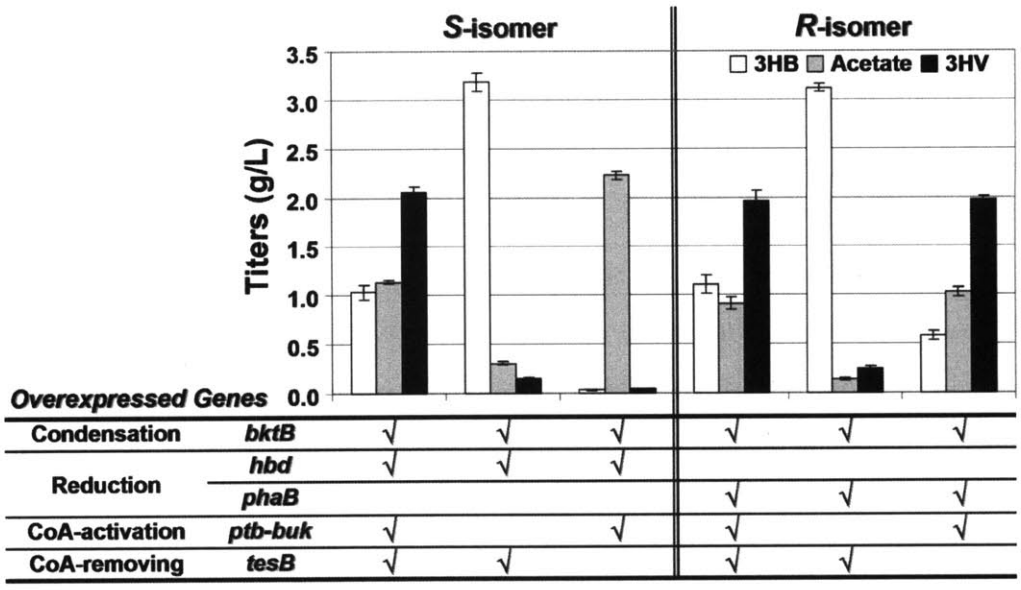

Figure 4-2 | 3HV biosynthesis from glucose and propionate. This figure shows shake-flask production of chiral 3HV by recombinant *E. coli* strain HCT 10 grown in LB supplemented with 20 g/L glucose and 20 mM sodium propionate. Over-expressed genes are indicated in the table below the graph.

4.3.2 3HV synthesis from glucose and 2-ketobutyrate

Propionyl-CoA can also be produced from 2-ketobutyrate, a common keto-acid intermediate for isoleucine biosynthesis, by the action of the endogenous pyruvate dehydrogenase complex enzyme (encoded by *PDHc*) (**Fig. 4-1**) (*Bisswanger, 1981*). We first compared 3HV production from glucose and 2-ketobutyrate using pathways with and without over-expression of the *ptb-buk* operon. The results showed that the presence of Ptb-Buk reduced production of propionate (only observed in the *R*-isomer construct) and 3HB while increasing production of acetate and 3HV, yielding (*S*)-3HV and (*R*)-3HV with titers up to 0.38 g/L and 1.02 g/L, respectively (**Fig. 4-3**). The increased production of acetate and 3HV was presumably due to the promiscuous activity of Ptb-Buk on cleaving excess acetyl-CoA and activating excess propionate. Given that 3HB production is a second-order reaction that should have a rate proportional to the square of the concentration of acetyl-CoA, a reduced acetyl-CoA pool resulting from the promiscuous activity of Ptb-Buk likely caused a significant decrease in 3HB production. In addition, propionyl-CoA is a competing substrate for BktB, so an increase in propionyl-CoA concentration may also reduce 3HB production.

In an effort to decrease acetate and increase 3HV production, several genes, including *atoDA* (encoding acetoacetyl-CoA transferase), *poxB* (encoding pyruvate oxidase), and *ackA-pta* (encoding acetate kinase and phosphate acetyltransferase) were deleted, and the resulting strain was designated as HCT 20. The production of (*S*)-3HV and (*R*)-3HV was further boosted to titers of 0.60 g/L and 2.04 g/L, respectively, in the recombinant acetate pathway knockout strains (HCT 20). In general, those strains produced less acetate and propionate and yielded more 3HB and 3HV compared to strains without these mutations (based on HCT 10), probably due to preserved acetyl-CoA and propionyl-CoA pools as a result of the introduced mutations. An empty-plasmid control experiment has also been conducted in the strain HCT 20 (that was not introduced with the 3HV pathway), yielding only trace amounts of acetate and propionate when grown in LB supplemented with glucose and 2-ketobutyrate (data not shown). This indicates that the production of acetate and propionate in the recombinant HCT 20 was attributed to the introduced CoA-cleaving activity conferred by *ptb-buk* and *tesB*.

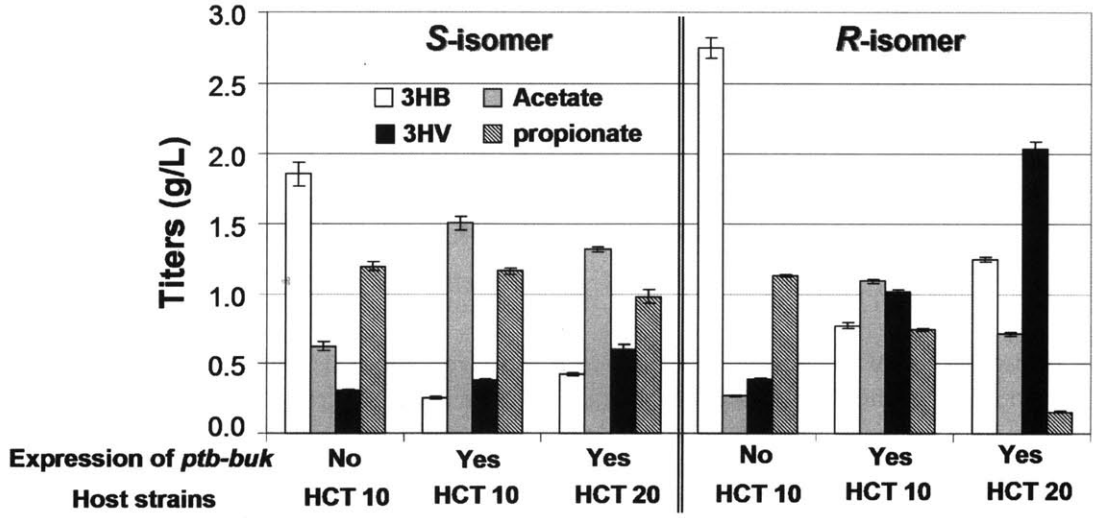

Figure 4-3 | 3HV biosynthesis from glucose and 2-ketobutyrate. This figure shows shake-flask production of chiral 3HV by recombinant *E. coli* grown in LB supplemented with 20 g/L glucose and 3 g/L sodium 2-ketobutyrate. Effects of overexpressing *ptb-buk* and using acetate pathway knockout strain HCT 20 (with additional deletions of *ackA-pta*. *poxB*, and *atoDA* genes compared to HCT 10) on 3HV production are compared. All strains contained the same set of plasmids pET-PB-B, and pCDF-T-H (for (*S*)-3HV synthesis) or pCDF-T-P (for (*R*)-3HV synthesis).

4.3.3 3HV synthesis from glucose and threonine

The metabolic intermediate 2-ketobutyrate can be produced from threonine by the action of threonine deaminase. Co-feeding of threonine with glucose, together with over-expression of *E. coli* threonine deaminase (encoded by *ilvA*), was able to achieve production of (*S*)-3HV and (*R*)-3HV with titers up to 0.11 g/L and 0.22 g/L, respectively (**Fig. 4-4**). Given that *E. coli* threonine deaminase is subject to feedback inhibition by isoleucine, a feedback resistant gene from *Corynebacterium glutamicum* (*Morbach et al., 1996*) was also used, and the production of (*S*)-3HV and (*R*)-3HV was further boosted to titers of 0.27 g/L and 0.91 g/L, respectively, under the same culture conditions. This experiment has also been conducted in the recombinant acetate pathway knockout strains (HCT 20); however, no improvement in production of 3HB and 3HV was observed (data not shown).

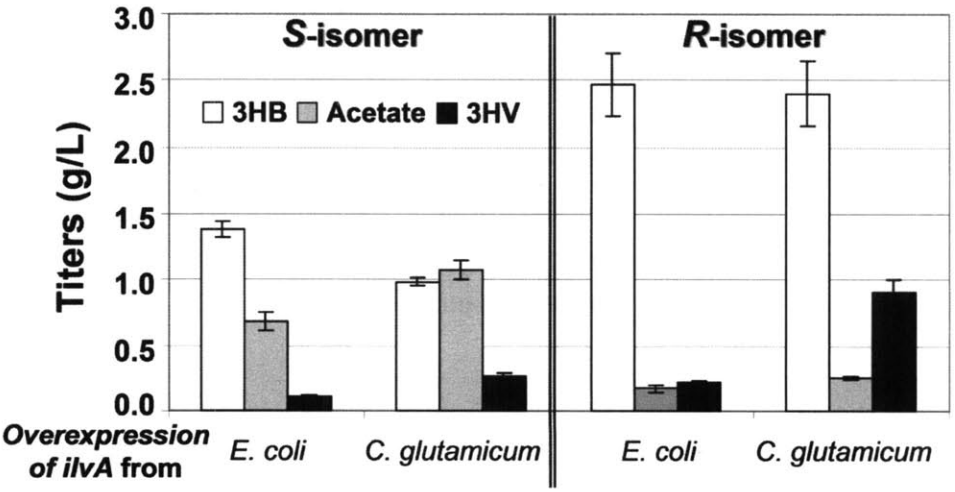

Figure 4-4 | 3HV biosynthesis from glucose and threonine. This figure shows shake-flask production of chiral 3HV by recombinant *E. coli* strain HCT 10 grown in LB supplemented with 20 g/L glucose and 3g/L threonine. Chiral 3HV production using alternative threonine deaminases (encoded by *ilvA)* from *E. coli* and *C. glutamicum* is compared. All strains contained the same set of plasmids pET-PB-B, pCOLA-lcg or pCOLA-lec as indicated, and pCDF-T-H (for (*S*)-3HV synthesis) or pCDF-T-P (for (*R*)-3HV synthesis).

4.3.4 3HV synthesis from glucose

We have demonstrated the production of chiral 3HV from glucose supplemented with propionate, 2-ketobutyrate, or threonine, in recombinant *E. coli*. The next step is to

construct a threonine over-producing strain in an attempt to achieve 3HV biosynthesis from a single carbon source. To do so, we up-regulated the threonine biosynthesis pathway by over-expressing the *thrABC* opeon, cloned from the wild type *E. coli* or the threonine producer *E. coli* ATCC 21277 that has a single amino acid alteration in the homoserine dehydrogenase (encoded by $thrA^{G1297A}$) for relieved feedback-inhibition (*Lee et al., 2009*). Transcriptional attenuation of those genes was removed by replacing the native promoter with a T7*lac* promoter, allowing for IPTG-inducible expression. In addition, the pathways that compete with threonine formation as well as degrade threonine were eliminated by knocking out *metA* (encoding homoserine O-succinyltransferase) and *tdh* (encoding threonine dehydrogenase) genes, yielding strain HCT 21.

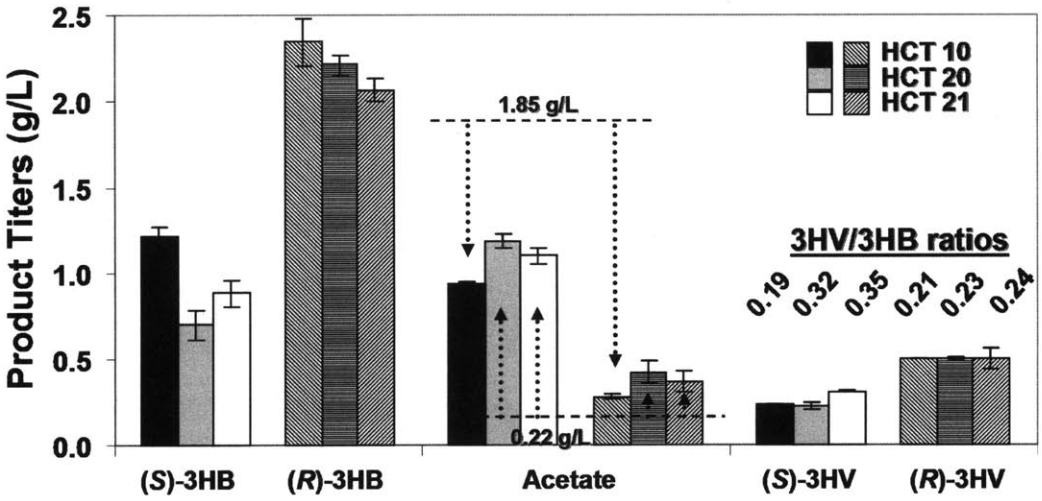

Figure 4-5 | 3HV biosynthesis solely from glucose. This figure shows shake-flask production of chiral 3HV in various knock-out strains as described in Table 1. Cells were grown in LB supplemented with 20 g/L glucose. The top and bottom dashed lines represent the acetate titers produced from *E. coli* strain HCT 10 and HCT 20 harboring empty plasmids, respectively. All strains contained the same set of plasmids pET-PB-B, pCOLA-Tecm-Icg, and pCDF-T-H (for (*S*)-3HV synthesis) or pCDF-T-P (for (*R*)-3HV synthesis). The recombinant HCT 10 strains carrying an empty pCOLAduet-1 in place of pCOLA-Tecm-Icg, as control strains, produced essentially no 3HV (data not shown).

Our results showed that there was essentially no difference in 3HV production between strains expressing the wild type and feedback resistant *thrA* (data not shown) probably because threonine did not accumulate or its level was not high enough to exert a feedback inhibition to ThrA. We also compared 3HV production across three

different *E. coli* strains, including HCT 10, HCT 20, and HCT 21. The mutants HCT 20 and HCT 21 carrying only empty plasmids significantly reduced acetate production to 0.22 g/L as opposed to 1.85 g/L by HCT 10 (**Fig. 4-5**); however, recombinant mutant HCT 20 or HCT 21 containing the 3HV pathway produced as much acetate as the recombinant HCT 10, a counterintuitive finding (see Discussion). The deletions of *metA* and *tdh* enhanced (*S*)-3HV production by 41% (recombinant HCT 21 relative to recombinant HCT 20), but essentially had no effect on (*R*)-3HV production. Nevertheless, those mutations were able to boost the ratios of 3HV/3HB by decreasing the 3HB titers and/or increase the 3HV titers. Overall, titers as high as 0.31 g/L and 0.50 g/L of (*S*)-3HV and (*R*)-3HV were achieved in the recombinant HCT 21 with 3HV/3HB ratios up to 0.35 and 0.24, respectively (**Fig. 4-5**).

4.3.5 3HV synthesis from glycerol

Glycerol has become a promising and abundant carbon source due to its generation as an inevitable byproduct of biodiesel production from vegetable oils or animal fats through a transesterification reaction (*Murarka et al., 2008*). There have been several reports on converting glycerol to more valuable compounds such as thymidine, ethanol, and 1,3-propanediol (*Gonzalez-Pajuelo et al., 2004, Lee et al., 2009, Shams Yazdani & Gonzalez, 2008*). Glycerol is also more reduced than glucose, leading to a higher reduced cofactor pool in the cytoplasm (*Lee et al., 2009*). Therefore, in addition to glucose, we investigated the ability of our recombinant *E. coli* to convert glycerol to chiral 3HV. Titers of 0.08 g/L and 0.96 g/L of (*S*)-3HV and (*R*)-3HV, respectively, were achieved in recombinant HCT 10, while recombinant HCT 21 produced 0.19 g/L and 0.60 g/L of (*S*)-3HV and (*R*)-3HV, respectively (**Fig. 4-6**). As mentioned in the Materials and Methods section, in this specific experiment, concentration of 3HB was quantified by DAD at 210 nm that had a detection limit at around 0.08 g/L. As a result, the amounts of (*S*)-3HB produced in both recombinant HCT 10 and HCT 21 strains were too low to be quantified so that we could not report the 3HV/3HB ratios. Nonetheless, in the case of (*R*)-isomers, 3HV/3HB ratios could be as

high as 0.88 and 1.10, respectively, in recombinant HCT 10 and HCT 21 strains. The high 3HV/3HB ratios can be beneficial in terms of product separation or biosynthesis of PHBV that enables high 3HV content.

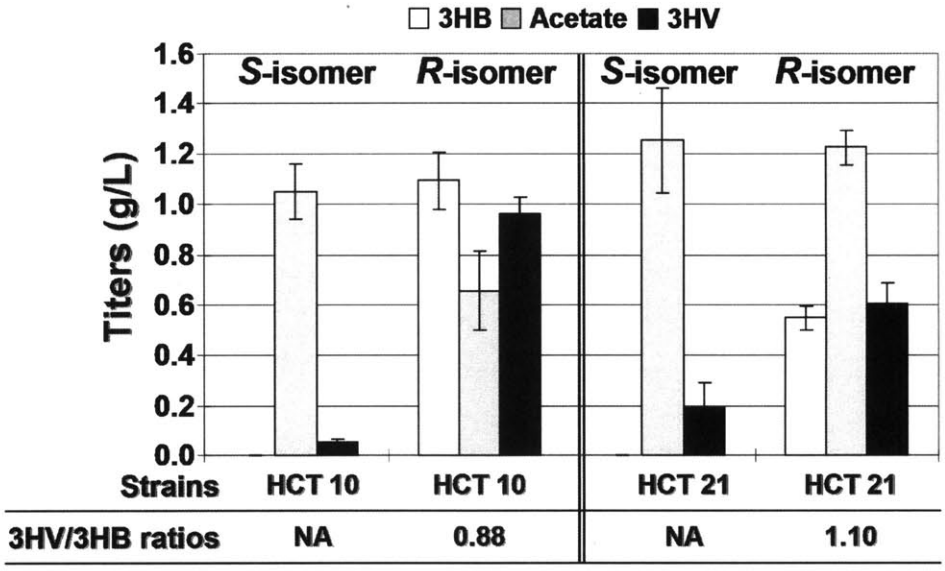

Figure 4-6 | 3HV biosynthesis solely from glycerol. This figure shows shake-flask production of chiral 3HV in various knock-out strains as described in Table 1. Cells were grown in LB medium supplemented with 20 g/L glycerol. The amounts of (*S*)-3HB produced in both recombinant HCT 10 and HCT 21 strains were too low to be quantified due to a low detection limit by DAD at 210 nm; therefore, the 3HV/3HB ratios were not applicable (NA) to the (*S*)-isomer. All strains contained the same set of plasmids pET-PB-B, pCOLA-Tecm-Icg, and pCDF-T-H (for (*S*)-3HV synthesis) or pCDF-T-P (for (*R*)-3HV synthesis).

4.3.6 Confirmation of 3HV stereochemistry

The stereochemistry of the resulting 3HV in the media from these cultures was determined by methyl esterification of the 3HV present followed by chiral HPLC analysis using our previously developed method (*Tseng et al., 2009*). However, we could not assign an absolute stereochemistry to each sample due to the unavailability of enantiopure 3HV standards. However, based on our previous results regarding the product stereochemistry of *pha*B and *hbd* and the observation that Me-(*R*)-3HB has a faster retention time relative to Me-(*S*)-3HB, we expect Me-(*R*)-3HV to have a faster retention time than Me-(*S*)-3HV when analyzed by the same method. Thus, the 6.9 and 9.2 min peaks likely represent Me-(*R*)-3HV and Me-(*S*)-3HV, respectively (**Fig. 4-7**). These results confirm the enantiopurity of biosynthesized 3HV.

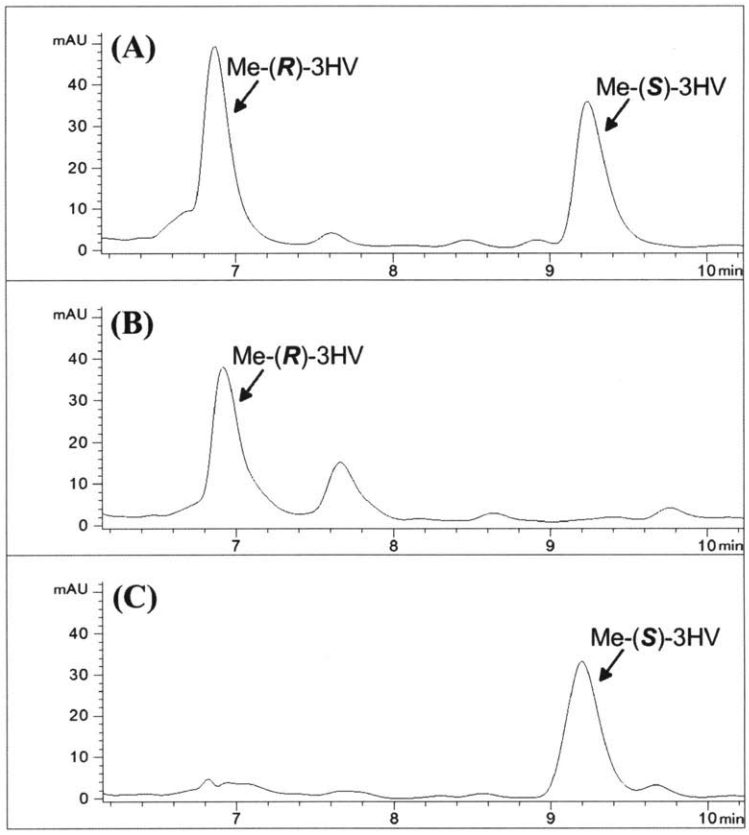

Figure 4-7 | Determination of the stereochemistry of 3HV. HPLC spectra of (A) racemic 3HV standards after boiling in methanol, (B) culture medium from the recombinant strain HCT 10 expressing *bktB, phaB, tesB, and ptb-buk* after boiling in methanol, and (C) culture medium from the recombinant strain HCT 10 expressing *bktB, hbd, tesB, and ptb-buk* after boiling in methanol are shown.

4.4 Discussion

In general, two approaches can be taken to engineer *E. coli* for direct 3HV production via the threonine biosynthesis pathway. The first is to utilize an existing threonine producer, such as *E. coli* ATCC 21277 (*Debabov, 2003*), followed by further engineering to introduce our constructed 3HV pathway. However, this and other available threonine producing strains have typically been developed through multiple rounds of random mutagenesis and selection due to the difficulty of engineering this highly regulated and complex metabolic network. Although there are several successful cases in developing industrial threonine producers by such approaches, resultant strains usually also suffer from undesired phenotypes including, for example, growth retardation, low transformation efficiency, and by-product formation as a result of

random mutations (*Lee et al., 2007*). In addition, other uncharacterized mutations may hinder further strain development as often needed. Fortunately, recent advances in computational genomics have allowed for rational development of production strains (*Lee et al., 2007*). Therefore, as a second approach, a genetically-defined threonine producing strain was established and introduced with the 3HV pathway to achieve direct microbial production of chiral 3HV from glucose or glycerol.

As seen in **Figure 4-5**, acetate is the major byproduct to the production of hydroxyacids (3HB and 3HV). In an effort to decrease acetate and increase 3HV production, a mutant strain HCT 20 with deletions on *atoDA*, *poxB*, and *ackA-pta* genes was developed. Counter-intuitively, the recombinant acetate pathway knockout strains of HCT 20 and HCT 21 produced slightly more acetate and less 3HB than recombinant HCT 10. We suspected that the enzymatic activity responsible for acetate production was restored by Ptb-Buk and TesB in the recombinant HCT 20 and HCT 21. In fact, in a separate experiment, both enzymes were found to have CoA-removing activities on acetyl-CoA and propionyl-CoA (data not shown), so an introduction of TesB and/or Ptb-Buk to strains HCT 20 or HCT 21 would likely restore the ability to produce acetate.

Apparently, knocking out enzymes responsible for acetate production failed to reduce acetate synthesis. Alternatively, to alleviate the substrate promiscuity of TesB and Ptb-Buk on acetyl-CoA, and thus reduce acetate production, one approach called enzyme co-localization could be implemented to allow substrate channeling between enzymes (*Conrado et al., 2008*). For example, pathway enzymes of Hbd and TesB, catalyzing successive reactions, can be co-localized in an attempt to reduce the amount of freely floating TesB that may hydrolyze acetyl-CoA as well as to increase accessibility of 3HV-CoA by TesB. The spatial organization of the enzymes can be achieved using either the leucine zipper, a dimer resulting from interaction between leucine residues (*Moll et al., 2001*), or the synthetic scaffolds, constructed from protein–protein interaction domains (*Dueber et al., 2009*). Furthermore, expressing enzymes that would assimilate produced acetate is another way to reduce acetate accumulation. For example, acetyl-CoA synthetase (encoded by *acs*) from *E. coli* can be over-expressed to

convert acetate to acetyl-CoA with the use of one ATP. While successfully demonstrated in one work (*Terpe, 2006*), in our case, over-expression of *acs* was found to have essentially no effect on acetate reduction (data not shown). Additionally, to overcome the hurdle of acetate reduction, approaches like protein engineering of TesB and/or Ptb-Buk to alleviate their substrate promiscuity, or utilization of better isozymes with more stringent substrate specificity could also mitigate the carbon loss in the form of acetate.

Among microbes, NADH and NADPH play a central role in energy metabolism by providing the cell with the reducing power for a variety of cellular redox reactions. The availability of such cofactors could impose a huge impact on the functionality of introduced biosynthetic pathways. In fact, we have previously shown that the $NADPH/NADP^+$ ratio was two- to three-fold higher than the $NADH/NAD^+$ ratio under the culture conditions examined, presumably affecting *in vivo* activities of PhaB and Hbd and resulting in greater production of (*R*)-3HB than (*S*)-3HB (*Tseng et al., 2009*). Given that our proposed 3HV pathway was based on the previously established 3HB pathway, it was also expected to see the same trend of greater production of (*R*)-3HV than (*S*)-3HV, even though the cofactor dependency of 3HV synthesis may be complicated by the energetically expensive threonine biosynthesis pathway with utilization of both ATP and NADPH. In an effort to perturb the cofactor balance within the cells, thereby tuning the production of (*R*)-3HV and (*S*)-3HV, we attempted to used glycerol, a promising, abundant, and highly-reduced carbon source, to support 3HV production. Based on our calculation of reducing equivalents (e^-) of glucose and glycerol, on the same basis of 2 moles of phosphoenolpyruvate synthesized, glucose and glycerol possess, respectively, 24 and 28 reducing equivalents. Potentially, the additional four reducing equivalents can be utilized to generate two NADPH or equivalent amount of ATP. In fact, it has been experimentally confirmed that a higher intracellular $NADPH/NADP^+$ ratio was observed when glycerol was used as a carbon source than glucose, and this higher ratio was also reflected in boosted production of thymidine as its biosynthesis requires NADPH as a cofactor (*Lee et al., 2009*). Given that both NADPH and ATP play a central role in

threonine biosynthesis, we hypothesized that the use of glycerol, which could generate more NADPH and ATP (**Fig. 4-1**) relative to glucose, may favor threonine biosynthesis by directing more carbon flux towards production of propionyl-CoA, thus favoring the formation of 3HV relative to 3HB. In agreement with our hypothesis, a higher 3HV/3HB ratio was obtained in the (*R*)-3HV production when glycerol was used as the carbon source (**Fig. 4-6**). In addition, much larger ratios of the total (R)-hydroxyacids (summation of (R)-3HB and (R)-3HV titers) to the total (S)-hydroxyacids (summation of (S)-3HB and (S)-3HV titers) were observed in glycerol-fed cultures (**Fig. 4-6**) compared to glucose-fed cultures (**Fig. 4-5**). We hypothesize that the higher intracellular NADPH/NADP+ ratio as a result of the use of glycerol would favor (R)-hydroxyacid biosynthesis compared to the use of glucose, thus yielding the larger ratios of total (R)-hydroxyacids to total (S)-hydroxyacids.

As mentioned previously, BktB was chosen as the primary thiolase due to its high enzymatic specificity towards the C_5 substrate. Given that *E. coli* has an endogenous thiolase (encoded by *atoB*), a deletion of *atoB* was expected to increase the ratio of 3HV/3HB as AtoB has been shown to prefer to condense two molecules of acetyl-CoA instead of one propionyl-CoA and one acetyl-CoA (*Slater et al., 1998*). However, our preliminary result showed that the recombinant HCT 11 with an *atoB* deletion behaved exactly as the recombinant HCT 10, and the deletion in *atoB* had essentially no effect on 3HV production (data not shown), implying that *atoB* may not be a constitutively expressed gene. In addition, it is noteworthy that increased 3HV production in the recombinant HCT 20 relative to the recombinant HCT 10 was observed only with 2-ketobutyrate supplementation (**Fig. 4-3**) but not with the threonine supplementation, solely glucose, or solely glycerol experiments (**Fig. 4-4**, **4-5** and **4-6**); similarly, an accumulation of propionate only occurred in the 2-ketobutyrate supplementation experiment (**Fig. 4-3**), altogether, indicating that 3HV biosynthesis from glucose or glycerol is most likely limited by the precursor propionyl-CoA. Therefore, approaches to increase the availability of propionyl-CoA could enhance the 3HV production.

4.5 Conclusions

Carbon skeletons with even-chain number are naturally found in fatty acid metabolism, but those with odd-chain number are pretty novel. As a result, there is a good deal of interest in making odd-carbon chain molecules such as 3HV (C5) and propionate (C3) because they are so much harder to produce than even-carbon chain ones such as acetate (C2) and butyrate/butanol (C4). This work opens the way for biosynthesis of the odd-carbon chain molecules from renewable feedstocks. Taking together, our work represents the first report of direct microbial production of enantiomerically pure 3HV from a single carbon source. In addition, we have explored the production of each stereoisomer of 3HV across different genetically altered *E. coli* strains, along with various enzyme homologs, for enhanced chiral 3HV production. Further engineering of host strains and pathway enzymes should lead to higher 3HV titers and a more economical bioprocess for the production of chiral 3HV.

Most importantly, the success in chiral 3HV production provides an initial proof-of-concept that high levels of five-carbon metabolite intermediates, especially 3-hydroxyvaleryl-CoA (3HV-CoA), can be obtained. Subsequent conversion of 3HV-CoA by the downstream *Clostridial* butanol pathway enzymes can potentially lead to production of pentanol. Validation of the rest steps of the six-step pentanol pathway is thus the focus in Chapter 5.

CHAPTER 5

Microbial Synthesis of Pentanol

Abstract

Butanol has emerged as the most promising alternative to ethanol as a biomass-derived fuel because it has a nearly 50% higher energy density than ethanol, representing about 90% of the energy density of gasoline. It is also significantly more hydrophobic than ethanol, improving its prospects as a blended or direct replacement fuel from both transport and utilization perspectives. Therefore, our first objective was the construction of heterologous organisms capable of synthesizing butanol as described in Chapter 2. However, we view butanol as only a first step in biofuels production as we believe the biochemical pathway towards butanol also lends itself towards the biosynthesis of other, longer-chain alcohols, especially pentanol, that have even higher energy density and more favorable physical properties. Thus, Chapter 5 describes how we extended the butanol biosynthetic pathway for pentanol biosynthesis. Here, a substrate feeding study was implemented to investigate the pentanol biosynthetic pathway with respect to the capacity of pathway enzymes to catalyze reactions of non-natural five-carbon analogues. Direct microbial synthesis of pentanol from glucose supplemented with propionate or solely from glucose or glycerol will also be discussed in Chapter 5.

This chapter will be submitted for publication as:

Tseng, H.-C., Prather, K.L.J. "Metabolic engineering of *E. coli* for production of bio-pentanol"

5.1 Introduction

The increasing demand for biomass-derived fuels has led to a resurgent interest in a number of candidate molecules to complement petroleum-derived transportation fuels. Chief among these, particularly in the US, has been ethanol. However, ethanol presents a number challenges towards large-scale integration into the fuels supply, including an unfavorable carbon balance with the dominant corn-based processes, as well as non-ideal physical-chemical properties, such as a lower energy density compared to existing fuels (e.g., ~60% that of gasoline) and its complete miscibility with water, which impacts the distribution infrastructure.

Butanol has emerged as the most promising alternative to because it has a nearly 50% higher energy density than ethanol, representing about 90% of the energy density of gasoline. The primary route for commercial butanol synthesis in the early part of the 20th century was microbial fermentation. The well-known Weizmann or "ABE" process utilizes a species of the *Clostridium* genus of bacteria, usually *Clostridium acetobutylicum*, to anaerobically produce a mixture of solvents with a typical ratio of 60% butanol, 30% acetone, and 10% ethanol. Research into the process continued in the subsequent years, as the pathway was fully defined and key solvent-producing enzymes identified. Significant advances have also been made with respect to the ability to engineer *Clostridium* (*Ezeji et al., 2004, Sillers et al., 2008, Tomas et al., 2003*); however, the development of such tools remains substantially behind that of other, more commonly used organisms. Given the relatively low yield of butanol and the challenges associated with engineering *Clostridium*, we considered the reconstitution of the butanol pathway in heterologous organisms to be a more promising strategy for improving its performance, which has been successfully demonstrated in Chapter 2. Another reason that we are particularly interested in construction of the butanol biosynthetic pathway in a more tractable host is because of the potential for modifying the pathway to produce other, structurally similar biofuels, such as pentanol in this work.

The butanol biosynthetic pathway begins with the condensation of two acetyl-CoA

molecules, followed by reduction of the ketone to an (*S*)-alcohol (**Fig. 5-1**). These initial condensation and ketone reduction steps mimic the first two steps for the production of poly(3-hydroxybutyrate-co-3-hydroxyvalerate) (poly(3HB-co-3HV)) co-polymer, one of various polyhydroxyalkanoate biopolymers (PHAs) (**Fig. 5-1**), except that the alcoholic ester produced is of the (*R*)-form. The bacterium *Ralstonia eutropha* is well-known for its ability to accumulate large amounts of PHAs, including the poly(3HB-co-3HV)). A BktB thiolase has been identified within *R. eutropha* that condenses acetyl-CoA with a longer chain precursor propionyl-CoA to produce five-carbon monomers, and that is distinct from the primary PhaA thiolase that condenses two acetyl-CoA (*Slater et al., 1998*) (**Fig. 5-1**).

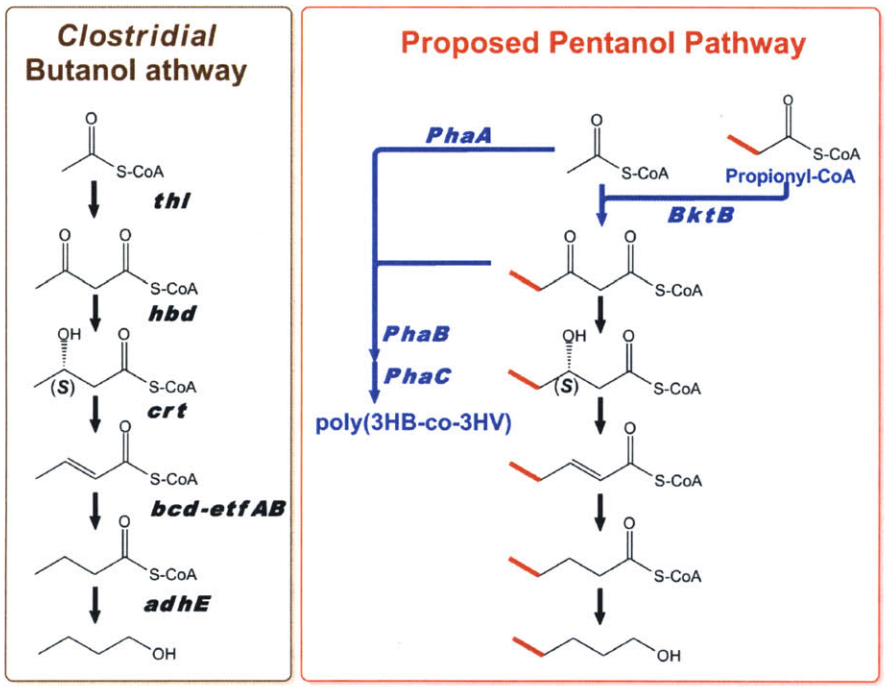

Figure 5-1 | Schematic of *Clostridial* butanol biosynthetic pathway (left panel), poly(3HB-co-3HV) biosynthetic pathway (in blue), and proposed pentanol biosynthetic pathway (right panel). Pentanol synthesis starts from condensation of one acetyl-CoA with one propionyl-CoA, instead of two acetyl-CoA molecules, to establish a five-carbon skeleton. Genes shown in black are from *C. acetobutylicum* while genes shown in blue are from *R. eutropha*.

BktB does act to form both four- and five-carbon molecules, but its activity is approximately three-fold higher for the latter. Thus, in the absence of the primary thiolase, the predominant products should be of the five-carbon variety. Based on the

successful reconstruction of the *Clostridial* butanol pathway in *E. coli* and identification of one versatile thiolase enzyme, in this chapter, we explored the possibility of incorporating the BktB thiolase, which preferentially condenses one acetyl-CoA and one propionyl-CoA, in place of the *C. acetobutylicum* Thl thiolase, into the basic butanol pathway for microbial synthesis of pentanol.

As described in Chapter 4, we have expressed the BktB thiolase along with the reductase PhaB utilized in PHA synthesis or Hbd employed in the butanol synthesis, and one additional thioesterase (TesB) that converts 3-hydroxyvaleryl-CoA (3HV-CoA) into 3-hydroxyvalerate (3HV), which served as a test pathway for examination of the capability of the upstream butanol pathway enzymes on five-carbon substrates. Using this test pathway and feeding propionate exogenously along with expression of a Ptb-Buk activator that converts propionate to propionyl-CoA, we have achieved up to 67% of produced 3-hydroxyacids as the five-carbon 3HV (*Tseng et al., 2010*). This provides the initial proof-of-concept that high levels of five-carbon intermediates can be obtained.

However, it is unknown in the extent to which each of the subsequent enzymes in the butanol pathway will accept five-carbon substrates. Therefore, in Chapter 5, we used a bypass strategy to examine the ability of the enzymes employed in the proposed pentanol biosynthetic pathway to accept five-carbon substrates. Particularly, certain coenzyme A (CoA) derivatives synthesized via reduction reactions along the pentanol pathway are targeted to be converted to their respective free acid forms, allowing for their extracellular detection. Alternatively, certain carboxylic acids are fed to serve as precursors of targeted CoA intermediates, both which can be achieved through the use of CoA-addition/removal tools, including broad-substrate-range enzymes of Ptb-Buk (from *C. acetobutylicum*) and TesB (from *E. coli*).

5.2 Materials and Methods

5.2.1 Plasmids

Codon-optimized genes, including *adhE* from *C. acetobutylicum* ATCC 824, *fdh1* from *S. cerevisiae*, and *fdh1* from *C. boidinii,* were purchased from Genscript (Piscataway, NJ). Genes derived from *C. acetobutylicum* ATCC 824 (*hbd*, *crt*, *bcd*, *etfAB*, *adhE,* and *ptb-buk*), *R. eutropha* H16 (*bktB* and *phaB*), *P. aeruginosa* (*phaJ1*), *M. elsdenii* (*pct*), *C. glutamicum* ATCC 13032 (*ilvA*), and *E. coli* ATCC 21277 ($thrA^{G1297A}BC$ opeon) were obtained by polymerase chain reaction (PCR) using genomic DNA (gDNA) templates. All gDNAs were prepared using the Wizard Genomic DNA Purification Kit (Promega, Madison, WI). Custom oligonucleotides (primers) were purchased for all PCR amplifications (Sigma-Genosys, St. Louis, MO). In all cases, Phusion High Fidelity DNA polymerase (Finnzymes, Espoo, Finland) was used for DNA amplification. Restriction enzymes and T4 DNA ligase were purchased from New England Biolabs (Ipswich, MA). Recombinant DNA techniques were performed according to standard procedures (*Sambrook & Russell, 2001*).

Compatible vectors pETDuet-1, pCDFDuet-1, pACYCDuet-1, and pCOLADuet-1 (Novagen, Darmstadt, Germany) were used to provide individual expression of each gene under a T7*lac* promoter and a ribosome binding site (RBS). These PCR products were digested with restriction enzymes corresponding to the restriction site incorporated into them by their respective primers and ligated directly into similarly digested Duet vectors. Ligation reactions using pETDuet-1, pACYCDuet-1, or pCOLADuet-1 as the vector were transformed into *E. coli* DH10B, while ligations using pCDFDuet-1 were transformed into *E. coli* ElectroTen-Blue. All constructs were confirmed to be correct by restriction enzyme digestion and nucleotide sequencing. Once all plasmids were constructed, they were co-transformed as appropriate into *E. coli* BL21Star(DE3) or Pal(DE3) to create production strains.

5.2.2 Strains

E. coli DH10B (Invitrogen, Carlsbad, CA) and ElectroTen-Blue (Stratagene, La Jolla, CA) were used for transformation of cloning reactions and propagation of all plasmids. *E. coli* MG1655(Δ*pta* Δ*adhE* Δ*ldhA*) was kindly donated by Professor Gregory

Stephanopoulos of the Department of Chemical Engineering at the Massachusetts Institute of Technology, USA. *E. coli* Pal(DE3) was then constructed from *E. coli* MG1655(Δ*pta* Δ*adhE* Δ*ldhA*) using a λDE3 Lysogenization Kit (Novagen, Darmstadt, Germany) to allow the expression of genes under the T7*lac* promoter (*Fischer et al., 2010*). *E. coli* BL21Star(DE3) (Invitrogen, Carlsbad, CA) was used as the host strain for substrate feeding experiments, including pentanol synthesis from valerate (strains BL1-BL4, **Table 5-1**) or trans-2-pentenoate (strains BL5-BL7, **Table 5-1**) while Pal(DE3) was the production host strain employed for the rest of experiments, including trans-2-pentenoate synthesis from glucose and propionate (strains Pal1-Pal4, **Table 5-1**), butanol synthesis from glucose (strains Pal5 and Pal6, **Table 5-1**), pentanol synthesis from glucose and propionate (strains Pal7-Pal11, **Table 5-1**), and pentanol synthesis solely from glucose or glycerol (strains Pal12-Pal17, **Table 5-1**).

Table 5-1 | *E. coli* strains and plasmids used in this work.

Name	Relevant Genotype	Reference
Strains		
DH10B	F⁻ *mcr*A Δ(*mrr-hsd*RMS-*mcr*BC) ϕ80*lacZ*ΔM15 Δ*lacX74 recA1 endA1 araD139*Δ(*ara, leu*)7697 *galU galK* λ⁻ *rpsL nupG*	Invitrogen
ElectroTen-Blue	Δ(*mcrA*)*183* Δ(*mcrCB-hsdSMR-mrr*)*173 endA1 supE44 thi-1 recA1 gyrA96 relA1 lac* Kan^r [F′ *proAB lacI*^{q}ZΔM15 Tn*10* (Tet^r)]	Stratagene
BL21Star(DE3)	F⁻ *ompT hsdS*$_B$ (r_B^- m_B^-) *gal dcm rne131* (DE3)	Invitrogen
BL1	pCDF/ptb-buk + pACYC/adhE	This study
BL2	pCDF/ptb-buk + pACYC/adhE$_{opt}$	This study
BL3	pCDF/pct + pACYC/adhE	This study
BL4	pCDF/pct + pACYC/ adhE$_{opt}$	This study
BL5	pET/bcd-etfAB/adhE$_{opt}$ + pCDF/ptb-buk	This study
BL6	pET/bcd-etfAB/adhE$_{opt}$ + pCDF/ptb-buk/fdh1$_{Sc}$	This study
BL7	pET/bcd-etfAB/adhE$_{opt}$ + pCDF/ptb-buk/fdh1$_{Cb}$	This study
MG1655	F⁻ λ⁻ *ilvG- rfb-50 rph-1*	ATCC 700926
Pal(DE3)	MG1655(DE3 Δ*pta* Δ*ldhA* Δ*adhE*)	(*Fischer et al., 2010*)
Pal1	pET/bktB/hbd + pCDF/ptb-buk/crt	This study
Pal2	pET/bktB/hbd + pCDF/ptb-buk	This study
Pal3	pET/bktB/phaB + pCDF/ptb-buk/phaJ1	This study
Pal4	pET/bktB/phaB + pCDF/ptb-buk	This study
Pal5	pET/bcd-etfAB/bktB + pCDF/crt/hbd + pACYC/adhE$_{opt}$	This study
Pal6	pET/bcd-etfAB/bktB + pCDF/phaJ1/phaB + pACYC/adhE$_{opt}$	This study
Pal7	pETDuet-1 + pCDFDuet-1 + pCOLADuet-1	This study
Pal8	pET/bcd-etfAB/bktB/pct + pCDF/crt/hbd + pACYC/fdh1$_{Sc}$/adhE$_{opt}$	This study
Pal9	pET/bcd-etfAB/bktB/pct + pCDF/crt/hbd + pACYC/fdh1$_{Cb}$/adhE$_{opt}$	This study
Pal10	pET/bcd-etfAB/bktB/pct + pCDF/phaJ1/phaB + pACYC/fdh1$_{Sc}$/adhE$_{opt}$	This study
Pal11	pET/bcd-etfAB/bktB/pct + pCDF/phaJ1/phaB + pACYC/fdh1$_{Cb}$/adhE$_{opt}$	This study
Pal12	pET/bcd-etfAB/bktB + pCDF/crt/hbd + pACYC/adhE$_{opt}$ + pCOLA/thrA^{fr}BC/ilvA	This study
Pal13	pET/bcd-etfAB/bktB + pCDF/crt/hbd + pACYC/fdh1$_{Sc}$/adhE$_{opt}$+ pCOLA/thrA^{fr}BC/ilvA	This study

Pal14	pET/bcd-etfAB/bktB + pCDF/crt/hbd + pACYC/fdh1$_{Cb}$/adhE$_{opt}$+ pCOLA/thrA^{fr}BC/ilvA	This study
Pal15	pET/bcd-etfAB/bktB + pCDF/phaJ1/phaB + pACYC/adhE$_{opt}$+ pCOLA/thrA^{fr}BC/ilvA	This study
Pal16	pET/bcd-etfAB/bktB + pCDF/phaJ1/phaB + pACYC/fdh1$_{Sc}$/adhE$_{opt}$+ pCOLA/thrA^{fr}BC/ilvA	This study
Pal17	pET/bcd-etfAB/bktB + pCDF/phaJ1/phaB + pACYC/fdh1$_{Cb}$/adhE$_{opt}$+ pCOLA/thrA^{fr}BC/ilvA	This study
Plasmids		
pETDuet-1	ColE1(pBR322) *ori*, *lacI*, T7*lac*, Amp^{R}	Novagen
pCDFDuet-1	CloDF13 *ori*, *lacI*, T7*lac*, Strep^{R}	Novagen
pACYCDuet-1	P15A *ori*, *lacI*, T7*lac*, Cm^{R}	Novagen
pCOLADuet-1	COLA *ori*, *lacI*, T7*lac*, Kan^{R}	Novagen
pET/bcd-etfAB/bktB	pETDuet-1 harboring *bcd-etfAB* operon from *C. acetobutylicum* ATCC 824, and *bktB* from *R. eutropha* H16	This study
pET/bcd-etfAB/bktB/pct	pETDuet-1 harboring *bcd-etfAB* operon from *C. acetobutylicum* ATCC 824, *bktB* from *R. eutropha* H16,and *pct* from *M. elsdenii*	This study
pET/bcd-etfAB/adhE$_{opt}$	pETDuet-1 harboring *bcd-etfAB* operon and codon-optimized *adhE*$_{opt}$ from *C. acetobutylicum* ATCC 824	This study
pET/bktB/hbd	pETDuet-1 harboring *bktB* from *R. eutropha* H16, and *hbd* from *C. acetobutylicum* ATCC 824	(*Tseng et al., 2009*)
pET/bktB/phaB	pETDuet-1 harboring *bktB* and *pha*B from *R. eutropha* H16	(*Tseng et al., 2009*)
pCDF/crt/hbd	pCDFDuet-1 harboring *crt* and *hbd* from *C. acetobutylicum* ATCC 824	This study
pCDF/phaJ1/phaB	pCDFDuet-1 harboring *phaJ1* from *P. aeruginosa*, and *pha*B from *R. eutropha* H16	This study
pCDF/ptb-buk	pCDFDuet-1 harboring *ptb-buk* operon from *C. acetobutylicum* ATCC 824	(*Tseng et al., 2009*)
pCDF/ptb-buk/fdh1$_{Sc}$	pCDFDuet-1 harboring *ptb-buk* operon from *C. acetobutylicum* ATCC 824, and codon-optimized *fdh1* from *S. cerevisiae*	This study
pCDF/ptb-buk/fdh1$_{Cb}$	pCDFDuet-1 harboring *ptb-buk* operon from *C. acetobutylicum* ATCC 824, and codon-optimized *fdh1* from *C. boidinii*	This study
pCDF/ptb-buk/crt	pCDFDuet-1 harboring *ptb-buk* operon and *crt* from *C. acetobutylicum* ATCC 824	This study
pCDF /ptb-buk/phaJ1	pCDFDuet-1 harboring *ptb-buk* operon from *C. acetobutylicum* ATCC 824, and *phaJ1* from *P. aeruginosa*	This study
pCDF/pct	pCDFDuet-1 harboring *pct* from *M. elsdenii*	This study
pACYC/adhE	pACYCDuet-1 harboring *adhE* from *C. acetobutylicum* ATCC 824	This study
pACYC/adhE$_{opt}$	pACYCDuet-1 harboring codon-optimized *adhE*$_{opt}$ from *C. acetobutylicum* ATCC 824	This study
pACYC /fdh1$_{Sc}$/adhE$_{opt}$	pACYCDuet-1 harboring codon-optimized *fdh1* from *S. cerevisiae*, and codon-optimized *adhE*$_{opt}$ from *C. acetobutylicum* ATCC 824	This study
pACYC /fdh1$_{Cb}$/adhE$_{opt}$	pACYCDuet-1 harboring codon-optimized *fdh1* from *C. boidinii*, and codon-optimized *adhE*$_{opt}$ from *C. acetobutylicum* ATCC 824	This study
pCOLA/thrA^{fr}BC/ilvA	pCOLADuet-1 harboring *thrA*^{G1297A}*BC* operon from *E. coli* ATCC 21277, and *ilvA* from *C. glutamicum* ATCC 13032	(*Tseng et al., 2010*)

5.2.3 Culture conditions

For trans-2-pentenoate synthesis from glucose and propionate, seed cultures of the recombinant strains (strains Pal1-Pal4) were grown in TB medium at 30°C overnight on a rotary shaker at 250 rpm, and were used to inoculate, at an inoculation volume of 10%, 50 mL TB medium in 250 ml flasks for aerobic growth, and 13 ml TB medium in 15 mL glass tubes (Bellco Glass, Inc.) stoppered with a butyl rubber septum for microaerobic or

anaerobic growth. The septum was pierced with a 26-gauge syringe needle to achieve microaerobic conditions. All cell cultures were supplemented with 10 g/L glucose. Cultures were induced with 0.5mM IPTG at 2h post-inoculation and incubated for another 24 h.

For the substrate feeding experiments, seed cultures of the recombinant strains (strains BL1-BL7, **Table 5-1**) were grown in TB medium at 30°C overnight on a rotary shaker at 250 rpm, and were used to inoculate 45 mL TB medium supplemented with 10 g/L glucose at an inoculation volume of 10% in 50mL glass culture tubes. Cultures were induced with 0.5 mM IPTG at 2h post-inoculation and incubated for another 72 h. One of the substrates, including neutralized valerate (10 mM or 20 mM) and trans-2-pentenoate (20 mM) was supplemented at the same time of induction to provide the precursor needed for pentanol synthesis.

For pentanol synthesis, seed cultures of the recombinant *E. coli* strains (strains BL7-BL17, **Table 5-1**) were grown in TB medium at 30°C overnight, and were used to inoculate 3 mL TB medium supplemented with 10 g/L glucose or 10 g/L glycerol at an inoculation volume of 10% in 15 mL Falcon tubes. Cultures were induced with 0.5mM IPTG at 2h post-inoculation and incubated for another 96 h. For strains BL12-BL17 (**Table 5-1**), 20 mM neutralized propionate was supplemented at the same time of induction.

For profiling experiments with various headspace to culture volume ratios, the seed cultures of the recombinant strains (strains Pal5 and Pal6, **Table 5-1**) were used to inoculate, at an inoculation volume of 10%, 10 mL, 5 mL, 3 mL of TB medium in 15 mL Falcon tubes, 25 mL and 10 mL of TB medium in 250 mL flasks with caps screwed on, and 25 mL of TB medium in 250 mL flask with loose caps. All cultures were supplemented with 10 g/L glucose and then incubated at 30°C on a rotary shaker. Cultures were induced with 0.5mM IPTG at 2h post-inoculation and incubated for another 48 h.

In all cases, culture medium was supplemented with 50 mg/L ampicillin, 50 mg/L streptomycin, 34 mg/L chloramphenicol, and 25 mg/L kanamycin as required. 1 mL of culture was withdrawn at the end of the incubation period for HPLC analysis. In general,

experiments were performed in triplicates, and data are presented as the averages and standard deviations of the results.

5.2.4 Metabolite analysis

Culture samples were pelleted by centrifugation and aqueous supernatant collected for HPLC analysis using an Agilent 1200 series instrument with a refractive index detector (RID) and a diode array detector (DAD) at 210 nm. Analytes were separated using an Aminex HPX-87H anion-exchange column (Bio-Rad Laboratories, Hercules, CA) and a 5 mM H_2SO_4 mobile phase. Glucose, glycerol, acetate, 3-hydroxybutyrate, 3-hydroxyvalerate, crotonate, trans-2-pentenoate, butyrate, valerate, butanol, pentenol, and pentanol were quantified using commercial standards on a 1200 series by linear extrapolation from calibration of external standards.

5.3 Results

5.3.1 Construction of pentanol biosynthetic pathway

We have constructed a synthetic pathway for producion of pentanol, which combines elements of the *Clostridial* butanol biosynthesis pathway with pathways of the poly(3HB-co-3HB) biosynthesis of *R. eutropha* and threonine biosynthesis of *E. coli* (**Fig. 5-2**). The pentanol biosynthesis begins with condensation of one acetyl-CoA and one propionyl-CoA to form 3-ketovaleryl-CoA. This reaction is catalyzed by an acetoacetyl-CoA thiolase from *R. eutropha* H16, which is encoded by *bktB*. The genes encoding for enzyme activities for the step-wise conversion of 3-ketovaleryl-CoA to valeryl-CoA are clustered together in a polycistronic operon, consisted of genes *crt*, *bcd*, *etfAB*, and *hbd* from *C. acetobutylicum*, encoding for crotonase, butyryl-CoA dehydrogenase, electron transfer proteins, and 3-hydroxybutyryl-CoA dehydrogenase, respectively. A bi-functional aldehyde/alcohol dehydrogenase, encoded by *adhE* from *C. acetobutylicum*, catalyzes the final steps of pentanol synthesis from valeryl-CoA. Alternatively, both *hbd* and *crt* genes can be replaced with *phaB* from *R. eutropha* H16 and *phaJ1* from *Pseudomonas aeruginosa*, respectively, to convert ketovaleryl-CoA to

trans-2-pentenoyl-CoA. While acetyl-CoA is an obligate central intermediate occurring in any organism and under any physiological condition, this is not the case for propionyl-CoA. Given that synthesis of 3-ketovaleryl-CoA requires propionyl-CoA biosynthesis, a pathway allowing for endogenous propionyl-CoA synthesis from glucose or glycerol was also introduced. Specifically, up-regulation of threonine biosynthesis by over-expressing an *E. coli thrA*^{fr}*BC* operon along with over-expression of *ilvA*^{fr} (encoding threonine deaminase) was performed to enhance synthesis of 2-ketobutyrate, a common keto-acid intermediate for isoleucine biosynthesis. 2-ketobutyrate can further be converted to propionyl-CoA by an endogenous pyruvate dehydrogenase complex (PDHc) or pyruvate-formate lyase (PflB).

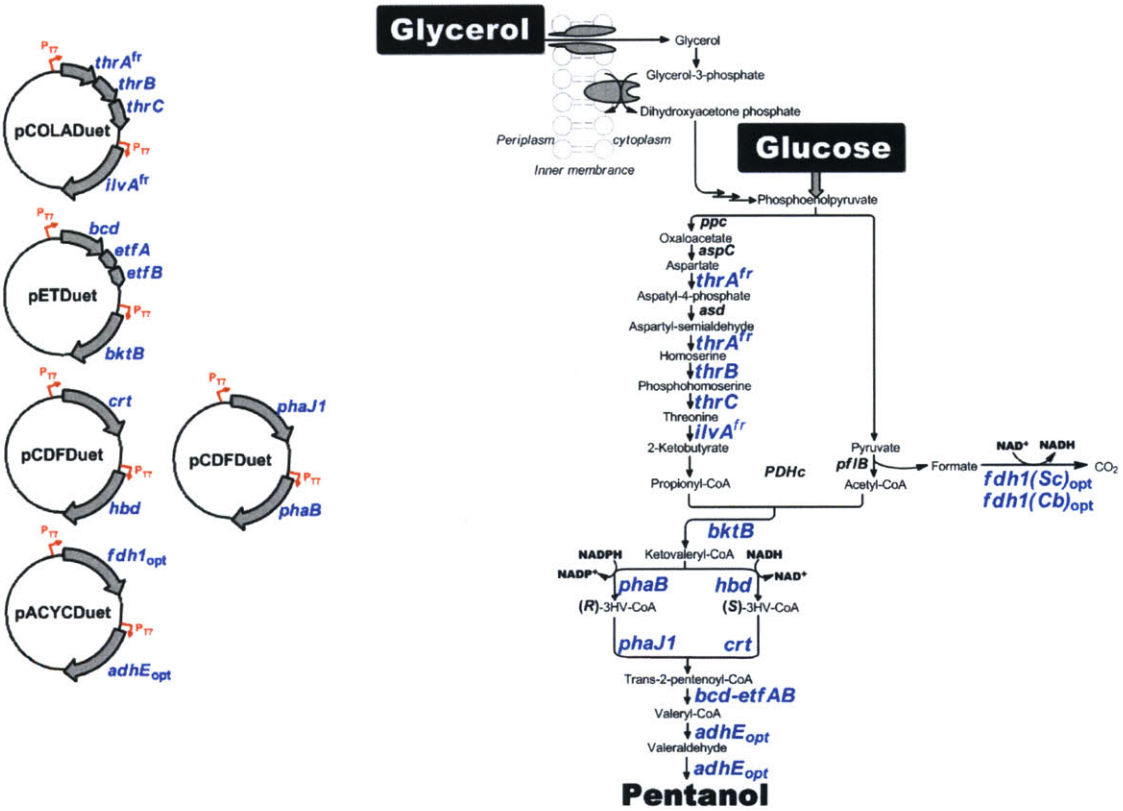

Figure 5-2 | Schematic of metabolic pathway and plasmids constructed for direct micriobial production of pentanol from glucose or glycerol. Overexpressed genes are shown in blue. Four compatible Duetvectors were used to carry all pathway genes.

5.3.2 Trans-2-pentenoate synthesis from glucose and propionate

To evaluate the ability of upstream pentanol pathway enzymes to accept five-carbon substrates, the pentanol pathway was shortcut towards production of

trans-2-pentenoate along with over-expression of a CoA activator Ptb-Buk. Here, two distinct metabolic routes, including one through (*S*)-3HV-CoA with an *hbd-crt* gene pair and the other through (*R*)-3HV-CoA with a *phaB-phaJ1* gene pair, were examined (**Fig. 5-3**).

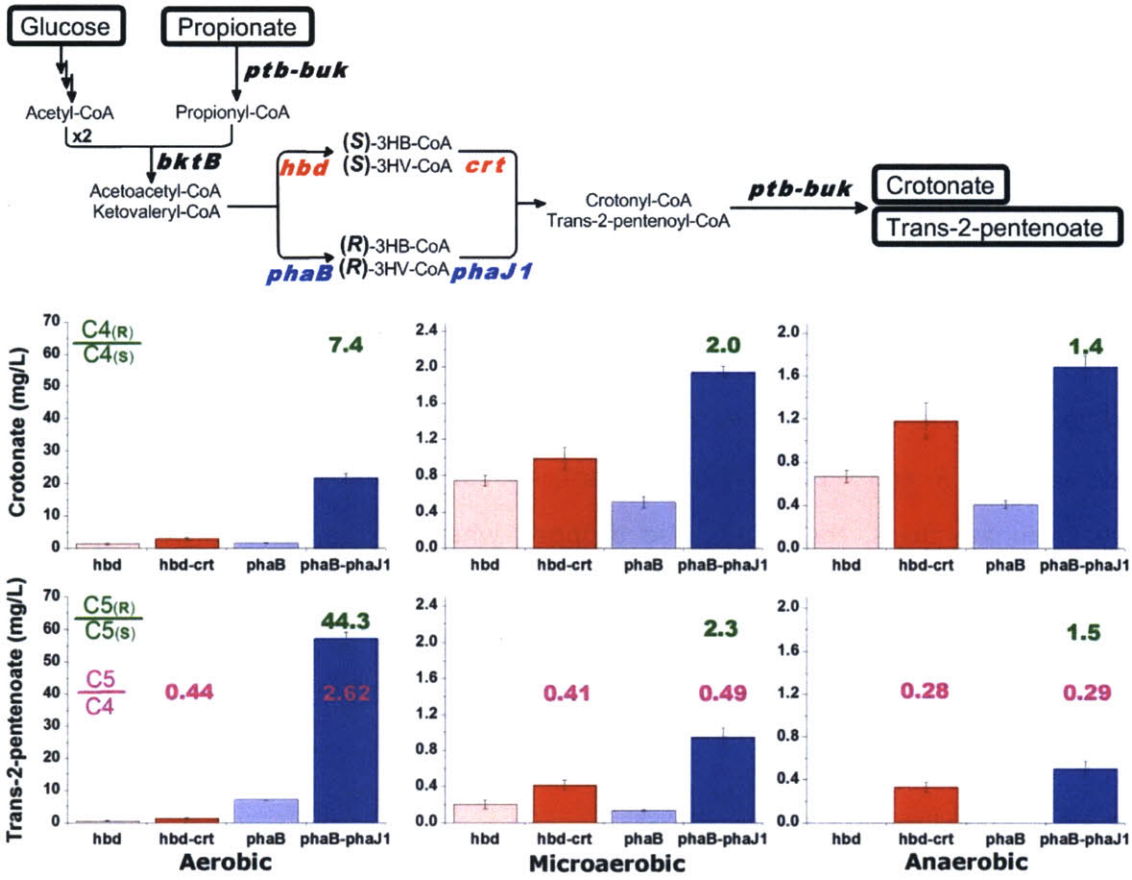

Figure 5-3 | Schematic of trans-2-pentenoate biosynthetic pathway (Top) and titers of products synthesized by recombinant *E. coli* grown under various conditions (Bottom). All constructs contain *ptb-buk* and *bktB* in addition to the genes indicated under each bar. The symbols of C4 and C5 denote crotonate and trans-2-pentenoate, respectively. Ratios of titers from *phaB-phaJ1* constructs to titers from *hbd-crt* constructs are shown in pink while ratios of trans-2-pentenoate titers to crotonate titers are shown in green. Cells were grown in TB supplemented with 10 g/L glucose and 20 mM propionate, and incubated at 30°C for 24 h.

Clearly, strains expressing *phaJ1* along with *phaB* were able to produce much more crotonate and trans-2-pentenoate than the no-*phaJ1* control under aerobic, microaerobic, and anaerobic conditions. Strains expressing *crt* along with *hbd* also produced both crotonate and trans-2-pentenoate, but the difference in titers between *crt*-expressing and *crt*-lacking strains was small. In general, there existed some

background crotonase activity (both *S*- and *R*- specific) that resulted in background production of crotonate and trans-2-pentenoate as observed in the no-*crt* and no-*phaJ1* controls. Altogether, the results show that all enzymes examined here, particularly Hbd, Crt, PhaB and PhaJ1, accepted five-carbon substrate analogues in addition to the natural four-carbon substrates.

Futhermore, to compare the two routes employed for the trans-2-pentenoate synthesis, two ratios, including one ratio of product titers from *phaB-phaJ1* constructs to those from *hbd-crt* and the other ratio of tran-2-pentenoate titers to crotonate titers (**Fig. 5-3**) were calculated. For the ratios of product titers from *phaB-phaJ1* constructs to those from *hbd-crt*, a value larger than one suggests that the *R*-pathway outperforms the *S*-pathway, which was the case under aerobic conditions. On the other hand, the ratio was close to one under anaerobic conditions, suggesting that the difference between the *R*- and *S*- pathway became smaller. For the ratios of tran-2-penenote titers to crotonate titers, the values also dropped when culture condition changes from aerobic to anaerobic. The difference in the two ratios between the *R*- and *S*- pathway implicates a correlation between oxygen availability and *R*- and *S*- pathway activities, to explain which a hypothesis was proposed in Discussion.

5.3.3 Pentanol synthesis from valerate

After validating the top pentanol pathway through synthesis of trans-2-pentenoate, we next wanted to evaluate whether the bottom pentanol pathway enzymes, including the butyryl-CoA dehydrogenase (encoded by *bcd-etfAB*) and the bi-functional alcohol/aldehyde dehydrogenase (encoded by *adhE*), can accept non-natural five-carbon substrates.

Valerate was initially supplemented to the culture in addition to glucose to test whether the AdhE enzyme could convert valeryl-CoA to pentanol (**Fig. 5-4**). Here, two versions of AdhE coding genes, including one original *adhE* from *C. acetobutylicum* and one codon-optimized *adhE* (denoted as $adhE_{opt}$), were explored. We found that cells containing $adhE_{opt}$ along with *ptb-buk* or *pct* were able to produce pentanol from

valerate while it was not the case for cells containing *adhE*. Such result is consistent with our observation on the protein gel that expression of *adhE* was significantly improved by codon-optimization as a strong protein band appeared on the protein gel from the soluble fraction of cell lysate (data not shown).

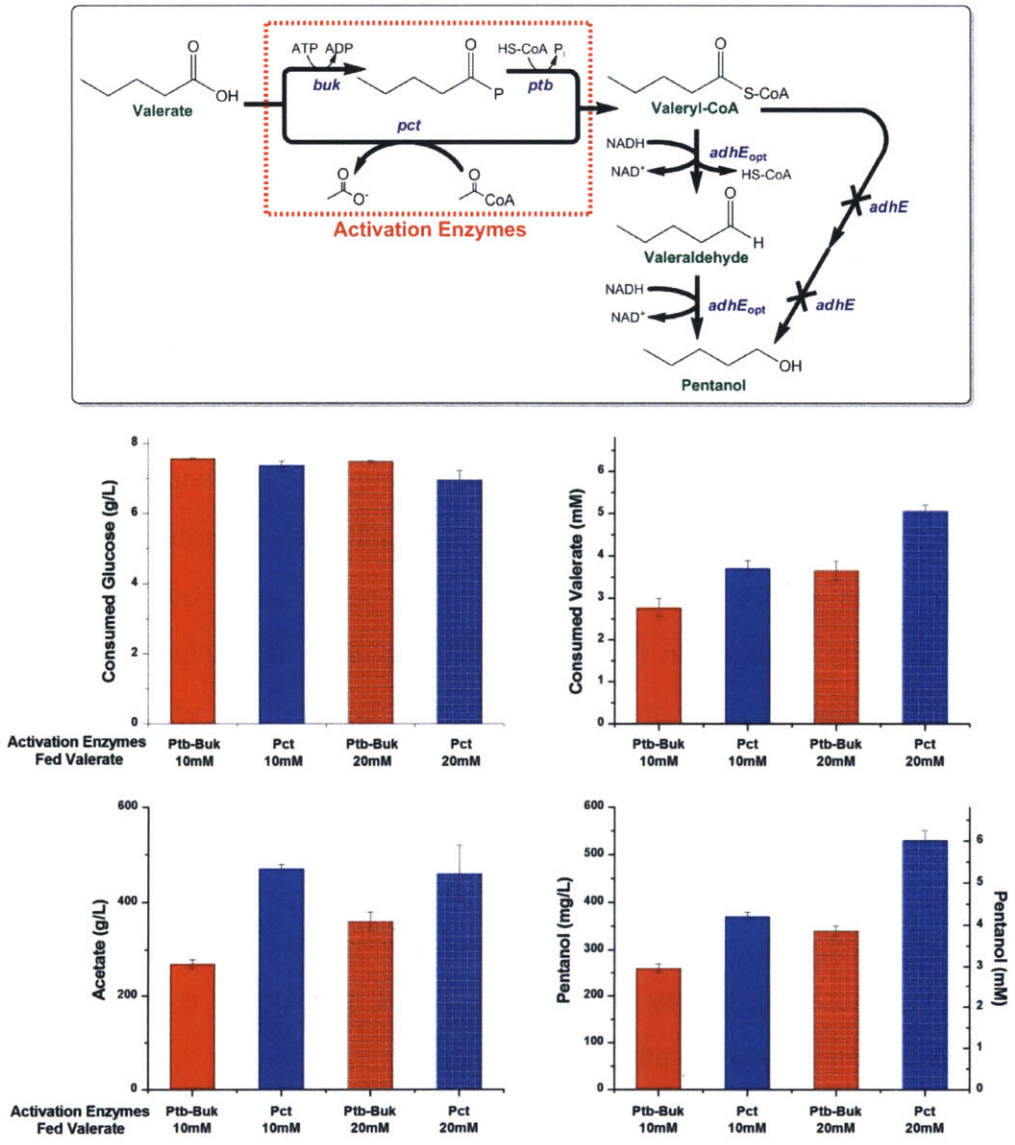

Figure 5-4 | Schematic diagram of pentanol synthesis from valerate and titers of substrates consumed and products synthesized by recombinant *E. coli*. Two activators, including Ptb-Buk and Pct, and two feed concentrations of valerate, were compared. The $adhE_{opt}$ gene was over-expressed in all constructs.

In addition, two activators were compared for valerate activation, and stains utilizing Pct as CoA-activation were found to consume more valerate and produce more

pentanol compared to stains utilizing Ptb-Buk as CoA-activation. Pentanol titers were further boosted when the valerate substrate concentration was increased from 10 mM to 20 mM (**Fig. 5-4**). Overall, the results presented here suggest that the AdhE enzyme, expressed from the codon-optimized $adhE_{opt}$, was able to catalyze the reaction of valeryl-CoA to pentanol.

5.3.4 Pentanol synthesis from trans-2-pentenoate

Next, one additional enzymatic step upstream to the AdhE reaction was examined through feeding of trans-2-pentenoate (**Fig. 5-5**). Trans-2-pentenoate was first activated to trans-2-pentenoyl-CoA by the activator Ptb-Buk, followed by sequential reduction to pentanol, catalyzed by Bcd and AdhE. Due to substrate promiscuity of those introduced enzymes together with endogenous fatty acid beta-oxidation activities, production of several other metabolites such as propionate, 3HV, pentenol, and valerate, was also expected. Cells containing the bottom pentanol pathway produced valerate with a molar yield of 30% on consumed trans-2-pentenoate, but resulted in undetectable pentanol production (top left plot in **Fig. 5-5**). The failure in pentanol production is most likely due to an intensive cofactor requirement of two moles of NADH for the reaction from valeryl-CoA to pentanol as opposed to zero for the reaction from valeryl-CoA to valerate while generating one mole of ATP. Energetically speaking, production of valerate would be more preferable for *E. coli* as opposed to production of pentanol. If that is the case, an increased NADH availability would be expected to allow for pentanol synthesis. One way to increase NADH availability is to utilize an NAD^+-dependent fomate dyhydrogenase from yeast.

The native *E. coli* formate dehydrogenase converts foramte to CO_2 and H_2 without generation of any NADH while the NAD^+-dependent formate dehydrogenase from several yeast strains could generate one mole of NADH with conversion of one mole of formate (*Berrios-Rivera et al., 2002*). It has been demonstrated that overexpression of the NAD^+-dependent FDH1 from *Candida boidinii* increased NADH

availability by extracting reducing power from formate and, consequently, enhanced ethanol production (*Berrios-Rivera et al., 2002*).

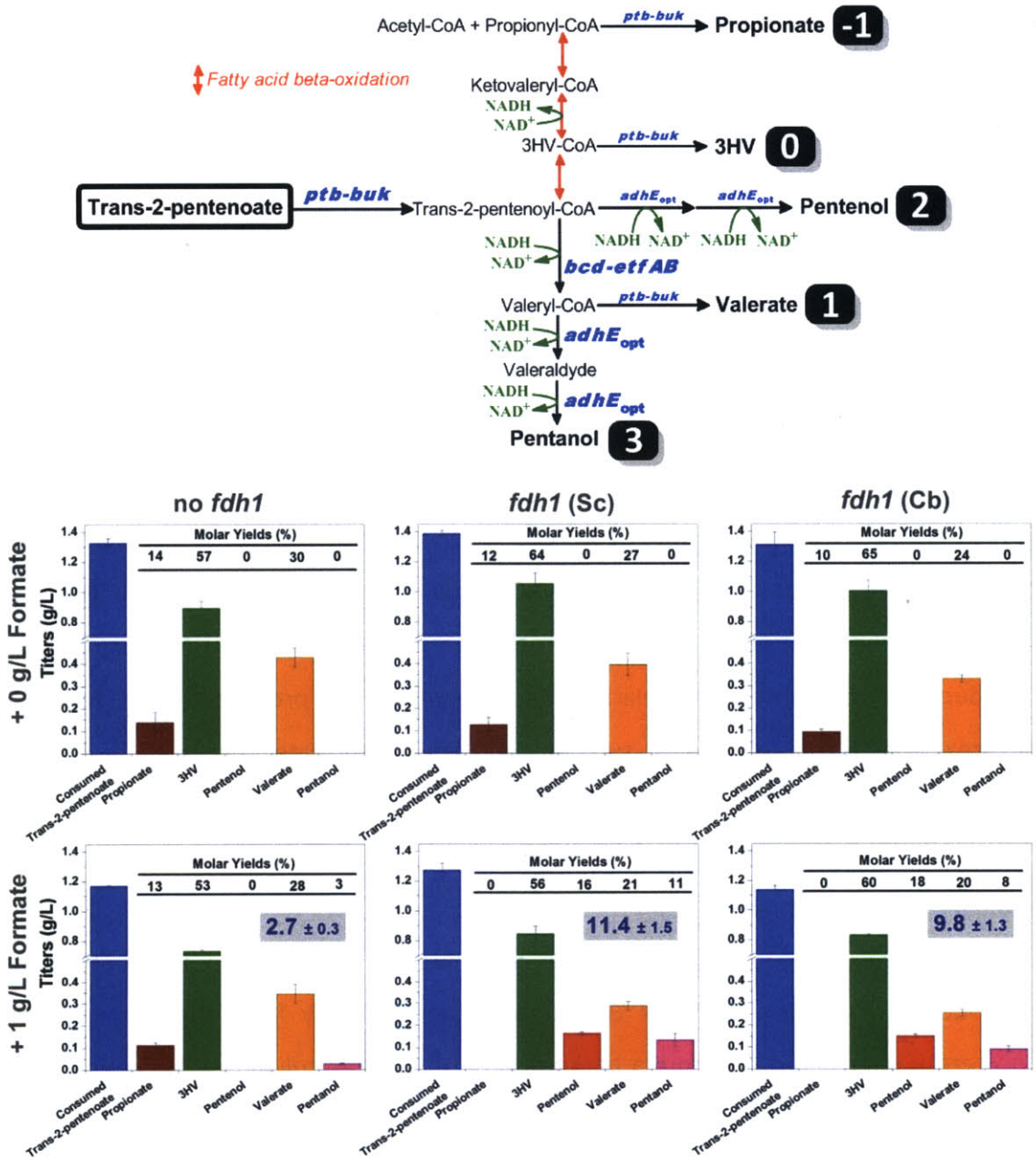

Figure 5-5 | Schematic diagram of pentanol synthesis from trans-2-pentenoate and titers of products resulting from the feeding of trans-2-pentenoate. All relevant products coming from trans-2-petenoate are shown. Genes of *ptb-buk*, *bcd-etfAB* and $adhE_{opt}$ were overexpressed. Two formate dehydrogenases (encoded by *fdh1* with codon-optimization) from *Saccharomyces cerevisiae* and *Candida boidinii* were over-expressed to increase availability of NADH. The effect of supplementation with 1 g/L formate was also compared. The calculated total NADH used for product formation was shown within each of bottom three plots.

In this work, two codon-optimized *fdh1* genes from *Saccharomyces cerevisiae and C. boidinii* were employed. The effect of overexpression of the two *fdh1* genes was then investigated with the bottom pentanol pathway (schematic in **Fig. 5-5**). Since the *E. coli* host strain used here was BL21Star(DE3), which normally produces little amount of formate under anaerobic conditions, supplementation of formate is required in this case. As expected, there was no effect of overexpression of either *fdh1* gene when formate was not supplemented (top three plots in **Fig. 5-5**). On the contrary, in the formate supplemented cultures, the overexpression of *fdh1* resulted in synthesis of more reduced products, including pentenol (a mono-unsaturated five-carbon alcohol) and pentanol (bottom three plots in **Fig. 5-5**).

To quantify the effect of overexpression of *fdh1*, one number was assigned to each product based on its relative redox state, for example, 2 for pentenol as its synthesis from trans-2-pentenoyl-CoA requires 2 moles of NADH and -1 for propionate as its synthesis from trans-2-pentenoyl-CoA generates 1 mole of NADH. Next, we calculated the total NADH used for product formation, which is the summation of products of multiplying the relative redox value by the product titer. Clearly, the overexpression of *fdh1* with supplementation of formate increased the NADH availability within the cells as the total NADH used for product formation increased from 2.7 in the no-*fdh1* control to 11.4 and 9.8 in cells expressing *S. cerevisiae fdh1* and *C. boidinii fdh1*, respectively.

Furthermore, one control experiment with a strain without *bcd-etfAB* was conducted to confirm that the Bcd activity came directly from the overexpressed *bcd-etfAB* operon but not from a background activity of *E. coli* as neither pentanol nor valerate was produced in such strain (data not shown). This and the other observation of production of valerate and pentanol in the *bcd-etfAB* containing strain suggest that Bcd employed in the bottom pentanol pathway can transform trans-2-pentenoyl-CoA, a five-carbon substrate, to valeryl-CoA.

5.3.5 Validation of the pentanol pathway by butanol synthesis

After verifying each of the top and bottom pentanol pathways, next, we assembled them together. Compared to the original *Clostridial* butanol pathway (left diagram in **Fig. 5-6**), three key changes occurred in our newly constructed pentanol pathway (right diagram in **Fig. 5-6**). First, a *bktB* thiolase with broader substrate specificity was used to do the initial condensation reaction as opposed to *thl* thiolase. Second, an alternative route through *phaB* and *phaJ1* was constructed in addition to that through *hbd* and *crt*. Third, a codon-optimized $adhE_{opt}$ gene was used, in place of the original *adhE* gene, to promote its functional expression in *E. coli*. To validate the newly constructed pentanol biosynthetic pathways, butanol synthesis was initially examined.

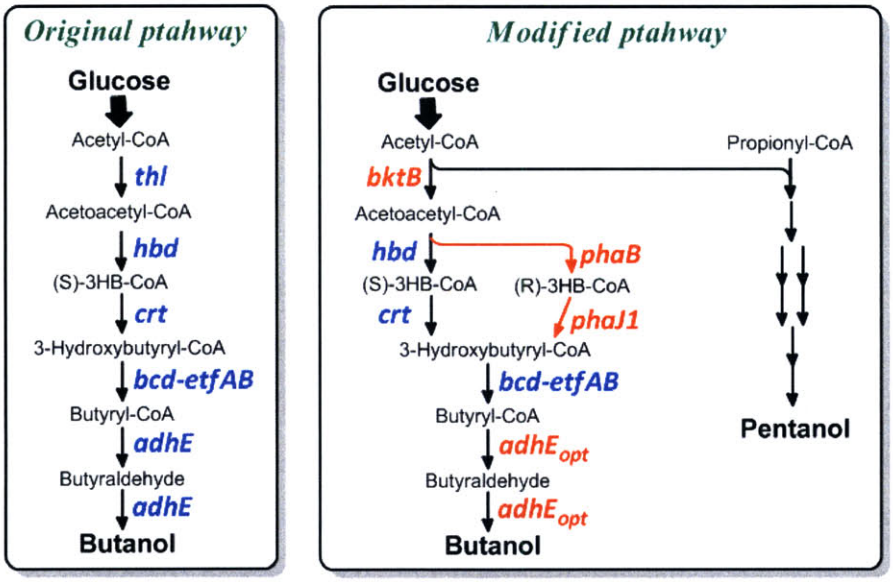

Figure 5-6 | Comparson of the *Clostridial* butanol pathway and the newly constructed pentanol pathway. The difference in genes between the *Clostridial* butanol pathway and the proposed pentanol pathway is shown in red.

Cells were cultivated in conditions with various ratios of headspace to culture volume for 48h. The reason of profiling the headspace to culture volume ratios is because of our previous observation on a correlation between oxygen availability and *R*- and *S*- pathway activity as seen in the experiment of trans-2-pentenoate production from glucose and propionate (**Fig. 5-3**). In general, strains containing either *R*- or *S*- pentanol biosynthetic pathway produced butanol, achieving the highest butanol specific titers at a headspace to culture volume ratio of 4 (**Fig. 5-7**).

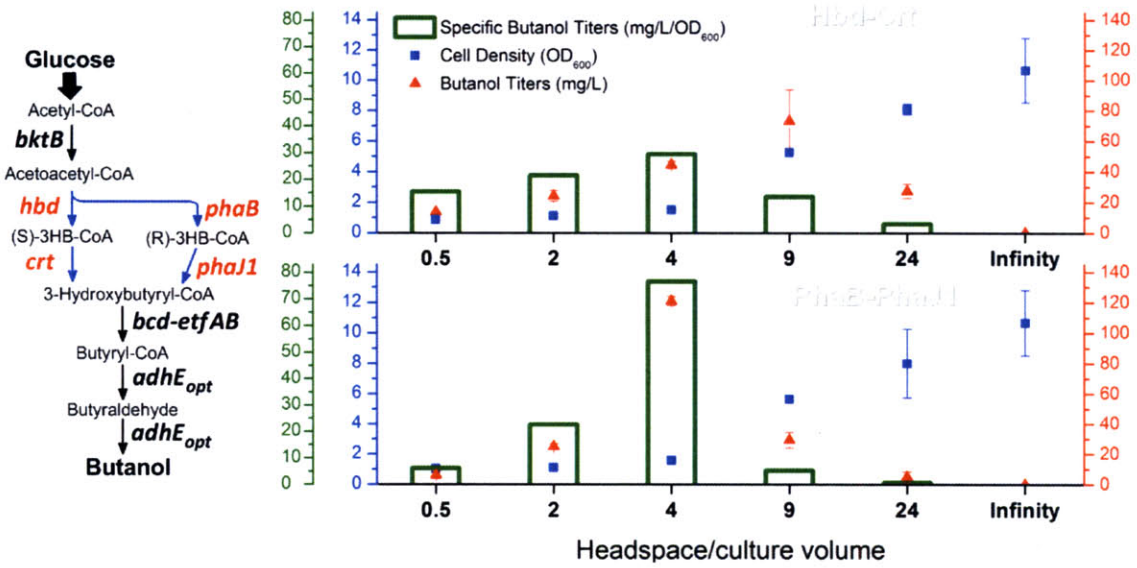

Figure 5-7 | Butanol synthesis from glucose via newly constructed pentanol pathways. This figure shows butanol titers, specific titers, and cell densities from cultures of recombinant *E. coli* containing the pentanol pathways. Cells were grown under various culture conditions with different ratios of headspace to culture volume for 48h. Two routes, including the *hbd-crt* route (Top) and the *phaB-phaJ1* (Bottom) route, were compared.

5.3.6 Pentanol synthesis from glucose and propionate

Next, we employed the pentanol pathway for pentanol synthesis from glucose and propionate. Here, Pct was expressed to activate propionate to propionyl-CoA, and each of the Fdh1 enzymes was utilized to increase NADH availability. In addition, cell cultures were performed under the condition at a headspace to culture volume ratio of 4 because of the previous observation that such ratio achieved highest butanol specific titers. In general, a boosted acetate production was observed compared to the control containing empty plasmids (**Fig. 5-8**), most likely due to the activation of propionate to propionyl-CoA with concomitant production of acetate from acetyl-CoA. Also, the propionyl-CoA seemed to be converted to propanol by the AdhE enzyme as propanol was produced with titers up to 350 mg/L and 700 mg/L in the *S*- and *R*-constructs, respectively, indicating a promiscuity of the AdhE enzyme. More importantly, all recombinant strains yielded pentanol from glucose and propionate with titers up to 85 mg/L (**Fig. 5-8**).

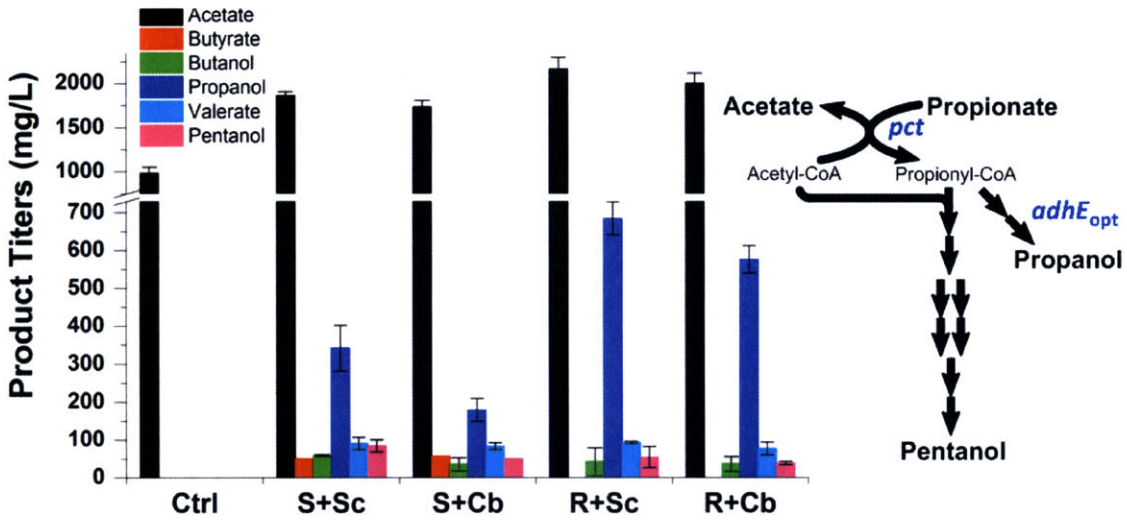

Figure 5-8 | Pentanol synthesis from glucose and propionate. Genes of *pct* and either *fdh1* (denoted as Sc) from *S. cerevisiae or fdh1* (denoted as Cb) from *C. boidinii* were overexpressed, in addition to the core pentanol pathway genes. Titers of pentanol and other relevant products are shown in the plot. The symbols of S and R denote the *hbd-crt* route and the *phaB-phaJ1* route, respectively.

5.3.7 Pentanol synthesis solely from glucose or glycerol

The results presented so far suggest that direct microbial synthesis of pentanol solely from glucose or glycerol can be realized upon recruiting all pathway enzymes together. So next, recombinant strains containing 4 compatible plasmids carrying all pentanol pathway genes were constructed and the resulting strains were tested for pentanol production solely from glucose or glycerol.

When glucose was used as the carbon source, only butyrate and butanol along with trace amount of propionate and proponal were produced. Neither valerate nor pentanol was synthesized (**Fig. 5-9**). On the contrary, when glycerol was used as the sole carbon source, titers of propionate, propanol, butyrate, and butanol were significantly increased compared to glucose as the carbon source. Particularly, the boosted production of propioante and propanol suggest a sufficient supply of propionyl-CoA from glycerol. Besides, direct valerate synthesis from glycerol was achieved. However, pentanol was not produced in either case.

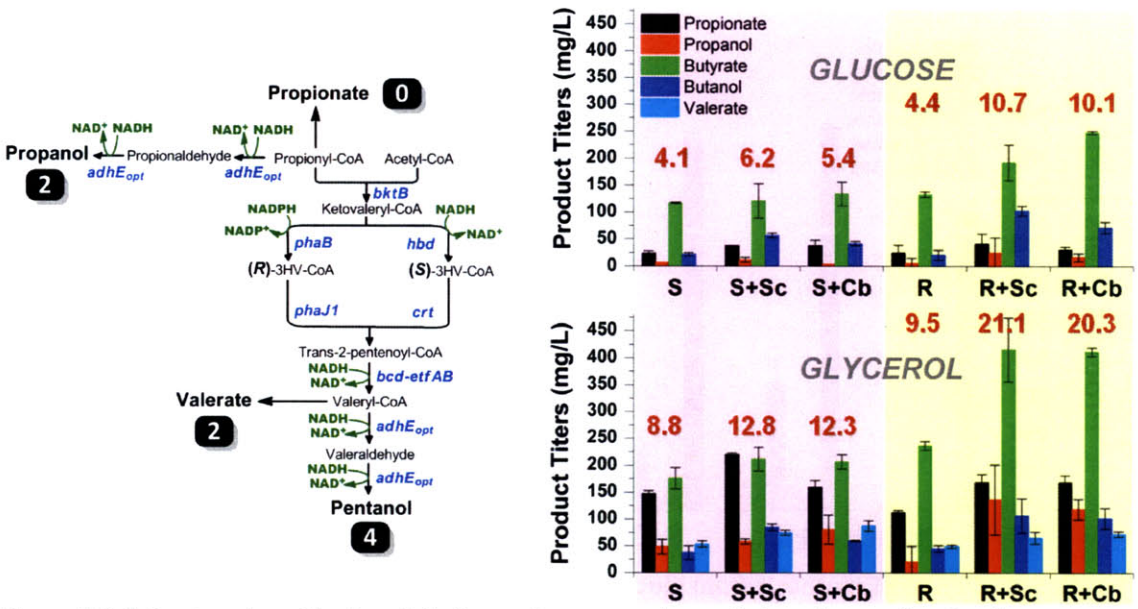

Figure 5-9 | Pentanol synthesis solely from glucose or glycerol. A pathway allowing for endogenous supply of propionyl-CoA was introduced along with overexpression of either *fdh1* (denoted as Sc) from *S. cerevisiae or fdh1* (denoted as Cb) from *C. boidinii*, in addition to the core pentanol pathway genes. The symbols of S and R denote the *hbd-crt* route and the *phaB-phaJ1* route, respectively. The relative redox values of relevant products are shown on the left panel and the calculated total NADH used for product formation was shown above each data set on the right panel.

We then calculated the total NADH used for product formation in a way similar to what we have done previously, by summing up the products of multiplying the relative redox value by the product titer. Again, the overexpression of *fdh1* was shown to enhance production of more reduced products. In addition, we found that the values of total NADH used for product formation in glycerol cultures were much larger than those in glucose cultures, consistent with the fact that glycerol is more reduced than glucose.

5.4 Discussion

The results of trans-2-pentenoate synthesis from glucose and glycerol under aerobic, microaerobic, and anaerobic culture conditions suggest that there may exist a correlation between oxygen availability and *R*- and *S*- pathway activities, to explain which a hypothesis was proposed (**Fig. 5-10**).

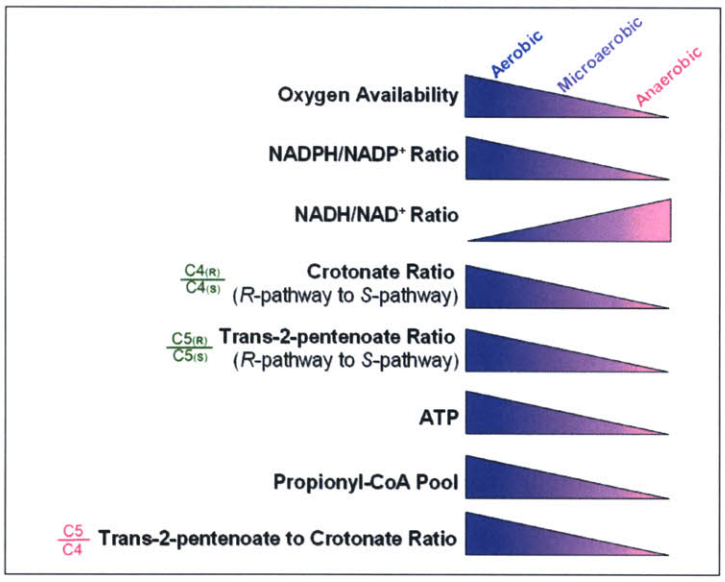

Figure 5-10 | Schematic representation of correlations between dissolved oxygen and various variables (cofactor ratios, ATP, and observed product ratios).

As generally known, NADPH/$NADP^+$ ratio is positively correlated with DOT (dissolved oxygen tension) while NADH/NAD^+ ratio is inversely correlated with DOT, so we could expect the NADPH-dependent *R*-pathway outperforms the NADH-dependent *S*-pathway under aerobic conditions, resulting in larger crotonate ratios (*R*-pathway to *S*-pathway) and trans-2-pentenoate ratios (*R*-pathway to *S*-pathway) (**Fig. 5-3**). When it comes to anaerobic conditions, the trend of cofactor ratios reverses, the difference in performance between the two pathways should become smaller, which is consistent with what we observed. In addition, we suspected that the activation of propionate is also affected by DOT as its activation by Ptb-Buk requires ATP, whose amount is positively correlated with DOT. Thus, a larger propionyl-CoA pool could be expected under the aerobic conditions, thus favoring the condensation reaction of acetyl-CoA with propionyl-CoA, and consequently resulting in larger trans-2-pentenoate to crotonate ratios (**Fig. 5-3**). Such observation gave us an insight into optimization of culture conditions, motivating us to profile the various headspace to culture volume ratios for production of butanol or pentanol (**Fig. 5-7**). In addition, this result and the other observation on undetectable pentanol production from the feeding of trans-2-pentenoate led us to think that our pentanol biosynthetic pathway activity may

be affected or limited by the intracellular NADH availability. To prove that, we investigated the effect of overexpression of yeast *fdh1* genes on pentanol synthesis from trans-2-pentenoate (**Fig. 5-5**), and found that such strategy successfully enabled pentanol production. We next assembled both the top and bottom pentanol pathway and introduced it to *E. coli*. The resulting recombinant *E. coli* achieved pentanol synthesis from glucose and propionate, demonstrating a functional and feasible pentanol biosynthetic pathway in *E. coli* (**Fig. 5-8**).

However, undetectable pentanol was observed in the experiment of direct production of pentanol solely from glucose or glycerol, most likely due to limited pathway activity as a result of limited availability of NADH. This is of particular concern with our pentanol biosynthetic pathway that combines an energetically expensive threonine biosynthesis pathway with the *Clostridial* butanol pathway which has intensive requirement for reducing equivalent, consuming 4 moles NADH per mole of butanol produced. The intensive requirement for NADH and other reducing equivalents in pentanol synthesis is expected to create a redox imbalance in *E. coli*, thus making the pentanol biosynthetic pathway unpreferable. To improve the pathway performance, we need to address such problem, and one solution, intuitively, is to engineer *E. coli* to further boost the NADH availability.

Under anaerobic growth conditions, one mole of glucose yields only two moles of NADH due to an inactive pyruvate dehydrogenase complex (PDHc) enzyme. Therefore, it would be interesting to construct a mutant that has an active PDHc under anaerobic conditions in an attempt to boosting NADH yield up to 4 moles of NADH per mole of glucose. Furthermore, the pentanol biosynthesis uses acetyl-CoA as one of precursor substrates that could possibly be limited in wild-type *E. coli* under anaerobic conditions. Therefore, an anaerobically active PDHc is also expected to enlarge acetyl-CoA pool, thereby enhancing the pentanol biosynthesis. In fact, an *E. coli* mutant SE2378 has been isolated with a mutant PDHc that functions under anaerobic conditions (*Kim et al., 2008*). In such case, four NADH molecules were re-oxidized by reduction of the two acetyl-CoA molecules to produce two ethanol molecules at a yield of 82% from glucose. However,

SE2378 demonstrated very poor transformation efficiency (as I have encountered first hand) as well as other undesired phenotypes resulting from random mutagenesis that could prevent from further strain development. Construction of a genetically-defined *E. coli* strain with a similar phenotype to mutant SE2378 will be preferable in the aspect of enriched NADH and acetyl-CoA pools, which is currently under investigation.

5.5 Conclusions

This work aims to use butanol synthesis as a platform from which microbial synthesis of pentanol can be obtained. Of particular note is the demonstration of direct production of valerate from a single carbon source of glycerol. Future pathway engineering will lead towards the production of the five-carbon alcohol (pentanol) instead of the five-carbon acid (valerate). Altogether, the results presented in Chapter 5 suggest that direct microbial synthesis of pentanol solely from glucose or glycerol can be realized once an efficient redox balancing within the recombinant strains is ensured. Specifically, by further engineering the internal redox metabolism in the recombinant strains, we should be able to redirect carbon flux towards the desired route for pentanol synthesis.

CHAPTER 6

Biosynthesis of Structurally Diverse 3-Hydroalkanoic Acids

Abstract

Chapter 6 focuses on the construction of a novel biosynthetic pathway, as an extension of the 3HV biosynthetic pathway described in Chapter 4, for production of value-added chiral 3-hydroxyalkanoic acids in *Escherichia coli*. The BktB thiolase implicated in polyhdroxyalkanote biosynthesis in *Ralstonia eutropha* was utilized for the initial condensation reaction. The required CoA-activated substrates were obtained intracellularly by feeding the precursor acids exogenously along with heterologous expression of the propionyl-CoA transferase gene (*pct*) from *Megasphaera elsdenii*. The PhaB reductase from *Ralstonia eutrophia* demonstrated the broadest capability for reduction of the ketone to produce the chiral alcohol, and the thioesterase B (TesB) of *E. coli* displayed broad substrate specificity for the hydrolysis of the thioester bond. Feeding of propionate, butyrate, and isobutyrate resulted in the production of 3-hydroxyvalerate, 3-hydroxyhexanoate, and 4-methyl-3-hydroxyvalerate, respectively. Of particular note is the observation that supplying glycolate resulted in the production of 3,4-dihydroxybutyrate and its related lactone, 3-hydroxy-γ-butyrolactone, a "top value-added chemical" from biomass.

This chapter will be submitted for publication as:

Martin, C.H. *, Tseng, H.-C. *, Dhamankar, H., Sheppard, M.J., Prather, K.L.J. "A platform pathway for the production of value-added biochemicals"

* These authors contributed equally to the work.

6.1 Introduction

Hydroxyacids are versatile, chiral compounds that contain both a carboxyl and a hydroxyl moiety, readily allowing for their modification into several useful derivatives (*Chen & Wu, 2005, Lee et al., 2002*) and making them suitable for applications in the synthesis of antibiotics (*Chiba & Nakai, 1985*), β- and γ-aminoacids and peptides (*Park & Kim, 2001, Seebach et al., 1986*), and as chiral synthetic building blocks (*Lee et al., 2002*). Direct biological production of hydroxyacid monomers has been successfully demonstrated for 3-hydroxybutyrate (3HB), and titers of 3 g L^{-1} and 12 g L^{-1} on the shake flask and fed-batch scales have been reported (*Gao et al., 2002*). In these reports, 3HB is made from acetyl-CoA through the use of acetyl-CoA acetyltransferase (*pha*A), 3-hydroxybutyryl-CoA dehydrogenase (*pha*B), phosphotransbutyrylase (*ptb*), and butyrate kinase (*buk*) (*Gao et al., 2002, Liu & Steinbuchel, 2000, Liu & Steinbüchel, 2000*). The last two of these enzymes were chosen to remove the CoA moiety from 3-hydroxybutyryl-CoA to yield free 3HB and were taken from *Clostridium acetobutylicum*, where they participate in the production of butyrate from butyryl-CoA (*Liu & Steinbüchel, 2000*). Recently, thioesterase II (*tes*B) from *Escherichia coli* K12 (*Naggert et al., 1991*) was successfully employed to directly hydrolyze the acyl-thioester of 3HB-CoA (*Liu et al., 2007, Tseng et al., 2009*). Tseng et al. (2009) investigated three different thiolases (*pha*A, *bkt*B, *thl*) and two different reductases (*pha*B, *hbd*) to exclusively produce both the *R*- and *S*-enantiomers, respectively, of 3HB. This work demonstrated that TesB is capable of hydrolysis of both enantiomers of 3HB-CoA, while the Ptb-Buk enzyme system is specific to the *R*-enantiomer.

The success of direct production of 3HB from the condensation of two acetyl-CoA caused us to consider the possibility of producing more structurally diverse hydroxyacids through generalizing this pathway to the condensation of an acyl-CoA molecule with acetyl-CoA (**Fig. 6-1**). In this platform pathway, referred to as the 3-hydroxyalkanoic acid pathway, a thiolase is employed to perform the condensation reaction to yield a 3-ketoacyl-CoA intermediate, which is subsequently reduced by either *pha*B or *hbd* to yield a 3-hydroxyacyl-CoA compound. Finally, *tes*B is used to hydrolyze the CoA moiety

from the 3-hydroxyacyl-CoA, liberating the free 3-hydroxyalkanoic acids. One complication in the 3-hydroxyalkanoic acid pathway is that unlike acetyl-CoA, short chain acyl-CoA compounds that would be candidate substrates for this pathway are not readily available metabolites in *E. coli*. To address this limitation, we recently utilized the platform pathway with the BktB thiolase to produce the 5-carbon analog 3-hydroxyvalerate (3HV) (*Tseng et al., 2010*). In this case, the required precursor substrate is propionyl-CoA, which was produced intracellularly by supplying propionate exogenously to the culture medium and utilizing the *ptb-buk* enzymes described previously, as the proteins are known to act reversibly (*Liu & Steinbüchel, 2000*). The resulting pathway yielded approximately 2 g L^{-1} of either enantiomer.

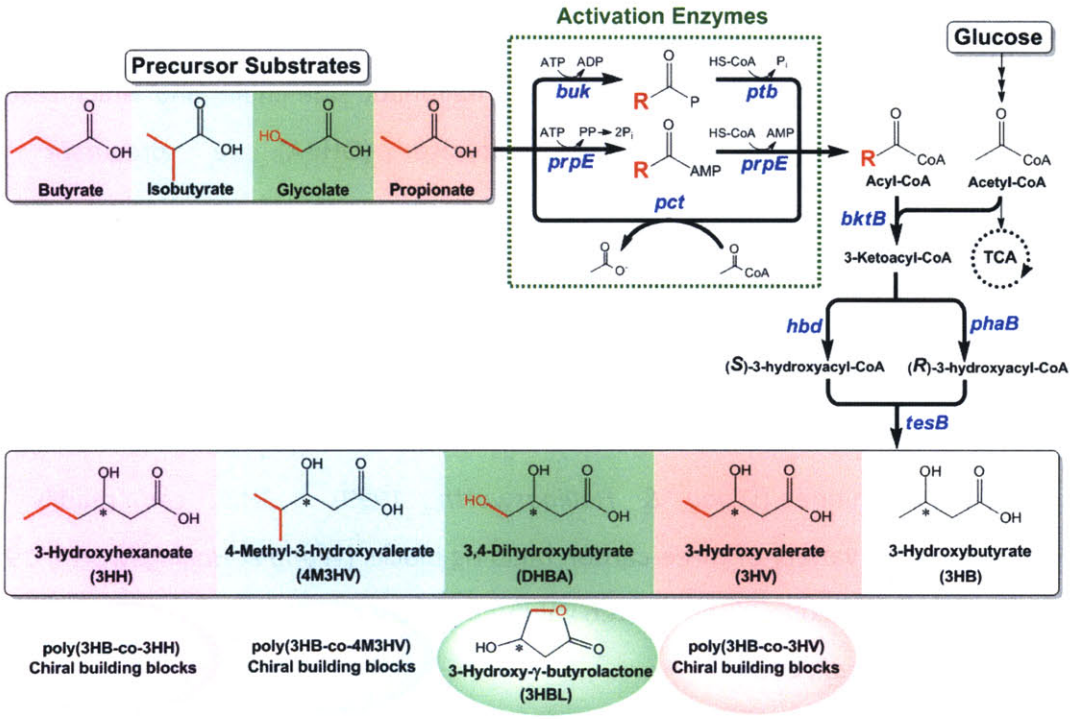

Figure 6-1 | Schematic representation of the 3-hydroxyalkanoic acid pathway. Genes in blue are overexpressed, including one of the activation enzymes (encoded by *pct*, *prpE*, or *ptb-buk*), one thiolase enzyme (encoded by *bkt*B), one of two 3-hydroxybutyryl-CoA reductases (encoded by *pha*B or *hbd*), and one thioesterase enzyme (encoded by *tes*B). The carbon sources used in the system are glucose and one of precursor substrates enclosed by a rectangular box. The precursor substrates and their corresponding products of 3-hydroxyalkanoic acids are color-coded accordingly.

The goal of the current work was to further explore the ability of this platform pathway to produce more structurally diverse compounds upon feeding the

corresponding precursor acids. Because of the diverse nature of the precursors, additional CoA-activation systems were investigated. These included propionyl-CoA transferase (*pct*), a broad substrate-specificity enzyme from *Megasphaera elsdenii* (*Schweiger & Buckel, 1984, Taguchi et al., 2008*) that exchanges CoA moieties between short-chain organic acids including acetyl-CoA, and propionyl-CoA synthetase (*prp*E) from *Salmonella typhimurium* LT2 (*Liu et al., 2008*), in addition to Ptb-Buk. Each of the CoA activation mechanisms were first validated with propionate feeding and 3HV production. A single thiolase, BktB, was employed because of its previously demonstrated ability to act efficiently to form both 4- and 5-carbon molecules (*Slater et al., 1998, Tseng et al., 2010*). We chose to explore the feeding of butyrate to determine whether longer chain hydroxyacids could be produced and isobutyrate to examine the potential for synthesis of branched substrates. Finally, we investigated the ability to feed glycolate, which carries a non-aliphatic side chain, and which results in the production of 3,4-dihydroxybutyrate (DHBA), a precursor to 3-hydroxy-γ-butyrolactone (3HBL). 3HBL is widely used in the pharmaceutical industry as a building block for the class of cholesterol-reducing drugs called statins such as Crestor$^{(R)}$ and Lipitor$^{(R)}$ as well as the antibiotic Zyvox$^{(R)}$ and the anti-hyperlipidemic medication Ezetimibe$^{(R)}$ (*Lee & Park, 2009, Lee et al., 2008*). Other pharmaceuticals derived from 3HBL include HIV inhibitors (*Kim et al., 1995*) and the nutritional supplement L-carnitine (*Wang & Hollingsworth, 1999*). 3HBL can readily be transformed into a variety of three-carbon building blocks (*Wang & Hollingsworth, 1999*) and has been listed as one of the top ten value-added chemicals by the U.S. Department of Energy (*Werpy et al., 2004*).

6.2 Materials and Methods

6.2.1 Strains

E. coli DH10B (Invitrogen, Carlsbad, CA) and ElectroTen-Blue (Stratagene, La Jolla, CA) were used for transformation of cloning reactions and propagation of all plasmids. *E. coli* MG1655(DE3) was constructed from *E. coli* MG1655 using a λDE3 Lysogenization Kit

(Novagen, Darmstadt, Germany). The *end*A and *rec*A genes in *E. coli* MG1655(DE3) were then knocked out by the method of Datsenko and Wanner (*Datsenko & Wanner, 2000*) to yield *E. coli* MG1655(DE3 Δ*end*A Δ*rec*A) as the production host for synthesis of 3HV, DHBA (and its related 3HBL), 4M3HB, and 3HH.

6.2.2 Plasmids and primers

Genes derived from *C. acetobutylicum* ATCC 824 (*ptb-buk* and *hbd*), *R. eutropha* H16 (*bkt*B and *pha*B), *E. coli* K-12 (*tes*B), *M. elsdenii* (*pct*), and *S. typhimurium* LT2 (*prp*E) were obtained by polymerase chain reaction (PCR) using genomic DNA (gDNA) templates. All gDNAs were prepared using the Wizard Genomic DNA Purification Kit (Promega, Madison, WI). Custom oligonucleotides (primers) were purchased for all PCR amplifications (Sigma-Genosys, St. Louis, MO) as listed in **Table 6-1**. In all cases, Phusion High Fidelity DNA polymerase (Finnzymes, Espoo, Finland) was used for DNA amplification. Restriction enzymes and T4 DNA ligase were purchased from New England Biolabs (Ipswich, MA). Recombinant DNA techniques were performed according to standard procedures (*Sambrook & Russell, 2001*).

Table 6-1 | List of DNA oligonucleotide primers used in the cloning of genes for the 3-hydroxyalkanoic acid pathway. Restriction sites used for cloning are underlined. Primer names correspond to the name of the gene that the primer amplifies, whether the primer is the forward primer (FP) or reverse primer (RP) of that gene, and the restriction site incorporated into the primer sequence for cloning.

Primer	Sequence 5'→3'	Source
bktB-FP-NcoI	GACACCATGGGCATGACGCGTGAAGTGGTAG	Sigma-Genosys
bktB-RP-EcoRI	GACAGAATTCTCAGATACGCTCGAAGATGG	Sigma-Genosys
hbd-FP-NdeI	TATCCATATGAAAAAGGTATGTGTTATAGGTGC	Sigma-Genosys
hbd-RP-XhoI	GACACTCGAGTTATTTTGAATAATCGTAGAAACCTTTTC	Sigma-Genosys
phaB-FP-NdeI	GACACATATGACTCAGCGCATTGC	Sigma-Genosys
phaB-RP-XhoI	GACACTCGAGTCAGCCCATGTGCAGG	Sigma-Genosys
pct-FP-EcoRI	GACAGAATTCATGAGAAAAGTAGAAATCATTACAGCTG	Sigma-Genosys
pct-RP-PstI	GACACTGCAGTTATTTTTTCAGTCCCATGGG	Sigma-Genosys
prpE-FP-EcoRI	ATAGAATTCCGTGATGTCTTTTAGCG	Sigma-Genosys
prpE-RP-NotI	TATGCGGCCGCTATTCTTCGATCGCC	Sigma-Genosys
tesB-FP-NdeI	GACACATATGAGTCAGGCGCTAAAAAAAT	Sigma-Genosys
tesB-RP-XhoI	GACACTCGAGTTAATTGTGAATTACGCATCACC	Sigma-Genosys

Two co-replicable vectors, pETDuet-1 and pCDFDuet-1 (Novagen, Darmstadt, Germany), were used for construction of the 3-hydroxyalkanoic acid pathway. Both

Duet vectors contain two multiple cloning sites (MCS), each of which is preceded by a T7*lac* promoter and a ribosome binding site (RBS), affording high-level expression of each individual gene. The sites, used for cloning the genes, are underlined in **Table 6-1**.

Table 6-2 | *E. coli* strains and plasmids used in the 3-hydroxyalkanoic acid pathway.

Name	Relevant Genotype	Reference
Strains		
DH10B	F⁻ *mcr*A Δ(*mrr-hsd*RMS-*mcr*BC) ϕ80*lac*ZΔM15 Δ*lacX74 recA1 endA1 araD139*Δ(*ara, leu*)7697 *galU galK* λ⁻ *rpsL nupG*	Invitrogen
ElectroTen-Blue	Δ(*mcrA*)*183* Δ(*mcrCB-hsdSMR-mrr*)*173 endA1 supE44 thi-1 recA1 gyrA96 relA1 lac* Kan^r [F′ *proAB lacI*^{q}ZΔM15 Tn*10* (Tet^r)]	Stratagene
MG1655	F⁻ λ⁻ *ilvG- rfb-50 rph-1*	ATCC 700926
MG0	MG1655 Δ*end*A Δ*rec*A (DE3)	(*Tseng et al., 2010*)
MG1	MG0 containing pET/bktB/hbd and pCDF/pct/tesB	This study
MG2	MG0 containing pET/bktB/hbd and pCDF/prpE/tesB	This study
MG3	MG0 containing pET/bktB/hbd and pCDF/ptb-buk/tesB	This study
MG3B	MG0 containing pET/bktB/hbd and pCDF/(ptb-buk)$_B$/tesB	This study
MG4	MG0 containing pET/bktB/phaB and pCDF/pct/tesB	This study
MG5	MG0 containing pET/bktB/phaB and pCDF/prpE/tesB	This study
MG6	MG0 containing pET/bktB/phaB and pCDF/ptb-buk/tesB	This study
MG6B	MG0 containing pET/bktB/phaB and pCDF/(ptb-buk)$_B$/tesB	This study
MG7	MG0 containing pETDuet-1 and pCDFDuet-1	This study
Plasmids		
pETDuet-1	ColE1(pBR322) *ori*, *lacI*, T7*lac*, Amp^R	Novagen
pCDFDuet-1	CloDF13 *ori*, *lacI*, T7*lac*, Strep^R	Novagen
pET/bktB/hbd	pETDuet-1 harboring *bkt*B from *R. eutropha* H16, and *hbd* from *C. acetobutylicum* ATCC 824	This study
pET/bktB/phaB	pETDuet-1 harboring *bkt*B and *pha*B from *R. eutropha* H16	This study
pCDF/pct/tesB	pCDFDuet-1 harboring *pct* from *M. elsdenii*, and *tes*B from *E. coli* MG1655	This study
pCDF/prpE/tesB	pCDFDuet-1 harboring *prp*E from *S. typhimurium* LT2, and *tes*B from *E. coli* MG1655	This study
pCDF/ptb-buk/tesB	pCDFDuet-1 harboring a *ptb-buk* operon from *C. acetobutylicum* ATCC 824, and *tes*B from *E. coli* MG1655	This study
pCDF/(ptb-buk)$_B$/tesB	pCDFDuet-1 harboring a *ptb-buk* artificial operon from *Bacillus subtilis*, and *tes*B from *E. coli* MG1655	This study

These PCR products were digested with restriction enzymes corresponding to the restriction site incorporated into them by their respective primers and ligated directly into similarly digested Duet vectors. Of particular note is that *ptb-buk* was generated by *Eco*RI and *Not*I digestion of pCDF-PB (*Tseng et al., 2009*). Ligation reactions using pETDuet-1 as the vector were transformed into *E. coli* DH10B, while ligations using pCDFDuet-1 were transformed into *E. coli* ElectroTen-Blue. One thiolase (*bkt*B) and one of two 3-hydroxybutyryl-CoA reductases (*pha*B and *hbd*) were cloned into pETDuet-1, resulting in two pETDuet-based plasmids. The pCDFDuet-based plasmids contained one

of three CoA-activation enzymes (*pct*, *ptb-buk*, and *prp*E) and one thioesterase (*tes*B). All constructs were confirmed to be correct by restriction enzyme digestion and nucleotide sequencing. Once all plasmids were constructed, one pETDuet-based plasmid and one pCDFDuet-based plasmid were co-transformed into *E. coli* MG1655(DE3 Δ*endA* Δ*recA*) to create production strains for synthesis of 3-hydroxyalkanoic acids.

6.2.3 Culturing conditions

Seed cultures of the recombinant *E. coli* strains (**Table 6-2**) were grown in LB medium at 30°C overnight, and were used to inoculate 50 mL LB medium supplemented with 10 g/L glucose at an inoculation volume of 2% in 250 mL flasks. Of particular note, due to peak overlapping between 3HH and one of LB components, 3HH biosynthesis was conducted in M9 minimal medium plus 10 g/L glucose where seed cultures were washed and resuspended with M9 minimal medium before inoculation. The shake flask cultures were then incubated at 30°C on a rotary shaker at 250rpm. Once the cells reached mid-exponential phase (when OD_{600} reached 0.8-1.0), cultures were supplemented (final concentrations in parentheses) with IPTG (1 mM) and one of the precursor substrates, including neutralized propionate (15 mM), butyrate (15 mM), isobutyrate (15 mM), and glycolate (40 mM) for induction of gene expression and to provide the substrates needed for the 3-hydroxyalkanoic acid pathway, respectively. In all cases, culture medium was supplemented with 50 mg/L ampicillin and 25 mg/L streptomycin to provide selective pressure for plasmid maintenance. 1 mL of culture was withdrawn at every 24 h interval for up to 96 h for HPLC analysis. Titers of 3-hydroxyalkanoic acids were found not to reach a plateau until 72 h and there was essentially no difference in the titers between 72 h and 96 h; accordingly, only the peak titers observed at 72 h were reported. In general, experiments were performed in triplicates, and data are presented as the averages and standard deviations of the results.

6.2.4 Metabolite analysis

Culture samples were pelleted by centrifugation and aqueous supernatant collected for HPLC analysis using an Agilent 1200 series instrument with a refractive index detector (RID). Analytes were separated using an Aminex HPX-87H anion-exchange column (Bio-Rad Laboratories, Hercules, CA) and a 5 mM H_2SO_4 mobile phase. Glucose (Sigma, St. Louis, MO), propionate (Sigma, St. Louis, MO), butyrate (Sigma, St. Louis, MO), isobutyrate (Sigma, St. Louis, MO), glycolate (MP Biomedicals, LLC., Solon, OH), acetate (Sigma, St. Louis, MO), 3-hydroxybutyrate (Sigma, St. Louis, MO), 3-hydroxyvalerate (Epsilon Chimie, Brest, France), 3-hydroxyhexanoate (Epsilon Chimie, Brest, France), and (*S*)-3-hydroxy-γ-butyrolactone (TCI America, Portland, OR) were quantified using commercial standards by linear extrapolation from calibration of external standards.

4M3HV analysis was analyzed using HPLC/MS since a commercial standard was not available. A Zorbax SB-Aq alkyl bonded phase column (Agilent Technologies, Wilmington, DE) with a 25 mM, pH 3 ammonium formate mobile phase was used to separate 4M3HV for detection with an Agilent 1100 series instrument equipped with either RID or 6120 Quadrapole MS with multi-mode source. The commercial 3HH isomer was used with RID to estimate the concentration of 4M3HV in supernatant samples. The ammonium adducts of 4M3HV and 3HH were detected at an m/z of +150.1 to confirm the presence of the branched isomer.

Due to the absence of a commercially available standard, the DHBA standard used for HPLC analysis was prepared from (*S*)-3-hydroxy-γ-butyrolactone by saponification at 37˚C for 3 hours at pH > 10 with 10N sodium hydroxide. Complete conversion of (*S*)-3HBL to (*S*)-DHBA (as confirmed by disappearance of the 3HBL peak on the HPLC time trace) was observed during this treatment. Additionally, DHBA synthesis was also confirmed using HPLC/MS analysis on an Agilent 1100 series instrument equipped with 6120 Quadrapole MS with multi-mode source and an Aminex column with 25mM ammonium formate as the mobile phase. The ammonium adduct of DHBA was detected at an m/z ratio of +138.1 to confirm DHBA synthesis in the samples. Due to co-elution of an unknown product with DHBA during separation of culture supernatants on the

Aminex Column during HPLC analysis, the DHBA titers were thus estimated indirectly, using the 3HBL titers before and after acid treatment and equilibrium constant post acid treatment as described below.

The conversion of DHBA to 3HBL can be effected by a simple acid and heat treatment via the acid catalyzed lactonization of DHBA to 3HBL. Thus, subjecting DHBA standards in LB to an overnight acid treatment at 37°C with increasing amounts of 50 mM hydrochloric acid results in lactonization under decreasing pH conditions, with the equilibrium progressively shifting in favor of the lactone (**Fig. 6-2**). At a pH of about 0.8, the highest K =1.9 is achieved.

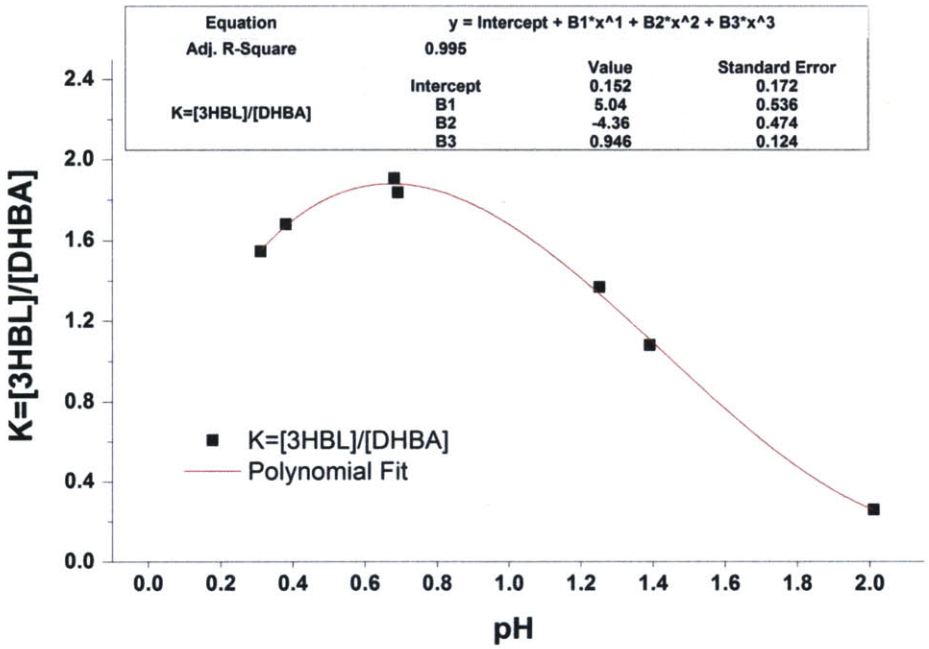

Figure 6-2 | Variation of equilibrium constant K with pH post acid treatment of DHBA standards in LB.

Co-elution of an unknown product along with DHBA on HPLC separation on the Aminex column was indicated by

a) slight shift in the peak corresponding to DHBA and this co-eluted product with respect to the DHBA standard and

b) K=[3HBL]/[DHBA] for samples, post acid treatment at pH=0.8, was between 0.6 and 0.7 as opposed to 1.9 observed for the DHBA standards. This decreased

value of K was attributed to incorrect quantification of DHBA using the standard calibration curve i.e. the peak observed on the LC results was not entirely because of DHBA and was resulting in an over-estimation of [DHBA], resulting in a reduced value of K

To resolve this discrepancy and quantify DHBA correctly, the 3HBL titers before and after acid treatment were used in conjunction with the following equations to estimate the DHBA concentration before and after acid treatment:

$$[\mathrm{DHBA}]_{\text{post acid treatment}} = \frac{[\mathrm{3HBL}]_{\text{post acid treatment}}}{\mathrm{K}} \quad \textbf{(Eq. 6-1)}$$

$$[\mathrm{DHBA}]_{\substack{\text{before acid}\\ \text{treatment}}} = [\mathrm{DHBA}]_{\substack{\text{post acid}\\ \text{treatment}}} + \left([\mathrm{3HBL}]_{\substack{\text{post acid}\\ \text{treatment}}} - [\mathrm{3HBL}]_{\substack{\text{before acid}\\ \text{treatment}}} \right) \quad \textbf{(Eq. 6-2)}$$

Since the prescribed acid treatment results in a drop in the pH of the culture supernatants from about 5.5 (before acid treatment) to 0.8 (post acid treatment), a value of K of about 2 (which results in more conservative estimates than the experimentally observed highest value of 1.9 observed for the DHBA standards at a pH of 0.8) was used in the above equations.

6.3 Results

6.3.1 Production of 3HV from glucose and propionate

The 3-hydroxyalkanoic acid pathway was first tested using propionate as a substrate. Neutralized propionate was supplied along with glucose to recombinant *E. coli* cells expressing one of three activators (Pct, PrpE, or Ptb-Buk), one of two 3-hydroxybutyryl-CoA reductases (*pha*B or *hbd*), *tes*B, and *bkt*B. In general, 3HV was produced in all six recombinant strains with all pathway gene combinations (**Fig. 6-3**). Among the three activation enzymes examined in this work, Pct (strain MG1) resulted in the most 3HV with titers up to 18.00 ± 0.23 mM (2130 ± 27 mg/L), followed by Ptb-Buk (strain MG3) and PrpE (strain MG2), in (*S*)-3HV biosynthesis where Hbd was utilized as the reductase. In the case of (*R*)-3HV biosynthesis employing PhaB as the reductase, all three activators were generally comparable to the achieved (*R*)-3HV titers, and up to 19.65 ± 1.81 mM (2320 ± 213 mg/L) of (*R*)-3HV was yielded in strain MG4. In addition,

the choice of reductases was found to have slight influence over both final 3HV titers and 3HV production rates based on our observation that strains utilizing PhaB (strains MG4-6) yielded more 3HV at a faster rate than strains employing Hbd (strains MG1-3) (**Fig. 6-3** and **Fig. 6-4**).

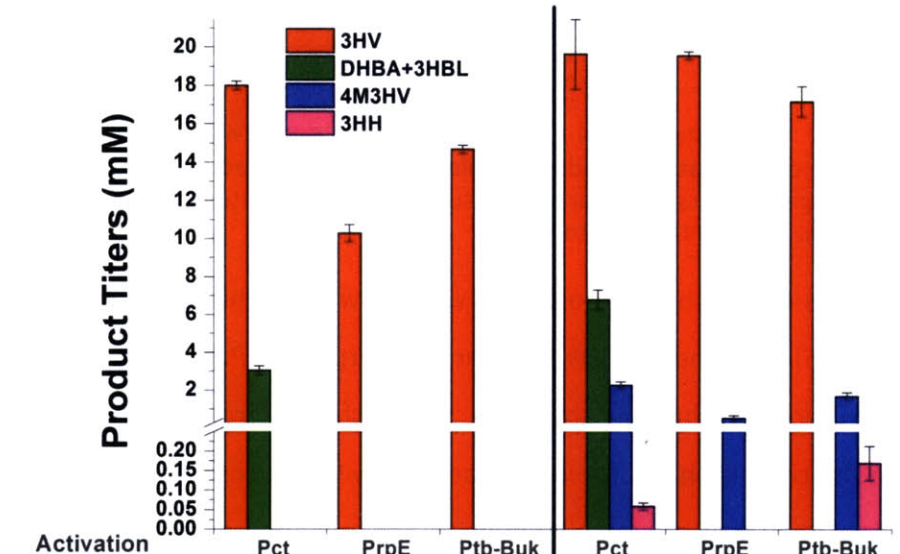

Activation	Pct	PrpE	Ptb-Buk	Pct	PrpE	Ptb-Buk
Reduction		Hbd			PhaB	
***E. coli* Strain**	**MG1**	**MG2**	**MG3**	**MG4**	**MG5**	**MG6**
3HV/3HB	3.60	0.37	0.85	1.46	0.76	0.68
(DHBA+3HBL)/3HB	1.05	0.00	0.00	1.25	0.00	0.00
4M3HV/3HB	0.00	0.00	0.00	0.21	0.02	0.15
3HH/3HB	0.00	0.00	0.00	0.04	0.00	0.03

Figure 6-3 | Biosynthesis of 3-hydroxyalkanoic acids through pathways with different pathway genes with feeding of various precursor substrates. This figure shows shake-flask production of chiral 3-hydroxyalokanoic acids at 72h. The various recombinant strains are described in **Table 6-2**. Production of 3HV (red bars), DHBA+3HBL (green bars), 4M3HV (blue bars) and 3HH (pink bars) were achieved with supplementation of propionate, glycolate, isobutyrate and butyrate, respectively, in addition to glucose. Data are presented in mean ± s.d. (n=3). The specific activation enzymes and reductases used in each pathway are shown on the x-axis. Product selectivity, defined as the ratio of the quantity of desired 3-hydroxyalkanoic acid to the quantity of concomitant product of 3HB, is shown below the x-axis.

Furthermore, control of product selectivity is an important consideration for synthesis of the structurally diverse 3-hydroxyalkanoic acids. 3HB, made from the initial condensation of two acetyl-CoA molecules, is the natural substrate for the enzymes employed in the 3-hydroxyalkanoic acid pathway and is considered as an inevitable byproduct. Therefore, comparison of product selectivity (the ratio of the quantity of desired 3-hydroxyalkanoic acid to the quantity of concomitant product of 3HB) across various activation enzymes and reductases was studied (**Fig. 6-3**).

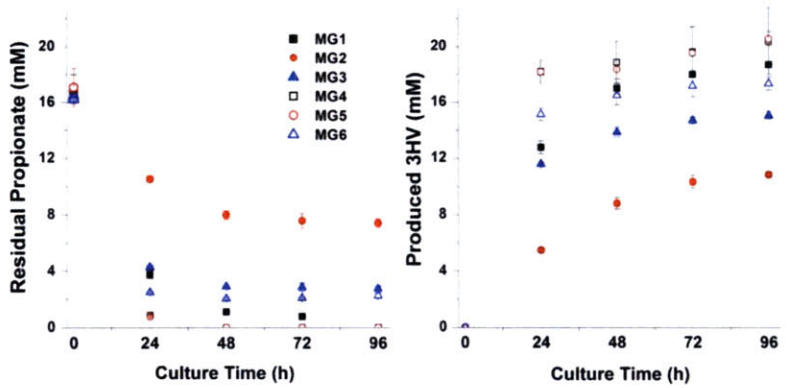

Figure 6-4 | Time course data in residual propionate and produced 3HV. This figure shows time course changes in titers of the precursor substrate (propionate) and the desired 3-hydroxyalkanoic acid (3HV) for up to 96h.

In the case of 3HV biosynthesis, Pct was shown to achieve the highest selectivity towards both (*S*)-3HV and (*R*)-3HV compared to PrpE and Ptb-Buk. Meanwhile, due to the Pct activation mechanism that CoA is transferred from acetyl-CoA to an acid supplied to the cells, such as propionate, acetate will be a concomitant byproduct along with propionate activation. Consistent with the metabolite profile (**Fig. 6-5**), strains using Pct resulted in the most acetate production among the three activators examined.

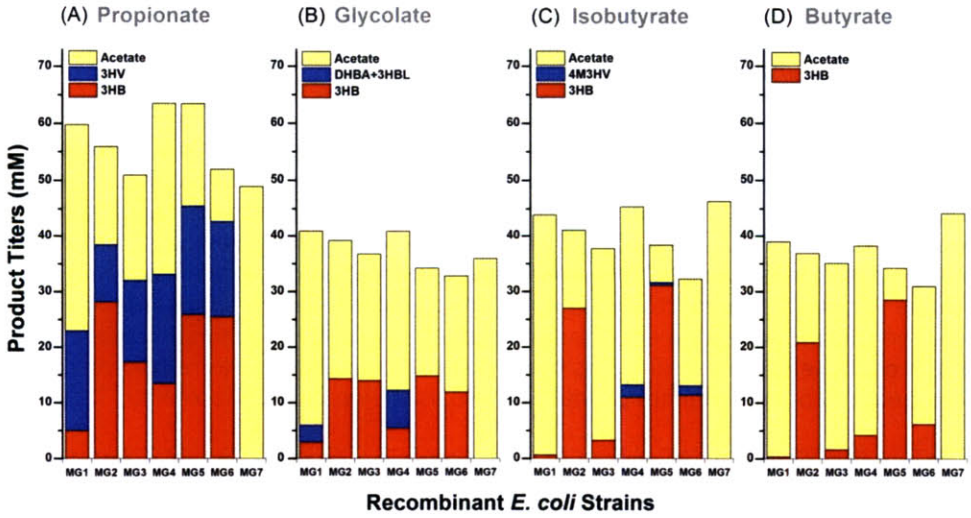

Figure 6-5 | Metabolite profile of the various recombinant *E. coli* cultures supplemented with various precursor substrates. This figure shows the profile of major products, including the desired 3-hydroxyalkanoic acid, 3HB, and acetate, from various combinations of pathway enzymes supplemented with various precursor substrates ((A) propionate; (B) glycolate; (C) isobutyrate; and (D) butyrate). The specific recombinant strains used are shown on the x-axis (**Table 6-2**). As mentioned in the METHODS, 3HH can not be resolved from one of LB peaks during the HPLC separation when cultures were conducted in the LB medium, so 3HH titers were not plotted in (D).

6.3.2 Production of 4M3HV from glucose and isobutyrate and 3HH from glucose and butyrate

Next, isobutyrate and butyrate were supplemented into the culture medium to explore the production of the six carbon isomers 4M3HV and 3HH. The results for 4M3HV and 3HH production highlight the utility of enzyme analog/homolog selection for tuning pathway product profiles (**Fig. 6-3** and **Fig. 6-5**). While five-carbon 3HV can be produced at greater than 10 mM for all pathway variants, six carbon 3-hydroxyalkanoic acids were produced only with the PhaB reductase (**Fig. 6-3**, strains MG4-6). Overall, 4M3HV titers were observed up to 2.27 ± 0.18 mM (300 ± 25 mg/L) in strain MG4 and 3HH titers up to 0.170 ± 0.04 mM (22.5 ± 5.9 mg/L) were achieved in strain MG6.

Acid activator analogs and homologs can further tune product and by-product synthesis both through substrate specificity and reaction chemistry. In 4M3HV synthesis, four activation systems were tested: *pct* transferase, *prpE* synthetase, and two *ptb-buk* transferase-kinase systems from *C. acetobutylicum* and *B. subtilis* (**Fig. 6-3**). As expected the transferase activity of Pct reduces the intracellular acetyl-CoA pool producing extracellular acetate while activating isobutyrate. This activation results in reduced 3HB synthesis and an increased 4M3HV titer (**Fig. 6-6**). The synthetase activity of PrpE irreversibly activates isobutyrate while consuming ATP without directly affecting the acetyl-CoA pool leading to high titers of 3HB. Lower 4M3HV titers are also observed. Isobutyrate can also be reversibly activated using the two enzyme Ptb-Buk system which consumes ATP to phosphorylate the free acid before transfer to CoA. Intuitively one may expect that the Ptb-Buk homologs would function more like each other than the other activation systems. The opposite appears to be true in the context of the 3-hydroxyalkanoic acid pathway. In previous work we have observed the *C. acetobutylicum* Ptb-Buk also works reversibly on acetate/acetyl-CoA (data not shown). With isobutyrate as a substrate, *C. acetobutylicum* Ptb-Buk functions analogously to Pct. Relatively high acetate and lower 3HB titers were observed with 4M3HV produced at 1.71 ± 0.19 mM (225 ± 25 mg/L). *B. subtilis* Ptb-Buk acts

analogously to PrpE with very low acetate titers and high 3HB titers. While displaying similar acetate and 3HB titers, *B. subtilis* Ptb-Buk appears to activate isobutyrate more efficiently than PrpE, leading to a 4M3HV titer of 1.66 ± 0.07 mM (218 ± 10 mg/L).

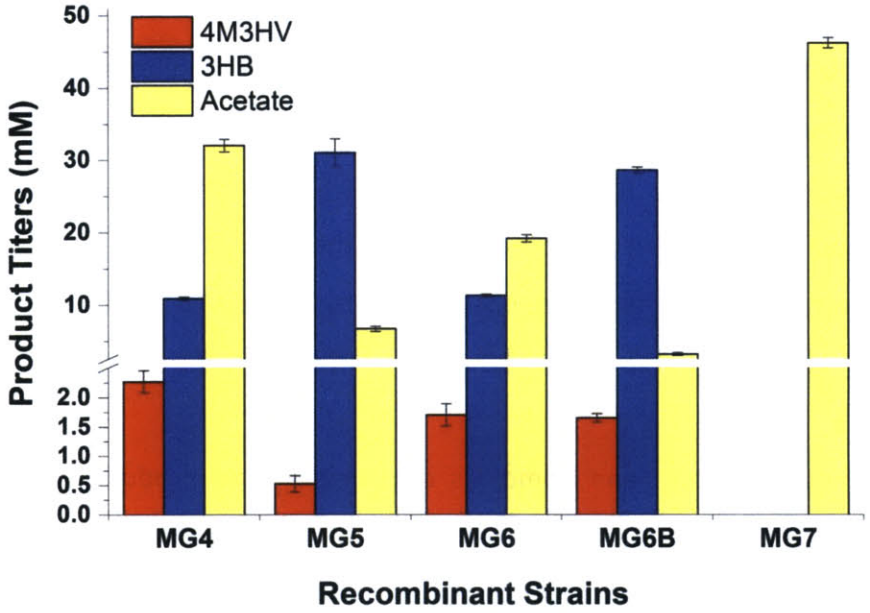

Figure 6-6 | 4M3HV biosynthesis from glucose and isobutyrate. Four activation systems, including *pct* transferase, *prpE* synthetase, and two *ptb-buk* transferase-kinase systems from *C. acetobutylicum* and *B. subtilis*, were examined for 4M3HV production.

6.3.3 Production of DHBA and 3HBL from glucose and glycolate

For the synthesis of the four carbon hydroxyacid DHBA, neutralized glycolate was supplied along with glucose to each recombinant *E. coli*. Only strains expressing the broad substrate range activator Pct showed DHBA synthesis with both PhaB and Hbd as reductases, while strains expressing the activators PrpE and Ptb-Buk only synthesized 3HB and acetate (**Fig. 6-3**). This again highlights the versatility of Pct in activating a variety of small acid molecules, including glycolate (carrying a hydroxyl group), butyrate and isobutyrate, in addition to its natural substrate propionate. PrpE and Ptb-Buk, on the other hand, did not show appreciable activation of glycolate, possibly due to unfavorable interactions with the hydroxyl group.

Further, these cultures were also observed to synthesize small quantities of 3HBL, formed either due to spontaneous lactonization of the 3,4-dihydroxybutyryl-CoA intermediate into 3HBL or from direct conversion of free DHBA on equilibration under

the culture conditions. If the former were true, then removal of *tes*B should result in increased 3HBL synthesis due to enhanced 3,4-dihydroxybutyryl-CoA accumulation, while if the latter were true, the opposite effect would be expected. In strains lacking *tes*B, 57% more 3HBL was produced on an average, with 95% less DHBA (data not shown). Moreover, equilibration of DHBA standards under culture conditions (pH≈5.5, 30˚C) did not result in lactonization of DHBA to 3HBL. These results suggests that the 3HBL observed was produced by the direct cyclization of the 3,4-dihydroxybutyryl-CoA intermediate. The identity of DHBA and 3HBL was confirmed through LC/MS analysis. Strain MG4 expressing Pct and PhaB in addition to BktB and TesB synthesized up to 4.62 ± 0.33 mM (555 ± 52 mg/L) of DHBA and 2.17 ± 0.15 mM (221 ± 15 mg/L) of 3HBL. The total DHBA and 3HBL titers estimated on a molar basis, employing PhaB as a reductase, were about two fold higher than those obtained with Hbd (**Fig. 6-3**), indicating limitations associated with the activity of Hbd towards the non-natural substrate 4-hydroxy-3-ketobutyryl-CoA.

6.3.4 DHBA to 3HBL conversion by acid treatment

In organic chemistry, it is well documented that lactonization is acid-catalyzed (*Carey et al., 2000*). The equilibrium between DHBA and 3HBL is hence expected to be governed by pH, amongst other factors. Indeed, the overnight acid treatment of DHBA standards in LB with 50 mM hydrochloric acid at 37˚C resulted in a progressive shift in the equilibrium towards 3HBL with decreasing pH, with a maximum K of 1.9 (K=[3HBL]/[DHBA]) being attained at a pH close to 0.8 (**Fig. 6-2**). Similar acid treatment of culture supernatants from strains MG1 and MG4 allowed effective conversion of DHBA to 3HBL with strain MG4 expressing the Pct-PhaB activator-reductase combination showing the highest post acid treatment 3HBL titers of 4.53 ± 0.33 mM (462 ± 35 mg/L) and corresponding DHBA titers of 2.27 ± 0.17 mM (272 ± 20 mg/L) (**Fig. 6-7**).

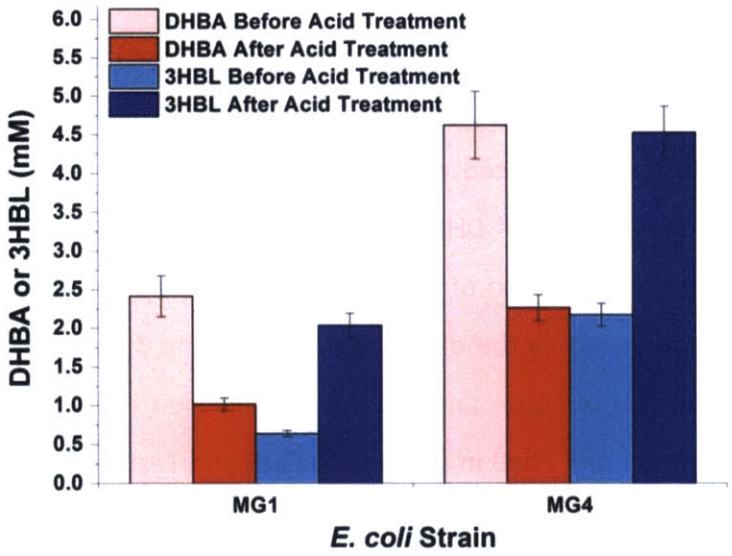

Figure 6-7 | DHBA and 3HBL titers before and after acid treatment. This figure shows overnight acid treatment of culture supernatants from strains MG1 and MG4 with 50 mM hydrochloric acid at 37˚C, allowing for effective conversion of DHBA to 3HBL. Bars in light colors represent samples before acid treatment while bars in dark colors represent samples after acid treatment.

6.4 Discussion

The 3-hydroxyalkanoic acid pathway has the key advantage that it and its constituent enzymes are flexible with respect to their substrates. Substrate flexibility was critical in realizing the production of 3HV, DHBA (and its related 3HBL), 4M3HV, and 3HH from this pathway. Experimentally, a combination of the four flexible enzymes (Pct, BktB, PhaB, and TesB) was found to yield the highest titers of novel 3-hydroxyalkanoic acid pathway products (**Fig. 6-3** and **Fig. 6-7**). Furthermore, the products obtained through the 3-hydroxyalkanoic acid pathway can be precisely controlled through the substrates and genes supplied to the pathway. For instance, 3HV is only produced in the presence of propionate, while DHBA and 3HBL are only made when glycolate is added.

Another interesting point is that in all of the 3-hydroxyalkanoic acid production experiments done in this work, much less 3HB was detected in strains utilizing Pct as CoA activation (**Fig. 6-5**, strains MG1 and MG4) compared to strains utilizing Ptb-Buk or PrpE, even though 3HB is the natural substrate for the enzymes employed in the 3-hydroxyalkanoic acid pathway. 3HB is made from the condensation of two acetyl-CoA

moieties (**Fig. 6-1**) and should theoretically be a major side product in the production of the other 3-hydroxyalkanoic acids. Given that Pct is a CoA-transferase that exchanges CoA moieties between short-chain organic acids, including acetate and acetyl-CoA (*Schweiger & Buckel, 1984*), the less amount of 3HB made in the presence of recombinant Pct suggests that the Pct protein may be removing CoA from acetyl-CoA in the cell and transferring it onto other supplementing acids, including propionate, glycolate, butyrate, and isobutyrate. This CoA transfer could significantly reduce intracellular acetyl-CoA concentrations, making the second-order condensation of two acetyl-CoA molecules much less likely than the condensation of acetyl-CoA with another acyl-CoA (a first-order reaction with respect to acetyl-CoA). The consequence of removing CoA from acetyl-CoA would be increased acetate production (**Fig. 6-5**). The significant increase in acetate production corroborates the hypothesis that Pct is harvesting CoA from acetyl-CoA for use in thiolating other short-chain acids within the cell.

The flexibility of the 3-hydroxyalkanoic acid pathway also extends to the stereochemistry of its final products where different stereochemical outcomes can be realized by using PhaB or Hbd as the 3-hydroxybutyryl-CoA reductase in the pathway. It is well documented in the literature that PhaB results in (*R*)-3-hydroxyalkanoic acids while Hbd results in the (*S*) stereoisomers (*Lee et al., 2008, Liu et al., 2007*). This phenomenon was experimentally verified both in pathways producing 3HB (*Tseng et al., 2009*) and 3HV (*Tseng et al., 2010*). Unfortunately, the methyl esterification chiral analysis method used to analyze the stereochemistry of 3HB and 3HV did not work on DHBA because of its ability to lactonize and because of the inability of the 3HBL lactone stereoisomers to resolve from one another during the analysis (data not shown). However, based on the observation that PhaB and Hbd produce different and completely enantiopure 3HB and 3HV products, there is no reason to expect that they will not do the same for DHBA and 3HBL. Similar assumption can also be made to the stereochemistry of both 3HH and 4M3HV produced from the 3-hydroxyalkanoic acid pathway. Interestingly, because DHBA has a hydroxyl group in the δ-position that

changes the stereochemical priority of the different parts of the molecule about its stereocenter, the stereochemistry of DHBA formed by PhaB should be (*S*)-DHBA while that formed by Hbd should be (*R*)-DHBA. Since PhaB is much better than Hbd at producing DHBA and 3HBL in the 3-hydroxyalkanoic acid pathway (**Fig. 6-3**), the pathway is better suited for the production of (*S*)-DHBA and (*S*)-3HBL than the (*R*) stereoisomers. Fortunately, the (*S*) stereoisomer is predominately used in the production of pharmaceuticals and high-value compounds (*Lee & Park, 2009*). The screening of *hbd* homologs could identify a 3-hydroxybutyryl-CoA reductase with identical stereochemical preference but with an increased substrate range for the production of (*R*)-DHBA and (*R*)-3HBL.

This work represents one of the first reports on the complete biological production of DHBA and 3HBL from inexpensive sugar and sugar-derived substrates. Further screening of additional 3-hydroxyalkanoic acid pathway homologs, aiming at improving product titers and broadening the substrate range of the pathway, should provide a rich resource of pathway combinations for the production of other high value 3-hydroxyalkanoic acids such as 3-hydroxypropionate from formyl-CoA and acetyl-CoA. Molecular analogs of DHBA and 3HBL could also be made using the platform pathway, such as 3,4-dihydroxyvalerate and its associated 4-methyl-3-hydroxybutyrolactone from the condensation of lactyl-CoA and acetyl-CoA, potentially leading to new intermediates for more effective pharmaceuticals. Furthermore, one promising route for increasing productivity is to engineer *E. coli* to produce pathway substrates "in-house" (**Fig. 6-8**). For instance, glycolate could be made intracellularly from glyoxylate through upregulation of the glyoxylate shunt (*Nunez et al., 2001*). Recently, the endogenous supply of propionyl-CoA has also been realized in our group through upregulation of the threonine biosynthesis, achieving direct microbial production of chiral 3HV solely from glucose or glycerol (*Tseng et al., 2010*). Intracellular production of pathway substrates would mitigate the cost and/or toxicity associated with the added secondary carbon sources as well as eliminate the need for substrate transport across the cellular envelope, accelerating production. Intracellular production of substrates would also

allow the feeding of just glucose to *E. coli* for product formation, simplifying the bioprocess while lowering material costs, as an efficient and sustainable avenue to the production of value-added biochemicals.

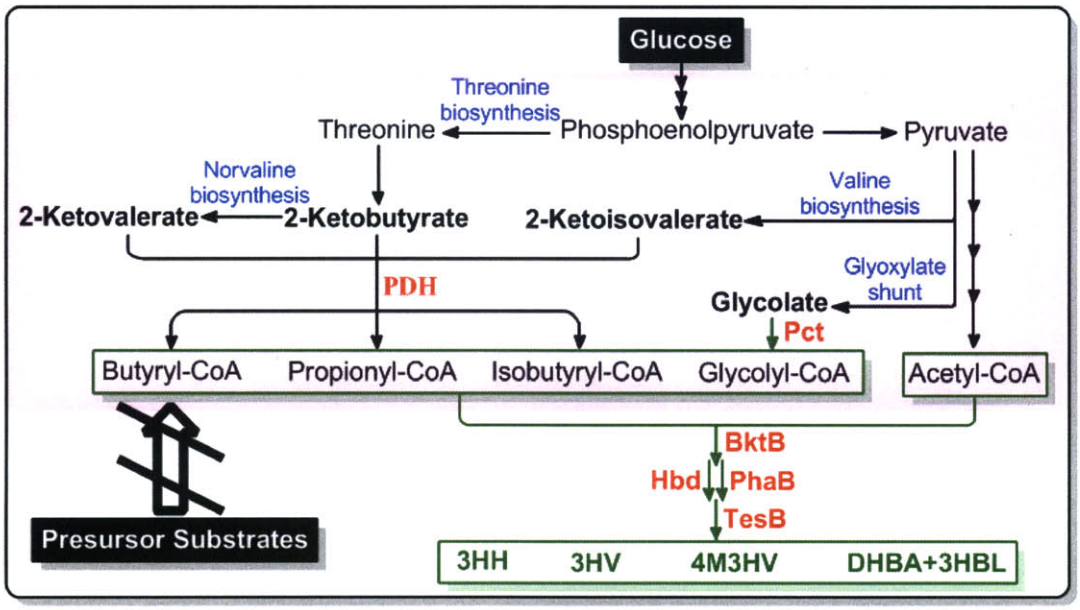

Figure 6-8 | Endogenous supply of pathway substrates from *E. coli* internal metabolism instead of exogenous supplementation of precursor acids. Potential metabolic routes allowing for endogenous production of butyryl-CoA, propionyl-CoA, isobutyryl-CoA, and glycolyl-CoA from glucose are shown in the pink box with corresponding pathways for their synthesis as indicated in blue. The core 3-hydroxyalkanoic acid platform pathway for production of 3HH, 3HV, 4M3HV and DHBA (and its associated 3HBL) is shown in green while the key enzymes involved in the pathway are shown in red.

6.5 Conclusions

In Chapter 6, a platform pathway was established and demonstrated for synthesis of value-added chiral 3HV, DHBA (and its related 3HBL), 4M3HV, and 3HH, with applications ranging from chiral building blocks to polymeric materials to high-value pharmaceuticals. This chapter illustrates how versatile our proposed pentanol pathway is as it can be modularized for synthesis of various chemicals.

CHAPTER 7

Conclusions and Recommendations

Abstract

This final chapter first describes the main findings and conclusions of the studies presented in this dissertation. Then, suggestions for directions for future research are provided.

7.1 Conclusions

Public concerns about global warming and energy security contribute to an ever-increasing focus on biomass-derived liquid fuels. As described in this thesis, pentanol has the potential to complement petroleum-derived fuel resources. To achieve pentanol production costs competitive with gasoline, several challenges associated with its production process have to be addressed, and amongst those challenges, the major one is the development of biocatalysts. As discussed throughout this work, a central goal of this thesis has been to construct a functional and feasible biosynthetic pathway for production of pentanol from renewable carbon sources.

We used butanol synthesis as a platform from which microbial synthesis of pentanol can be obtained. The successful production of butanol in *E. coli* with titers up to 580 mg/L demonstrated the feasibility of a synthetic butanol pathway in *E. coli* (Chapter 2), giving a feasible platform for pentanol biosynthesis. To better understand the butanol pathway, we shortcut it towards 3HB synthesis and demonstrated the functional expression of various thiolase enzymes and 3-hydroxybutyryl-CoA dehydrogenase enzymes that allowed for chiral 3HB production (Chapter 3). In addition, a complementary technique was employed to directly assess the performance of the individual steps of the butanol pathway under *in vivo* conditions. Such analysis identified the Bcd-catalyzed reaction to be the bottleneck reaction involved in the butanol biosynthesis (Appendix A). To explore the possibility of employing the butanol pathway enzymes for pentanol biosynthesis, similar approach to the 3HB production was conducted to assess capability of the pathway enzymes on five carbon substrate analogues. We succeed in chiral 3HV production, providing an initial proof-of-concept that high levels of five-carbon metabolite intermediates, particularly 3HV-CoA, can be obtained (Chapter 4). To explore the potential of subsequent conversion of 3HV-CoA to pentanol by the downstream *Clostridial* butanol pathway enzymes, we used a bypass/substrate feeding strategy to thoroughly evaluate plasticity of those enzymes on catalyzing formation of five-carbon precursors for pentanol synthesis. Additionally, by boosting the intracellular NADH availability, we finally achieved up to 85 mg/L pentanol

from glucose and propionate, demonstrating a functional and feasible pentanol biosynthetic pathway in *E. coli* (Chapter 5). Furthermore, a platform pathway was established and demonstrated for synthesis of value-added chiral 3-hydroxyalkanoic acids with applications ranging from chiral building blocks to polymeric materials to high-value pharmaceuticals (Chapter 6). Of significance, such pathway was constructed as one portion of the pentanol pathway, illustrating how versatile the pentanol pathway is in that it can be modularized for synthesis of various valuable chemicals.

Despite the initial failure of direct pentanol synthesis solely from glucose or glycerol, once an efficient redox balancing within the recombinant strains is ensured, we should be able to redirect carbon flux towards our desired route for pentanol production. As construction of desired biosynthetic pathways is just the first step toward economically viable bio-pentanol production, increasing the titer, yield, and productivity will ultimately determine the feasibility of such pathway.

7.2 Recommendations for Future Works

Undetectable pentanol was observed in the experiment of direct production of pentanol solely from glucose or glycerol, most likely due to limited pathway activity as a result of limited availability of NADH. This is of particular concern with our pentanol biosynthetic pathway that combines energetically expensive threonine biosynthesis pathway and the *Clostridial* butanol pathway, both of which have intensive requirement for reducing equivalent, which is expected to create a redox imbalance in *E. coli*, thus making the pentanol biosynthetic pathway unpreferable. To improve the pathway performance, we need to address such problem, and one solution, intuitively, is to engineer *E. coli* to further boost the NADH availability. For example, we can overexpress a mutated PDH enzyme (as described in Chapter 5) that is less sensitive to high NADH, which is expected to boost NADH yield up to 4 moles of NADH per mole of glucose under anaerobic conditions, thereby enabling/enhancing the pentanol biosynthesis.

In addition, we need to consider kinetics of the individual enzymes in the pentanol pathway, Bcd-EtfAB enzyme has been shown problematic and the reaction it catalyzes

has been considered as the bottleneck reaction (Chapter 2 and Appendix A). Thus, with the aim to facilitate the carbon flux going through the desired pentanol pathway, we can use a crotonyl-CoA specific trans-enoyl-CoA reductase (Ter) from *Treponema denticola* as a replacement for Bcd-EtfAB, which has been demonstrated to enhance butanol production (*Bond-Watts et al., 2011*).

A four-plasmid system is currently used to construct the pentanol biosynthesis pathway in *E. coli*, which requires supplementation of appropriate antibiotics to maintain each of compatible plasmids. Such multiple high-copy plasmids can impose a metabolic burden on their hosts. Therefore, chromosomal integration of the pathway genes or construction of an artificial operon containing all required genes for pentanol synthesis would be a way to relieve the metabolic burden.

As several other metabolites were co-synthesized along with the desire product of pentanol, an action could be taken to reduce byproduct formation, and meanwhile, redirect the carbon flux to the pentanol synthesis. Knocking out enzymes responsible for byproduct formation may promote the pentanol biosynthesis. Alternatively, to alleviate the substrate promiscuity of pathway enzymes, one approach called enzyme co-localization could be implemented to allow substrates channeling between enzymes (*Conrado et al., 2008*). The spatial organization of the enzymes can be achieved using either the leucine zipper, a dimer resulting from interaction between leucine residues (*Moll et al., 2001*), or the synthetic scaffolds, constructed from protein–protein interaction domains. In addition, approaches like protein engineering of the pathway enzymes to alleviate their substrate promiscuity, or utilization of better isozymes with more stringent substrate specificity could also mitigate the carbon loss.

REFERENCES

Abramson, J., Riistama, S., Larsson, G., Jasaitis, A., Svensson-Ek, M., Laakkonen, L., Puustinen, A., Iwata, S., and Wikstrom, M. (2000) The structure of the ubiquinol oxidase from Escherichia coli and its ubiquinone binding site, *Nat Struct Biol* **7**, 910-917.

Alberty, R. A. (2005) *Thermodynamics of biochemical reactions*, Wiley-Interscience.

Aldor, I. S., Kim, S. W., Prather, K. L., and Keasling, J. D. (2002) Metabolic engineering of a novel propionate-independent pathway for the production of poly(3-hydroxybutyrate-co-3-hydroxyvalerate) in recombinant Salmonella enterica serovar typhimurium, *Appl Environ Microbiol* **68**, 3848-3854.

Alexeyev, M. F., Shokolenko, I. N., and Croughan, T. P. (1995) Improved Antibiotic-Resistance Gene Cassettes and Omega-Elements for Escherichia-Coli Vector Construction and in-Vitro Deletion Insertion Mutagenesis, *Gene* **160**, 63-67.

Alper, H., Moxley, J., Nevoigt, E., Fink, G. R., and Stephanopoulos, G. (2006) Engineering yeast transcription machinery for improved ethanol tolerance and production, *Science* **314**, 1565-1568.

Alper, H., and Stephanopoulos, G. (2007) Global transcription machinery engineering: a new approach for improving cellular phenotype, *Metab Eng* **9**, 258-267.

Alper, H., and Stephanopoulos, G. (2009) Engineering for biofuels: exploiting innate microbial capacity or importing biosynthetic potential, *Nat Rev Microbiol* **7**, 715 - 723.

Antoni, D., Zverlov, V. V., and Schwarz, W. H. (2007) Biofuels from microbes, *Applied microbiology and biotechnology* **77**, 23-35.

Aristidou, A., and Penttil, M. (2000) Metabolic engineering applications to renewable resource utilization, *Current Opinion in Biotechnology* **11**, 187-198.

Atsumi, S., Cann, A. F., Connor, M. R., Shen, C. R., Smith, K. M., Brynildsen, M. P., Chou, K. J., Hanai, T., and Liao, J. C. (2008) Metabolic engineering of Escherichia coli for 1-butanol production, *Metab Eng* **10**, 305-311.

Atsumi, S., Hanai, T., and Liao, J. C. (2008) Non-fermentative pathways for synthesis of branched-chain higher alcohols as biofuels, *Nature* **451**, 86-89.

Baba, T., Ara, T., Hasegawa, M., Takai, Y., Okumura, Y., Baba, M., Datsenko, K. A., Tomita, M., Wanner, B. L., and Mori, H. (2006) Construction of Escherichia coli K-12 in-frame, single-gene knockout mutants: the Keio collection, *Mol Syst Biol* **2**, 2006 0008.

Berrios-Rivera, S. J., Bennett, G. N., and San, K. Y. (2002) Metabolic engineering of Escherichia coli: increase of NADH availability by overexpressing an NAD(+)-dependent formate dehydrogenase, *Metab Eng* **4**, 217-229.

Berrios-Rivera, S. J., San, K. Y., and Bennett, G. N. (2003) The effect of carbon sources and lactate dehydrogenase deletion on 1,2-propanediol production in Escherichia coli, *Journal of industrial microbiology & biotechnology* **30**, 34-40.

Bischoff, K. M., Liu, S., Leathers, T. D., Worthington, R. E., and Rich, J. O. (2009) Modeling bacterial contamination of fuel ethanol fermentation, *Biotechnol Bioeng* **103**, 117-122.

Bisswanger, H. (1981) Substrate specificity of the pyruvate dehydrogenase complex from Escherichia coli, *J Biol Chem* **256**, 815-822.

Bond-Watts, B. B., Bellerose, R. J., and Chang, M. C. (2011) Enzyme mechanism as a kinetic control element for designing synthetic biofuel pathways, *Nat Chem Biol* **7**, 222-227.

Bonomo, J., Warnecke, T., Hume, P., Marizcurrena, A., and Gill, R. T. (2006) A comparative study of metabolic engineering anti-metabolite tolerance in Escherichia coli, *Metabolic Engineering* **8**, 227-239.

Borden, J. R., and Papoutsakis, E. T. (2007) Dynamics of genomic-library enrichment and identification of solvent tolerance genes for *Clostridium acetobutylicum*, *Applied and Environmental Microbiology* **73**, 3061-3068.

Bowles, L. K., and Ellefson, W. L. (1985) Effects of butanol on *Clostridium acetobutylicum*, *Applied and Environmental Microbiology* **50**, 1165-1170.

Boynton, Z. L., Bennet, G. N., and Rudolph, F. B. (1996) Cloning, sequencing, and expression of clustered genes encoding beta-hydroxybutyryl-coenzyme A (CoA) dehydrogenase, crotonase, and butyryl-CoA dehydrogenase from Clostridium acetobutylicum ATCC 824, *Journal of bacteriology* **178**, 3015-3024.

Bradford, M. M. (1976) A rapid and sensitive method for the quantitation of microgram quantities of protein utilizing the principle of protein-dye binding, *Anal. Biochem.* **72**, 248-254.

Bramucci, M., Nagarajan, V., Sedkova, N., and Singh, M. (2007) Solvent tolerant microorganisms and methods of isolation, EI DuPont de Nemours and Co.

Bramucci, M. G., Dicosimo, Robert , Fallon, Robert , Gavagan, John E., Herkes, Frank , Wilczek, Lech (2006) 3-Hydroxycarboxylic acid production and use in branched polymers, *United States Patent 7138480*

Britton, R. A., Eichenberger, P., Gonzalez-Pastor, J. E., Fawcett, P., Monson, R., Losick, R., and Grossman, A. D. (2002) Genome-wide analysis of the stationary-phase sigma factor (sigma-H) regulon of Bacillus subtilis, *Journal of bacteriology* **184**, 4881-4890.

Brumaghim, J. L., Li, Y., Henle, E., and Linn, S. (2003) Effects of hydrogen peroxide upon nicotinamide nucleotide metabolism in *Escherichia coli*: changes in enzyme levels and nicotinamide nucleotide pools and studies of the oxidation of NAD(P)H by Fe(III), *J. Biol. Chem.* **278**, 42495-42504.

Buday, Z., Linden, J., and Karim, M. (1990) Improved acetone-butanol fermentation analysis using subambient HPLC column temperature, *Enzyme Microb. Technol.* **12**, 24-27.

Campbell, J. W., Morgan-Kiss, R. M., and Cronan, J. E. (2003) A new Escherichia coli metabolic competency: growth on fatty acids by a novel anaerobic beta-oxidation pathway, *Molecular Microbiology* **47**, 793-805.

Cann, A. F., and Liao, J. C. (2008) Production of 2-methyl-1-butanol in engineered Escherichia coli, *Appl Microbiol Biotechnol* **81**, 89-98.

Carey, F. A., McGraw, N. Y., and New, H. (2000) *Organic Chemistry*.

Cascone, R. (2008) Biobutanol - A Replacement for Bioethanol?, *Chem Eng Progr* **104**, S4-S9.

Causey, T. B., Shanmugam, K. T., Yomano, L. P., and Ingram, L. O. (2004) Engineering Escherichia coli for efficient conversion of glucose to pyruvate, *Proc Natl Acad Sci U S A* **101**, 2235-2240.

Chen, C. K., and Blaschek, H. P. (1999) Examination of physiological and molecular factors involved in enhanced solvent production by clostridium beijerinckii BA101, *Applied and environmental microbiology* **65**, 2269-2271.

Chen, G. Q., and Wu, Q. (2005) Microbial production and applications of chiral hydroxyalkanoates, *Appl. Microbiol. Biotechnol.* **67**, 592-599.

Chiba, T., and Nakai, T. (1987) A new synthetic approach to the carbapenem antibiotic PS-5 from ethyl(*S*)-3-hydroxybutanoate., *Chem. Lett.* **11**, 2187-2188.

Chiba, T., and Nakai, T. A. (1985) Synthetic approach to (1)-thienamycin from methyl (*R*)-(2)-3-hydroxybutanoate. A new entry to (3*R*,4*R*)-3-[(*R*)-1-hydroxyethyl]-4-acetoxy-2-azetidinone, *Chem. Lett.* **161**, 651-654.

Clomburg, J. M., and Gonzalez, R. (2010) Biofuel production in Escherichia coli: the role of metabolic engineering and synthetic biology, *Appl Microbiol Biotechnol* **86**, 419-434.

Connor, M. R., and Liao, J. C. (2008) Engineering of an Escherichia coli strain for the production of 3-methyl-1-butanol, *Appl Environ Microbiol* **74**, 5769 - 5775.

Conrado, R. J., Varner, J. D., and DeLisa, M. P. (2008) Engineering the spatial organization of metabolic enzymes: mimicking nature's synergy, *Curr Opin Biotechnol* **19**, 492-499.

Datsenko, K. A., and Wanner, B. L. (2000) One-step inactivation of chromosomal genes in Escherichia coli K-12 using PCR products, *Proc Natl Acad Sci U S A* **97**, 6640-6645.

de Bont, J. A. M. (1998) Solvent-tolerant bacteria in biocatalysis, *Trends in Biotechnology* **16**, 493-499.

de Carvalho, C. C., da Cruz, A. A., Pons, M. N., Pinheiro, H. M., Cabral, J. M., da Fonseca, M. M., Ferreira, B. S., and Fernandes, P. (2004) Mycobacterium sp., Rhodococcus erythropolis, and Pseudomonas putida behavior in the presence of organic solvents, *Microscopy research and technique* **64**, 215-222.

de Graef, M. R., Alexeeva, S., Snoep, J. L., and de Mattos, M. J. T. (1999) The steady-state internal redox state (NADH/NAD) reflects the external redox state and is correlated with catabolic adaptation in Escherichia coli, *Journal of bacteriology* **181**, 2351-2357.

de Roo, G., Kellerhals, M. B., Ren, Q., Witholt, B., and Kessler, B. (2002) Production of chiral *R*-3-hydroxyalkanoic acids and *R*-3-hydroxyalkanoic acid methylesters via hydrolytic degradation of polyhydroxyalkanoate synthesized by *pseudomonads*, *Biotechnol. Bioeng.* **77**, 717-722.

Debabov, V. G. (2003) The threonine story, *Adv Biochem Eng Biotechnol* **79**, 113-136.

Dueber, J. E., Wu, G. C., Malmirchegini, G. R., Moon, T. S., Petzold, C. J., Ullal, A. V., Prather, K. L., and Keasling, J. D. (2009) Synthetic protein scaffolds provide modular control over metabolic flux, *Nat Biotechnol* **27**, 753-759.

Edwards, J. S., and Palsson, B. O. (2000) The Escherichia coli MG1655 in silico metabolic genotype: its definition, characteristics, and capabilities, *Proc Natl Acad Sci U S A* **97**, 5528-5533.

Elowitz, M. B., and Leibler, S. (2000) A synthetic oscillatory network of transcriptional regulators, *Nature* **403**, 335-338.

Errington, J., and Mandelstam, J. (1983) Variety of Sporulation Phenotypes Resulting from Mutations in a Single Regulatory Locus, Spoiia, in Bacillus-Subtilis, *Journal of General Microbiology* **129**, 2091-2101.

Eschenlauer, A. C., Stoup, S. K., Srienc, F., and Somers, D. A. (1996) Production of heteropolymeric polyhydroxyalkanoate in Escherichia coli from a single carbon source, *Int J Biol Macromol* **19**, 121-130.

Ezeji, T. C., Qureshi, N., and Blaschek, H. P. (2004) Butanol fermentation research: upstream and downstream manipulations, *Chem Rec* **4**, 305-314.

Ezeji, T. C., Qureshi, N., and Blaschek, H. P. (2007) Bioproduction of butanol from biomass: from genes to bioreactors, *Current opinion in biotechnology* **18**, 220-227.

Fischer, C. R., Klein-Marcuschamer, D., and Stephanopoulos, G. (2008) Selection and optimization of microbial hosts for biofuels production, *Metabolic Engineering* **10**, 295-304.

Fischer, C. R., Tseng, H. C., Tai, M., Prather, K. L., and Stephanopoulos, G. (2010) Assessment of heterologous butyrate and butanol pathway activity by measurement of intracellular pathway intermediates in recombinant Escherichia coli, *Appl Microbiol Biotechnol* **88**, 265-275.

Fontaine, L., Meynial-Salles, I., Girbal, L., Yang, X., Croux, C., and Soucaille, P. (2002) Molecular characterization and transcriptional analysis of adhE2, the gene encoding the NADH-dependent aldehyde/alcohol dehydrogenase responsible for butanol production in alcohologenic cultures of Clostridium acetobutylicum ATCC 824, *Journal of bacteriology* **184**, 821-830.

Foust, T., Aden, A., Dutta, A., and Phillips, S. (2009) An economic and environmental comparison of a biochemical and a thermochemical lignocellulosic ethanol conversion processes, *Cellulose* **16**, 547-565.

Gao, H. J., Wu, Q., and Chen, G. Q. (2002) Enhanced production of *D*-(-)-3-hydroxybutyric acid by recombinant *Escherichia coli*, *FEMS Microbiol. Lett.* **213**, 59-65.

Gheshlaghi, R., Scharer, J. M., Moo-Young, M., and Chou, C. P. (2009) Metabolic pathways of clostridia for producing butanol, *Biotechnol Adv* **27**, 764-781.

Gonzalez-Pajuelo, M., Andrade, J. C., and Vasconcelos, I. (2004) Production of 1,3-propanediol by Clostridium butyricum VPI 3266 using a synthetic medium and raw glycerol, *J Ind Microbiol Biotechnol* **31**, 442-446.

Guerout-Fleury, A. M., Frandsen, N., and Stragier, P. (1996) Plasmids for ectopic integration in Bacillus subtilis, *Gene* **180**, 57-61.

Harris, L. M., Desai, R. P., Welker, N. E., and Papoutsakis, E. T. (2000) Characterization of recombinant strains of the *Clostridium acetobutylicum* butyrate kinase inactivation mutant: need for new phenomenological models for solventogenesis and butanol inhibition?, *Biotechnology and bioengineering* **67**, 1-11.

Hartmanis, M. G., and Gatenbeck, S. (1984) Intermediary Metabolism in Clostridium acetobutylicum: Levels of Enzymes Involved in the Formation of Acetate and Butyrate, *Applied and environmental microbiology* **47**, 1277-1283.

Hasegawa J, H. S., Ogura M, Watanabe K. (1981) Production of beta-hydroxycarboxylic acids from aliphatic carboxylic acids by microorganisms, *J Ferment Technol.* **59**, 257-262.

Heipieper, H. J., and Debont, J. A. M. (1994) Adaptation of Pseudomonas-Putida S12 to Ethanol and Toluene at the Level of Fatty-Acid Composition of Membranes, *Applied and environmental microbiology* **60**, 4440-4444.

Hempfling, W. P., and Mainzer, S. E. (1975) Effects of varying the carbon source limiting growth on yield and maintenance characteristics of Escherichia coli in continuous culture, *J Bacteriol* **123**, 1076-1087.

Hornsten, E. G. (1995) On Culturing Escherichia-Coli on a Mineral Salts Medium during Anaerobic Conditions, *Bioprocess Engineering* **12**, 157-162.

Hwang, E. I., Kaneko, M., Ohnishi, Y., and Horinouchi, S. (2003) Production of plant-specific flavanones by Escherichia coli containing an artificial gene cluster, *Applied and environmental microbiology* **69**, 2699-2706.

Inui, M., Suda, M., Kimura, S., Yasuda, K., Suzuki, H., Toda, H., Yamamoto, S., Okino, S., Suzuki, N., and Yukawa, H. (2008) Expression of *Clostridium acetobutylicum* butanol synthetic genes in *Escherichia coli*, *Appl. Microbiol. Biotechnol.* **77**, 1305-1316.

Isken, S., and de Bont, J. A. M. (1998) Bacteria tolerant to organic solvents, *Extremophiles* **2**, 229-238.

Jarboe, L. R., Zhang, X., Wang, X., Moore, J. C., Shanmugam, K. T., and Ingram, L. O. Metabolic engineering for production of biorenewable fuels and chemicals: contributions of synthetic biology, *J Biomed Biotechnol* **2010**, 761042.

Jones, D. T., and Woods, D. R. (1986) Acetone-butanol fermentation revisited, *Microbiol Rev* **50**, 484-524.

Kang, H. J., Heo, D. H., Choi, S. W., Kim, K. N., Shim, J., Kim, C. W., Sung, H. C., and Yun, C. W. (2007) Functional characterization of Hsp33 protein from Bacillus psychrosaccharolyticus; additional function of HSP33 on resistance to solvent stress, *Biochemical and biophysical research communications* **358**, 743-750.

Kaup, B., Bringer-Meyer, S., and Sahm, H. (2004) Metabolic engineering of Escherichia coli: construction of an efficient biocatalyst for D-mannitol formation in a whole-cell biotransformation, *Appl Microbiol Biotechnol* **64**, 333-339.

Keasling, J. D., and Chou, H. (2008) Metabolic engineering delivers next-generation biofuels, *Nat Biotechnol* **26**, 298-299.

Keen, N. T., Tamaki, S., Kobayashi, D., and Trollinger, D. (1988) Improved broad-host-range plasmids for DNA cloning in gram-negative bacteria, *Gene* **70**, 191-197.

Kim, E. E., Baker, C. T., Dwyer, M. D., Murcko, M. A., Rao, B. G., Tung, R. D., and Navia, M. A. (1995) Crystal structure of HIV-1 protease in complex with VX-478, a potent and orally bioavailable inhibitor of the enzyme, *J Am Chem Soc* **117**, 1181-1182.

Kim, Y., Ingram, L. O., and Shanmugam, K. T. (2008) Dihydrolipoamide dehydrogenase mutation alters the NADH sensitivity of pyruvate dehydrogenase complex of Escherichia coli K-12, *J Bacteriol* **190**, 3851-3858.

Knoshaug, E. P., and Zhang, M. (2008) Butanol Tolerance in a Selection of Microorganisms, *Applied biochemistry and biotechnology* **153**, 13-20.

Kwok, R. (2009) Cellulosic ethanol hits roadblocks, *Nature* **461**, 582-583.

Lau, M. W., and Dale, B. E. (2009) Cellulosic ethanol production from AFEX-treated corn stover using Saccharomyces cerevisiae 424A(LNH-ST), *Proc Natl Acad Sci* **106**, 1368-1373.

Lee, H. C., Kim, J. S., Jang, W., and Kim, S. Y. (2009) Thymidine production by overexpressing NAD+ kinase in an Escherichia coli recombinant strain, *Biotechnol Lett* **31**, 1929-1936.

Lee, I. Y., Kim, M. K., Park, Y. H., and Lee, S. Y. (1996) Regulatory effects of cellular nicotinamide nucleotides and enzyme activities on poly(3-hydroxybutyrate) synthesis in recombinant *Escherichia coli*, *Biotechnol. Bioeng.* **52**, 707-712.

Lee, J. H., Sung, B. H., Kim, M. S., Blattner, F. R., Yoon, B. H., Kim, J. H., and Kim, S. C. (2009) Metabolic engineering of a reduced-genome strain of Escherichia coli for L-threonine production, *Microb Cell Fact* **8**, 2.

Lee, K. H., Park, J. H., Kim, T. Y., Kim, H. U., and Lee, S. Y. (2007) Systems metabolic engineering of Escherichia coli for L-threonine production, *Mol Syst Biol* **3**, 149.

Lee, S.-H., and Park, O.-J. (2009) Uses and production of chiral 3-hydroxy-gamma-butyrolactones and structurally related chemicals, *Applied microbiology and biotechnology* **84**, 817-828.

Lee, S. H., Park, S. J., Lee, S. Y., and Hong, S. H. (2008) Biosynthesis of enantiopure (*S*)-3-hydroxybutyric acid in metabolically engineered *Escherichia coli*, *Appl. Microbiol. Biotechnol.* **79**, 633-641.

Lee, S. K., Chou, H., Ham, T. S., Lee, T. S., and Keasling, J. D. (2008) Metabolic engineering of microorganisms for biofuels production: from bugs to synthetic biology to fuels, *Curr Opin Biotechnol* **19**, 556 - 563.

Lee, S. Y., and Lee, Y. (2003) Metabolic engineering of *Escherichia coli* for production of enantiomerically pure (*R*)-(-)-hydroxycarboxylic acids, *Appl. Environ. Microbiol.* **69**, 3421-3426.

Lee, S. Y., Park, S. H., Lee, Y., Lee, S. H., and Dio, Y. (2002) Production of chiral and other valuable compounds from microbial polyesters, *In Steinbchel A eds Biopolymers polyesters III WileyVCH Weinheim pp*, 375-387

Li, F., Hinderberger, J., Seedorf, H., Zhang, J., Buckel, W., and Thauer, R. K. (2008) Coupled ferredoxin and crotonyl coenzyme A (CoA) reduction with NADH catalyzed by the butyryl-CoA dehydrogenase/Etf complex from Clostridium kluyveri, *Journal of bacteriology* **190**, 843-850.

Li, H., Cann, A. F., and Liao, J. C. (2010) Biofuels: Biomolecular Engineering Fundamentals and Advances, *Annual Review of Chemical and Biomolecular Engineering* **1**.

Lin, H., Bennett, G. N., and San, K. Y. (2005) Metabolic engineering of aerobic succinate production systems in *Escherichia coli* to improve process productivity and achieve the maximum theoretical succinate yield, *Metab. Eng.* **7**, 116-127.

Liu, Q., Ouyang, S. P., Chung, A., Wu, Q., and Chen, G. Q. (2007) Microbial production of *R*-3-hydroxybutyric acid by recombinant *E. coli* harboring genes of *phbA*, *phbB*, and *tesB*, *Appl. Microbiol. Biotechnol.* **76**, 811-818.

Liu, S. J., and Steinbuchel, A. (2000) Exploitation of butyrate kinase and phosphotransbutyrylase from *Clostridium acetobutylicum* for the in vitro biosynthesis of poly(hydroxyalkanoic acid), *Appl Microbiol Biotechnol* **53**, 545-552.

Liu, S. J., and Steinbüchel, A. (2000) A novel genetically engineered pathway for synthesis of poly(hydroxyalkanoic acids) in Escherichia coli, *Applied and environmental microbiology* **66**, 739-743.

Liu, X.-W., Wang, H.-H., Chen, J.-Y., Li, X.-T., and Chen, G.-Q. (2008) Biosynthesis of poly(3-hydroxybutyrate-co-3-hydroxyvalerate) by recombinant *Escherichia coli* harboring propionyl-CoA synthase gene (*prpE*) or propionate permease gene (*prpP*) *Biochem. Eng. J.* **43**, 72-77.

Liu, X., Zhu, Y., and Yang, S. T. (2006) Construction and characterization of ack deleted mutant of Clostridium tyrobutyricum for enhanced butyric acid and hydrogen production, *Biotechnol Prog* **22**, 1265-1275.

Lutz, R., and Bujard, H. (1997) Independent and tight regulation of transcriptional units in Escherichia coli via the LacR/O, the TetR/O and AraC/I1-I2 regulatory elements, *Nucleic Acids Res* **25**, 1203-1210.

Madison, L. L., and Huisman, G. W. (1999) Metabolic engineering of poly(3-hydroxyalkanoates): from DNA to plastic, *Microbiol Mol Biol Rev* **63**, 21-53.

Martin, C. H., Nielsen, D. R., Solomon, K. V., and Prather, K. L. (2009) Synthetic metabolism: engineering biology at the protein and pathway scales, *Chem Biol* **16**, 277-286.

Martin, C. H., and Prather, K. L. J. (2009) High-titer production of monomeric hydroxyvalerates from levulinic acid in Pseudomonas putida, *Journal of Biotechnology* **139**, 61-67.

Masamune, S., Walsh, C. T., Sinskey, A. J., and Peoples, O. P. (1989) Poly-(*R*)-3-hydroxybutyrate (PHB) biosynthesis: mechanistic studies on the biological Claisen condensation catalyzed by β-ketoacyl thiolase, *Pure Appl. Chem.* **61**, 303-312.

McMahon, B., Gallagher, M. E., and Mayhew, S. G. (2005) The protein coded by the PP2216 gene of Pseudomonas putida KT2440 is an acyl-CoA dehydrogenase that oxidises only short-chain aliphatic substrates, *FEMS Microbiol Lett* **250**, 121-127.

Mermelstein, L. D., Welker, N. E., Petersen, D. J., Bennett, G. N., and Papoutsakis, E. T. (1994) Genetic and metabolic engineering of Clostridium acetobutylicum ATCC 824, *Ann N Y Acad Sci* **721**, 54-68.

Meynial Salles, I., Forchhammer, N., Croux, C., Girbal, L., and Soucaille, P. (2007) Evolution of a Saccharomyces cerevisiae metabolic pathway in Escherichia coli, *Metab Eng* **9**, 152-159.

Middleton, R., and Hofmeister, A. (2004) New shuttle vectors for ectopic insertion of genes into Bacillus subtilis, *Plasmid* **51**, 238-245.

Minkler, P. E., Kerner, J., Kasumov, T., Parland, W., and Hoppel, C. L. (2006) Quantification of malonyl-coenzyme A in tissue specimens by high-performance liquid chromatography/mass spectrometry, *Anal Biochem* **352**, 24--32.

Moll, J. R., Ruvinov, S. B., Pastan, I., and Vinson, C. (2001) Designed heterodimerizing leucine zippers with a ranger of pIs and stabilities up to 10(-15) M, *Protein Sci* **10**, 649-655.

Morales, V. M., Backman, A., and Bagdasarian, M. (1991) A Series of Wide-Host-Range Low-Copy-Number Vectors That Allow Direct Screening for Recombinants, *Gene* **97**, 39-47.

Morbach, S., Sahm, H., and Eggeling, L. (1996) l-Isoleucine Production with Corynebacterium glutamicum: Further Flux Increase and Limitation of Export, *Appl Environ Microbiol* **62**, 4345-4351.

Mori, K. (1981) A simple synthesis of (*S*)-(+)-sulcatol, the pheromone of *Gnathotrichus tetusus* employing baker's yeast for asymmetric reduction., *Tetrahedron* **37**, 1341-1342.

Murarka, A., Dharmadi, Y., Yazdani, S. S., and Gonzalez, R. (2008) Fermentative utilization of glycerol by Escherichia coli and its implications for the production of fuels and chemicals, *Appl Environ Microbiol* **74**, 1124-1135.

Naggert, J., Narasimhan, M. L., DeVeaux, L., Cho, H., Randhawa, Z. I., Cronan, J. E., Green, B. N., and Smith, S. (1991) Cloning, sequencing, and characterization of Escherichia coli thioesterase II, *The Journal of biological chemistry* **266**, 11044-11050.

Ni, Y., and Sun, Z. (2009) Recent progress on industrial fermentative production of acetone-butanol-ethanol by Clostridium acetobutylicum in China, *Appl Microbiol Biotechnol* **83**, 415-423.

Nielsen, D. R., Leonard, E., Yoon, S. H., Tseng, H. C., Yuan, C., and Prather, K. L. (2009) Engineering alternative butanol production platforms in heterologous bacteria, *Metab Eng* **11**, 262-273.

Nijkamp, K., van Luijk, N., de Bont, J. A. M., and Wery, J. (2005) The solvent-tolerant Pseudomonas putida S12 as host for the production of cinnamic acid from glucose, *Applied Microbiology and Biotechnology* **69**, 170-177.

Nunez, M. F., Pellicer, M. T., Badia, J., Aguilar, J., and Baldoma, L. (2001) Biochemical characterization of the 2-ketoacid reductases encoded by ycdW and yiaE genes in Escherichia coli, *Biochem J* **354**, 707-715.

Osborne, S. J., Leaver, J., Turner, M. K., and Dunnill, P. (1990) Correlation of biocatalytic activity in an organic-aqueous two-liquid phase system with solvent concentration in the cell membrane, *Enzyme Microb Technol* **12**, 281-291.

Park, J. I., and Kim, D. H. (2001) 2-Benzyl-3,4-iminobutanoic acid as inhibitor of carboxypeptidase A, *Bioorganic & medicinal chemistry letters* **11**, 2967-2970.

Park, J. W., Jung, W. S., Park, S. R., Park, B. C., and Yoon, Y. J. (2007) Analysis of intracellular short organic acid-coenzyme A esters from actinomycetes using liquid chromatography-electrospray ionization-mass spectrometry, *J Mass Spectrom* **42**, 1136--1147.

Patel, R. N. (2000) *Stereoselective Biocatalysis*, CRC Press, Boca Raton, FL.

Patel, R. N. (2006) Biocatalysis: synthesis of chiral intermediates for drugs, *Curr. Opin. Drug Discov. Devel.* **9**, 741-764.

Phue, J. N., Noronha, S. B., Hattacharyya, R., Wolfe, A. J., and Shiloach, J. (2005) Glucose metabolism at high density growth of *E. coli* B and *E. coli* K: Differences in metabolic pathways are responsible for efficient glucose utilization in *E. coli* B as determined by microarrays and Northern blot analyses, *Biotechnol. Bioeng.* **90**, 805-820.

Phue, J. N., and Shiloach, J. (2004) Transcription levels of key metabolic genes are the cause for different glucose utilization pathways in E. coli B (BL21) and E. coli K (JM109), *Journal of biotechnology* **109**, 21-30.

Poirier, Y., Nawrath, C., and Somerville, C. (1995) Production of polyhydroxyalkanoates, a family of biodegradable plastics and elastomers, in bacteria and plants, *Biotechnology (N Y)* **13**, 142-150.

Pollard, D. J., and Woodley, J. M. (2007) Biocatalysis for pharmaceutical intermediates: the future is now, *Trends Biotechnol.* **25**, 66-73.

Regalbuto, J. R. (2009) Engineering. Cellulosic biofuels--got gasoline?, *Science* **325**, 822-824.

Ren, Q., Ruth, K., Th?ny-Meyer, L., and Zinn, M. (2010) *Enatiomerically pure hydroxycarboxylic acids: current approaches and future perspectives*, Vol. 87.

Rubin, E. M. (2008) Genomics of cellulosic biofuels, *Nature* **454**, 841-845.

Ruhl, J., Schmid, A., and Blank, L. M. (2009) Selected Pseudomonas putida strains can grow in the presence of high butanol concentrations, *Applied and environmental microbiology* **75**, 4653-4656.

Sambrook, J., and Russell, D. (2001) *Molecular Cloning: A Laboratory Manual*, Third ed., Cold Spring Harbor Laboratory Press, Cold Spring Harbor, NY.

Sanchez, A. M., Bennett, G. N., and San, K. Y. (2005) Effect of different levels of NADH availability on metabolic fluxes of Escherichia coli chemostat cultures in defined medium, *Journal of biotechnology* **117**, 395-405.

Sardessai, Y., and Bhosle, S. (2002) Organic solvent-tolerant bacteria in mangrove ecosystem, *Curr Sci* **82**, 622-623.

Saxena, R. C., Adhikari, D. K., and Goyal, H. B. (2009) Biomass-based energy fuel through biochemical routes: A review, *Renewable and Sustainable Energy Reviews* **13**, 167-178.

Schmid, A., Dordick, J. S., Hauer, B., Kiener, A., Wubbolts, M., and Witholt, B. (2001) Industrial biocatalysis today and tomorrow, *Nature* **409**, 258-268.

Schneider, D., Duperchy, E., Depeyrot, J., Coursange, E., Lenski, R., and Blot, M. (2002) Genomic comparisons among *Escherichia coli* strains B, K-12, and O157:H7 using IS elements as molecular markers, *BMC Microbiol.* **2**, 18-25.

Schubert, P., Steinbuchel, A., and Schlegel, H. G. (1988) Cloning of the *Alcaligenes eutrophus* genes for synthesis of poly-beta-hydroxybutyric acid (PHB) and synthesis of PHB in *Escherichia coli*, *J. Bacteriol.* **170**, 5837-5847.

Schweiger, G., and Buckel, W. (1984) On the dehydration of (R)-lactate in the fermentation of alanine to propionate by Clostridium propionicum, *FEBS Lett* **171**, 79-84.

Secchi, S., Gassman, P. W., Williams, J. R., and Babcock, B. A. (2009) Corn-based ethanol production and environmental quality: a case of Iowa and the conservation reserve program, *Environ Manage* **44**, 732-744.

Seebach, D., Chow, H. F., Jackson, R. F. W., Sutter, M. A., Thaisrivongs, S., and Zimmermann, J. (1986) (+)-11,11'-di-O-methylelaiophylidene-preparation from Elaiophylin and total synthesis from (*R*)-3-hydroxybutyrate and (*S*)-malate, *Liebigs Ann. Chem.* **1986**, 1281-1308.

Shams Yazdani, S., and Gonzalez, R. (2008) Engineering Escherichia coli for the efficient conversion of glycerol to ethanol and co-products, *Metab Eng* **10**, 340-351.

Shen, C. R., and Liao, J. C. (2008) Metabolic engineering of Escherichia coli for 1-butanol and 1-propanol production via the keto-acid pathways, *Metabolic Engineering* **10**, 312-320.

Shimazu, M., Vetcher, L., Galazzo, J. L., Licari, P., and Santi, D. V. (2004) A sensitive and robust method for quantification of intracellular short-chain coenzyme A esters, *Anal Biochem* **328**, 51--59.

Shiraki, M., Endo, T., and Saito, T. (2006) Fermentative production of (*R*)-(-)-3-hydroxybutyrate using 3-hydroxybutyrate dehydrogenase null mutant of *Ralstonia eutropha* and recombinant *Escherichia coli*, *J. Biosci. Bioeng.* **102**, 529-534.

Si Jae Park, S. Y. L. (2004) New *fadB* homologous enzymes and their use in enhanced biosynthesis of medium-chain-length polyhydroxyalkanoates in *fadB* mutant *Escherichia coli*, *Biotechnol. Bioeng.* **86**, 681-686.

Sillers, R., Chow, A., Tracy, B., and Papoutsakis, E. T. (2008) Metabolic engineering of the non-sporulating, non-solventogenic Clostridium acetobutylicum strain M5 to produce butanol without acetone demonstrate the robustness of the acid-formation pathways and the importance of the electron balance, *Metab Eng* **10**, 321-332.

Slater, S., Gallaher, T., and Dennis, D. (1992) Production of poly-(3-hydroxybutyrate-co-3-hydroxyvalerate) in a recombinant *Escherichia coli* strain, *Appl Environ Microbiol* **58**, 1089-1094.

Slater, S., Houmiel, K. L., Tran, M., Mitsky, T. A., Taylor, N. B., Padgette, S. R., and Gruys, K. J. (1998) Multiple beta-ketothiolases mediate poly(beta-hydroxyalkanoate) copolymer synthesis in *Ralstonia eutropha*, *J Bacteriol* **180**, 1979-1987.

Snell, K. D., Feng, F., Zhong, L., Martin, D., and Madison, L. L. (2002) YfcX enables medium-chain-length poly(3-hydroxyalkanoate) formation from fatty acids in recombinant *Escherichia coli fadB* strains, *J. Bacteriol.* **184**, 5696-5705.

Steen, E. J., Chan, R., Prasad, N., Myers, S., Petzold, C. J., Redding, A., Ouellet, M., and Keasling, J. D. (2008) Metabolic engineering of Saccharomyces cerevisiae for the production of n-butanol, *Microb Cell Fact* **7**, 8.

Steen, E. J., Kang, Y., Bokinsky, G., Hu, Z., Schirmer, A., McClure, A., Del Cardayre, S. B., and Keasling, J. D. (2010) Microbial production of fatty-acid-derived fuels and chemicals from plant biomass, *Nature* **463**, 559-562.

Steinbuchel, A., and Valentin, H. E. (1995) Diversity of bacterial polyhydroxyalkanoic acids, *FEMS Microbiology Letters* **128**, 219-228.

Stelling, J., Klamt, S., Bettenbrock, K., Schuster, S., and Gilles, E. D. (2002) Metabolic network structure determines key aspects of functionality and regulation, *Nature* **420**, 190-193.

Taguchi, S., Yamada, M., Matsumoto, K. i., Tajima, K., Satoh, Y., Munekata, M., Ohno, K., Kohda, K., Shimamura, T., Kambe, H., and Obata, S. (2008) A microbial factory for lactate-based polyesters using a lactate-polymerizing enzyme, *Proceedings of the National Academy of Sciences of the United States of America* **105**, 17323-17327.

Terpe, K. (2006) Overview of bacterial expression systems for heterologous protein production: from molecular and biochemical fundamentals to commercial systems, *Appl Microbiol Biotechnol* **72**, 211-222.

Tishkov, V. I., and Popov, V. O. (2004) Catalytic mechanism and application of formate dehydrogenase, *Biochemistry (Mosc)* **69**, 1252-1267.

Tokiwa, Y., and Calabia, B. P. (2008) Biological production of functional chemicals from renewable resources, *Can. J. Chem.* **86**, 548-555.

Tolia, N. H., and Joshua-Tor, L. (2006) Strategies for protein coexpression in *Escherichia coli*, *Nat. Methods* **3**, 55-64.

Tomas, C. A., Welker, N. E., and Papoutsakis, E. T. (2003) Overexpression of groESL in Clostridium acetobutylicum results in increased solvent production and tolerance, prolonged metabolism, and changes in the cell's transcriptional program, *Appl Environ Microbiol* **69**, 4951 - 4965.

Tseng, H.-C., Martin, C. H., Nielsen, D. R., and Prather, K. L. J. (2009) Metabolic engineering of Escherichia coli for the enhanced production of (R)- and (S)-3-hydroxybutyrate, *Appl. Environ. Microbiol.*

Tseng, H. C., Harwell, C. L., Martin, C. H., and Prather, K. L. (2010) Biosynthesis of chiral 3-hydroxyvalerate from single propionate-unrelated carbon sources in metabolically engineered E. coli, *Microb Cell Fact* **9**, 96.

Tyo, K. E., Fischer, C. R., and Stephanopoulos, G. (2008) Genetic and Metabolic Perturbation Analysis of the Polyhydroxybutyrate Pathway, *submitted*.

Vermue, M., Sikkema, J., Verheul, A., Bakker, R., and Tramper, J. (1993) Toxicity of homologous series of organic-solvents for the Gram-positive bacteria *Arthrobacter* and *Nocardia* Sp

and the Gram-negative bacteria *Acinetobacter* and *Pseudomonas* Sp, *Biotechnology and Bioengineering* **42**, 747-758.

Wakeley, H. L., Hendrickson, C. T., Griffin, W. M., and Matthews, H. S. (2009) Economic and environmental transportation effects of large-scale ethanol production and distribution in the United States, *Environ Sci Technol* **43**, 2228-2233.

Wallace, K. K., Bao, Z. Y., Dai, H., Digate, R., Schuler, G., Speedie, M. K., and Reynolds, K. A. (1995) Purification of crotonyl-CoA reductase from Streptomyces collinus and cloning, sequencing and expression of the corresponding gene in Escherichia coli, *European journal of biochemistry / FEBS* **233**, 954-962.

Walle, M. v. d., and Shiloach, J. (1998) Proposed mechanism of acetate accumulation in two recombinant *Escherichia coli* strains during high density fermentation, *Biotechnol. Bioeng.* **57**, 71-78.

Waltz, E. (2009) Cellulosic ethanol stimulus, *Nat Biotechnol* **27**, 304.

Wang, G., and Hollingsworth, R. I. (1999) Direct Conversion of (S)-3-Hydroxy-gamma-butyrolactone to Chiral Three-Carbon Building Blocks, *The Journal of organic chemistry* **64**, 1036-1038.

Welch, R. W., Rudolph, F. B., and Papoutsakis, E. T. (1989) Purification and characterization of the NADH-dependent butanol dehydrogenase from Clostridium acetobutylicum (ATCC 824), *Archives of biochemistry and biophysics* **273**, 309-318.

Werpy, T., Petersen, G., Oak, U. S., and Ridge, T. N. (2004) Top value added chemicals from biomass, Vol results of screening for potential candidates from sugars and synthesis gas, *Department of Energy August*.

Wierckx, N. J. P., Ballerstedt, H., de Bont, J. A. M., and Wery, J. (2005) Engineering of solvent-tolerant Pseudomonas putida S12 for bioproduction of phenol from glucose, *Applied and environmental microbiology* **71**, 8221-8227.

Xia, X. X., Han, M. J., Lee, S. Y., and Yoo, J. S. (2008) Comparison of the extracellular proteomes of *Escherichia coli* B and K-12 strains during high cell density cultivation, *Proteomics* **8**, 2089-2103.

Yeh, J. I., Chinte, U., and Du, S. (2008) Structure of glycerol-3-phosphate dehydrogenase, an essential monotopic membrane enzyme involved in respiration and metabolism, *Proc Natl Acad Sci U S A* **105**, 3280-3285.

Zhang, H., Wang, Y., and Pfeifer, B. A. (2008) Bacterial hosts for natural product production, *Molecular pharmaceutics* **5**, 212-225.

Zhang, K., Sawaya, M. R., Eisenberg, D. S., and Liao, J. C. (2008) Expanding metabolism for biosynthesis of nonnatural alcohols, *Proc Natl Acad Sci* **105**, 20653-20658.

Zhang, Y. H. (2008) Reviving the carbohydrate economy via multi-product lignocellulose biorefineries, *J Ind Microbiol Biotechnol* **35**, 367-375.

Zhao, K., Tian, G., Zheng, Z., Chen, J. C., and Chen, G. Q. (2003) Production of *D*-(-)-3-hydroxyalkanoic acid by recombinant *Escherichia coli*, *FEMS Microbiol. Lett.* **218**, 59-64.

Zheng, Y. N., Li, L. Z., Xian, M., Ma, Y. J., Yang, J. M., Xu, X., and He, D. Z. (2009) Problems with the microbial production of butanol, *J Ind Microbiol Biotechnol* **36**, 1127-1138.

Zheng, Z., Gong, Q., Liu, T., Deng, Y., Chen, J. C., and Chen, G. Q. (2004) Thioesterase II of *Escherichia coli* plays an important role in 3-hydroxydecanoic acid production, *Appl. Environ. Microbiol.* **70**, 3807-3813.

APPENDIX A

Assessment of *Clostridium acetobutylicum* Butanol and Butyrate Pathway Activity by CoA Pool Size Measurements

Abstract

In clostridia, *n*-butanol production from carbohydrates at yields of up to 76% of the theoretical maximum and at titers of up to 13 g/L has been reported. However, in *E. coli*, several groups have reported butyric acid or butanol production from recombinant expression of clostridial genes, at much lower titers and yields. To pinpoint deficient steps in the recombinant pathway, we developed an analytical procedure for the determination of intracellular pools of key pathway intermediates, and applied the technique to the analysis of three sets of *E. coli* strains expressing various combinations of butyrate biosynthesis genes. Low expression levels of the *hbd*-encoded *S*-3-hydroxybutyryl-CoA dehydrogenase were insufficient to convert acetyl-CoA to 3-hydroxybutyryl-CoA, indicating that *hbd* was a rate-limiting step in the production of butyryl-CoA. Increasing *hbd* expression alleviated this bottleneck, but in resulting strains, our pool size measurements and thermodynamic analysis showed that the reaction step catalyzed by the *bcd*-encoded butyryl-CoA dehydrogenase was rate-limiting. Such thermodynamic interpretation of pool size measurements is applicable to the analysis of other metabolic pathways.

This chapter was published as:

Fischer, C.R., Tseng, H.-C., Tai, M., Prather, K.L.J., Stephanopoulos G. 2010. "Assessment of *Clostridium acetobutylicum* butanol and butyrate pathway activity in recombinant *Escherichia coli* strains by measurement of intracellular pathway intermediates" ***Appl Microbiol Biotechnol*** 88(1): 265–275.

A.1 Introduction

Butyric acid is a saturated C4 fatty acid and intermediate in the clostridial biosynthesis of butanol. As such, an efficient means to produce it from glucose or other biomass-derived carbohydrates could enable efficient biofuels production from renewable biomass. In *Clostridium beijerinckii*, *n*-butanol production at yields of up to 74% of the theoretical maximum and at titers of up to 13 g/L has been reported (*Ezeji et al., 2004*). In *Clostridium tyrobutyricum*, which ends its fermentation at butyrate and does not produce butanol, butyrate yields of 78% of the theoretical maximum and titers of up to 50 g/L have been reported (*Liu et al., 2006*). Butyrate biosynthesis in clostridia is believed to proceed by the pathway shown in **Figure A-1**.

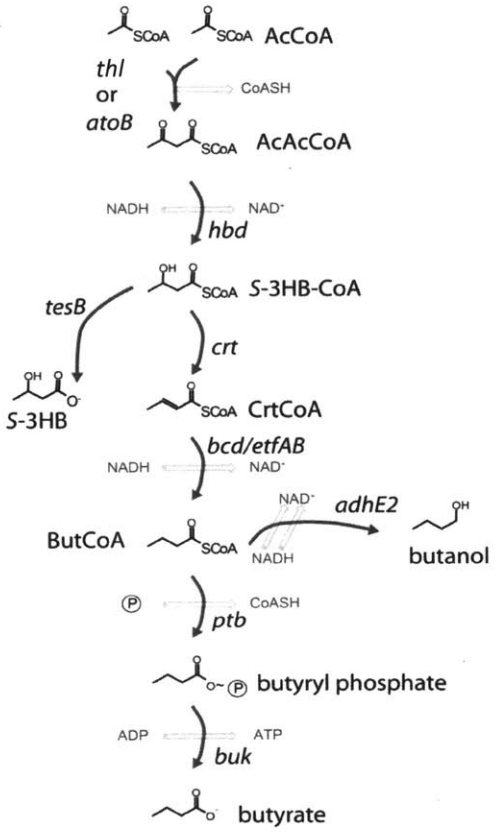

Figure A-1 | Pathways of butyrate and butanol biosynthesis from acetyl-CoA (AcCoA) in *Clostridium acetobutylicum*. Also shown is the reaction for the non-clostridial *tesB* gene product (thioesterase II), which can hydrolyze acyl-CoAs directly to free carboxylic acids in a single step.

Because clostridia are more difficult to transform, are sensitive to oxygen, exhibit complex fermentation kinetics, and can form spores, they can be difficult to engineer.

Synthetic biology promises to simplify and expedite the design and engineering of metabolic pathways for the bioconversion of various feedstocks to desired fuels and chemicals. Several groups have recently applied synthetic biology approaches to the synthesis of *n*-butanol in a well-studied, robust host organism such as *E. coli* (*Atsumi et al., 2008, Inui et al., 2008, Nielsen et al., 2009*), but always at yields under 15% of the theoretical, and with titers less than 0.7 g/L. Two groups have assayed butanol pathway enzymes in cell extracts of heterologous hosts (*Inui et al., 2008, Nielsen et al., 2009*), and found that activity levels of the butyryl-CoA dehydrogenase, encoded by *bcd* and accompanying electron transfer flavoproteins encoded by *etfA* and *etfB*, were either much lower than other pathway enzymes (*Inui et al., 2008*) or not detectable in cell extracts (*Nielsen et al., 2009*). However, despite the low or non-measureable activity of the *bcd-etfAB* encoded butyryl-CoA dehydrogenase enzyme, *bcd* and *etfAB* is required for production of butanol in recombinant *E. coli*. Butyryl-CoA dehydrogenase is known to be very oxygen-sensitive, and yet expression of *bcd* and *etfAB* under aerobic conditions led to measureable butanol production in *E. coli* (*Atsumi et al., 2008*).

The *bcd-etfAB* encoded enzyme is thus a prime candidate as a bottleneck in the production of butanol from recombinant *E. coli* strains expressing the clostridial butanol biosynthesis genes, but bottlenecks may also occur in other reaction steps, and the role of oxygen is yet unclear. To bear futher light on these questions, we measured acyl CoA and related pool sizes in a battery of *E. coli* strains expressing clostridial genes for butyrate and butanol biosynthesis in a background strain engineered to favor butyrate production and to be an obligate aerobe.

A.2 Materials and Methods

A.2.1 Strains

E. coli K12 Δ*pta*, *E. coli* K12 Δ*ldhA*, and *E. coli* K12 Δ*adhE* were constructed via the method of Datsenko and Wanner (*Datsenko & Wanner, 2000*) starting from *E. coli* K12 MG1655. These genotypes were combined through a series of P1 mediated transductions of the corresponding *pta*::*kan*, *ldhA*::*kan*, and *adhE*::*kan* alleles followed

by elimination of the kanamycin marker with FLP-mediated recombination by pCP20. The resulting triple Δ*pta* Δ*ldhA* Δ*adhE* triple knockout was called the pal strain. For expression of the lambda Red expressing electrocompetent cells, an IPTG-inducible variant of the pKD46 plasmid described by Wanner was used. The pal(DE3) derivative of pal was created with the DE3 lysogenization kit (Merck KGaA, Darmstadt, Germany) as per the manufacturer's directions.

The pal-1e strain was created by evolving *E. coli* pal pZE21-pab pHATet-CBEH (see below) in MOPS-butyrate medium for 130 hours after inoculation from an overnight 4 mL culture in LB broth. No noticeable growth occurred until after 110 hr, when a population arose that could grow on butyrate as a sole carbon source. Colonies from this population were streaked from the exponentially growing culture in MOPS-butyrate onto LB agar. Two colonies were picked from the resulting plates, and grown overnight in LB broth, and re-inoculated into MOPS butyrate, where they were found to exhibit a lag phase of less than 1 hr. This strain may be a *fadR* deletion mutant (*Campbell et al., 2003*) but has not been exhaustively characterized.

A.2.2 Plasmids

The ptb-buk operon was cloned from *Clostridium acetobutylicum* ATCC 824 genomic DNA using primers "MT ptb-buk Sense" (TCCC**CCCGGG**GGGAGTTTATA GGGCAAAAGTTTTATAAACATGGGTACTGG) and "MT ptb-buk Anti" (GG**GGTACC** CCGAGTGTACGACCAGTGATTAAGAGTTTTAA) endowed with XmaI and KpnI restriction sites (emphasized in primer sequences. This PCR product was digested and ligated to KpnI/XmaI digested pZE21-gfp(ASV) (*Elowitz & Leibler, 2000*) in order to create pZE21ptb-buk. The *atoB* gene was cloned from *E. coli* K12 MG1655 genomic DNA with primers "CF184 atoB Sense KpnI" (ACTCG**GGTACC**ATGAAAAATTGTGTCATCGTCAGTG) and "CF185 atoB anti HindIII" (AGAGG**AAGCTT**TTAATTCAACCGTTCAATCACCATC), digested with HindIII and KpnI, and ligated to the HindIII/KpnI fragment of pZE21-gfp(ASV) to create pZE21-atoB. The promoter-gene PLTetO1 -atoB expression cassette from pZE21-atoB was amplified with primers "CF188 P(LTetO1) atoB Sense

(AatII)" (GGCTTCCCAACCTTACCAGAGG)and "CF189 P(LTetO1) atoB Anti AatII(XbaI)" (CCTCGACGTCTAGATATTACCGCCTTTGAGTGAGCTG), and the resulting fragment was digested with AatII and ligated into an AatII-digested fragment of pZE21-ptb-buk in order to create pZE21-pab. pRK415-BCS (*Nielsen et al., 2009*) was digested with SacI and AvrII, and the fragment containing the BCS operon with genes *crt*, *etfAB*, *bcd*,and *hbd* was ligated to XbaI-digested pHACm (*Alper & Stephanopoulos, 2007*) in order to create pHACm-CBEH. This plasmid carries genes for both tetracycline resistance (from pRK415-BCS) and chloramphenicol resistance (from pHACm). The CmR-conferring cat gene was disrupted in pHACm-CBEH by removing the 38bp MscI and NcoI linker region and re-ligating the plasmid, in order to form pHATet-CBEH.

A.2.3 Culturing conditions

Batch oxygen-limiting cultures were maintained in 15 mL glass tubes (Bellco Glass, Inc.) stoppered with a butyl rubber septum. The septum was pierced with a 26-gauge or 27-gauge syringe needle. Antibiotics were used as required (*Sambrook & Russell, 2001*). Anaerobically, *E. coli* requires bicarbonate for growth at low cell densities (*Hornsten, 1995*). In batch oxygen-limiting cultures without bicarbonate or CO_2 supplementation, this requirement results in long lag phases as sufficient bicarbonate must be accumulated by the metabolism of inoculated cells before growth can begin. In continuous cultures, gas sparging can strip away bicarbonate as CO_2, stopping growth. To avoid either possibility, MOPS minimal medium (Teknova Inc., Hollister, CA) was supplemented with 10 mM ammonium bicarbonate.

A.2.4 Stoichiometric modeling of the pal strain

We used a stoichiometric model of *E. coli* metabolism considered derived from the iJE660 model constructed by Jeremy Edwards and his co-workers (*Edwards & Palsson, 2000*). The model as originally formulated by Edwards et al. included redundant columns (fluxes) in an attempt to model stoichiometrically equivalent reactions. For example, the original model included 5 duplicate columns for the NADH-driven reduction of L-lactate

to lactaldehyde (column indices were 109, 110, 111, 113, and 114). This model was simplified by removing 117 stoichiometrically duplicated fluxes, resulting in a stoichiometric matrix with dimensions 536 × 836. This simplified model was called "iJE660b". To construct stoichiometric product-growth envelopes, the growth yield was fixed at μ_f gDCW / mol glucose, and then fluxes to either succinate or butyrate were minimized and maximized subject to iJE660b and the additional growth = μ_f constraint. This procedure was repeated for many values of μ_f between zero and the maximum growth rate possible in iJE660b.

A.2.5 Determination of intracellular acyl CoAs

Our method for the determination of intracellular levels of short-chain acyl-CoA esters is derived from the method reported by Shimazu et al (*Shimazu et al., 2004*), but is modified in several aspects. Briefly, in a 1.5 mL eppendorf tube, a 1-mL aliquot of exponential growth-phase bacterial culture was suspended above 400 µL of bromododecane, which itself was layered above 100 µL of metabolite extraction fluid. Because this cell harvesting method requires a dense, hexane-and bromododecane-immiscible polar, extraction fluid, we formulated an extraction fluid of acetonitrile, 2,2,2-trifluoroethanol, water, and trifluoroacetic acid in a 45:45:9:1 ratio ($\rho \sim 1.08$ g/cm^3). Samples were centrifuged for 30 s at 18,000 *g*. Cells were thus quickly centrifuged through the bromododecane layer into the metabolite extraction fluid, where they were rapidly lysed. Trials with GFP-expressing *E. coli* showed that cells pelleted in bromododecane alone retained fluorescence, but cell debris pelleted in extraction fluid had lost fluorescence after retrieval from the centrifuge. The culture medium and bromododecane supernatants were removed by aspiration; the crude extract was twice washed by the addition of 0.5 mL of hexanes (mixture of isomers) and subsequent vortexing and re-centrifugation. 70 µL of the original 100 µL of extract was transferred to a clean microcentrifuge tube in order to separate metabolite extracts from cell debris, and all samples were evaporated to dryness in a vacuum centrifuge (Vaccufuge, Eppendorf AG, Hamburg, Germany) at 30 ◦C. Dried samples were stored

indefinitely at -20 ◦C. This procedure avoids the use of both exotic extractants like Freon and trioctylamine (*Shimazu et al., 2004*) as well as solid-phase extraction columns (*Minkler et al., 2006, Park et al., 2007*). Instead of post-column derivatization with bromoacetaldehyde, and fluorescent detection of the resulting *1,N*^{6}-ethenoadenine adduct, we used pre-column derivatization with 150 µL of 1M chloroacetaldehyde in 150 mM sodium citrate buffer (pH=4.0) and fluorescent detection.

We used two chromatographic methods: one which we called Method A was a simple modification of the protocol of Shimazu "Method 1"(*Shimazu et al., 2004*), with identical HPLC setup but for a switch of Shimazu's buffer A with a 50% mixture of (100 mM sodium phosphate, 75 mM sodium acetate, pH 4.5) and 50% 60 mM magnesium chloride, with both buffers amended by addition of 1% v/v unstabilized tetrahydrofuran. The addition of magnesium chloride was necessary for chromatographic resolution of AcCoA and 3HB-CoA, which co-elute in the method originally reported by Shimazu and co-workers. As such, data reported by Shimazu for AcCoA pool sizes in *E. coli* and *Mixococcus xanthus* may be overestimates, due to conflation of 3HB-CoA and AcCoA pool sizes. Method A was used for all analyses of Strain Set I.

In a second method we called Method B, buffer A was 5 mM ammonium phosphate / 1%v/v THF adjusted to pH 6.5 with phosphoric acid, and buffer B was 99:1 methanol:THF. The column temperature was 60 ◦C and flow rate was 1.2 mL/min and the gradient regime was: 0% B for 2 min; then from 0 % B to 6.25%B by 3 min; from 6.25% B to 14.6% B by 7.5 min; from 14.6% B to 75% B by 13.3 min; a constant flow of 75% B until 15.3 min; to 0% B by 16 min; and a constant flow of 0% B for 2 min. We found this method is preferred for measurement of adenosine phosphates and free CoASH. For all samples analyzed with this method, hexanoyl-CoA was used as an internal standard by 1000× dilution of a 10 mM stock of hexanoyl-CoA (Sigma-Aldrich, St. Louis, MO) dissolved in PBS into metabolite extraction fluid, immediately before beginning the extractions. The peak areas of all analytes were normalized to the HexCoA peak size, and the normalized peak area was calibrated against known standards in

order to quantify metabolite pool sizes. Method B was used for all analyses of Strain Set II and III.

The concentrations of acyl-CoAs were calculated from linear ($R^2 > 0.9$) standard curves obtained from stock solutions (AcCoA, ATP, ADP, AMP, and CoASH), or from spiking known amounts of acyl-CoA into wild-type *E. coli* K12 metabolite extracts (all other acyl-CoAs). The uncertainty in measured pool sizes was the root-mean-square of the standard error between duplicate or triplicate measurements and the standard error associated with the linear regression. This latter error term was dominant for low pool-size measurements (< 100 pmol/(A600 · mL)).

A.2.6 Calculation of $\Delta_{IPTG}\Delta G'$

The strains used in this study express butyrate or butanol biosynthesis genes from IPTG-inducible promoters. If the induction of gene expression with IPTG changes the pool sizes of pathway metabolites, the free energy change associated with any given pathway step will also change. The difference between the induced state of the pathway and uninduced state of the pathway is shown in **Equation A-1**, where *Q* indicates the measured, possibly non-equilibrated reaction quotient $\prod_i (C_i)^{\nu_i}$, where C_i is the concentration of reactant or product *i* and *vi* is the stoichiometric coefficient of the reactant or product in the biochemical reaction of interest, and *K'* is the biochemical equilibrium constant (*Alberty, 2005*). In the calculation of $\Delta_{IPTG}\Delta G'$, the thermodynamic equilibrium constant *K'* cancels out, and thus uncertainty in $\Delta G'$ stemming from uncertainty in ln *K'* cancels out. To the extent that assumed physiological parameters like the NADH:NAD ratio or the energy charge stay constant after induction, the uncertainty in these values will also cancel out. The prime mark on *K'* and $\Delta G'$ indicates a biochemical standard state, where the pH, rather than the absolute number of moles of H^+ is taken as the independent variable (*Alberty, 2005*).

$$\Delta_{\mathrm{IPTG}}\Delta G' = -RT\left[\left(\ln K' - \ln Q_{\mathrm{IPTG}}\right) - \left(\ln K' - \ln Q_{\mathrm{no\,IPTG}}\right)\right] = RT\ln\left(\frac{Q_{\mathrm{IPTG}}}{Q_{\mathrm{no\,IPTG}}}\right) \qquad \textbf{(Eq. A-1)}$$

A.3 Results

A.3.1 Design of the pal strain and a stoichiometric driving force for butyrate production

In order to balance reducing equivalents, the native metabolism of *E. coli* ferments glucose to produce acetate, ethanol, and lactate, all of which could conceivably compete with butyrate production. To test the effects of removing these pathways on stoichiometrically possible space for butyrate production, the genes *pta*, *adhE*, and *ldhA*, responsible for the fermentative production of acetate, ethanol, and lactate, respectively, were deleted from the constraints-based stoichiometric model of *E. coli* metabolism (*Edwards & Palsson, 2000*).

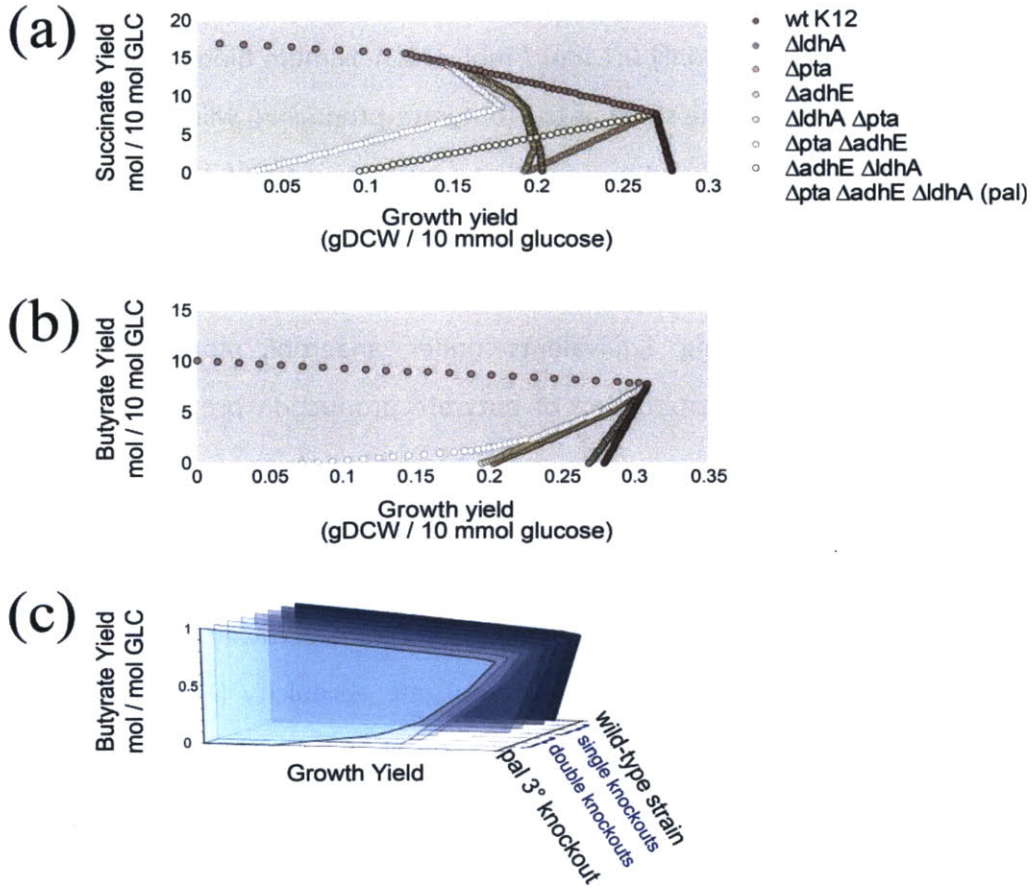

Figure A-2 | Stoichiometrically feasible region for the anaerobic biosynthesis of (a) succinate and *E. coli* cell biomass from glucose and carbon dioxide; (b) butyric acid and *E. coli* cell biomass from glucose as the sole carbon source. Panel (c) shows the data in (b) from an alternate visual perspective for clarity.

In stoichiometric models not including clostridial butyrate biosynthesis reactions, these deletions led to a stoichiometric correlation between biomass formation and succinate production, as shown in **Figure A-2(a)**. In the Δ*pta*, Δ*adhE*, and Δ*ldhA* strain model (hereafter, the pal strain model), growth without any succinate production was possible only up to biomass yields on glucose of 0.003 gDCW / 1 mmol glucose, or about 0.017 gDCW / g glucose. This is about ten times lower than usual anaerobic biomass yields on glucose for *E. coli* (*Hempfling & Mainzer, 1975*). Introduction of the clostridial butyrate biosynthesis pathway reactions shown in **Figure A-1** into the stoichiometric model of *E. coli pal* metabolism caused a shift in the growth-optimal outlet for reducing equivalents, as shown in **Figure A-2(b)**. When the butyrate pathway was made available, growth yields exceed 0.094 gDCW / g glucose at a butyrate yield on glucose of only 0.1 mol / mol. The maximum biomass yield of the *pal* triple knockout model was the same as the (butyrate-producing) wild-type strain model, 0.032 gDCW / mmol glucose, and it occured at a butyrate yield of 7.5 mol butyrate / 10 mol glucose.

Thus, although the *E. coli* metabolic network has alternate routes for clearing glycolysis-generated reducing equivalents under anaerobic conditions (e.g., the production of succinate), introduction of butyrate production provides a more facile route for anaerobic biomass production, at least stoichiometrically. To ensure that the activity of clostridial butyrate biosynthesis enzymes expressed in *E. coli* was not obscured or outcompeted by native *E. coli* metabolism, the *pal* strain background was used for all measurements of the pool sizes of butyrate pathway intermediates. An unexpected property of the *pal* strain was obligate aerobicity (*Fischer et al., 2010*), which allowed for growth under strict oxygen limitation, where the rate of oxygen to supply to the culture limits the rate of growth, similar to conditions previously shown to improve performance of the butanol fermentations (*Atsumi et al., 2008*).

A.3.2 Assessment of butyrate pathway activity by CoA pool size measurements in three strain sets

Table A-1 | Strains and plasmids used in this study.

Source strains	Description	Reference or Source
E. coli K12 MG1655	wild-type	ATCC 47076
pal	K12 Δ*pta* Δ*ldhA* Δ*adhE*	this work
TGD(cat+PHB)	K12 with chromosomally inserted PHB biosynthesis pathway	(*Tyo et al., 2008*)
Plasmids		
pKD46	temperature-sensitive, low-copy AmpR plasmid for chromosomal modification	(*Datsenko & Wanner, 2000*)
pCP20	temperature sensitive, AmpR expression module for the FRT recombinase	(*Datsenko & Wanner, 2000*)
pJM12	derivative of pKD46 with PBAD promoter replaced by Plac	this work
pRK415-BCS	source of cloned clostridial CBEH operon	(*Nielsen et al., 2009*)
pZE21-gfp(ASV)	medium-copy kanR plasmid with constitutive P(LTetO1) promoter	(*Elowitz & Leibler, 2000*), (*Lutz & Bujard, 1997*)
pZE21-ptb-buk	pZE21 with gfp replaced by the ptb/buk polycistron from C. acetobutylicum	this work
pZE21-pab	Inserts a P(LTetO1)-atoB expression cassette into pZE21-ptb-buk	this work
pHACm-CBEH	low-copy SC101 derivative for the aTc-inducible expression of the CBEH operon from *C. acetobutylicum*	this work
pHATet-CBEH	variant of pHACm-CBEH with chloramphenicol marker removed	this work
pRARE	p15a-derived, CmR plasmid expressing tRNAs for rare codons in *E. coli*	Novagen
pHACm-	low-copy SC101 derivative without any expression cassette	(*Alper & Stephanopoulos, 2007*)
pETDuet1-thl-hbd	Medium-copy T7 expression vector for clostridial ketothiolase *thl* and *S*-specific ketoacid reductase *hbd*	(*Tseng et al., 2009*)
pETDuet1-thl-phaB	Replaces *S*-3HB-CoA specific *hbd* in pETDuet1-thl-hbd with *R*-3HB-CoA specific *phaB*	(*Tseng et al., 2009*)
pCDFDuet1-ptb-buk	Medium-copy T7 expression vector for clostridial energy-conserving acyl-CoA phosphatase *ptb* and acyl phosphate kinase *buk*	(*Tseng et al., 2009*)
pCDFDuet1-tesB	Replaces *ptb-buk* operon in pCDFDuet1-ptb-buk with *tesB* thioesterase	(*Tseng et al., 2009*)
pETDuet1-atoB, pETDuet1-atoB-gapA	Medium-copy T7 expression vector for native *E. coli* ketothiolase *atoB* (and NADH-regenerating enzyme *gapA*)	(*Nielsen et al., 2009*)
pCDF-hbd-crt	Medium-copy T7 expression vector for clostridial ketoacid reductase *hbd* and crotonase *crt*	(*Nielsen et al., 2009*)
pCOLA-bcd-etfAB	Medium-copy T7 expression vector for clostridial butyryl-CoA reductase *bcd* and accessory electron transfer flavoprotein genes *etfAB*	(*Nielsen et al., 2009*)
pACYC-adhE2	Medium-copy T7 expression vector for clostridial alcohol dehydrogenase *adhE2*	(*Nielsen et al., 2009*)
pETDuet1-bktB-acd	Medium-copy T7 expression vector for alternate ketothiolase *bktB* and acyl CoA dehydrogenase *acd*	(*Nielsen et al., 2009*)
Strain Set I		
1	*pal* pZE21-pab pHATet-CBEH	this work
1e	*strain 1 evolved to grow on butyrate as a sole carbon source*	this work
2	*pal* pZE21-ptb/buk pHATet-CBEH	this work
3	*pal* pZE21-atoB pHATet-CBEH	this work
4	*pal* pZE21-pab pHACm-	this work
5	*pal* pZE21-gfp pHACm-	this work
6	*pal* pZE21-pab pHATet-CBEH pRARE	this work
7	*pal* pZE21-ptb/buk pHATet-CBEH pRARE	this work
8	*pal* pZE21-atoB pHATet-CBEH pRARE	this work
9	*pal* pZE21-pab pHACm- pRARE	this work
Strain Set II		
11	*pal(DE3)* pETDuet1-thl-hbd pCDFDuet1-tesB	this work
12	*pal(DE3)* pETDuet1-thl-hbd pCDFDuet1-ptb-buk	this work
13	*pal(DE3)* pETDuet1-thl-phaB pCDFDuet1-tesB	this work
14	*pal(DE3)* pETDuet1-thl-phaB pCDFDuet1-ptb-buk	this work
911	Strain #11 transformed with pHATet-CBEH	this work
912	Strain #12 transformed with pHATet-CBEH	this work
914	Strain #14 transformed with pHATet-CBEH	this work
Strain Set III		
21	*pal*(DE3) pETDuet1-atoB pCDF-hbd-crt pCOLA-bcd-etfAB pACYC-adhE2	this work
22	*pal*(DE3) pETDuet1-atoB-gapA pCDF-hbd-crt pCOLA-bcd-etfAB pACYC-adhE2	this work
23	*pal*(DE3) pETDuet1-bktB-acd pCDF-hbd-crt pCOLA-bcd-etfAB pACYC-adhE2	this work

To examine the factors that control performance of the clostridial butyrate biosynthesis pathway in the *E. coli* pal strain, we measured in three strain sets the pool sizes of the pathway intermediates coenzyme A (CoASH), acetyl CoA (AcCoA), acetoacetyl-CoA (AcAcCoA), 3-hydroxybutyryl-CoA (3HB-CoA), crotonoyl-CoA (CrtCoA), and butyryl-CoA (ButCoA). None of the strain sets produced measurable quantities of butyric acid, but proved to differ markedly in the pool sizes of various pathway intermediates. Strain Set I includes strains expressing clostridial butyrate biosynthesis genes from low- or medium copy pSC101 and pZE-derived plasmids, and medium strength P_{LTetO1} derived promoters. No strains in Strain Set I produced measureable quanitites of butyric acid during growth on minimal glucose medium. In all of these strains (#1-#9 in **Table A-1**), AcCoA was the sole short-chain acyl-CoA detected from growth-phase cultures. The levels of AcCoA were similar in all of the strains, ranging from between 700 to 1800 pmol/(A_{600}·mL) for strains #1-#5. Strain #1, containing all genes in the clostridial butyrate biosynthesis pathway (**Fig. A-1**), did not have significantly different AcCoA pool sizes than strains #2-5, "dropout" strains missing one or more pathway genes. Pool sizes were generally lower in strains #6-9, which were identical to strains #1-4 except for introduction of a pRARE plasmid which facilitates the translation of genes containing rare codons. Quantitative data are given in **Table A-2**.

Table A-2 | AcCoA pool sizes in induced cultures of strain set I, expressing clostridial butyrate biosynthesis genes from low and medium copy plasmids using P_{LTetO1}-derived promoters.

Strain # (see Table A-1 in main text)	AcCoA Pool Size, pmol/(A_{600}·mL)	3HB-CoA Pool Size, pmol/(A_{600}·mL)
1	1595 ± 422	n.d.
2	1804 ± 754	n.d.
3	1007 ± 383	n.d.
4	1181 ± 486	n.d.
5	704 ± 129	n.d.
6	1338 ± 355	n.d.
7	306 ± 114	n.d.
8	513 ± 171	n.d.
9	779 ± 379	n.d.
TGD(cat+PHB)	147 ± 45	97 ± 30

A strain of *E. coli* with the entire *Ralstonia eutropha*-derived pathway for polyhydroxybutyrate biosynthesis chromosomally integrated contains an alternate route

for the synthesis of 3-hydroxybutyryl-CoA by use of the *R. eutropha* gene *phaB*. In contrast to the results with Strain Set I, a clone of this strain transformed with pHATet-CBEH and pZE21-pab (the same butyrate-producing plasmids used in Strain Set I), 3HB-CoA was detectable in cell extracts (**Table A-2**). This result suggested that either the expression level of *hbd* in Strain Set #1 was insufficient for production of the first two pathway intermediates AcAcCoA and 3HBCoA, or that availability of the redox cofactor NADH was limiting the activity of the *hbd*-encoded enzyme. In the first case, the bottleneck could be alleviated by increasing the expression of *hbd*, and in the second, the bottleneck might be eliminated by swapping NADH-requiring *hbd* for NADPH-requiring 3-hydroxybutyryl-CoA reductases, such as *phaB*.

Further pool size measurements were made on Strain Set II, which express *hbd* and other genes for the production of 3-hydroxybutyric acid from monocistronic operons driven by much stronger IPTG-inducible, T7-derived promoters (*Tseng et al., 2009*). Measurements of intracellular acyl-CoAs in induced cultures of strains from Strain Set II revealed detectable quantities of 3HB-CoA, showing that expression levels of *hbd* in Strain Set I had been insufficient for measureable intracellular conversion of AcCoA to 3HB-CoA, and that intracellular NADH levels were sufficient for production of 3HB-CoA. To test the effect of alleviating this bottleneck on the performance of the entire clostridial butanol biosynthesis pathways, pool sizes in a third set of strains was analyzed. This strain set bears plasmids containing the complete clostridial pathway for butanol fermentation (*Nielsen et al., 2009*), and these plasmids have previously been used to produce small amounts (<600 mg/L) of butanol. In this third strain set, butyryl-CoA was not reliably detected in IPTG-induced cultures (**Table A-3**). In contrast, slight amounts of butyryl-CoA were detected in non-induced strains, but the uncertainty in the level of butyryl-CoA detected under non-inducing conditions was still quite large. Butyryl-CoA levels were too low to be reliably detected in these extracts, as illustrated by the uncertainties given in **Table A-3** for ButCoA.

Our HPLC technique also allows determination of intracellular ATP, ADP, and AMP. From these universal energy metabolites, the adenylate energy charge (EC), a ratio of

the ATP pool plus one-half the ADP pool to total adenine phosphate pool, can be calculated. This ratio is an indicator of the energetic state of the cell. AMP and ADP pool sizes measured in Strain Sets II and III are generally consistent with previously obtained measurements (*Shimazu et al., 2004*). The extremely low values for EC obtained in strains #11 and #13 after IPTG induction reflect the activity of the *tesB* gene product: the TesB enzyme does not regenerate ATP during the hydrolysis of 3HB-CoA to form free 3-hydroxybutyric acid; whereas with Ptb and Buk, ATP is regenerated during the two-step formation of 3-hydroxybutyric acid from 3HB-CoA. Pathway intermediates AcAcCoA and CrtCoA were not detected in any of the strain sets we studied.

Table A-3 | Intracellular pool sizes in pmol/(A600·mL) of free coenzyme A, acyl CoAs, and adenosine phosphates in *E. coli* strains expressing clostridial butanol biosynthesis genes.
Uncertainties shown are the root-mean-square of the standard error in the mean calculated from either 2 or 3 duplicate measurements and (ii) the standard error stemming from linear regression against HPLC calibration curves.

Strain	CoASH	AcCoA	AcCoA/CoASH ratio	3HB-CoA	ButCoA	ATP	ADP	AMP	EC
NO IPTG									
11	676±41	1,170±46	1.7±0.13	18±5	8±4	347±37	214±31	179±58	0.61±0.051
12	278±13	1,059±45	3.8±0.24	27±6	19±4	220±46	150±10	105±29	0.62±0.039
13	477±23	1,116±200	2.3±0.43	96±49	16±1	478±61	184±29	71±15	0.78±0.022
14	412±77	1,216±123	3.0±0.63	14±8	10±4	379±105	195±27	113±29	0.69±0.033
21	391±220	627±109	1.6±0.94	120±54	16±2	250±68	148±32	78±5	0.68±0.026
22	635±26	943±197	1.5±0.32	109±10	13±4	583±305	228±63	76±17	0.79±0.032
23	262±148	503±69	1.9±1.12	25±25	16±2	164±2	114±13	104±37	0.58±0.058
pal w.t.	570±201	1,031±254	1.8±0.78	62±41	13±8	441±197	181±56	131±61	0.71±0.065
+ IPTG									
11	342±42	1,218±96	3.6±0.52	6±4	20±20	5±1	4±1	31±20	0.17±0.028
12	528±51	1,305±111	2.5±0.31	210±94	n.d.	450±188	159±21	144±79	0.70±0.088
13	818±80	861±309	1.1±0.39	170±173	16±2	n.d.	n.d.	247±104	0.00±0.000
14	1,442±539	1,564±316	1.1±0.46	763±872	25±20	910±504	289±80	331±170	0.69±0.066
21	981±1,105	665±231	0.7±0.80	322±290	35±9	542±295	78±34	211±27	0.70±0.054
22	364±30	676±282	1.9±0.79	33±6	9±6	218±229	94±52	60±27	0.71±0.057
23	1,244±1,404	788±216	0.6±0.74	407±813	32±8	611±15	126±29	235±167	0.69±0.138
pal w.t.	298±210	1,134±559	3.8±3.27	87±116	13±17	337±301	177±109	187±174	0.61±0.113

A.3.3 A thermodynamic framework for relating pool size measurements to pathway activity

Enzymes accelerate the rate at which biochemical reactions reach equilibrium. The addition of IPTG leads to high-level overexpression of pathway enzymes, and thus should tend to push pathway reactions towards equilibrium. This push can be

quantified using pool size measurements, if reaction thermodynamic data and pool size measurements are available. Because AcAcCoA and CrtCoA were not detectable in any of the strain sets we studied, we lumped the butyrate biosynthesis pathway into two reactions, the first being synthesis of 3HB-CoA from AcCoA and the second being the synthesis of ButCoA from 3HB-CoA.

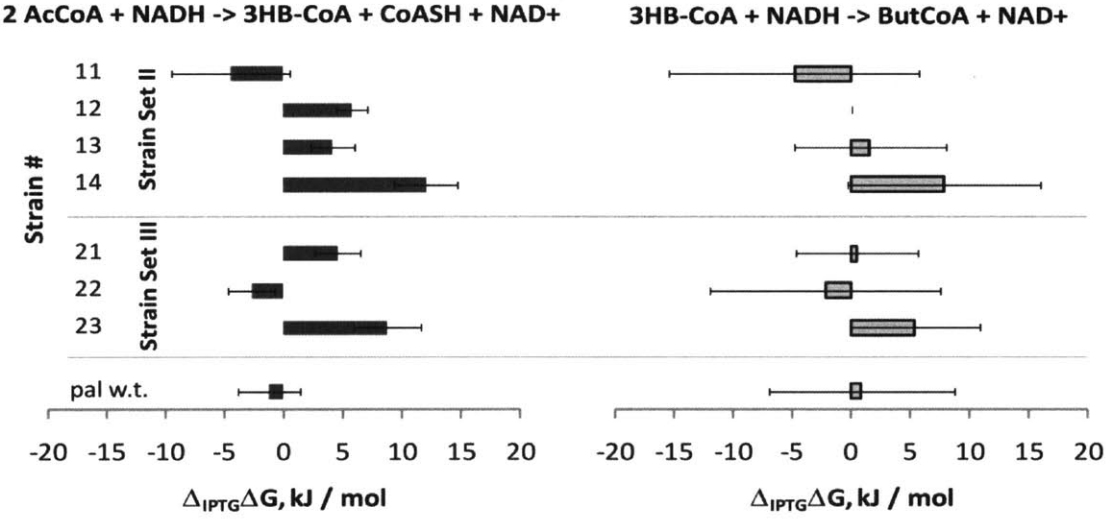

Figure A-3 | The change from adding IPTG inducer in measured ΔG' values for component reactions of the clostridial butyrate or butanol biosynthesis pathway. A positive $\Delta_{IPTG}\Delta G'$ indicates that induction of pathway genes has filled pool sizes for reaction products (or depleted pool sizes for reactants) of the given reaction, and as such, represents evidence that pathway induction leads to conversion of thermodynamic chemical potential into flux through the given reaction. The graph shows $\Delta_{IPTG}\Delta G'$ for nine strains numbered according to **Table A-1**. For some strains, induction clearly shifts the 3HBCoA synthesis reaction toward equilibrium. In contrast, no such change is shown for the ButCoA synthesis reaction, indicating that this pathway step is likely rate-limiting.

Using the pool sizes in **Table A-3** and relevant thermodynamic parameters from the literature (*Fischer et al., 2010*), we estimated the effect of IPTG on equilibration of pathway reactions by computing $\Delta_{IPTG}\Delta G'$ (see Materials and Methods), as shown in **Figure A-3**. This figure shows that IPTG increased (made less thermodynamically favorable) the $\Delta_{IPTG}\Delta G'$ for conversion of AcCoA to 3HB-CoA for two of the 3HB producing strains (strain #12 and #14), as shown by the positive values for $\Delta_{IPTG}\Delta G'$. The $\Delta_{IPTG}\Delta G'$ value for the 3HBCoA-from-AcCoA reactions for strain #13 was also likely positive, but a value of 0 cannot be excluded because of the slight overlap of the error

bar and the $\Delta_{IPTG}\Delta G' = 0$ center axis. In strain #11, measurements did not reliably detect intracellular 3HB-CoA, increasing the uncertainty in $\Delta_{IPTG}\Delta G'$ values.

The failure to detect appreciable levels of butyryl-CoA in Strain Set II and III under either inducing or non-inducing conditions made accurate estimation of $\Delta_{IPTG}\Delta G'$ fraught with uncertainty. However, it is notable that the estimated ranges for $\Delta_{IPTG}\Delta G'$ shown for the 3HBCoA → ButCoA set of pathway reactions all overlap 0. The parent pal strain, with no plasmids or pathway genes, also had estimated $\Delta_{IPTG}\Delta G'$ values near 0 kJ / mol, as would be expected for a strain with no pathway activity of any type.

A.3.4 Unexpected behavior of ptb and buk

Strain #12 (in the *pal* background) expressing both *hbd* and *ptb-buk* also produced much higher amounts of crotonic acid than control strains. **Figure A-4** shows crotonate production for several strains growing under various conditions in MOPS minimal media. Strain #1, expressing all the genes of the clostridial butyrate biosynthesis pathway at relatively low levels, produced 76 μM crotonic acid during growth on MOPS glucose medium. In MOPS *butyrate* medium, this strain did not show signs of growth until more than 110 hours of culture, after which growth eventually began. Two colonies isolated by streaking onto LB agar after growth in MOPS butyrate showed no lag phase on reinoculation into MOPS butyrate. This mutant evolved from Strain #1, called Strain #1e, produced 10× more crotonate than its parent in growth on MOPS glucose. Crotonic acid production was much lower in Strain #1e growing on MOPS butyrate, where flux through butyrate biosynthetic reactions (**Fig. A-1**) is reversed.

Strain #12 gave 3× more crotonic acid than strain #1. These strains differ in two important ways: (i) *hbd* is expressed using the high-copy pETDuet1-*thl-hbd* plasmid and the strong T7 promoter, and (ii) *crt* and thus the crotonase enzyme is not present in strain 12. Thus, the production of crotonate does not depend on the crotonase enzyme or the *crt* gene. Also, crotonate was produced at much, much lower levels in strains expressing *tesB* in place of *ptb-buk* such as 911, 11, or 13, illustrating that crotonate

production depends on expression of both *hbd* and *ptb-buk*, but not *crt*. Strains expressing *phaB* in place of *or in addition* to *hbd* also showed very low or indetectable crotonate production. This may be related to the difference in stereochemistry of the 3-hydroxybutyryl-CoA that results from PhaB versus Hbd. That is, dehydration of 3-hydroxybutyryl-CoA to crotonyl-CoA may require the *S*-enantiomer produced by Hbd. While the inclusion of *phaB* in addition to *hbd* should enable the production of both enantiomers, differences in pathway activity could account for the greatly reduced crotonate production in the presence of *phaB*. Thus, these conditions seemed necessary and sufficient for crotonate production of over 100 μM: (i) co-expression of the *hbd* and *ptb-buk* operons; (ii) the absence of alternative pathway genes including *tesB* and *phaB*, (iii) operation of the butyrate pathway in the forward direction as in growth on glucose. The expression of the *crt* gene was unrelated to crotonate production.

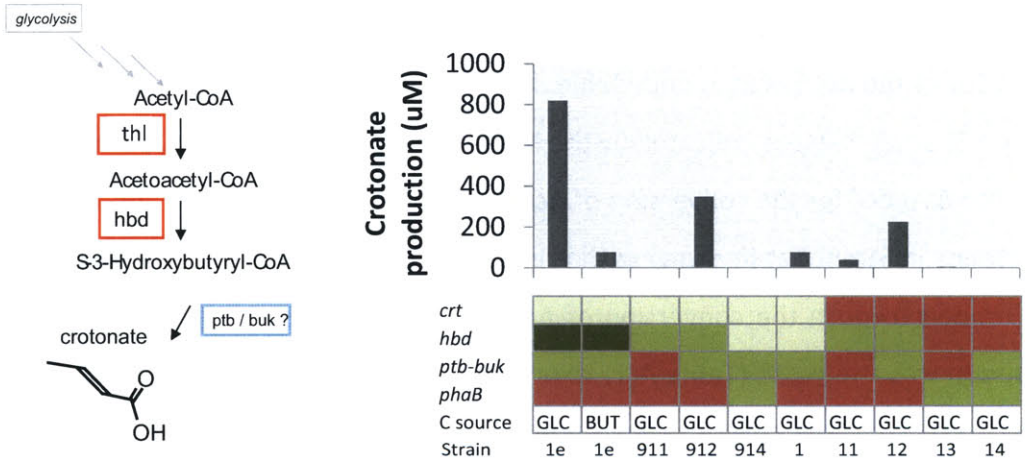

Figure A-4 | Unexpected activity of the clostridial *ptb-buk* operons in recombinant *E. coli*. Crotonic acid is a byproduct of co-expressing both *hbd* (*S*-3-hydroxybutyryl-CoA dehydrogenase) and *ptb-buk*. The expression of butyrate biosynthesis genes (crotonase, *crt*; *hbd*; *ptb-buk*; or the *R*-3-hydroxybutyryl-CoA dehydrogenase-encoding *phaB* gene) is shown semi-quantitatively by color. Red indicates omission of a gene; shades of green indicate semiquantitative expression level. Crotonate production does not depend on the presence of *crt*, correlates with the expression level of *hbd*, and is much higher when growing on glucose than when growing on butyrate. Strain numbers refer to **Table A-1**.

The results shown in **Figure A-4** suggest that *E. coli* strains expressing both *hbd* and *ptb-buk* produce crotonate as a minor fermentation product. Crotonate production

may involve a side reaction of the *ptb-buk* system whereby *S*-3HBCoA, *S*-3-hydroxybutyryl phosphate, or *S*-3-hydroxybutyric acid is converted to crotonate; however, background activities present on the *E. coli* genome may also be involved. We also observed 3HB production in *E. coli* pal(DE3) strains expressing both *hbd* and *ptb-buk*, but the level of production was not reproducible and varied in duplicate experiments between background levels and those previously measured (*Tseng et al., 2009*) for *E. coli* BL21(DE3) strains expressing both *tesB* and *ptb-buk* (data not shown).

A.4 Discussion

Analysis of short chain acyl CoAs and adenosine phosphates in three sets of *E. coli* strains expressing clostridial genes for the biosynthesis of butyrate and butanol showed that *hbd* expression leads to observable 3HB-CoA pools only in Strain Set II, in which strong T7 promoters drive the expression of *hbd* (*Tseng et al., 2009*). The P_{LTetO1}-derived promoter and low-copy pSC101-derived plasmid used to express *hbd* in Strain Set #1 did not result in detectable 3HB-CoA. ButCoA was not reliably detected in any of the strain sets, as indicated by the large relative uncertainties given in **Table A-3**.

The $\Delta_{IPTG}\Delta G'$ for the conversion of AcCoA to 3HB-CoA was positive for all but one of the strains in Strain Set II, showing that induction of ketoacid reductase genes *phaB* or *hbd* tended to push the conversion of AcCoA to 3HB-CoA closer to equilibrium. The exception was strain #11 (**Table A-1**), expressing the clostridial *hbd* gene for reduction of AcAcCoA to 3HB-CoA as well as the non-energy conserving *tesB* gene for conversion of 3HB-CoA to free 3HB. In this strain $\Delta_{IPTG}\Delta G'$ was negative, indicating that induction may have pushed the AcCoA to 3HB-CoA reaction further away from equilibrium. One possible explanation is that induction boosted the activity of TesB more than Hbd, thus draining away 3HB-CoA and indirectly dis-equilibrating the AcCoA to 3HB-CoA reaction.

A thermodynamic framework centered on the calculation of $\Delta_{IPTG}\Delta G'$ revealed that the conversion of 3HB-CoA to ButCoA was not accelerated by induction of the *crt* or *bcd* enzymes, even under the oxygen-limiting conditions we studied. This finding is a confirmation of several other independent analyses that also pinpointed *bcd* as

encoding the enzyme whose activity prevents *E. coli* from reaching its stoichiometric potential (*Inui et al., 2008, Nielsen et al., 2009*). One possibility is that the stoichiometry of the reaction catalyzed by the proteins coded by the *bcd/etfAB* genes has been misunderstood (*Li et al., 2008*), at least in some species of *Clostridia.*

A.5 Conclusions

Overall, pool size measurements can directly assess the performance of the individual steps of a recombinant pathway under *in vivo* conditions, and are thus complementary to other techniques for dissecting the activity of recombinant pathways, such as enzyme assays or bypass studies (Chapters 3-5). We expect that combining pool size measurements with calculation of $\Delta_{inducer}\Delta G'$ will be useful for the dissection and analysis of any metabolically engineered pathway whose performance is not yet satisfactory.

APPENDIX B

Pentanol Theoretical Yield Analysis

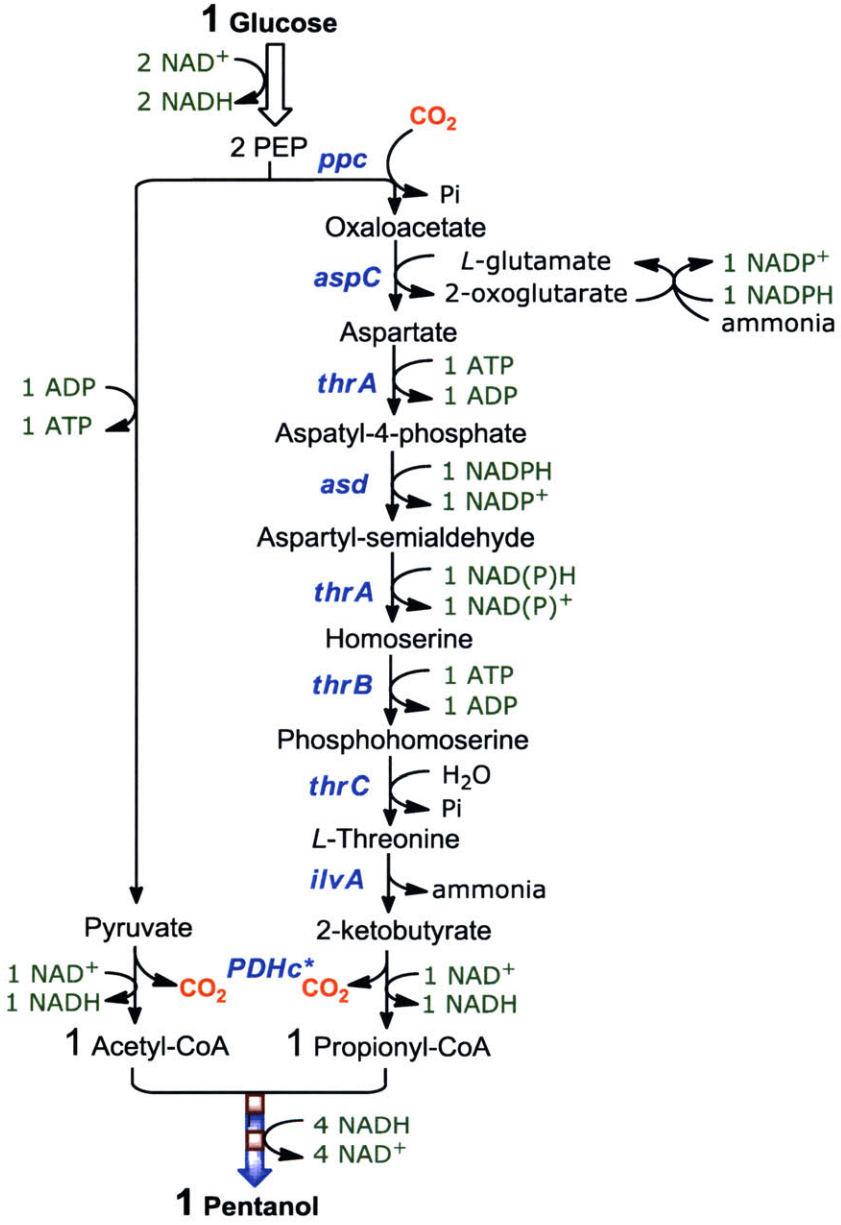

Figure B-1 | Pentanol biosynthetic pathway with cofactor and energy requirement shown in green.

Once the target pathway for pentanol biosynthesis is specified (**Fig. B-1**), maximum theoretical mass yield can then be calculated based on the stoichiometry of the pathway. The detailed calculation for various theortical yields is shown below.

Stoichiometry Yield:

$$Y^S = \frac{1 \text{ mole of pentanol produced} \times 88}{1 \text{ mole of glucose consumed} \times 180} = 0.489$$

Equivalence Yield:

***Method 1**: Deficiency with 3 moles of NADPH per mole of pentanol produced*

$$\text{Pentose Phosphate Pathway} \Rightarrow \frac{2 \text{ moles of NADPH generated}}{1 \text{ mole of } CO_2 \text{ consumed}}$$

1 mole of glucose $\Rightarrow$ 6 moles of CO_2 $\Rightarrow$ 12 moles of NADPH

3 mole of NADPH require $\frac{1}{4}$ mole of glucose

***Method 2**: Calculation of reducing equivalents:*

C = +4; H = +1; O = -2

Glucose ($C_6H_{12}O_6$) = 24

Pentanol ($C_5H_{12}O$) = 30

$\frac{30}{24}(=1+\frac{1}{4})$ moles of glucose is needed to produce 1 mole of pentanol

$$Y^E = \frac{1 \text{ mole of pentanol produced} \times 88}{\left(1+\frac{1}{4}\right) \text{ mole of glucose consumed} \times 180} = 0.391$$

Pathway Yield:

Deficiency with 1 mole of ATP per mole of pentanol produced

1 mole of glucose $\Rightarrow$ 34 moles of ATP under aerobic conditions

1 mole of ATP requires $\frac{1}{34}$ mole of glucose

$$Y^P = \frac{1 \text{ mole of pentanol produced} \times 88}{\left(1+\frac{1}{4}+\frac{1}{34}\right) \text{ mole of glucose consumed} \times 180} = 0.382$$

APPENDIX C

Sequences of Synthesized Genes

GenScript
The Biology CRO

Your Innovation Partner in Drug Discovery!

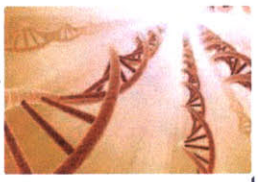

Quotation #:
Gene name: **Sc_fdh1**
Customer:
Optimized for expression in: ***E. coli***
Gene length: **1143**
Optimization region: **7-1137**
Analysis conducted by: **Jason Zhou, Ph.D**
Analysis created: **12/02/2010 02:56:17**

QA: *James*

OptimumGene™ Codon Optimization Analysis

Optimization Parameters

OptimumGene™ algorithm optimizes a variety of parameters that are critical to the efficiency of gene expression, including but not limited to:

- Codon usage bias
- GC content
- CpG dinucleotides content
- mRNA secondary structure
- Cryptic splicing sites
- Premature PolyA sites
- Internal chi sites and ribosomal binding sites
- Negative CpG islands
- RNA instability motif (ARE)
- Repeat sequences (direct repeat, reverse repeat, and Dyad repeat)
- Restriction sites that may interfere with cloning

Additional sequences we propose to improve translational performance:

(1) To increase the efficiency of translational initiation
- Kozak sequence
- Shine-Dalgarno Sequence

(2) To increase the efficiency of translational termination
- Stop codon (TAA)

860 Centennial Ave., Piscataway, NJ 08854, U.S.
Tel: 1-732-885-9188 Fax: 1-732-210-0262 Email: gene@genscript.com Web: www.genscript.com

Results *E. coli*

1. Codon usage bias adjustment

Codon Adaptation Index (CAI)

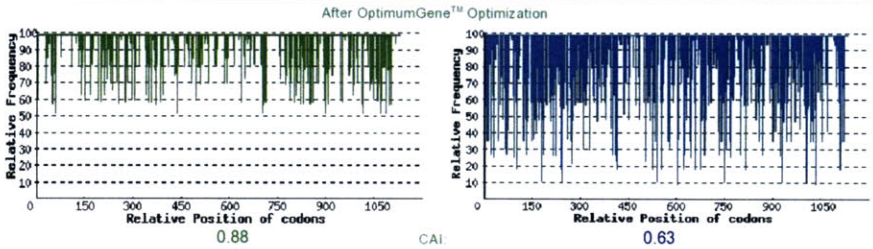

Figure 1a. The distribution of codon usage frequency along the length of the gene sequence. A CAI of 1.0 is considered to be perfect in the desired expression organism, and a CAI of > 0.9 is regarded as very good, in terms of high gene expression level.

Frequency of Optimal Codons (FOP)

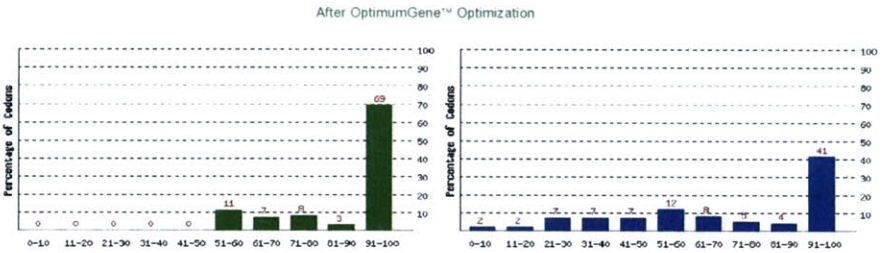

Figure 1b. The percentage distribution of codons in computed codon quality groups. The value of 100 is set for the codon with the highest usage frequency for a given amino acid in the desired expression organism.

2. GC Content Adjustment

GC Content Adjustment

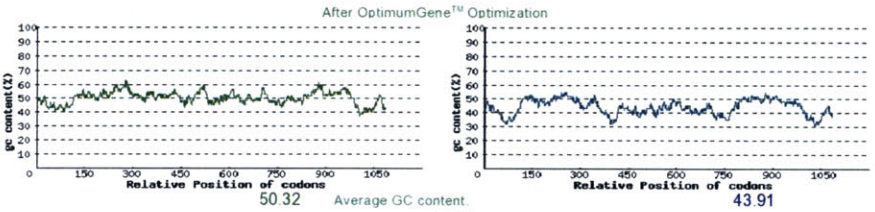

Figure 2. The ideal percentage range of GC content is between 30-70 %. Peaks of %GC content in a 60 bp window have been removed.

860 Centennial Ave., Piscataway, NJ 08854, U.S.
Tel: 1-732-885-9188 Fax: 1-732-210-0262 Email: gene@genscript.com Web: www.genscript.com

3. Restriction Enzymes and CIS-Acting Elements

Restriction Enzymes	Optimized	Original
(Green: filtered sites; Blue: checked sites (not filtered); Red: kept sites)		
NdeI(CATATG)	1(1)	1(1)
AvrII(CCTAGG)	1(1138)	1(1138)
Ribosome binding site	0	0

CIS-Acting Elements	Optimized	Original
E.coli_RBS(AGGAGG)	0	0
PolyT(TTTTTT)	0	0
PolyA(AAAAAAA)	0	0
Chi_sites(GCTGGTGG)	0	0
T7Cis(ATCTGTT)	0	0

4. Remove Repeat Sequences

After Optimization

Max Direct Repeat: Size:11 Distance:510 Frequency:2
Max Inverted Repeat: None
Max Dyad Repeat: None

Before Optimization

Max Direct Repeat: Size:10 Distance:342 Frequency:2
Max Inverted Repeat: None
Max Dyad Repeat: Size: 11 Tm: 27.2 Start Positions: 577, 113

5. Optimized Sequence (Optimized Sequence Length:1143, GC%:50.32)

ATGTCCAAAGGCAAAGTGCTGCTGGTGCTGTACGAAGGTGGTAAACACGCTGAAGAACAAGAAAAACTGCTGGGC
TGTATTGAAAACGAACTGGGCATTCGCAACTTTATCGAAGAACAGGGTTATGAACTGGTTACCACGATCGATAAA
GACCCGGAACCGACCAGCACGGTTGATCGTGAACTGAAAGACGCGGAAATTGTCATCACCACGCCGTTTTTCCCG
GCCTACATTAGTCGTAACCGCATCGCAGAAGCTCCGAATCTGAAACTGTGCGTCACCGCAGGCGTGGGTTCCGAT
CATGTTGACCTGGAAGCGGCCAACGAACGCAAAATTACCGTTACGGAAGTCACCGGCTCAAATGTGGTTTCGGTT
GCGGAACATGTCATGGCCACGATTCTGGTGCTGATCCGTAACTATAATGGCGGTCACCAGCAAGCCATTAACGGC
GAATGGGATATCGCGGGTGTGGCCAAAAACGAATACGATCTGGAAGACAAAATCATCTCTACCGTTGGCGCGGGT
CGTATTGGTTACCGCGTGCTGGAACGTCTGGTTGCCTTTAACCCGAAAAAACTGCTGTATTACGATTACCAGGAA
CTGCCGGCGGAAGCCATTAACCGCCTGAATGAAGCGTCAAAACTGTTCAATGGCCGCGGTGATATCGTGCAGCGT
GTTGAAAAACTGGAAGATATGGTTGCCCAATCGGACGTCGTGACCATTAACTGCCCGCTGCATAAAGATAGCCGC
GGCCTGTTCAACAAAAAACTGATCTCTCACATGAAAGACGGCGCATATCTGGTCAATACGGCACGTGGTGCTATT
TGTGTGGCTGAAGATGTTGCAGAAGCTGTCAAATCAGGCAAACTGGCAGGTTACGGCGGTGATGTGTGGGACAAA
CAACCGGCTCCGAAAGATCACCCGTGGCGTACCATGGATAACAAAGACCATGTCGGCAATGCGATGACCGTGCAC
ATCAGCGGCACGTCTCTGGATGCACAGAAACGCTATGCTCAAGGTGTGAAAAACATCCTGAACAGTTACTTCTCC
AAAAAATTCGACTACCGTCCGCAAGACATCATCGTTCAAAATGGCTCGTATGCTACCCGTGCGTATGGTCAGAAA
AAATAA

6. DNA Alignment (Optimized Region)

```
Optimized     7   ATGTCCAAAGGCAAAGTGCTGCTGGTGCTGTACGAAGGTGGTAAACACGCTGAAGAACAA
Original      7   ATGTCGAAGGGAAAGGTTTTGCTGGTTCTTTACGAAGGTGGTAAGCATGCTGAAGAGCAG

Optimized    67   GAAAAACTGCTGGGCTGTATTGAAAACGAACTGGGCATTCGCAACTTTATCGAAGAACAG
Original     67   GAAAAGTTATTGGGGTGTATTGAAAATGAACTTGGTATCAGAAATTTCATTGAAGAACAG

Optimized   127   GGTTATGAACTGGTTACCACGATCGATAAAGACCCGGAACCGACCAGCACGGTTGATCGT
Original    127   GGATACGAGTTGGTTACTACCATTGACAAGGACCCTGAGCCAACCTCAACGGTAGACAGG

Optimized   187   GAACTGAAAGACGCGGAAATTGTCATCACCACGCCGTTTTTCCCGGCCTACATTAGTCGT
Original    187   GAGTTGAAAGACGCTGAAATTGTCATTACTACGCCCTTTTTCCCCGCCTACATCTCGAGA

Optimized   247   AACCGCATCGCAGAAGCTCCGAATCTGAAACTGTGCGTCACCGCAGGCGTGGGTTCCGAT
Original    247   AACAGGATTGCAGAAGCTCCTAACCTGAAGCTCTGTGTAACCGCTGGCGTCGGTTCAGAC

Optimized   307   CATGTTGACCTGGAAGCGGCCAACGAACGCAAAATTACCGTTACGGAAGTCACCGGCTCA
Original    307   CATGTCGATTTAGAAGCTGCAAATGAACGGAAAATCACGGTCACCGAAGTTACTGGTTCT
```

```
Optimized   367   AATGTGGTTTCGGTTGCGGAACATGTCATGGCCACGATTCTGGTGCTGATCCGTAACTAT
Original    367   AACGTCGTTTCTGTCGCAGAGCACGTTATGGCCACAATTTTGGTTTTGATAAGAAACTAT

Optimized   427   AATGGCGGTCACCAGCAAGCCATTAACGGCGAATGGGATATCGCGGGTGTGGCCAAAAAC
Original    427   AATGGTGGTCATCAACAAGCAATTAATGGTGAGTGGGATATTGCCGGCGTGGCTAAAAAT

Optimized   487   GAATACGATCTGGAAGACAAAATCATCTCTACCGTTGGCGCGGGTCGTATTGGTTACCGC
Original    487   GAGTATGATCTGGAAGACAAAATAATTTCAACGGTAGGTGCCGGTAGAATTGGATATAGG

Optimized   547   GTGCTGGAACGTCTGGTTGCCTTTAACCCGAAAAAACTGCTGTATTACGATTACCAGGAA
Original    547   GTTCTGGAAAGATTGGTCGCATTTAATCCGAAGAAGTTACTGTACTACGACTACCAGGAA

Optimized   607   CTGCCGGCGGAAGCCATTAACCGCCTGAATGAAGCGTCAAAACTGTTCAATGGCCGCGGT
Original    607   CTACCTGCGGAAGCAATCAATAGATTGAACGAGGCCAGCAAGCTTTTCAATGGCAGAGGT

Optimized   667   GATATCGTGCAGCGTGTTGAAAAACTGGAAGATATGGTTGCCCAATCGGACGTCGTGACC
Original    667   GATATTGTTCAGAGAGTAGAGAAATTGGAGGATATGGTTGCTCAGTCAGATGTTGTTACC

Optimized   727   ATTAACTGCCCGCTGCATAAAGATAGCCGCGGCCTGTTCAACAAAAAACTGATCTCTCAC
Original    727   ATCAACTGTCCATTGCACAAGGACTCAAGGGGTTTATTCAATAAAAAGCTTATTTCCCAC

Optimized   787   ATGAAAGACGGCGCATATCTGGTCAATACGGCACGTGGTGCTATTTGTGTGGCTGAAGAT
Original    787   ATGAAAGATGGTGCATACTTGGTGAATACCGCTAGAGGTGCTATTTGTGTCGCAGAAGAT

Optimized   847   GTTGCAGAAGCTGTCAAATCAGGCAAACTGGCAGGTTACGGCGGTGATGTGTGGGACAAA
Original    847   GTTGCCGAGGCAGTCAAGTCTGGTAAATTGGCTGGCTATGGTGGTGATGTCTGGGATAAG

Optimized   907   CAACCGGCTCCGAAAGATCACCCGTGGCGTACCATGGATAACAAAGACCATGTCGGCAAT
Original    907   CAACCAGCACCAAAAGACCATCCCTGGAGGACTATGGACAATAAGGACCACGTGGGAAAC

Optimized   967   GCGATGACCGTGCACATCAGCGGCACGTCTCTGGATGCACAGAAACGCTATGCTCAAGGT
Original    967   GCAATGACTGTTCATATCAGTGGCACATCTCTGGATGCTCAAAAGAGGTACGCTCAGGGA

Optimized  1027   GTGAAAAACATCCTGAACAGTTACTTCTCCAAAAAATTCGACTACCGTCCGCAAGACATC
Original   1027   GTAAAGAACATCCTAAATAGTTACTTTTCCAAAAAGTTTGATTACCGTCCACAGGATATT

Optimized  1087   ATCGTTCAAAATGGCTCGTATGCTACCCGTGCGTATGGTCAGAAAAAATAA
Original   1087   ATTGTGCAGAATGGTTCTTATGCCACCAGAGCTTATGGACAGAAGAAATAA
```

Conclusion

A wide variety of factors regulate and influence gene expression levels, and our OptimumGene™ algorithm takes into consideration as many of them as possible, producing the single gene that can reach the highest possible level of expression.

In this case, the native gene employs tandem rare codons that can reduce the efficiency of translation or even disengage the translational machinery. We changed the codon usage bias in E. coli by upgrading the CAI from 0.63 to 0.88 . GC content and unfavorable peaks have been optimized to prolong the half-life of the mRNA. The Stem-Loop structures, which impact ribosomal binding and stability of mRNA, were broken. In addition, our optimization process has screened and successfully modified those negative cis-acting sites as listed in the introduction.

We are honored to deliver the analysis that you requested. We hope that you are pleased with your GenScript OptimumGene™ results.

860 Centennial Ave., Piscataway, NJ 08854, U.S.
Tel: 1-732-885-9188 Fax: 1-732-210-0262 Email: gene@genscript.com Web: www.genscript.com

Supplementary

1. Codon Frequency Table Used: (Primary Host)

TTT 22.1(80995)	TCT 10.4(38027)	TAT 17.5(63937)	TGT 5.2(19138)
TTC 16.0(58774)	TCC 9.1(33430)	TAC 12.2(44631)	TGC 6.1(22188)
TTA 14.3(52382)	TCA 8.9(32715)	TAA 2.0(7356)	TGA 1.0(3623)
TTG 13.0(47500)	TCG 8.5(31146)	TAG 0.3(989)	TGG 13.9(50991)
CTT 11.9(43449)	CCT 7.5(27340)	CAT 12.5(45879)	CGT 20.0(73197)
CTC 10.2(37347)	CCC 5.4(19666)	CAC 9.3(34078)	CGC 19.7(72212)
CTA 4.2(15409)	CCA 8.6(31534)	CAA 14.6(53394)	CGA 3.8(13844)
CTG 48.4(177210)	CCG 20.9(76644)	CAG 28.4(104171)	CGG 5.9(21552)
ATT 29.8(109072)	ACT 10.3(37842)	AAT 20.6(75436)	AGT 9.9(36097)
ATC 23.7(86796)	ACC 22.0(80547)	AAC 21.4(78443)	AGC 15.2(55551)
ATA 6.8(24984)	ACA 9.3(33910)	AAA 35.3(129137)	AGA 3.6(13152)
ATG 26.4(96695)	ACG 13.7(50269)	AAG 12.4(45459)	AGG 2.1(7607)
GTT 19.8(72584)	GCT 17.1(62479)	GAT 32.7(119939)	GGT 25.5(93325)
GTC 14.3(52439)	GCC 24.2(88721)	GAC 19.2(70394)	GGC 27.1(99390)
GTA 11.6(42420)	GCA 21.2(77547)	GAA 39.1(143353)	GGA 9.5(34799)
GTG 24.4(89265)	GCG 30.1(110308)	GAG 18.7(68609)	GGG 11.3(41277)

2. Protein Alignment (Optimized Region)

```
Optimized    1    MSKGKVLLVLYEGGKHAEEQEKLLGCIENELGIRNFIEEQGYELVTTIDKDPEPTSTVDR
Original     1    MSKGKVLLVLYEGGKHAEEQEKLLGCIENELGIRNFIEEQGYELVTTIDKDPEPTSTVDR

Optimized   61    ELKDAEIVITTPFFPAYISRNRIAEAPNLKLCVTAGVGSDHVDLEAANERKITVTEVTGS
Original    61    ELKDAEIVITTPFFPAYISRNRIAEAPNLKLCVTAGVGSDHVDLEAANERKITVTEVTGS

Optimized  121    NVVSVAEHVMATILVLIRNYNGGHQQAINGEWDIAGVAKNEYDLEDKIISTVGAGRIGYR
Original   121    NVVSVAEHVMATILVLIRNYNGGHQQAINGEWDIAGVAKNEYDLEDKIISTVGAGRIGYR

Optimized  181    VLERLVAFNPKKLLYYDYQELPAEAINRLNEASKLFNGRGDIVQRVEKLEDMVAQSDVVT
Original   181    VLERLVAFNPKKLLYYDYQELPAEAINRLNEASKLFNGRGDIVQRVEKLEDMVAQSDVVT

Optimized  241    INCPLHKDSRGLFNKKLISHMKDGAYLVNTARGAICVAEDVAEAVKSGKLAGYGGDVWDK
Original   241    INCPLHKDSRGLFNKKLISHMKDGAYLVNTARGAICVAEDVAEAVKSGKLAGYGGDVWDK
```

```
Optimized  301    QPAPKDHPWRTMDNKDHVGNAMTVHISGTSLDAQKRYAQGVKNILNSYFSKKFDYRPQDI
Original   301    QPAPKDHPWRTMDNKDHVGNAMTVHISGTSLDAQKRYAQGVKNILNSYFSKKFDYRPQDI

Optimized  361    IVQNGSYATRAYGQKK*
Original   361    IVQNGSYATRAYGQKK*
```

GenScript
The Biology CRO

Your Innovation Partner in Drug Discovery!

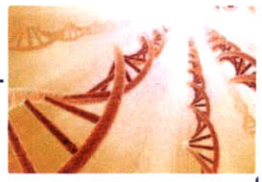

Quotation #:
Gene name: **Cb_fdh1**
Customer:
Optimized for expression in: ***E. coli***
Gene length: **1107**
Optimization region: **7-1101**
Analysis conducted by: **Jason Zhou, Ph.D**
Analysis created: **12/02/2010 03:01:32**

QA: *James*

ACCORDING TO ISO 9001 CERTIFIED

OptimumGene™ GenScript Codon Optimization

OptimumGene™ Codon Optimization Analysis

Optimization Parameters

OptimumGene™ algorithm optimizes a variety of parameters that are critical to the efficiency of gene expression, including but not limited to:

- Codon usage bias
- GC content
- CpG dinucleotides content
- mRNA secondary structure
- Cryptic splicing sites
- Premature PolyA sites
- Internal chi sites and ribosomal binding sites
- Negative CpG islands
- RNA instability motif (ARE)
- Repeat sequences (direct repeat, reverse repeat, and Dyad repeat)
- Restriction sites that may interfere with cloning

Additional sequences we propose to improve translational performance:

(1) To increase the efficiency of translational initiation
- Kozak sequence
- Shine-Dalgarno Sequence

(2) To increase the efficiency of translational termination
- Stop codon (TAA)

860 Centennial Ave., Piscataway, NJ 08854, U.S.
Tel: 1-732-885-9188 Fax: 1-732-210-0262 Email: gene@genscript.com Web: www.genscript.com

Results *E. coli*

1. Codon usage bias adjustment

Codon Adaptation Index (CAI)

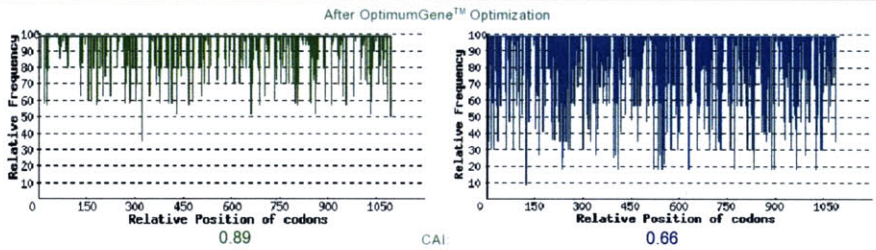

Figure 1a. The distribution of codon usage frequency along the length of the gene sequence. A CAI of 1.0 is considered to be perfect in the desired expression organism, and a CAI of > 0.9 is regarded as very good, in terms of high gene expression level.

Frequency of Optimal Codons (FOP)

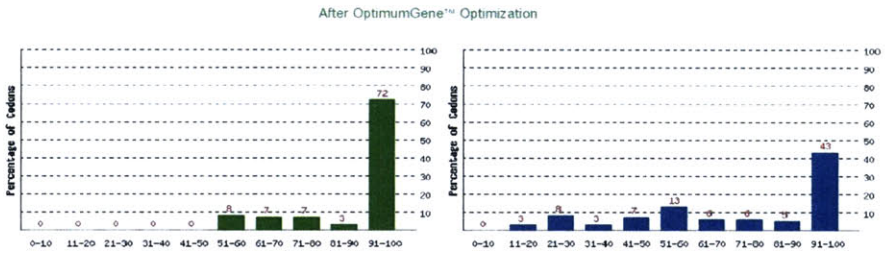

Figure 1b. The percentage distribution of codons in computed codon quality groups. The value of 100 is set for the codon with the highest usage frequency for a given amino acid in the desired expression organism.

2. GC Content Adjustment

GC Content Adjustment

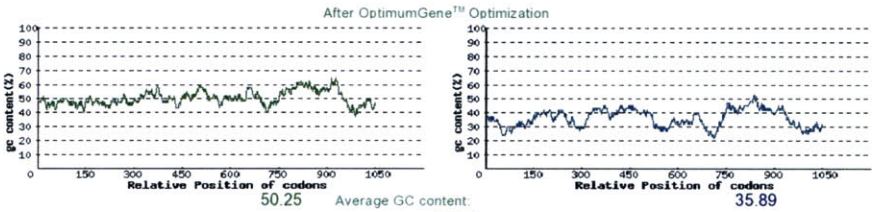

Figure 2. The ideal percentage range of GC content is between 30-70 %. Peaks of %GC content in a 60 bp window have been removed.

860 Centennial Ave., Piscataway, NJ 08854, U.S.
Tel: 1-732-885-9188 Fax: 1-732-210-0262 Email: gene@genscript.com Web: www.genscript.com

3. Restriction Enzymes and CIS-Acting Elements

Restriction Enzymes	Optimized	Original
* Green: filtered sites. Blue: checked sites (not filtered). Red: kept sites.		
NdeI(CATATG)	1(1)	1(1)
AvrII(CCTAGG)	1(1102)	1(1102)
Ribosome binding site	0	0

CIS-Acting Elements	Optimized	Original
E.coli_RBS(AGGAGG)	0	0
PolyT(TTTTTT)	0	0
PolyA(AAAAAAA)	0	0
Chi_sites(GCTGGTGG)	0	0
T7Cis(ATCTGTT)	0	0

4. Remove Repeat Sequences

After Optimization

Max Direct Repeat: Size:13 Distance:156 Frequency:2
Max Inverted Repeat: None
Max Dyad Repeat: None

Before Optimization

Max Direct Repeat: Size:11 Distance:396 Frequency:2
Max Inverted Repeat: None
Max Dyad Repeat: None

5. Optimized Sequence (Optimized Sequence Length:1107, GC%:50.25)

ATGAAAATCGTGCTGGTCCTGTATGACGCTGGCAAACATGCGGCGGATGAAGAAAAACTGTATGGTTGTACCGAA
AATAAACTGGGCATCGCCAACTGGCTGAAAGATCAGGGCCATGAACTGATTACCACGAGTGATAAAGAAGGTGAA
ACCTCCGAACTGGACAAACATATCCCGGATGCTGACATTATCATTACCACGCCGTTTCACCCGGCGTATATTACG
AAAGAACGCCTGGATAAAGCCAAAAATCTGAAACTGGTGGTTGTCGCAGGCGTTGGTTCAGACCATATCGATCTG
GACTACATTAACCAGACCGGCAAGAAAATTAGCGTGCTGGAAGTGACGGGTAGCAATGTGGTTTCTGTGGCGGAA
CACGTCGTGATGACCATGCTGGTTCTGGTCCGTAACTTTGTCCCGGCCCATGAACAAATCATTAATCACGATTGG
GAAGTGGCGGCCATCGCTAAAGATGCGTATGACATTGAAGGCAAAACCATCGCCACGATTGGCGCAGGTCGTATT
GGTTACCGCGTTCTGGAACGTCTGCTGCCGTTCAACCCGAAAGAACTGCTGTATTACGATTATCAGGCCCTGCCG
AAAGAAGCAGAAGAAAAAGTGGGCGCACGTCGCGTTGAAAATATCGAAGAACTGGTGGCCCAAGCAGATATTGTG
ACCGTTAACGCTCCGCTGCATGCGGGCACGAAAGGTCTGATCAACAAAGAACTGCTGTCCAAATTCAAAAAAGGT
GCATGGCTGGTTAACACCGCACGTGGTGCAATTTGCGTTGCAGAAGATGTCGCAGCTGCACTGGAAAGCGGTCAG
CTGCGTGGTTATGGTGGTGACGTCTGGTTCCCGCAACCGGCACCGAAAGATCATCCGTGGCGTGACATGCGCAAC
AAATATGGCGCTGGTAATGCGATGACCCCGCACTACAGCGGTACCACGCTGGATGCTCAGACCCGCTATGCGGAA
GGCACGAAAAATATTCTGGAAAGCTTTTTCACCGGTAAATTCGATTACCGTCCGCAAGACATTATCCTGCTGAAT
GGCGAATACGTTACCAAAGCCTACGGCAAACACGACAAAAAATGA

6. DNA Alignment (Optimized Region)

```
Optimized     7   ATGAAAATCGTGCTGGTCCTGTATGACGCTGGCAAACATGCGGCGGATGAAGAAAAACTG
Original      7   ATGAAGATCGTTTTAGTCTTATATGATGCTGGTAAGCACGCTGCTGATGAAGAAAAATTA

Optimized    67   TATGGTTGTACCGAAAATAAACTGGGCATCGCCAACTGGCTGAAAGATCAGGGCCATGAA
Original     67   TATGGTTGTACTGAAAATAAATTAGGTATTGCTAATTGGTTAAAAGATCAAGGTCATGAA

Optimized   127   CTGATTACCACGAGTGATAAAGAAGGTGAAACCTCCGAACTGGACAAACATATCCCGGAT
Original    127   CTAATTACTACTTCTGATAAAGAAGGTGAAACAAGTGAATTGGATAAACATATCCCAGAT

Optimized   187   GCTGACATTATCATTACCACGCCGTTTCACCCGGCGTATATTACGAAAGAACGCCTGGAT
Original    187   GCTGATATTATCATCACCACTCCTTTCCATCCTGCTTATATCACTAAGGAAAGACTTGAC

Optimized   247   AAAGCCAAAAATCTGAAACTGGTGGTTGTCGCAGGCGTTGGTTCAGACCATATCGATCTG
Original    247   AAGGCTAAGAACTTAAAATTAGTCGTTGTCGCTGGTGTTGGTTCTGATCACATTGATTTA

Optimized   307   GACTACATTAACCAGACCGGCAAGAAAATTAGCGTGCTGGAAGTGACGGGTAGCAATGTG
Original    307   GATTATATTAATCAAACAGGTAAGAAAATCTCAGTCTTGGAAGTTACAGGTTCTAATGTT
```

```
Optimized    367   GTTTCTGTGGCGGAACACGTCGTGATGACCATGCTGGTTCTGGTCCGTAACTTTGTCCCG
Original     367   GTCTCTGTTGCTGAACACGTTGTCATGACCATGCTTGTCTTGGTTAGAAATTTCGTTCCA

Optimized    427   GCCCATGAACAAATCATTAATCACGATTGGGAAGTGGCGGCCATCGCTAAAGATGCGTAT
Original     427   GCACATGAACAAATTATTAACCACGATTGGGAGGTTGCTGCTATCGCTAAGGATGCTTAC

Optimized    487   GACATTGAAGGCAAAACCATCGCCACGATTGGCGCAGGTCGTATTGGTTACCGCGTTCTG
Original     487   GATATCGAAGGTAAAACTATTGCTACCATTGGTGCTGGTAGAATTGGTTACAGAGTCTTG

Optimized    547   GAACGTCTGCTGCCGTTCAACCCGAAAGAACTGCTGTATTACGATTATCAGGCCCTGCCG
Original     547   GAAAGATTACTCCCTTTTAATCCAAAAGAATTATTATACTACGATTATCAAGCTTTACCA

Optimized    607   AAAGAAGCAGAAGAAAAAGTGGGCGCACGTCGCGTTGAAAATATCGAAGAACTGGTGGCC
Original     607   AAAGAAGCTGAAGAAAAAGTTGGTGCTAGAAGAGTTGAAAATATTGAAGAATTAGTTGCT

Optimized    667   CAAGCAGATATTGTGACCGTTAACGCTCCGCTGCATGCGGGCACGAAAGGTCTGATCAAC
Original     667   CAAGCTGATATCGTTACAGTTAATGCTCCATTACACGCAGGTACAAAAGGTTTAATTAAT

Optimized    727   AAAGAACTGCTGTCCAAATTCAAAAAAGGTGCATGGCTGGTTAACACCGCACGTGGTGCA
Original     727   AAGGAATTATTATCTAAATTTAAAAAAGGTGCTTGGTTAGTCAATACCGCAAGAGGTGCT

Optimized    787   ATTTGCGTTGCAGAAGATGTCGCAGCTGCACTGGAAAGCGGTCAGCTGCGTGGTTATGGT
Original     787   ATTTGTGTTGCTGAAGATGTTGCAGCAGCTTTAGAATCTGGTCAATTAAGAGGTTACGGT

Optimized    847   GGTGACGTCTGGTTCCCGCAACCGGCACCGAAAGATCATCCGTGGCGTGACATGCGCAAC
Original     847   GGTGATGTTTGGTTCCCACAACCAGCTCCAAAGGATCACCCATGGAGAGATATGAGAAAT

Optimized    907   AAATATGGCGCTGGTAATGCGATGACCCCGCACTACAGCGGTACCACGCTGGATGCTCAG
Original     907   AAATATGGTGCTGGTAATGCCATGACTCCTCACTACTCTGGTACTACTTTAGATGCTCAA

Optimized    967   ACCCGCTATGCGGAAGGCACGAAAAATATTCTGGAAAGCTTTTTCACCGGTAAATTCGAT
Original     967   ACAAGATACGCTGAAGGTACTAAAAATATCTTGGAATCATTCTTTACTGGTAAATTTGAT

Optimized   1027   TACCGTCCGCAAGACATTATCCTGCTGAATGGCGAATACGTTACCAAAGCCTACGGCAAA
Original    1027   TACAGACCACAAGATATTATCTTATTAAATGGTGAATACGTTACTAAAGCTTACGGTAAA

Optimized   1087   CACGACAAAAAATGA
Original    1087   CACGATAAGAAATAA
```

Conclusion

A wide variety of factors regulate and influence gene expression levels, and our OptimumGene™ algorithm takes into consideration as many of them as possible, producing the single gene that can reach the highest possible level of expression.

In this case, the native gene employs tandem rare codons that can reduce the efficiency of translation or even disengage the translational machinery. We changed the codon usage bias in E. coli by upgrading the CAI from 0.66 to 0.89 . GC content and unfavorable peaks have been optimized to prolong the half-life of the mRNA. The Stem-Loop structures, which impact ribosomal binding and stability of mRNA, were broken. In addition, our optimization process has screened and successfully modified those negative cis-acting sites as listed in the introduction.

We are honored to deliver the analysis that you requested. We hope that you are pleased with your GenScript OptimumGene™ results.

860 Centennial Ave., Piscataway, NJ 08854, U.S.
Tel: 1-732-885-9188 Fax: 1-732-210-0262 Email: gene@genscript.com Web: www.genscript.com

Supplementary

1. Codon Frequency Table Used: (Primary Host)

TTT 22.1(80995)	TCT 10.4(38027)	TAT 17.5(63937)	TGT 5.2(19138)
TTC 16.0(58774)	TCC 9.1(33430)	TAC 12.2(44631)	TGC 6.1(22188)
TTA 14.3(52382)	TCA 8.9(32715)	TAA 2.0(7356)	TGA 1.0(3623)
TTG 13.0(47500)	TCG 8.5(31146)	TAG 0.3(989)	TGG 13.9(50991)
CTT 11.9(43449)	CCT 7.5(27340)	CAT 12.5(45879)	CGT 20.0(73197)
CTC 10.2(37347)	CCC 5.4(19666)	CAC 9.3(34078)	CGC 19.7(72212)
CTA 4.2(15409)	CCA 8.6(31534)	CAA 14.6(53394)	CGA 3.8(13844)
CTG 48.4(177210)	CCG 20.9(76644)	CAG 28.4(104171)	CGG 5.9(21552)
ATT 29.8(109072)	ACT 10.3(37842)	AAT 20.6(75436)	AGT 9.9(36097)
ATC 23.7(86796)	ACC 22.0(80547)	AAC 21.4(78443)	AGC 15.2(55551)
ATA 6.8(24984)	ACA 9.3(33910)	AAA 35.3(129137)	AGA 3.6(13152)
ATG 26.4(96695)	ACG 13.7(50269)	AAG 12.4(45459)	AGG 2.1(7607)
GTT 19.8(72584)	GCT 17.1(62479)	GAT 32.7(119939)	GGT 25.5(93325)
GTC 14.3(52439)	GCC 24.2(88721)	GAC 19.2(70394)	GGC 27.1(99390)
GTA 11.6(42420)	GCA 21.2(77547)	GAA 39.1(143353)	GGA 9.5(34799)
GTG 24.4(89265)	GCG 30.1(110308)	GAG 18.7(68609)	GGG 11.3(41277)

2. Protein Alignment (Optimized Region)

```
Optimized    1    MKIVLVLYDAGKHAADEEKLYGCTENKLGIANWLKDQGHELITTSDKEGETSELDKHIPD
Original     1    MKIVLVLYDAGKHAADEEKLYGCTENKLGIANWLKDQGHELITTSDKEGETSELDKHIPD

Optimized   61    ADIIITTPFHPAYITKERLDKAKNLKLVVVAGVGSDHIDLDYINQTGKKISVLEVTGSNV
Original    61    ADIIITTPFHPAYITKERLDKAKNLKLVVVAGVGSDHIDLDYINQTGKKISVLEVTGSNV

Optimized  121    VSVAEHVVMTMLVLVRNFVPAHEQIINHDWEVAAIAKDAYDIEGKTIATIGAGRIGYRVL
Original   121    VSVAEHVVMTMLVLVRNFVPAHEQIINHDWEVAAIAKDAYDIEGKTIATIGAGRIGYRVL

Optimized  181    ERLLPFNPKELLYYDYQALPKEAEEKVGARRVENIEELVAQADIVTVNAPLHAGTKGLIN
Original   181    ERLLPFNPKELLYYDYQALPKEAEEKVGARRVENIEELVAQADIVTVNAPLHAGTKGLIN

Optimized  241    KELLSKFKKGAWLVNTARGAICVAEDVAAALESGQLRGYGGDVWFPQPAPKDHPWRDMRN
Original   241    KELLSKFKKGAWLVNTARGAICVAEDVAAALESGQLRGYGGDVWFPQPAPKDHPWRDMRN
```

```
Optimized  301    KYGAGNAMTPHYSGTTLDAQTRYAEGTKNILESFFTGKFDYRPQDIILLNGEYVTKAYGK
Original   301    KYGAGNAMTPHYSGTTLDAQTRYAEGTKNILESFFTGKFDYRPQDIILLNGEYVTKAYGK

Optimized  361    HDKK*
Original   361    HDKK*
```